INFORMATION TO USERS

This manuscript has been reproduced from the microfilm master. UMI films the text directly from the original or copy submitted. Thus, some thesis and dissertation copies are in typewriter face, while others may be from any type of computer printer.

The quality of this reproduction is dependent upon the quality of the copy submitted. Broken or indistinct print, colored or poor quality illustrations and photographs, print bleedthrough, substandard margins, and improper alignment can adversely affect reproduction.

In the unlikely event that the author did not send UMI a complete manuscript and there are missing pages, these will be noted. Also, if unauthorized copyright material had to be removed, a note will indicate the deletion.

Oversize materials (e.g., maps, drawings, charts) are reproduced by sectioning the original, beginning at the upper left-hand corner and continuing from left to right in equal sections with small overlaps.

Photographs included in the original manuscript have been reproduced xerographically in this copy. Higher quality 6" x 9" black and white photographic prints are available for any photographs or illustrations appearing in this copy for an additional charge. Contact UMI directly to order.

Bell & Howell Information and Learning
300 North Zeeb Road, Ann Arbor, MI 48106-1346 USA

UMI®
800-521-0600

THE UNIVERSITY OF OKLAHOMA

GRADUATE COLLEGE

An Investigation of Alcohol Tracer Partition Coefficients and a Study of Simulations

A Dissertation

SUBMITTED TO THE GRADUATE FACULTY

in partial fulfillment of the requirements for the

degree of

Doctor of Philosophy

By

Alfred E. Thal, Jr.
Norman, Oklahoma
1999

UMI Number: 9952417

UMI Microform 9952417

Bell & Howell Information and Learning Company
300 North Zeeb Road
P.O. Box 1346
Ann Arbor, MI 48106-1346

An Investigation of Alcohol Tracer Partition Coefficients and a Study of Simulations

A Dissertation
APPROVED FOR THE SCHOOL OF CIVIL ENGINEERING
AND ENVIRONMENTAL SCIENCE

BY

Robert C. Knox, Chairperson

David A Sabatini
David A. Sabatini

Randall L. Kolar
Randall L. Kolar

Mark A. Nanny
Mark A. Nanny

Anuj Gupta

Dedication

To Susan, my wife, soulmate, and confidante

And to Jennifer, my daughter of whom I couldn't be prouder
and who will always be "my little girl"

Thank you for your tremendous sacrifices, unbelievable understanding,
and enduring patience

Most of all, thank you for your love,
All that I have become is because of the two of you

I love you both more than words will ever describe,
and more than the dew on the leaves

Acknowledgements

There are a great many people to whom I owe a great deal of gratitude. It is only right that the list begin with the two people who have inspired me the most. It began with "cookie lessons" when my daughter was just a toddler and continues to this day with talks about "the game of life." After all, a large part of being a good parent is being a good teacher. To Susan, my co-teacher in this game of life, and to Jennifer, our "student for life," any words I might choose to describe what I feel for both of you would be an overwhelming understatement and woefully inadequate. To both of you then, I simply say thank you. Without your love and support, the past few years would not have been worth it.

To my committee chair and advisor, Dr. Bob Knox, thank you for the thought-provoking discussions, sessions at the "dry-wipe board," and the autonomy with which you released me to accomplish my research. You are truly the master, despite what Hans might say. To Dr. David Sabatini, whom I consider the consummate teacher, thank you for the opportunity to learn from you. You have a unique gift, and I can only pray that I come close to the same level of excellence that you bring to the art of teaching. To Dr. Randy Kolar, thank you for clearing the fog and helping me to better understand governing equations and the effort required to develop mathematical models. I particularly want to thank you for pointing out my unwitting attempts at re-writing the Thomas algorithm. To Dr. Anuj Gupta, thank you for a solid background in numerical methods. The material you presented and the analytical approach you showed us continue to remain with me. To Dr. Mark Nanny, thank you for opening your door when I came knocking, and for helping break down the mental block that has kept me from understanding even the most basic principles of organic chemistry. To all of you, thank you for agreeing to take the time to serve on my committee. More importantly, thank you for greatly enriching my learning experience at The University of Oklahoma. The guidance, encouragement, and patience will never be forgotten.

There are a number of people who made the many days and nights in the lab more enjoyable. I particularly want to thank Bin Wu for taking the time to teach me how to conduct various experiments and how to use the analytical equipment. His expertise and wealth of knowledge were of great benefit. To Micah Goodspeed, thank you for the company and conversations during the weekends and evenings in the lab. Your kindness and friendship meant a lot.

A note of thanks must also be given to Dr. Gary Pope, Dr. Mojdeh Delshad, and a number of graduate students at the University of Texas at Austin. The seminar they hosted to present the development and concepts behind UTCHEM was the genesis of my research. I especially want to thank Mojdeh for the articles and reports she provided, as well as the patience she showed in answering my many questions.

I also want to thank my fellow AFIT students for their friendship and camaraderie. Without it, the last few years would have been much less enjoyable. Additionally, I want to thank Colonel Bob Warner, Commander of the AFROTC detachment on campus, his successor, Colonel Phil Brown, and their respective staffs.

Their support and friendships were a blessing. TSgt Eddie Grooms and TSgt Derek Gadberry deserve special mention. They are truly at the top of their profession. The administrative support and guidance regarding my AFIT Liaison responsibilities were superb. I must also thank the Engineering and Environmental Management Department in the Graduate School of Engineering at the Air Force Institute of Technology for sponsoring me and displaying a mountain of patience as I struggled to complete my degree requirements.

Finally, I want to thank all of my friends and relatives for their support and encouragement. I would especially like to thank Denny, Susie, Marquis, and Angela for their friendship, the fun we've had together, and the use of their "pool house." The memories will be with us forever, and the bonds of friendship will remain strong.

To everyone I've mentioned, and to those countless others I haven't, I say once again, thank you. In no small way, each of you has had a significant impact on me during the last few years. In closing, I leave you with a few notable quotes regarding this profession of teaching in which we are all involved one way or another.

I hear and I forget. I see and I remember. I do and I understand.

- Chinese Proverb

A teacher affects eternity, he can never tell where his influence stops.

- Henry Adams

The whole art of teaching is only the art of awakening the natural curiosity of young minds for the purpose of satisfying it afterwards.

- Anatole France

Table of Contents

List of Tables

List of Figures

Abstract

In any industrial society, the production and use of liquid petroleum products and industrial solvents are widespread. Since little was known about the hazards associated with these chemicals until the 1970s, management and disposal practices were inadequate in the past and provided only minimal protection to human health and the environment. The presence of these chemicals in the subsurface, whether from improper management or poor disposal practices, poses a serious threat to groundwater systems.

Regardless of the cleanup technology selected for a contaminated site, proper characterization of subsurface nonaqueous phase liquids (NAPLs) is essential for effective remediation efforts. Since partitioning tracers are increasingly being used for characterization efforts, the primary objective of this research was to determine if a correlation existed between the distribution of a tracer between water and organic solvents such that researchers could estimate partition coefficients. After validating the equivalent alkane carbon number (EACN) concept, a correlation ($R_2 = 0.9910$) was found to exist in which there is a bilinear relationship between tracer partition coefficients and the EACNs of both the contaminant and alcohol (9 contaminants and 13 alcohols were used). The ability to estimate partition coefficients, when coupled with modeling efforts, enables the researcher to focus work on tracers possessing partitioning characteristics most suitable for a given site.

A closely related objective was to determine the composition changes in a synthetic NAPL during surfactant enhanced remediation. Composition changes would result in changes to the NAPL's EACN and affect the estimated partition coefficient determined from the previous correlation. However, composition changes during this research were negligible and the NAPL EACN remained essentially constant. During the remediation process, analysis of the effluent validated preferential solubilization. A Solubility Ratio Index (SRI) was developed which easily identified the order of preferential solubilization for the contaminants. Furthermore, a linear relationship between the SRI and aqueous solubility was discovered.

The secondary objective of this research was to demonstrate the advantages of the UTCHEM simulator in developing effective design strategies for tracer tests and surfactant flooding processes. During a column study, there was generally good agreement between the simulation results and the experimental data. At the field scale, simulation results were only able to illustrate general trends in the experimental data. Obtaining good agreement was not possible because of a lack of information regarding site heterogeneities and NAPL distribution.

CHAPTER 1

INTRODUCTION

The material presented and discussed in this work is an outgrowth of ongoing research at The University of Oklahoma concerning surfactant-enhanced remediation of subsurface nonaqueous phase liquid (NAPL) contamination. During a recent field demonstration, university researchers used the partitioning interwell tracer test (PITT) technique for the first time. While the PITT technique offers many advantages and was found to be very effective in measuring residual NAPL saturation levels, its use prompted the realization that a better understanding of partitioning tracers is needed.

Therefore, one focus of this work is to determine the relationship between the partitioning coefficients of alcohol tracers and NAPL composition. This requires that the variable nature of NAPL composition during surfactant-enhanced remediation be investigated as well. Another focus of this research is the application of UTCHEM (a three-dimensional chemical flooding simulator developed at The University of Texas at Austin) in modeling partitioning interwell tracer tests, as well as the surfactant remediation process. The following sections of this chapter further describe the motivation for this work as well as the specific objectives and hypotheses guiding the research. A review of subsequent chapters is also provided.

1.1 Motivation

In any industrial society, the production and use of liquid petroleum products and industrial solvents are widespread. Petroleum products have been an integral part of civilization since the industrial revolution and solvents have been heavily used for a better part of this century. Since little was known about the hazards associated with these chemicals until the 1970s, management and disposal practices were inadequate in the past and provided only minimal protection to human health and the environment. As a result, subsurface contamination from chlorinated solvents at existing hazardous waste sites is considered a common occurrence (Mackay and Cherry, 1989; Mercer and Cohen, 1990; Oolman *et al.*, 1995). Releases from underground storage tanks, pipeline ruptures, and illegal disposal of waste materials are additional sources of contamination (Feenstra and Coburn, 1986; Mercer and Cohen, 1990). The presence of these chemicals in the subsurface, whether from improper management or poor disposal practices, poses a serious threat to groundwater systems.

The literature is replete with examples and a long history of documentation illustrating the existence of subsurface contamination and its effects on groundwater systems (Atwater, 1984; Feenstra and Coburn, 1986; Cohen *et al.*, 1987; Schwille, 1987). In the United States, there are thousands of sites where the groundwater has become contaminated because of releases of chemical substances (Korfiatis and Makarigakis, 1996). The Environmental Protection Agency (EPA) has identified over 300,000 of these sites as hazardous (Ratnam *et al.*, 1996). Additionally, there have been more than 300,000 releases from underground storage tanks reported by state and local environmental agencies (Phillips, 1995). Contamination may result from single sources impacting relatively small areas up to multiple sources constituting a problem of regional dimensions (Fusillo *et al.*, 1985; USEPA, 1985). Regardless of the extent of the contamination, the removal of chemical substances from the subsurface is complicated by many factors.

Many contaminants exist in the subsurface as virtually immiscible or nonaqueous phase liquids (NAPLs). The term immiscible is used to describe fluids exhibiting significant capillary pressures resulting from interfacial surface tension (Knox and Sabatini, 1992). As NAPLs migrate through a porous formation, they flow vertically and horizontally under the influence of capillary, viscous, and buoyancy forces (Sleep and Sykes, 1993). During migration, a portion of the NAPL is retained within the pores of the soil matrix as immobile ganglia due to the action of capillary forces. This volume of NAPL may occupy between 5 and 40 percent of the pore volume (Hunt *et al.*, 1988; Schwille, 1984; Wilson and Conrad, 1984) and is commonly referred to as residual saturation. Since the entrapped residual is typically immobile and retained in the subsurface for indefinite time periods, it is often considered a long-term source of groundwater contamination. Despite their limited aqueous solubility, NAPL groundwater concentrations of many chemical substances are often one to two orders of magnitude greater than their Maximum Contaminant Levels (MCLs) promulgated under the Safe Drinking Water Act (Kueper and Frind, 1991; Geller and Hunt, 1993; Oolman *et al.*, 1995).

Throughout the 1970s and 1980s, attempts at remediating groundwater contamination in the United States relied heavily upon "pump-and-treat" systems. These systems are used at nearly 75 percent of the Superfund sites where groundwater is contaminated and at most sites governed by either the Resource Conservation and Recovery Act (RCRA) or state laws (MacDonald and Kavanaugh, 1994). By the late 1980s and early 1990s, most of these remediation projects were considered unsuccessful. The limitations of pump-and-treat methods are attributed to (1) the low aqueous solubility of most NAPLs which results in extremely low concentrations of contaminants that require large volumes of water to be treated and (2) the relatively large interfacial tension between water and NAPLs which results in large capillary forces that act to immobilize the NAPL (Fountain, 1992).

It is now generally recognized that conventional pump-and-treat methods are an ineffective, time-consuming, and costly means of remediating groundwater contamination (Knox *et al.*, 1986; Mackay and Cherry, 1989; Haley *et al.*, 1991; Pennell *et al.*, 1993, MacDonald and Kavanaugh, 1994). However, researchers have demonstrated during the past decade that the efficiency of pump-and-treat methods can be improved by using surfactants (e.g., Nash, 1987; Harwell, 1992; West and Harwell, 1992; Kueper *et al.*; 1993; Fountain *et al.*, 1995; Pennell *et al.*, 1996; Knox *et al.*, 1997). The use of surfactants in remediation efforts is based on their ability to increase the aqueous solubility of NAPLs and to displace entrapped ganglia (Pennell *et al.*, 1996). The fundamentals of surfactant performance were developed from earlier research on their use for enhanced oil recovery (Pope and Wade, 1995).

Regardless of the method, NAPL zones must be properly characterized for any remediation effort to be effective (Mackay and Cherry, 1989). Locating and characterizing these zones is a difficult problem that has traditionally been approached using inefficient techniques such as soil coring, cone penetrometers, or geophysical logging (James *et al.*, 1997). The inefficiencies associated with these techniques have resulted in a trend toward fewer and less time-consuming site characterization requirements. While such a streamlined approach may be adequate if the remediation goal is to simply prevent migration, detailed site characterization is a prerequisite for successful cleanup efforts (Mackay and Cherry, 1989).

In the last few years, the use of partitioning tracers has been proposed as an effective method for characterizing NAPL zones. Although tracers have been extensively used in petroleum reservoir characterization for almost 30 years, their use in NAPL characterization applications is in its infancy. As discussed by Jin (1995), the partitioning interwell tracer test (PITT) technique can be used very effectively for the detection and estimation of nonaqueous phase liquids in the subsurface, as well as for the performance assessment of remediation efforts.

The PITT technique assumes a constant NAPL composition and, therefore, a constant NAPL-water partition coefficient for the tracer throughout the remediation process. However, as surfactant enhanced remediation of a NAPL proceeds through either solubilization or mobilization, the composition of the NAPL can be expected to change. A review of the literature did not reveal any attempts to qualitatively or quantitatively explain the impact of changing composition on the partition coefficient for tracer studies conducted in conjunction with surfactant enhanced remediation of subsurface contamination.

There have been recent attempts in the physical chemistry literature to explain the partitioning of solutes in liquid-liquid systems with multi-parameter linear free-energy models (Kamlet *et al.*, 1982; Rutan *et al.*, 1989; Marcus, 1991), quantitative structure-activity relationship (QSAR) techniques (Nirmalakhandan and Speece, 1989), and group-contribution models (Wang *et al.*, 1998). Although useful from a physical chemistry perspective, these models involve many variables and would be difficult to use in the field as a screening tool. A more practical tool for field use, based upon the equivalent alkane carbon number (EACN) concept and reported by Dwarakanath and Pope (1998), will be explored in this research.

1.2 Objectives and Hypotheses

Part of this research focuses on the use of partitioning and non-partitioning tracers to determine residual NAPL saturation levels in conjunction with surfactant-enhanced remediation of subsurface contamination. The primary objective of this research is to determine if a relationship exists between the mole fraction of individual components comprising a NAPL, the type of alcohol tracer, and the tracer partition coefficient. The EACN approach will be the basis of determining whether such a relationship exists. After validating the EACN concept through phase behavior studies (i.e., salinity scans) and determining the partition coefficient of several alcohol tracers with a number of neat compounds and mixtures, a column study will be conducted to assess the manner in which NAPL composition changes during the remediation process. Field data from Hill AFB will also be reviewed to investigate the effect of surfactant on NAPL composition. At each point that observations are made regarding NAPL composition, the partition coefficient correlation determined through this research can be used to assess the variability of the partition coefficient. The secondary objective of this research is to demonstrate the advantages of the UTCHEM simulator in developing effective design strategies for tracer tests and surfactant flooding processes. This will be demonstrated by simulating tracer tests and surfactant floods from both laboratory and pilot-scale field tests.

In association with the above objectives, the following hypotheses will be investigated during the course of this research.

1. There is a linear relationship between the NAPL equivalent alkane carbon number (EACN) and the logarithm of the optimal salinity (on a weight percentage basis).

2. There is a linear relationship between alcohol tracer partition coefficients and the equivalent alkane carbon number of the alcohol and the NAPL.

3. The partitioning of tracers is rate limited and can impact residual saturation calculations.

4. UTCHEM will adequately model the partitioning interwell tracer tests as well as the surfactant remediation processes.

1.3 Review of Chapters

Chapter 2 provides a brief literature review of topics relevant to this research. Besides describing the general principals of NAPL migration and distribution, it also describes the difficulties of conventional pump-and-treat efforts and the advantages of surfactant enhanced remediation. Chapter 3 introduces the equivalent alkane carbon number (EACN) concept and presents the results of phase behavior studies that were conducted to confirm the linear relationship between EACNs and the natural logarithm of optimal salinities. Chapter 4 focuses on the relationship between tracer partition coefficients and NAPL composition under static (i.e., equilibrium) conditions. The development of an estimation technique for partition coefficients based on the EACN concept is also provided. Chapter 5 presents the results of a column study used to analyze the variable nature of NAPL composition during surfactant enhanced remediation efforts. Chapter 6 describes simulations conducted with UTCHEM and compares the results with the data gathered during laboratory column studies. Chapter 7 compares simulation results with data collected from a test cell as part of a treatability study. Finally, Chapter 8 summarizes the conclusions determined from this research and offers potential topics for future research.

CHAPTER 2

LITERATURE REVIEW

To establish a foundation upon which to build, a literature review was conducted to gather information relative to this research. Areas to be covered in this chapter include nonaqueous phase liquid (NAPL) migration, subsurface distribution, and remediation efforts; chromatographic theory and the use of tracers to locate and quantify subsurface contamination; surfactant fundamentals; and efforts to model multiphase flow in porous media.

2.1 NAPL Migration and Distribution

2.1.1 NAPL Migration

NAPL migration in porous media is affected by a combination of forces. While gravity and viscous forces are important, the predominant force impacting NAPL movement is that provided by capillary action. The extent of capillary forces depends upon the NAPL-water interfacial tension, wettability of the fluids to the soil (contact angle), and geometry of the pore spaces in the soil matrix (Mace and Wilson, 1992). Other factors include the (1) NAPL release volume, (2) infiltration surface area, (3) release duration, (4) NAPL properties, (5) subsurface media properties, and (6) underlying subsurface flow conditions (Feenstra and Cherry, 1988).

After a release has occurred, NAPL migration in the subsurface system is a complex process. Initially, the NAPL enters the vadose zone as a discrete liquid phase and migrates downward as a result of gravitational forces. The rate of downward migration is a function of the porosity and relative permeability of the soil, as well as the density and viscosity of the contaminant (Lesage and Brown, 1994). As the contaminant moves downward, some degree of lateral spreading occurs due to the effect of capillary forces (Schwille, 1988) and the spatial variability (e.g., layering) of the subsurface media (Mercer and Cohen, 1990). Some of the contaminant also volatilizes in the vadose zone and causes a vapor plume to develop.

As a NAPL continues to migrate downward, a residual amount becomes trapped in pore spaces of the soil matrix due to capillary effects. The degree of saturation at a particular point can be defined as the fraction of pore space occupied by NAPL within a representative elementary volume around the point of interest (Bear, 1972). Similar to porosity, saturation can thus be conceptualized as a point property that varies in space (Corey, 1986).

If a NAPL release is sufficiently large, it eventually reaches the water table. A contaminant less dense than water, termed a light nonaqueous phase liquid (LNAPL), tends to spread laterally along the capillary fringe (i.e., "float") where it may depress natural groundwater levels and form a lens of free product. However, water table fluctuations due to severe rain events or seasonal variations can cause vertical displacement of the free product and its subsequent redistribution (Schwille, 1967, 1988; McKee *et al.*, 1972; Pennell *et al.*, 1993). Infiltrating rainwater, water table fluctuations, and the contact area between the LNAPL and the aqueous phase cause soluble components of the NAPL to dissolve into the groundwater, resulting in a contaminant plume extending in the direction of the hydraulic gradient. The precise distribution depends on the type of LNAPL (e.g., specific gravity, viscosity, surface tension), air pressures, and the pore size distribution (Mercer and Cohen, 1990).

If a contaminant more dense than water, termed a dense nonaqueous phase liquid (DNAPL), reaches the water table in sufficient volume to overcome capillary entry pressures, it continues to migrate vertically (i.e., "sink") through the saturated zone and displaces aquifer pore water (Schwille, 1988; Mackay *et al*, 1985). During this downward migration, a DNAPL undergoes preferential spreading as it encounters more permeable layers, fractures, and other pathways providing less capillary resistance than the underlying media (Mercer and Cohen, 1990). Regions of water-saturated media are subsequently bypassed by the flowing DNAPL and a portion of the DNAPL may become separated from the bulk flow as a result of interfacial instabilities and heterogeneities (Kueper and Frind, 1988) in a process commonly referred to as "fingering." Migration of the bulk organic phase eventually ceases when all of the fluid has become trapped as discontinuous blobs, or when the NAPL encounters a low permeability stratum (Kueper *et al.*, 1989) and has insufficient pressure to force the nonwetting NAPL into the small pores of this layer (Powers *et al.*, 1991). Provided there is sufficient volume, the DNAPL migrates downward until it reaches an impermeable barrier; at this point, it essentially remains in place or continues to flow under pressure and gravity forces.

As a NAPL migrates through a porous formation, interfacial forces act to retain a residual portion of it within soil pores as immobile ganglia (also referred to as blobs and globules) in both the unsaturated and saturated zones (Powers *et al.*, 1991; Pennell *et al.*, 1993). This volume of NAPL is commonly referred to as residual saturation and may occupy between 5 and 40 percent of the pore volume (Hunt *et al.*, 1988; Schwille, 1988; Wilson and Conrad, 1984). Mercer and Cohen (1990) found that residual saturation levels for DNAPLs typically ranged from 1 to 25 percent of the pore volume. Research by Hunt *et al.* (1988) shows that trapped residual segments of organic liquid are immobile under typical hydraulic conditions.

Residual NAPL in the subsurface presents a potential long-term source of contamination. In the vadose zone, entrapped organic chemicals can solubilize into infiltrating rainwater or volatilize and be transported by either diffusion or convection (Schwille, 1988; Hinchee and Reisinger, 1987; Cohen and Ryan, 1985). Infiltrating rainwater may dissolve organic vapors and transport contaminants to the saturated region (Mercer and Cohen, 1990). In the saturated zone, NAPL can partition directly into the aqueous phase (Schwille, 1988; Mackay *et al.*, 1985). The overall extent and persistence of residual NAPLs will be a function of the respective volatilization and solubilization rates (Pennell *et al.*, 1993). For NAPL pools formed at the water table surface or along impermeable boundaries, dissolution will result in much lower aqueous concentrations than those resulting from the dissolution of residual NAPL zones (Schwille, 1988). An additional contaminant source is thus provided with a life expectancy greater than residual NAPL (Kueper and Frind, 1991).

2.1.2 NAPL Distribution

More insight into subsurface NAPL distribution can be gained by examining displacement mechanisms at the pore level. In addition to capillary effects, NAPLs can become trapped in saturated, water-wet porous media through snap-off and by-passing (Chatzis *et al.*, 1983; Wilson and Conrad, 1984; Wilson *et al.*, 1990). These mechanisms are illustrated in Figure 2.1.

During snap-off, a wetting fluid (water) enters a pore body and displaces a non-wetting fluid (NAPL) as it preferentially flows along the pore walls. Depending on pore geometry and soil wettability, the wetting fluid may reach the pore throat before the non-wetting fluid is completely displaced and cause a portion of it to "snap-off" in the pore body. If the pore aspect ratio (ratio between diameter of pore body to pore throat) is small, complete displacement of the non-wetting fluid may occur (Mace and Wilson, 1992). If the pore aspect ratio is large, the non-wetting phase will tend to snap-off and become trapped. Therefore, the snap-off mechanism is more common in well-sorted, unconsolidated sands (Powers *et al.*, 1991).

By-passing occurs when a wetting fluid preferentially displaces a non-wetting fluid within the pore body due to differences in capillary forces caused by pore geometries (Mace and Wilson, 1992). Larger blobs of a non-wetting fluid are by-passed in areas where several large pore bodies are well connected (i.e., high pore aspect ratios) and isolated from other pores by smaller pore aspect ratios (Powers *et al.*, 1991). In heterogeneous soils, it is not uncommon for large pockets of organic contaminant to be by-passed in coarse lenses (Wilson *et al.*, 1990).

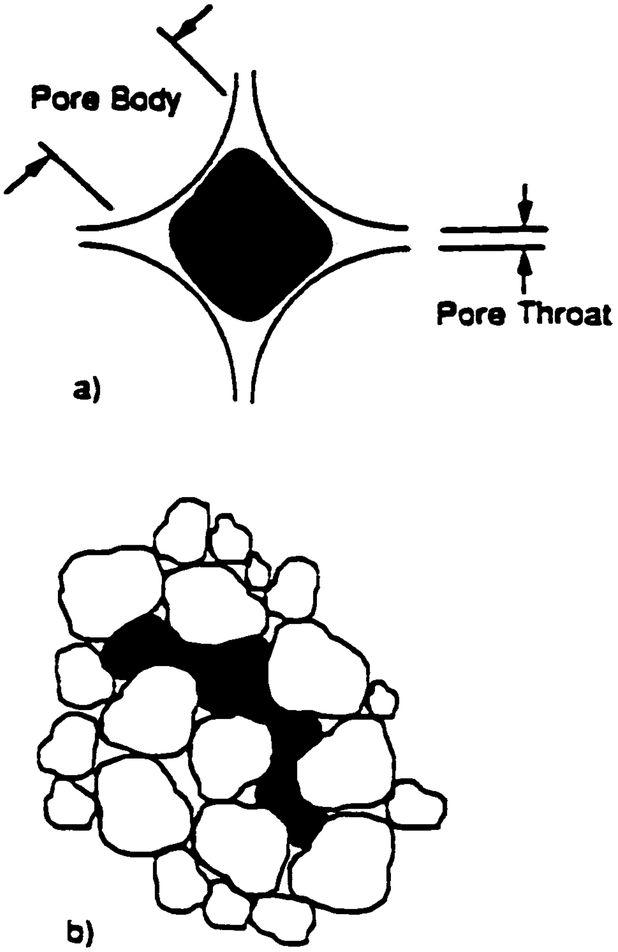

Figure 2.1 NAPL Entrapment Mechanisms: a) Snap-off and b) By-passing (Powers *et al.*, 1991)

The form and structure of NAPL blobs in the subsurface depend upon the properties of the porous medium (e.g., permeability, pore space geometry, and pore size distribution) with blob sizes ranging over several orders of magnitude. The viscous forces required to remove residual saturation are related to blob length. Similarly, blob volume and surface area affect the rate of NAPL dissolution into the aqueous phase and thus the fate and transport properties of subsurface contaminants (Mayer and Miller, 1992). However, little research has been performed to determine relationships among blob size characteristics, porous medium characteristics, and meaningful macroscopic aquifer parameters.

Waterflooding investigations have shown that residual NAPL saturation in porous media is strongly dependent upon the interfacial tension between immiscible liquids, the wettability of solids with respect to immiscible liquids (i.e., the contact angle), and the pore-water velocity (Dawson and Roberts, 1997). It has long been recognized that immiscible displacement of NAPLs through waterflooding is controlled by two dimensionless groups, the Capillary Number and the Bond Number (Foster, 1973). The Capillary Number (N_C) is defined as the ratio of viscous to capillary forces, while the Bond Number (N_B) is defined as the ratio of gravitational to capillary forces (Perry and Chilton, 1973). Capillary forces promote trapping while the viscous and/or buoyancy forces discourage trapping. The equations for these dimensionless groups are given as (Morrow and Songkran, 1981; Ng et al., 1978):

$$N_C = \frac{u\mu}{\sigma} \tag{2.1}$$

$$N_C = \frac{\Delta \rho g k k_w}{\sigma} \tag{2.2}$$

where u is the displacing fluid velocity, μ is the displacing fluid viscosity, σ is the interfacial tension, $\Delta\rho$ is the fluid density contrast, g is the acceleration force due to gravity, k is the intrinsic permeability, and k_W is the relative permeability to water.

The Capillary Number has been used extensively in the petroleum literature to determine the residual saturation of oil (Stegemeier, 1976; Foster, 1973). Since it relates viscous forces associated with groundwater flow to interfacial forces between the aqueous and NAPL phases, it can also be used to qualitatively assess residual NAPL saturations (Powers *et al.*, 1991). However, experiments have shown that residual NAPL saturation is independent of the Capillary Number during most horizontal waterfloods (Dawson and Roberts, 1997). In fact, Lake (1989) reported that Capillary Numbers greater than about 10^{-5} can only be attained through the use of chemicals which act to lower the interfacial tension between NAPL and water.

The importance of the Bond Number remained unrecognized until the use of surfactants increased (Ratman *et al.*, 1996). Since surfactants cause greater fluid density contrasts, the influence of buoyancy properties on entrapment mechanisms became more pronounced and identifiable. In contrast to the numerous studies involving Capillary Numbers, there have been relatively few studies investigating the relationship between buoyancy forces and NAPL saturations (Dawson and Roberts, 1997). A few researchers have shown that NAPL saturation is inversely correlated with the Bond Number (Morrow and Songkran, 1981; Morrow *et al*, 1988).

Morrow and Songkran (1981) reported that the effects of viscous and gravitational forces could be superimposed and derived an empirical linear combination of the Capillary and Bond Numbers that correlated well with NAPL saturations. More recently, one-dimensional and two-dimensional trapping numbers have been developed to show the combined effects of viscous and gravity forces (Pennell *et al.*, 1996). Additionally, Jin (1995) described the theoretical development of a three-dimensional trapping number that combines the effects of buoyancy and viscous forces on the mobilization of trapped NAPLs.

2.1.3 NAPL Dissolution

The literature is abundant with conflicting examples comparing aqueous concentrations with aqueous solubilities. In laboratory experiments, various researchers have shown that concentrations approximately equal to aqueous solubility are obtained in water flowing at 10 to 100 cm/day through NAPL-contaminated sands (e.g., Anderson, 1988; Schwille, 1988). However, the literature also reports many cases in which organic compounds are commonly found in groundwater at concentrations less than 10 percent of their solubility limits (e.g., Mackay *et al.*, 1985; Pennell *et al.*, 1993). Other researchers have reported similar results indicating that solute concentrations are typically lower than their corresponding equilibrium values (Feenstra and Coburn, 1986; Mercer and Cohen, 1990). Additionally, Cherry *et al.* (1990) observed that the rate of removal of organic species decreased substantially over time during waterflooding experiments. From the research available, it is reasonable to expect nonequilibrium mass transfer rates to influence contaminant concentrations most often in situations involving small (areal extent) spills, high Darcy velocities, large blob sizes (i.e., in well-graded or heterogeneous aquifers), and low residual saturation (Powers *et al.*, 1991).

Four hypotheses have been suggested to explain these discrepancies: (1) rate limited mass transfer between phases, (2) physical by-passing of the aqueous phase around contaminated regions due to lower permeabilities, (3) non-uniform flow caused by aquifer heterogeneities, and (4) the effect of NAPL composition on equilibrium solubility values (Feenstra and Coburn, 1986; Mackay and Cherry, 1989; Feenstra, 1990). Regardless of which hypothesis is more strongly supported, it is clear that a better understanding of the complex mechanisms governing multiphase flow and NAPL dissolution is needed before effective remediation efforts can be implemented (Mercer and Cohen, 1990; Bedient, 1991).

Early multiphase flow models used the "local equilibrium assumption" to describe the partitioning between NAPLs and the aqueous phase (Powers *et al.*, 1991). This implies that the concentration of a contaminant in a particular phase can be described by equilibrium partitioning relationships if the concentration in another phase at the same spatial location is known (Abriola and Pinder, 1985a). However, the examples cited in the previous paragraph indicate that this is not always true.

In fact, the Damkohler number has been the most widely used criterion for identifying conditions under which the local equilibrium assumption is valid for mass transfer processes (Brusseau, 1992). The Damkohler number (ω) represents the ratio of hydrodynamic residence time to characteristic time of reaction,

$$\omega = \frac{\alpha l}{q} \tag{2.3}$$

where α is the first-order mass transfer constant, l is the length of the system, and q is the Darcy velocity (Brusseau, 1992). The Damkohler number also quantifies the relationship between the degree of nonequilibrium and pore-water velocity. Brusseau (1992) reports that the local equilibrium assumption is valid only when the Damkohler number is greater than about 100 and that mass transfer is significantly rate limited when the Damkohler number is less than about 10.

Mass transfer between phases involves several steps: (1) diffusion and convection through the bulk phase of one fluid toward the interface between the two phases; (2) accumulation, adsorption/ desorption, convection, diffusion, or chemical reaction at the interface; and (3) diffusion and convection away from the interface into the bulk phase of the second liquid (Giavedoni and Deiber, 1986). The rate of mass transfer is a function of aqueous solubility of the NAPL components, aqueous phase velocity, contact area between the aqueous and NAPL phases, and the molecular diffusivity of the NAPL components in water (Pfannkuch, 1984; Anderson, 1988; Feenstra and Cherry, 1988; Hunt *et al.*, 1988; Schwille, 1988). Numerous studies have indicated that mass transfer between NAPL and water phases is rate limited (e.g., Powers *et al.*, 1992; Geller and Hunt, 1993; Powers *et al.*, 1994). After all, the net flux of a chemical species across an interface between two phases (i.e., the mass transfer rate) is caused by differences in the temporal and equilibrium concentrations (more appropriately chemical potentials) of that species in the respective phases (Powers *et al.*, 1991). Some researchers have suggested three distinct phases to the dissolution process: (1) an initial period in which effluent concentrations are observed at, or nearly at, solubility limits, (2) a transition period in which there is a rapid drop in effluent concentrations, and (3) a longer period of time in which effluent concentrations are virtually steady at levels less than 0.01 percent of solubility (Lamarche, 1991; Borden and Kao, 1992; Reynolds, 1995; Reynolds *et al.*, 1996).

A common concept implicit in many mass transfer theories is that the rate of mass transfer between any two phases is a function of a driving force and the interfacial contact area (Miller *et al.*, 1990). This mass transfer relationship is commonly represented as,

$$J = k_l (C_S - C) \tag{2.4}$$

where J is the solute mass flux from the immiscible liquid phase to the aqueous phase, k_l is the mass transfer coefficient, C_S is the equilibrium aqueous concentration at the interface, and C is the aqueous phase solute concentration. The total rate of mass transfer of the organic from the NAPL to the aqueous phase is the product of the mass flux and the specific interfacial area between the phases. Thus, the aspect of residual saturation most important to the mass transfer process is the shape and size distribution of the NAPL blobs.

Ideally, a complete description of the mass transfer process requires accurate measurement of the interfacial area of the NAPL blobs. Due to the heterogeneous nature of the subsurface though, it is extremely difficult to quantify the contact area between the phases, either experimentally or mathematically (Pfannkuch, 1984). As previously mentioned, blob shape and size are a function of pore geometry and cause NAPL ganglia to take on a variety of complex shapes and a wide distribution of sizes (Wilson *et al.*, 1990). This wide diversity in entrapped blobs indicates the inadequacies of trying to characterize all blobs with a single geometric shape (Powers *et al.*, 1992). Conrad *et al.* (1992) reached a similar conclusion when they proposed the use of an "effective" sphere diameter for multiple-pore space blobs. An additional difficulty arises from the fact that interfacial area will decrease throughout the dissolution process.

A change in NAPL composition during the remediation process will also affect the driving force and cause difficulties in quantifying the contact area between phases. Several researchers have reported preferential leaching of various species from a mixed NAPL in accordance with Raoult's law (Razakarisoa *et al.*, 1989; Geller and Hunt, 1993). As more soluble compounds are transferred, NAPL composition will change and cause a decrease in the driving force. Another problem is the difficulty in estimating the curvature of the NAPL-aqueous phase interface since it is dependent upon the NAPL and water pressures and saturations, interfacial tension, pore geometry, and the chemical and physical properties of the solid surface (Rose and Bruce, 1949). Still another problem is the accessibility of the interphase area to the flowing aqueous phase caused by NAPL blobs exhibiting "neck" and "head" menisci (Mohanty *et al.*, 1987). It is interesting to note that the contact area of a given mass of residual NAPL ganglia is much greater than that of an equivalent mass of pooled NAPL. This explains why dissolution of residual NAPL results in higher NAPL concentrations in the groundwater and depletes the source more quickly than the dissolution of a NAPL pool of equivalent mass (Mercer and Cohen, 1990).

2.1.4 NAPL Remediation

Initial attempts at remediating the subsurface environment relied heavily on the pump-and-treat method. In fact, it was highly touted as the panacea for most contaminated sites. However, the low aqueous solubilities of most NAPLs and the mass transfer considerations discussed above result in very low groundwater contaminant concentrations that will require large volumes of water to be treated (Mackay and Cherry, 1989; Mercer and Cohen, 1990). Additionally, relatively large interfacial tensions between NAPL and water result in large capillary forces that act to immobilize the majority of the NAPL (Wilson and Conrad, 1984) and prevent displacement of residual NAPL blobs at realistic pumping rates (Pennell *et al.*, 1994).

General limitations of pump-and-treat include geological conditions limiting groundwater flow: low permeability lenses, hydrodynamically isolated "dead spots," water table fluctuations, and hydraulic conductivities less than about 10^{-3} cm/sec (Fountain *et al.*, 1995). Other factors limiting pump-and-treat efforts include desorption of contaminants from media surfaces and dissolution of entrapped NAPLs

(Keely, 1989; Haley *et al.*, 1991). It is now generally recognized that remediation technologies relying on conventional pump-and-treat methods are an ineffective, time-consuming, and costly means of restoration for NAPL contaminants (Knox *et al.*, 1986; MacDonald and Kavanaugh, 1994; Pennell *et al.*, 1993; Mackay and Cherry, 1989; Haley *et al.*, 1991). Most researchers agree that pump-and-treat should be used only for containment purposes to prevent migration of the dissolved contaminants (e.g., Haley *et al.*, 1991; Cherry *et al.*, 1992).

Numerous researchers have shown that the efficiency of pump-and-treat methods can be improved through the use of surfactants (Nash, 1987; Fountain *et al.*, 1995; West and Harwell, 1992; Fountain, 1992; Harwell, 1992; Kueper *et al.*, 1993; Pennell *et al.*, 1993; Pennell *et al.*, 1996). In fact, it was over 40 years ago that surfactant-based technologies were initially recognized for their abilities to enhance the recovery of NAPLs from subsurface environments (Schwille, 1975). The concept of using surfactants to improve pump-and-treat systems is based on the ability of surfactants to increase the aqueous solubility of NAPLs and displace entrapped NAPL ganglia (Pennell *et al.*, 1996). Despite many successes though, mixed results have demonstrated that surfactants are not applicable in all situations (TRI, 1985; Nash, 1987; Ziegenfuss, 1987; Ang and Abdul, 1991; Pennell *et al.*, 1993). A more detailed discussion of the use of surfactants to remediate subsurface contamination can be found in a later section of this chapter.

The amount, distribution, and aerial extent of residual NAPL in the subsurface are significant factors in deciding whether remedial action is appropriate and, if so, what type of technology is the most cost effective. However, locating and characterizing these sources is a difficult problem that is often compounded by complex subsurface heterogeneities that cause complicated and widespread distributions of NAPL (Kueper *et al.*, 1989; Poulsen and Kueper, 1992). The literature contains numerous articles in which authors state that very little success has been achieved in locating subsurface NAPL sources (Mackay and Cherry, 1989; National Research Council, 1994).

The reason for this lack of success is the statistical sampling approach and inefficient techniques that are often taken in terms of (1) conventional core analysis, (2) cone penetrometer testing, and (3) geophysical logging (James *et al.*, 1997). As each of these methods provides information at discrete points, the probability of the test method actually encountering a NAPL zone is quite small (Nelson and Brusseau, 1996). There is compelling evidence that a much larger sample volume is necessary to adequately characterize the subsurface (Mayer and Miller, 1995). A method to detect and quantify subsurface NAPLs that has received increasing attention over the last few years is through the use of tracers having different magnitudes of organic phase partitioning (Jin *et al.*, 1995). The advantage of tracer tests is that they allow the testing of large zones of aquifers by transmitting partitioning tracers between separate injection and extraction wells (Jin *et al.*, 1997).

2.2 Tracers and Chromatographic Theory

For the use of partitioning tracers to be most effective, it would be helpful if a correlation concerning the distribution of a tracer between water and organic solvents existed. With such a correlation, it would be much easier to describe the partitioning process itself. It would also allow for the estimation of partition coefficients and the use of the correlation as a screening tool during preliminary planning stages. The literature provides examples of various types of correlations that have been explored.

Kamlet *et al.* (1988) found that many solute-solvent properties are well correlated by equations that include linear combinations of dependences on up to five solute parameters. With a database of 245 solutes, they reported the linear solvation energy relationship (LSER) for octanol/water partition coefficients as,

$$\log K_{ow} = 0.35 + 5.35V_I/100 - 1.04(\pi^* - 0.35\delta) - 3.84\beta_m + 0.10\alpha_m, \qquad (2.5)$$

where K_{ow} is the octanol/water partition coefficient, V_I is the intrinsic volume, π^* is the solvatochromic polarity parameter, δ is a polarizability correction factor, β_m is the hydrogen bonding acceptance ability, and α_m is the hydrogen bonding donation ability. The coefficient of determination (R^2 value) for this equation was 0.9959. The difficulty in using a relationship such as this is the fact that π^* is a mixture of polarity and polarizability. Determining its value for each functional group is as difficult and time-consuming as measuring the partition coefficient (Hansch and Fujita, 1995).

Nirmalakhandan and Speece (1989) applied quantitative structure-activity relationship (QSAR) techniques to develop a model for aqueous solubility. The

QSAR method uses molecular connectivity indexes and a polarizability parameter that are both calculated strictly from the molecular structure of the solute. The resulting model from their research ($R^2 = 0.941$) was,

$$\log S = 1.506 + 1.750\,{}^0\chi - 1.469\,{}^0\chi^v + 1.01\Phi \tag{2.6}$$

where S is the aqueous solubility, ${}^0\chi$ and ${}^0\chi^v$ are valence molecular connectivity indexes, and Φ is a polarizability parameter.

There have also been a number of articles in the literature related to UNIFAC, a group-contribution activity-coefficient model. The theory behind the UNIFAC method is that a compound can be structurally decomposed into functional groups, with each functional group having a unique contribution toward the activity coefficient of the compound (Kan and Tomson, 1996). Furthermore, despite the large number of compounds that exist, the number of functional groups is relatively small. Wang *et al.* (1998) used the UNIFAC model to estimate the partition coefficients of alcohol tracers between water and a NAPL using the formula,

$$K_i = (\gamma_i^A M^A \rho^N) / (\gamma_i^N M^N \rho^A) \tag{2.7}$$

where K_i is the partition coefficient for chemical component i, M is the molecular weight, ρ is the density (g/cm^3), and γ_i is the activity coefficients for component i, with the superscripts N and A representing NAPL and aqueous phases, respectively. During their research, they found a linear relationship between the logarithm of tracer partition coefficients and the logarithm of tracer aqueous solubility.

The above discussions serve to illustrate the point that different methodologies have been used to identify relationships involving partition coefficients and solubility. However, these methods are somewhat complex and require extensive knowledge of physical chemistry principles. An easier method, which allows estimation of partition coefficients, is presented in this research and involves partitioning tracers, chromatographic theory, and the equivalent alkane carbon number (EACN) concept.

2.2.1 Tracer Fundamentals

Tracers are chemicals or radioactive materials with properties such that they can be added to fluids in small concentrations without affecting any of the intrinsic properties of the fluid. Since they are injected into the subsurface, tracers must be non-toxic to avoid potentially adverse impacts on human health or the environment. For mass balance analysis to be effective, tracers should not absorb to soil particles or break down in the chemical and biological environment of the subsurface. Tracers must also be easily detectable and quantifiable in minute concentrations; therefore, the chemicals used as tracers should occur at very low background concentrations.

Hydrogeologists routinely study the movement of tracers in the subsurface to determine the flow rate and direction of groundwater. Tracer breakthrough curves can also help define the following hydrogeologic parameters: hydraulic conductivity, porosity, flux, hydrodynamic dispersion, and retardation. In the petroleum industry, various types of tracers have been used in reservoir floods to determine interwell flow characteristics such as reservoir heterogeneity and dispersion characteristics, flow barriers, preferential flow paths, and sweep efficiencies (Agca *et al.*, 1990).

Tracers that are soluble in both the water phase and the oil phase in the subsurface are called partitioning tracers (Lichtenberger, 1991). Partitioning tracers have been used in the oil industry since the 1970s to determine residual oil saturations using chromatographic separation theory (Sheely and Baldwin, 1982; Tang and Harker, 1991; Tang, 1995). More recently, they have also been used in the environmental arena to measure NAPL residual saturations (Jin *et al.*, 1995; Wilson and Mackay, 1995; Nelson and Brusseau, 1996).

2.2.2 Chromatographic Theory

Chromatography, an analytical technique used to separate and identify components of complex chemical mixtures, relies on the differential affinities of a substance for mobile and stationary mediums. Similarly, the use of tracers to determine residual NAPL levels relies on chromatographic separation (or retardation) of a tracer. Four mechanisms are associated with chromatographic separation of tracers in porous media: (1) fluid partitioning, (2) adsorption, (3) ion exchange, and (4) size exclusion (Tang, 1995). The most common mechanism used by industry for in situ measurements of fluid saturations is fluid partitioning (Tang, 1995). This is accomplished by comparing the transit time for a nonpartitioning (conservative) tracer, which is only soluble in an injected fluid phase such as water, with the transit time of a partitioning (nonconservative) tracer that is soluble in both water and oil.

While conservative tracers are unaffected by NAPL presence, nonconservative tracers are retarded because of their partitioning behavior into and from NAPL. Driven by the tracer concentration gradient, tracer molecules diffuse from the aqueous phase into the residual (immobile) oil phase. At some point, the concentration gradient is reversed and tracer molecules diffuse from the oil phase back into the aqueous phase. The transport time of a partitioning tracer is thus retarded with respect to that of a nonpartitioning tracer; its frontal advance rate will be less than that of the injection fluid velocity. This chromatographic separation provides the basis for the determination of residual saturation levels (Cooke, 1971).

Two types of tracer tests have been widely performed. The single well tracer test (SWTT), developed by Exxon in 1971 (Chang *et al.*, 1988), has been used in over 300 oil field reservoirs (Jin, 1995). Often referred to as a backflow tracer test, the SWTT involves the injection and extraction of a primary partitioning tracer and a non-partitioning tracer through the same well (Tang, 1995). During a shut-in period of 3-20 days, the partitioning tracer undergoes hydrolysis to generate a non-partitioning secondary tracer. Used primarily in the oil industry, the SWTT measures average oil saturation in the portion of the reservoir contacted by the injected water. The large depth of investigation and control over the depth are unique properties that enhance the usefulness of the SWTT (Sheely and Baldwin, 1982). The accuracy of the SWTT (2-3 percent PV) has been confirmed through laboratory results and mathematical models. However, the efficiency is affected by the permeability distribution (sweep efficiency) of the injected tracer (Chang *et al.*, 1988).

Cooke (1971) developed the interwell tracer test to expand the coverage area of the SWTT and measure the residual oil saturation between wells. The test is conducted at steady state to ensure a consistent streamline distribution. However, a lack of suitable chemicals and interpretation techniques hindered further development of the method. Tang (1991) provided the first systematic approach to the study of tracers used in interwell tracer tests. The benefits of an interwell tracer test over an SWTT are: (1) residual oil saturation can be determined directly at any point on the tracer profile, (2) drift and heterogeneity effects are less significant, (3) greater depth of investigation, and (4) it is easier to design, operate, and interpret (Tang, 1991).

In Cooke's original method, the residual oil saturation was determined by comparing the breakthrough times of a partitioning and nonpartitioning tracer. However, a comparison involving the full profile is more appropriate since breakthrough times can be affected by dispersion, the tracer detection limit, and streamline and layer distributions (Tang, 1995). In this process, simulators or models are used to match the partitioning and nonpartitioning tracer profiles. This is obviously very time consuming and requires a large number of input parameters.

To simplify the process, Tang (1995) proposed a chromatographic transformation theory that used the relative separation of the respective tracer profiles to calculate the residual oil saturation. According to this theory, the ratio of the production (i.e., arrival) times for the partitioning and nonpartitioning tracers at the same normalized concentration will result in the retardation factor of $1 + \beta$. In other words, if the following equation is satisfied,

$$\frac{C_p(\tau)}{C_{p,\max}}=\frac{C_n(t)}{C_{n,\max}} \tag{2.8}$$

then the following equation is true,

$$\tau=t(1+\beta) \tag{2.9}$$

where $C_n(t)$ and $C_{n,\max}$ are the non-partitioning tracer concentrations at time t and at the peak, $C_p(\tau)$ and $C_{p,\max}$ are the partitioning tracer concentrations at time τ and at the peak, and t and τ are the production times for the non-partitioning and partitioning tracers. From the retardation factor of $1 + \beta$, the residual saturation can be determined from,

$$1+\beta=1+\frac{KS}{1-S} \tag{2.10}$$

where K is the tracer partition coefficient and S is the residual saturation.

In an unrelated effort, Jin (1995) described the development of the partitioning interwell tracer test (PITT) technique. The purposes of the PITT are to (1) detect and locate subsurface NAPLs, (2) estimate the NAPL volume, (3) provide a mechanism to evaluate the performance of remedial efforts, and (4) determine the spatial distribution of the NAPL (Jin *et al.*, 1995; Jin *et al.*, 1997). The technique consists of the simultaneous injection of tracers with different partition coefficients at one or more injection wells and the subsequent measurement of tracer concentrations at one or more production or monitoring wells. The flow of tracers with higher partition coefficients is retarded to a greater degree. The separation of the tracer profiles, a function of both the amount of NAPL present in the swept zone and the partition coefficient, is determined by the amount of time the tracer spends in the NAPL phase compared to the amount of time it spends in the aqueous phase.

The mean residence time of a tracer in the subsurface can be determined by integrating the area under the tracer response curve. The difference between the first temporal moments of the respective tracers is then used to determine the amount of residual NAPL saturation according to the following equation,

$$S = \frac{t_2 - t_1}{\left(K_{N,w}^2 - 1\right)t_1 - \left(K_{N,w}^1 - 1\right)t_2} \tag{2.11}$$

where t_1 and t_2 are the mean residence times of the tracers, $K^2_{\mathrm{N,w}}$ and $K^1_{\mathrm{N,w}}$ are the respective tracer partition coefficients, and S is the residual saturation of the NAPL phase. If one of the tracers is non-partitioning (i.e., the partition coefficient is zero), the equation above reduces to the following,

$$S = \frac{t_p - t_n}{\left(K_{N,w}^2 - 1\right)t_n + t_p} \tag{2.12}$$

where the previous subscripts of 1 and 2 are replaced with n and p to denote the non-partitioning and partitioning tracers.

With a known residual saturation value, the swept pore volume and volume of NAPL detected by the tracer can be estimated from the following two equations, respectively.

$$V_p = \frac{qt_1}{1-S\left(1-K_{N,w}^1\right)} = \frac{qt_2}{1-S\left(1-K_{N,w}^2\right)} \tag{2.13}$$

$$V_n = SV_p = \frac{q\left(t_2-t_1\right)}{K_{N,w}^2 - K_{N,w}^1} \tag{2.14}$$

If the detailed development of the PITT technique is desired, the reader is referred to the original work of Jin as presented in his dissertation of 1995. A set of typical breakthrough curves, and an example of the PITT calculations are shown in Appendix A.

2.3 Surfactants

The concept of using surfactants to remediate subsurface contamination originated from their successful use in the petroleum industry for enhanced oil recovery. In the oil fields, primary recovery efforts remove 20 to 60 percent of the subsurface product. After petroleum sulfonates were patented in 1963, a significant portion of the remaining product has often been removed through secondary recovery efforts involving aqueous surfactant solutions (Abdul *et al.*, 1990). A huge body of scientific and practical data regarding the use of surfactants in the subsurface has thus been generated over the past 30 years. Whether surfactants are used for enhanced oil recovery or remediation efforts, the basic principles are the same; however, significant differences exist regarding operating conditions and criteria for success. An excellent review of these differences and "lessons learned" from the petroleum industry is provided by Pope and Wade (1995), with the primary difference being the potential contamination of the porous medium from the surfactant itself.

2.3.1 Surfactant Fundamentals

The term surfactant, derived from the phrase "surface active agent," is used to describe a substance that accumulates at an interface and thereby alters interfacial properties (Rosen, 1989). The surface activity of surfactants, and their propensity to accumulate at interfaces, is due to their amphiphilic structure. In aqueous systems, a surfactant has a polar or ionic hydrophilic moiety (i.e., part) and a nonpolar lipophilic moiety that are referred to as the head and tail group, respectively (West and Harwell, 1992). In NAPL-aqueous systems, a surfactant will orient itself at the oil-water interface such that its hydrophilic head is in the water phase and its lipophilic tail is in the oil phase. Oriented in this way, both moieties of the surfactant molecule are in a preferred phase and the free energy of the system is minimized (Sabatini *et al.*, 1995). Surfactants are typically classified according to the hydrophilic nature of the molecule as anionic, cationic, nonionic, and zwitterionic (both cationic and anionic groups).

A phenomenon unique to surfactants is their ability to self-assemble into aggregates of 50-200 molecules known as micelles (Sabatini *et al.*, 1995; West and Harwell, 1992; Harwell, 1992). West (1992) defines micelles as organized surfactant structures that form spontaneously in solution when the surfactant concentration is above a level referred to as the critical micelle concentration (CMC). A function of the surfactant structure, surfactant solution temperature, concentration of electrolytes, and concentration of solubilizates and other amphiphiles, the typical range of most CMCs is 0.1 to 10 mM (Harwell, 1992). As Figure 2.2 illustrates, micelle formation causes a sudden change in a number of solution properties, indicating that a radical change in the aqueous surfactant environment has occurred (Christian, 1995).

At concentrations below the CMC, surfactant molecules exist solely as monomers and have a minimal effect on the solubility of most hydrocarbons (Pennell *et al.*, 1993). Once the CMC has been reached, any surfactant added to the solution will result in the formation of micelles and the extramicellar surfactant concentration (the aqueous surfactant activity) remains constant (Sabatini *et al.*, 1995) as illustrated in Figure 2.3. When micelles form, their hydrophilic (polar) moieties are oriented towards the aqueous phase and their lipophilic (non-polar) moieties are positioned towards the interior of the aggregate. The organic interior core formed by this orientation acts as an oil sink into which hydrophobic contaminants can partition. Micelles thus serve as an organic pseudophase possessing a high capacity for solubilizing an organic contaminant (West, 1992).

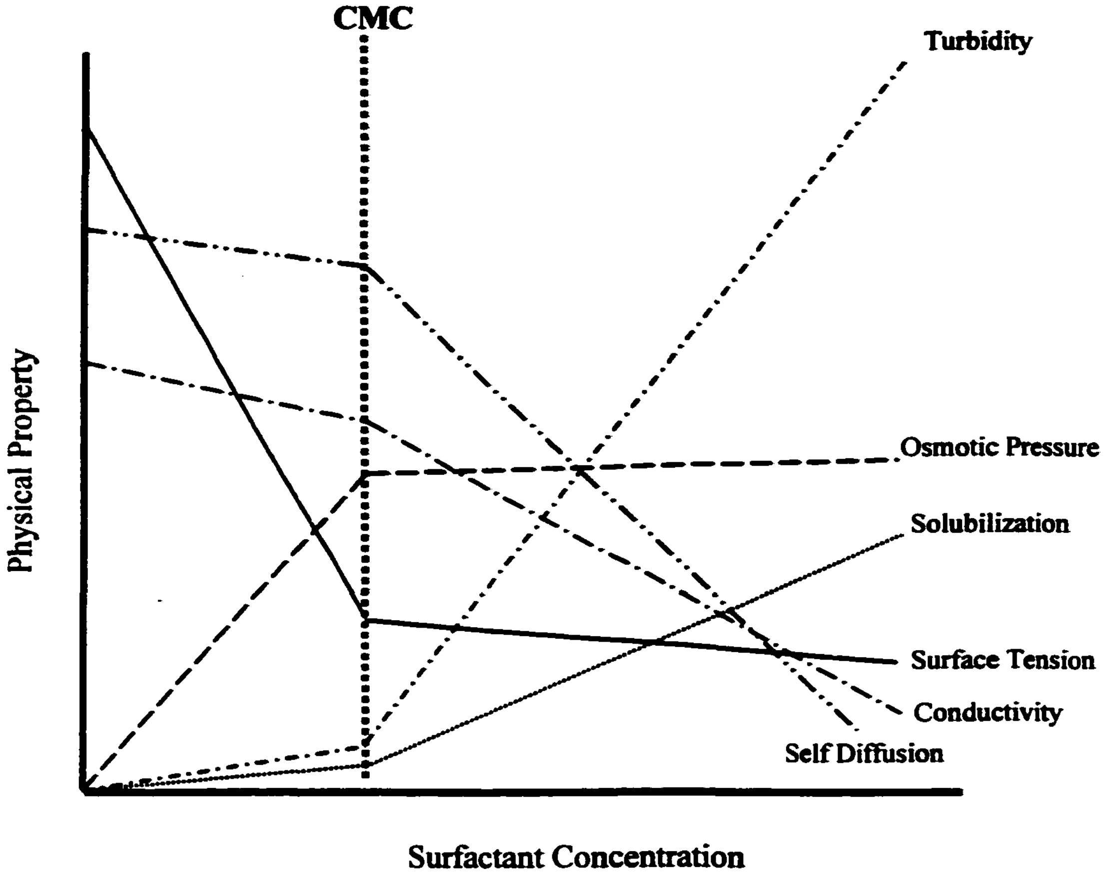

Figure 2.2 Variation of Measured Properties Near the Critical Micelle Concentration (modified from Christian, 1995)

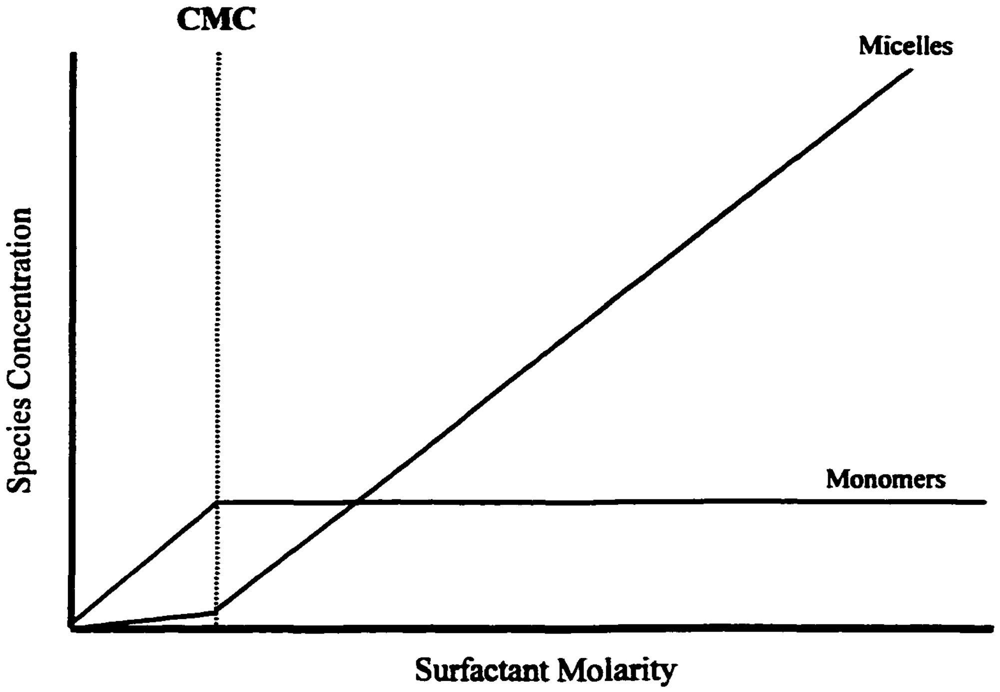

Figure 2.3 Schematic of Typical Monomer and Micelle Concentrations in Surfactant Systems (modified from Christian, 1995)

In general, micellar systems transition from normal to swollen micelles (Winsor Type I), to middle phase systems (Winsor Type III), and finally to reverse micelles (Winsor Type II) (Shiau *et al.*, 1995). In a Type I system where salinity values are relatively low, the surfactant is too water soluble and is in the form of oil-swollen micelles in equilibrium with the aqueous and excess organic phase. As the salinity of the system is increased, more oil is solubilized. At an initial critical salinity value, the Type I system converts into a Type III system in which the surfactant is said to be balanced and is in equilibrium with both the excess water and organic phase. This "middle phase" (often called a microemulsion) contains almost all of the surfactant and large quantities of the organic and aqueous phases (West and Harwell, 1992). At an optimum salinity value, the volume of organic and aqueous phases incorporated in the surfactant microemulsion is equal. At a second critical salinity value, the Type III system converts to a Type II system in which the surfactant is too oil soluble and is mostly found in the form of water-swollen reverse micelles in equilibrium with the oil and excess aqueous phase. Figure 2.4 shows this typical change in phase behavior as a function of salinity for anionic surfactants.

Two parameters represent the solubilization capacity of a particular surfactant: the molar solubilization ratio (MSR) and the micelle-water partition coefficient (K_m). The MSR is defined as the ratio of the number of moles of hydrocarbon solubilized to the number of moles of surfactant in the micellar form (Pennell *et al.*, 1993). When surfactant concentrations are expressed on a molar basis and plotted against aqueous contaminant solubility, the slope of the straight-line portion above the CMC is the

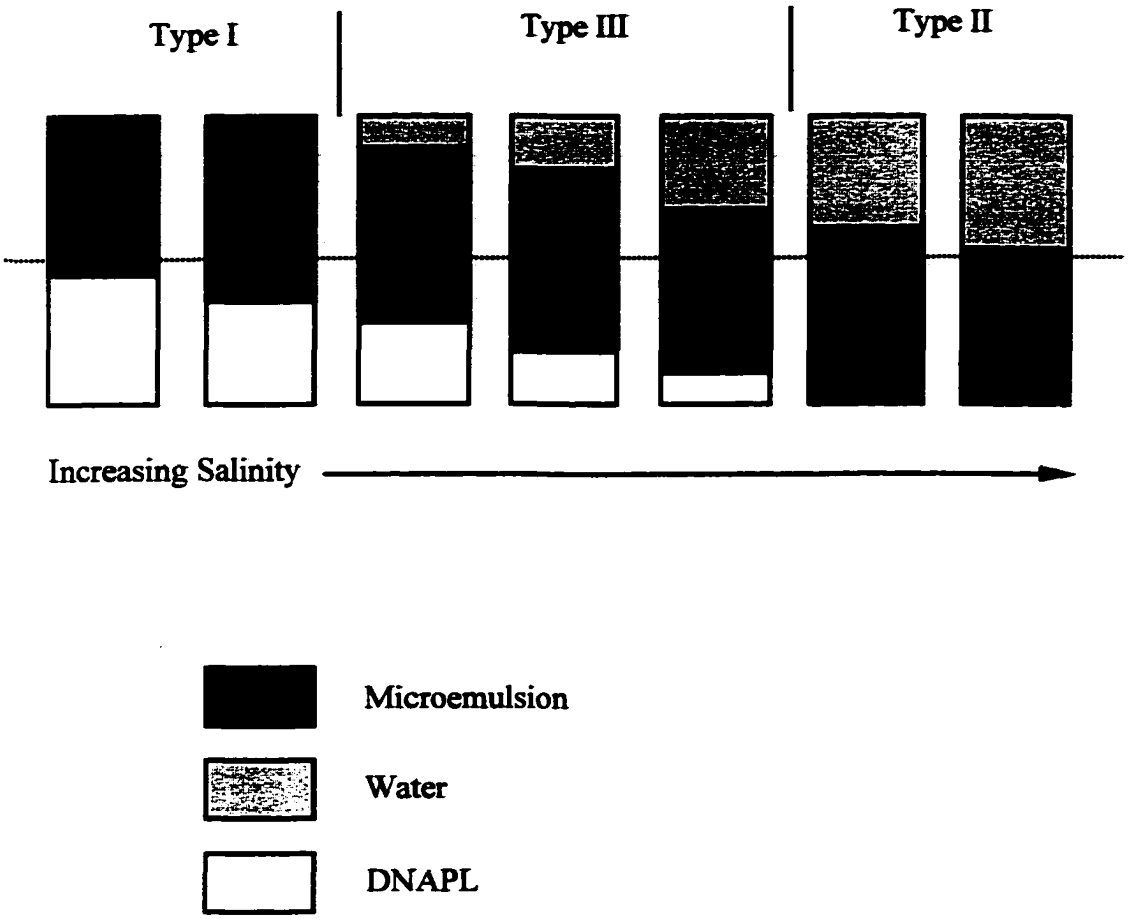

Figure 2.4 Typical Phase Behavior

MSR. The micellar partitioning coefficient can be defined as the ratio of the micellar to aqueous mole fraction of the contaminant (Lipe *et al.*, 1996). It is used to describe the extent to which a specific compound will solubilize into a given surfactant micelle.

Two methods are commonly used to examine a surfactant's appropriateness with a given contaminant: the hydrophilic/lipophilic balance (HLB) method and the Winsor method (West and Harwell, 1992). The relationship between the methods is illustrated in Figure 2.5. In the HLB method, an empirical scale from 0 to 40 (a higher number indicates more water solubility) has been developed which is related to the surfactant behavior and balance between hydrophilic and lipophilic portions of the surfactant molecule (Rosen, 1989). HLB numbers have subsequently been assigned to many commercial surfactant products and contaminants. An appropriate surfactant type for a given contaminant is one in which the respective HLB numbers are similar. In this manner, the HLB method serves as a screening tool in matching surfactants and contaminants. Since the impacts of temperature and electrolytes on surfactant performance have not been quantitatively incorporated into it, the HLB method should not be used to make final surfactant selections (West and Harwell, 1992).

2.3.2 Surfactant-Enhanced Remediation

Surfactant enhanced remediation is based on two mechanisms: micellar solubilization of NAPL and mobilization of entrapped NAPLs. Micellar solubilization is based on the tendency of micelles to increase the aqueous solubility

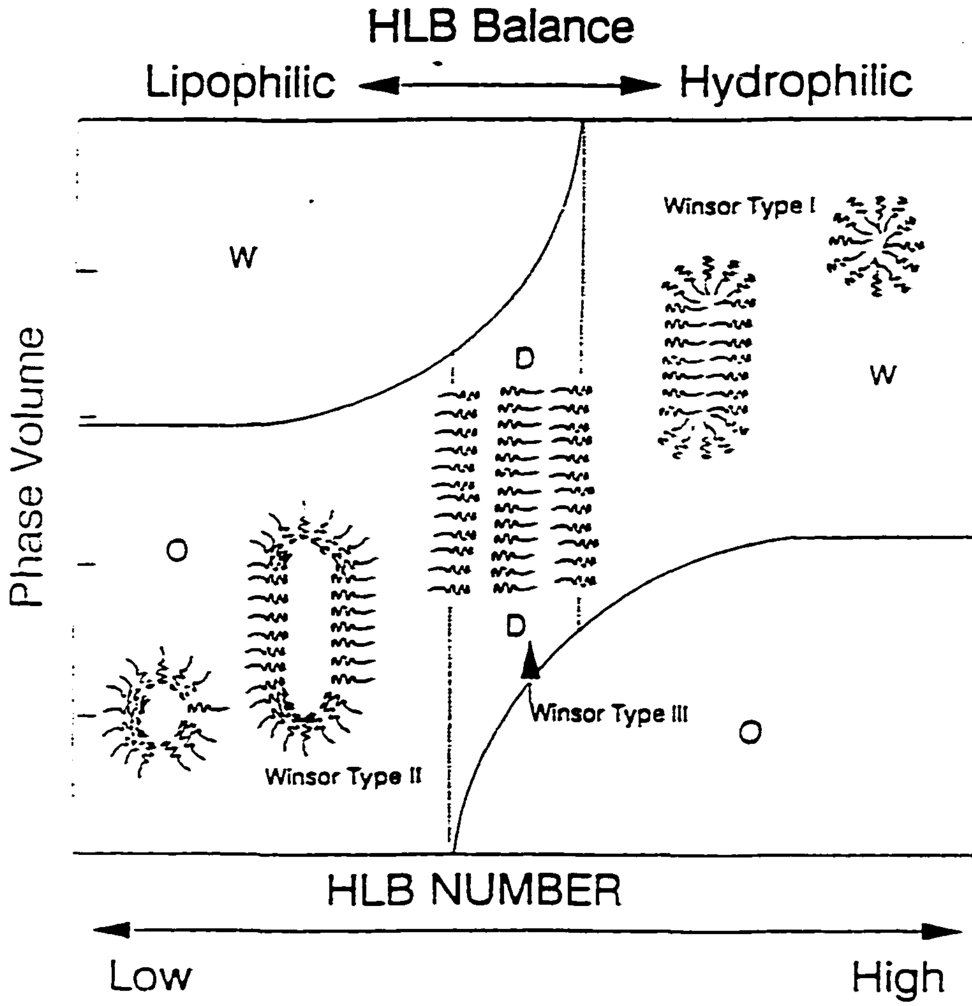

Figure 2.5 Relationship Between the HLB Method and the Winsor Method (Shiau, 1995, as adapted from Shinoda and Friberg, 1986)

of hydrophobic compounds. As a general rule of thumb, the larger the K_{ow} of a solute, the greater will be its tendency to concentrate inside the micelle. It is interesting to note that the process of solubilization is equally appropriate for enhancing the desorption of highly hydrophobic contaminants and the dissolution of residual saturation (Sabatini *et al.*, 1995). Mobilization is the result of a surfactant's ability to establish ultralow interfacial tensions ($<10^{-3}$ dyn/cm) between the organic and aqueous phases (Pennell *et al.*, 1993). If solubilization is the goal, Winsor Type I systems should be appropriately designed to prevent mobilization. However, if mobilization is the goal, Winsor Type III systems should be designed.

The mobilization and solubilization effects of surfactant are strongly linked properties (Oolman *et al.*, 1995). The Chun Huh correlation is used to determine the relationship between surface tension effects and solubilization effects as follows,

$$0.35 = \sigma S^2 \tag{2.15}$$

where σ is the interfacial tension in dynes per centimeter between the surfactant solution and air and S is the aqueous solubility ratio of the solute to the surfactant. From this correlation, it is evident that there is a clear limit on the efficiency of solubilization that can be achieved without simultaneously enhancing mobilization. Thus, if mobilization is not desired, a surfactant that does not substantially reduce the interfacial tension should be chosen.

To ensure surfactants remain active and that losses to sorption, precipitation, and phase changes are minimized, surfactants must be selected so as to be compatible with the contaminated medium (West and Harwell, 1992). Selection of the best surfactant is dependent upon (1) solubilization of the contaminant, (2) interfacial tension, (3) surfactant adsorption, and (4) surfactant toxicity and biodegradation (Fountain *et al.*, 1995). Since the potential for vertical migration is a critical factor, interfacial tension should be an important criterion for surfactant selection. Pope and Wade (1995) list the following criteria for screening surfactants for use in SEAR applications: solubilization potential, phase behavior, environmental acceptability, viscosity of surfactant solutions, coalescence behavior, cost and availability, transport characteristics in permeable media, stability, and sorption characteristics.

2.3.3 Surfactant Success Stories

To illustrate the usefulness of surfactants, various findings reported in the literature are briefly reviewed. Simulations by Brown *et al.* (1994) indicated that 21,700 m^3 of water had to be injected for each cubic meter of PCE removed during conventional pump-and-treat methods, whereas only 417 m^3 of surfactant solution were necessary. Fountain (1992) reported that the PCE concentration of the effluent in one experiment rose to about 4,000 ppm (20 times the aqueous solubility) within one pore volume. In subsequent experiments, Fountain *et al.* (1995) concluded that surfactant flushing can be useful under a wide range of aquifer conditions as long as hydraulic conductivity is high enough (greater than 10^{-3} cm/sec) to make pump-and-treat a viable method. In other words, the ultimate success of surfactants is controlled primarily by site characteristics. The solubility of TCE in the aqueous solution also changed dramatically with the addition of surfactant in experiments by Oolman *et al.* (1995). They reported that the TCE solubility in the surfactant solution was 204,000 mg/L, compared to a literature value if 100 mg/L in clean water, and that residual saturation was reduced from 22.4% to 2.7%.

Pennell *et al.* (1993) reported that the solubility of dodecane (3500 mg/L) in a surfactant solution was about 6 orders of magnitude greater than the reported solubility of dodecane in water (3.7 μg/L). After surfactant flushing, dodecane effluent concentrations in column experiments represented a 5 order of magnitude increase in solubility, but was still 7 times less than the equilibrium value measured in batch experiments. This was attributed to rate-limited solubilization based on (a) the increase in effluent concentrations following flow interruption, and (b) the reduction in steady-state effluent concentrations as the pore-water velocity was increased. Similar observations were reported for dissolution experiments by Geller and Hunt (1993) and Powers *et al* (1994). Results of various studies suggest that rate-limited mass transfer is more prevalent during micellar solubilization of NAPLs than during dissolution of NAPLs into water (Pennell *et al.*, 1994).

In field-scale studies, Abdul *et al.* (1990) evaluated surfactant enhanced remediation of PCB contamination and found that about 10 percent of the PCB was solubilized with six pore volumes. Fountain (1995) reported PCE effluent concentrations 20 times greater than aqueous solubility during experiments at the Borden site and found that vertical mobility can be controlled if interfacial tensions are not reduced below a few dynes/cm. A field demonstration study in Traverse City, Michigan, the PCE and total hydrocarbon mass removed using surfactants was 40 and 90 times higher, respectively, that what would have been removed with a traditional pump-and-treat system (Sabatini *et al.*, 1997; Knox *et al.*, 1997). During our field work at Hill AFB, an average of over 57 percent of contaminants were removed from a test cell with surfactant flushing.

Much work has also been done to determine the most efficient and cost-effective use of surfactants. Harwell (1992) identified numerous factors that could potentially reduce a surfactant's ability to remove contaminants and should be incorporated in the design process. Rouse *et al.* (1993) found that disulfonated surfactants did not precipitate and exhibited an order of magnitude less sorption compared to monosulfonated surfactants. Vertical circulation wells (VCWs) have been proposed to maximize surfactant recovery and were subsequently used with great success in the field (Knox *et al.*, 1997). An economic analysis by Krebs-Yuill *et al.*, (1996) concluded that surfactant enhanced remediation will outperform conventional pump-and-treat if the source zone is one acre or less, surfactant losses are minimized, and the surfactant is recovered and reused.

2.4 Modeling Multiphase Flow in Porous Media

The development of mathematical equations to describe multiphase flow in porous media is well documented in the petroleum industry (Crichlow, 1977; Peaceman, 1977; Aziz and Settari, 1979), with numerical solutions of compositional systems for petroleum reservoirs being first reported in the 1960s (Sleep and Sykes, 1993). The compositional modeling approach solves discrete mass balance equations for each chemical component in the system. Similar approaches are now being used in the groundwater field to model multiphase and multicomponent flow of NAPL contaminants. However, these models are typically limited in practical application due to the sheer magnitude of site-specific data that is required. That is not to say that these models are not useful. To the contrary, compositional models can be very useful in conceptualizing subsurface NAPL behavior under both natural conditions and various remediation scenarios (Mercer and Cohen, 1990).

One of the first multiphase flow and transport models reported in the contaminant hydrogeology literature was presented by Abriola and Pinder (1985b). Osborne and Sykes (1986) developed a two-dimensional model to simulate two-phase immiscible flow. This model was limited to transport processes and did not include mass transfer. A similar model that accounted for three-phase immiscible flow was developed the following year (Kuppasamy *et al.*, 1987). Faust *et al.* (1989) described a three-dimensional model, but did not include multicomponent transport. The development of a multiphase, multicomponent model that accounted for adsorption was described by Kaluarachchi and Parker (1990). A comprehensive compositional simulator was developed specifically for contaminants and remediation of groundwater systems (Sleep and Sykes, 1993). Since these models have been sufficiently documented by the respective researchers, readers wishing more detailed information regarding them are referred to the literature.

2.4.1 Overview of UTCHEM

The model used during this research is the University of Texas Chemical flooding simulator (UTCHEM) capable of three-dimensional, multicomponent, multiphase flow. In its genesis, UTCHEM was a one-dimensional, compositional chemical flooding simulator developed to simulate enhanced recovery of tertiary oil using surfactants and polymers (Pope and Nelson, 1978). In subsequent work, the researchers focused on accurate treatment of phase relationship and improved the modeling of physical properties. They also incorporated numerical dispersion control schemes to improve the effectiveness of simulations. Hong (1982) developed a two-dimensional version of the simulator and Datta Gupta *et al.* (1986) reported a three-dimensional version of it. A series of three companion papers describing the model in more detail and comparing simulation results to experimental data were published shortly thereafter (Camilleri *et al.*, 1987a; Camilleri *et al.*, 1987b; Camilleri *et al.*, 1987c). Subsequent improvements to UTCHEM are explained in an environmental research brief prepared for the United States Environmental Protection Agency (Pope *et al.*, 1996). The intent of this section is to provide a brief overview of UTCHEM; for a more detailed description, the reader is referred to the listed references.

2.4.2 UTCHEM Mathematical Formulation

The mathematical formulation of UTCHEM is based on the simultaneous solution of two types of equations: mass conservation and pressure. If temperature is to be considered, energy conservation is added as a third type of equation. Mass balance equations (which incorporate phase velocity and dispersive flux) are solved for any number of user-specified chemical components (water, organic species, surfactant, polymer, electrolytes, alcohols, biological species, tracers, and geochemical species). These components can form up to four fluid phases (aqueous, oleic, microemulsion, and gas). The pressure equation is written explicitly in terms of the aqueous phase pressure and results from applying the mass balance equations to all volume-occupying components (water, oil, surfactant, and gas). Pressures for other phases are determined by factoring in the capillary pressure between the phases.

2.4.3 UTCHEM Capabilities

UTCHEM (version 6.0) can model the physical properties listed in Table 2.1. Some of the more interesting aspects of the model are briefly discussed below. For more detailed information, the reader is referred to both the user's guide (University of Texas at Austin, 1996) and the technical documentation (Delshad, undated). Phase behavior relationships in UTCHEM are based on either the binodal curve or the solubilization ratio. For the binodal curve option, equilibrium phase behavior is described by either the original or modified version of Hand's rule. Hand's rule is based upon the empirical observation that equilibrium phase concentration ratios taken from a ternary diagram form a linear relationship when plotted on a log-log scale (Delshad, 1996). For the solubilization ratio option, the term "solubilization ratio" is defined as the ratio of the volume of oil/water solubilized and the volume of surfactant (Bourrel and Schecter, 1988). In either case, the resulting parameters are

Table 2.1: Major Physical Properties Modeled by UTCHEM

Surfactant/cosolvent phase behavior
Interfacial tension
Equilibrium and nonequilibrium dissolution in aqueous phase
Relative permeability
Capillary pressure
Phase viscosity and density
Multiple organic species
Diffusion and dispersion
Adsorption (organic, surfactant, and polymer)
Tracers and tracer reactions
Dead-end pore space
Dual porosity (for single phase water flow and one tracer)
High pH chemical flooding
Biodegradation
Hysteresis (for relative permeability and capillary pressure)
Cation exchange
Aqueous reactions
Partitioning of chemical species between oil and water
Dissolution and precipitation
Polymers and gels

used in UTCHEM to calculate the interfacial tension between the microemulsion and the excess phases. Interfacial tensions can be calculated with either a correlation developed by Reed and Healy and later modified by Hirasaki (1981) or a correlation developed by Huh (1979).

2.4.4 UTCHEM Numerical Simulation Method

The solution method used in UTCHEM is analogous to the implicit in pressure and explicit in saturation (IMPES) method used in the petroleum industry (Brown, 1993). It is more accurately described as "IMPES-like" since it uses an implicit in pressure and explicit in concentration method (Pope *et al.*, 1996). To be more specific, the pressure equation is solved implicitly using the Jacobi conjugate gradient method. After back-substituting the results, the mass conservation equations are solved explicitly for the overall concentration of each component.

UTCHEM uses a block-centered finite-difference discretization scheme with four possible coordinate systems: Cartesian, radial, Cartesian with variable width, or curvilinear. Gridblock sizes can be constant, or they may vary either on a regional basis or independently on a unit basis. First-order approximations are available for time derivatives; however, temporal accuracy can be enhanced through the use of a time-correction technique developed by Liu (1993) that is considered second-order. The UTCHEM user's guide recommends using second-order time approximations only with higher-order dispersion methods. For spatial discretization of the advective term, three methods are available to control numerical dispersion. The first two methods, standard single-point and two-point upstream methods, provide first-order and second-order results, respectively. To obtain third order results free of oscillations, a total-variation-diminishing (TVD) scheme developed by Harten (1983) is the third method.

CHAPTER 3

RELATIONSHIP BETWEEN OPTIMAL SALINITY AND EACN VALUES

Part of the focus of this research is to establish a relationship between the partition coefficient of an alcohol tracer and the composition of the nonaqueous phase liquid (NAPL) with which the tracer is being used. The basis of this relationship will be the equivalent alkane carbon number (EACN) concept, which was first identified in the petroleum literature over 40 years ago during research involving surfactant enhanced oil recovery. The concept has been applied to the use of surfactants in groundwater remediation efforts by a single group of researchers since the mid-1990s. Therefore, this chapter will serve to introduce the concept and validate its applicability to the objectives of this research. In doing so, this chapter will also develop a better understanding of phase behavior resulting from the use of surfactants.

3.1 Introduction of the EACN Concept

Before introducing the EACN concept, it should be noted that the alkane carbon number (ACN) is simply the number of carbon atoms in an alkane. Alkanes are hydrocarbons that consist of carbon atoms bonded to either hydrogen or other carbon atoms by four single bonds and have the general formula C_nH_{2n+2} where n is any integer. For other hydrocarbons, the ACN is the number of carbons in the alkane chain (longest continuous chain of carbon atoms present). Cayias *et al.* (1976) found that hydrocarbon mixtures behave like pure hydrocarbons with respect to the relationships between optimal salinity, surfactant concentration, and surfactant average equivalent weight. Therefore, an equivalent alkane carbon number (EACN) can be calculated on a mole fraction basis and assigned to the mixtures. This EACN value was found to vary linearly with surfactant equivalent average weight (Cayias *et al.*, 1976). Furthermore, Salager *et al.* (1979) discovered a linear relationship between the logarithm of the optimal salinity and the ACN/EACN. Chlorinated hydrocarbons and complex mixtures were found to exhibit similar behavior (Baran *et al.*, 1994).

The basis of the EACN concept can be attributed to research by Cayias *et al.* (1977) in which the interfacial tensions of three homologous series of hydrocarbons (alkanes, alkylbenzenes, and alkylcyclohexanes) were investigated. Various compounds from each of the three homologous series were combined with an aqueous phase containing 0.2 wt% Witco TRS 10-80 (a petroleum sulfonate) and 1.0 wt% NaCl. To explore the effects of the surfactant on interfacial tension, they plotted the ACNs against the interfacial tension for each compound as shown in Figure 3.1. From the plot, a trend is evident in which octane, octylbenzene, and butylcyclohexane exhibited the minimum tensions for each series, respectively.

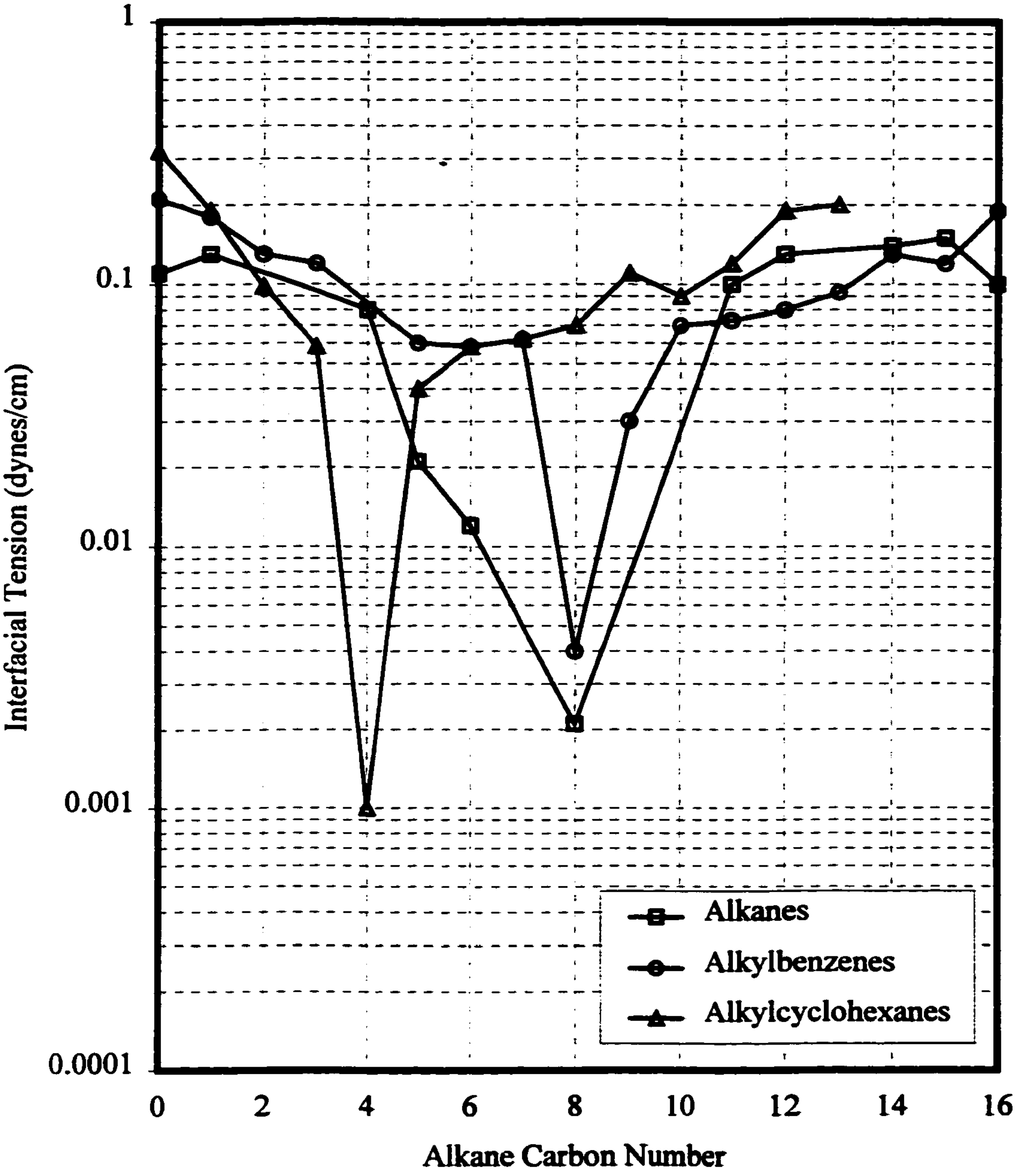

Figure 3.1 Relationship Between Interfacial Tension and Alkane Carbon Number for Three Homologous Series and a 0.2 wt% Witco Surfactant Solution (adapted from Cayias *et al*., 1977)

Cayias *et al.* (1977) made three important observations from their research. First, they concluded that the alkyl groups dominate in this system and that the aromatic nature of the molecules is not important. Secondly, by observing the minimum interfacial tension at an ACN of 4, they also determined that the cyclohexane ring for the alkyl cyclohexanes resembles a four-carbon alkyl increment. Finally, the fact that the interfacial tensions approach nearly the same value at large ACN values supports the contention that the alkyl groups dominate in determining the interfacial tensions. By varying the weight percentage of the surfactant, they further discovered a correlation between the surfactant equivalent weight and the molecular weight of the compound within each homologous series that exhibited the minimum interfacial tension. They found that the optimal surfactant equivalent weight increases as the molecular weight of a hydrocarbon is increased within a homologous series (Cayias *et al.*, 1977).

Cash *et al.* (1977) extended the above research to investigate binary mixtures within and between each of the three homologous series. Using the same concentrations of surfactant and electrolyte, they found that the interfacial tension of a binary mixture varied linearly with mole fraction. More interestingly, they also discovered that the critical parameter in matching a binary mixture to a given surfactant weight percentage to obtain minimal interfacial tensions is the paraffinicity of the oil phase.

Figure 3.2 was adapted from the article by Cash *et al.* (1977) to illustrate the relationship between ACNs and interfacial tension. For this plot, average ACN values for binary mixtures were obtained from the formula,

$$C_{avg} = X_A C_A + X_B C_B \tag{3.1}$$

where X_A and X_B are the mole fractions of components A and B, respectively; and C_A and C_B are the number of carbons in the alkyl group of each component. As Figure 3.2 indicates, the plots for four alkane pairs overlay each other with each mixture exhibiting minimum interfacial tension at an average ACN of approximately 7.7. The nature of the curve shown in Figure 3.2 also fits the interfacial tension data for the individual components with a shift of 0.3 units.

Cash *et al.* (1977) also conducted similar experiments with three binary mixtures of alkylbenzenes, three binary mixtures of alkylcyclohexanes, and with five binary mixtures of components selected from different homologous series. When the average ACN values were plotted against the interfacial tension, the resulting curves for all three experiments were similar to the curve for the alkane pairs in Figure 3.2. The only difference was the ACN value corresponding to the minimum interfacial tension: 7.6 for the alkylbenzene pairs, 4.0 for the alkylcyclohexane pairs, and 8.0 for the mixed series.

Cash *et al.* (1977) concluded that the correlating variable in each case was the number of carbons for alkanes and the number of carbons in the side chain for alkylbenzenes. For cyclohexanes, they found that the cyclohexyl ring was equivalent

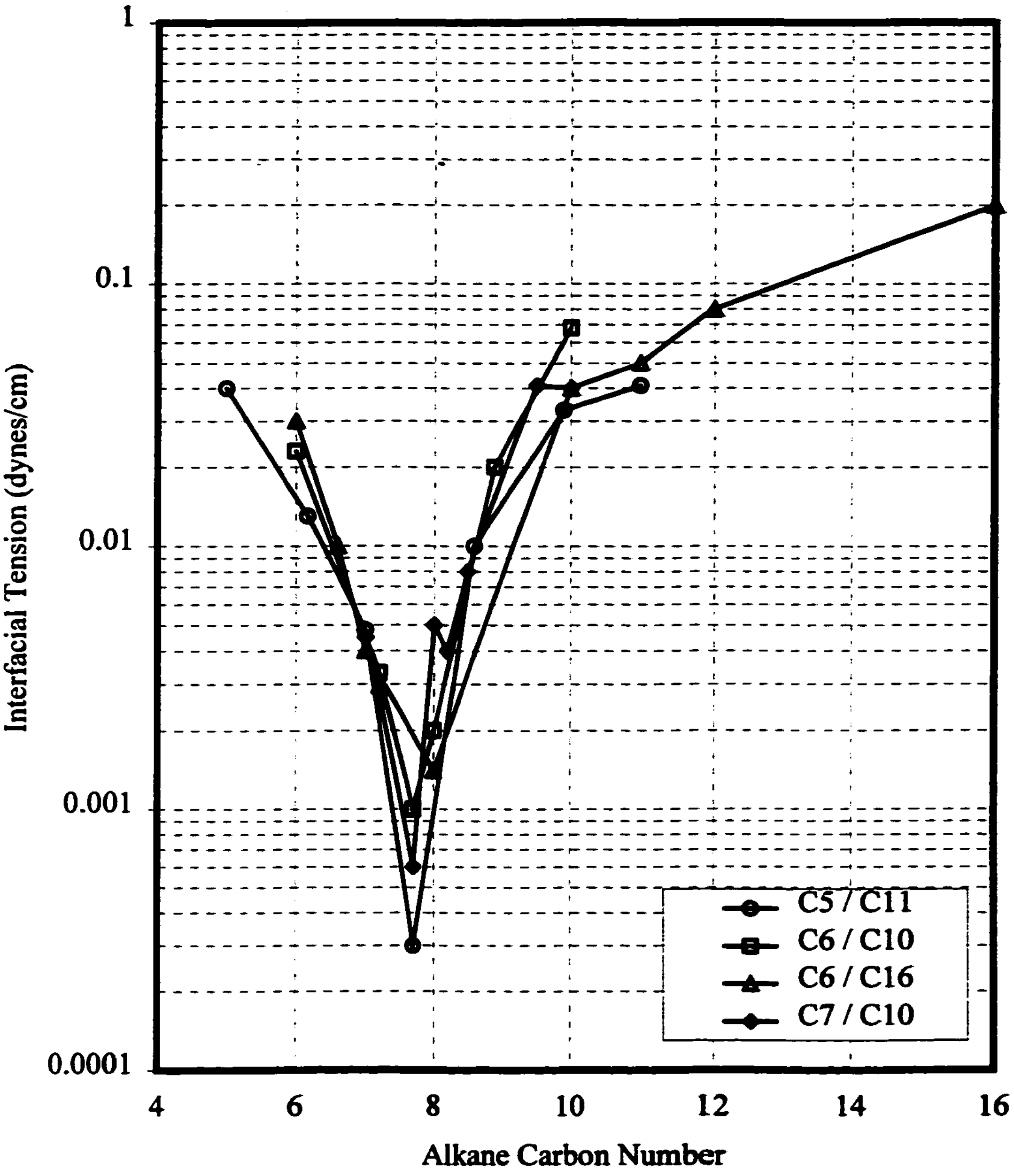

Figure 3.2 Relationship Between Interfacial Tension and Average Alkane Carbon Number for Indicated Binary Mixtures and a 0.2 wt% Witco Surfactant Solution (adapted from Cash *et al*., 1977)

to about four carbons and a scaling factor of 3.7 can be added to the number of carbons in the alkyl side chains. Cash *et al.* (1977) proposed that the trends depicted in Figure 3.2 are universal and clearly illustrate the affinity of a surfactant for a particular hydrocarbon composition to attain a minimal interfacial tension.

Cayias *et al.* (1976) applied the principles identified above to complex hydrocarbon mixtures and found that it was possible to predict the resulting interfacial tensions. They also discovered that hydrocarbon mixtures behave like pure hydrocarbons with respect to changes in salinity, surfactant concentration, and surfactant average equivalent weight. More specifically, they found that the behavior of crude oils is similar to that of alkanes in the range of hexane to nonane. Pertinent to this research is the fact that they were able to model complex mixtures with a unique EACN and found that the EACN, which resulted in minimal interfacial tension, varied linearly with surfactant average equivalent weight.

In similar work investigating the phase behavior of surfactant/brine/oil systems, several researchers found that low interfacial tensions and high solubilizations in the microemulsion phase occurred in or near the salinity ranges resulting in three-phase behavior (Healy and Reed, 1974; Healy *et al.*, 1975). Expanding on this work, Salager *et al.* (1979) concluded that the optimum formulation of a system is characterized by (1) minimal interfacial tension, (2) three-phase behavior, and (3) high solubilization of both water and oil in the microemulsion phase. Thus, the determination of optimal formulations can be accomplished through the measurement of interfacial tensions or the observance of three-phase behavior.

In either case, Salager *et al.* (1979) discovered a correlation between optimal formulation and several variables: structure of the surfactant, ACN of the oil, salinity, and the type and concentration of alcohol used as a cosurfactant. For the alkylbenzene sulfonates and NaCl brine used in their experiments, it was shown that an optimal formulation was obtained whenever the following correlation was satisfied,

$$\ln S^* = k(\text{EACN}) + f(A) - \sigma \tag{3.2}$$

where S^* is the optimal salinity, k is a constant (equal to 0.16 for alkyl aryl sulfonates and 0.10 for alkyl sulfates and alkanoates), EACN is the equivalent alkane carbon number, $f(A)$ is a function that depends on the alcohol cosurfactant and its concentration, and σ is a parameter specific to the surfactant.

After this initial work, the literature appears to be void of further efforts concerning optimal formations and EACNs until the early 1990s. Baran *et al.* (1994) investigated the formation of a microemulsion in surfactant systems combined with mixed chlorinated hydrocarbons and reported that the behavior of chlorocarbons parallels that previously established for hydrocarbons. They proposed that the following relationship is applicable to both hydrocarbons and chlorocarbons,

$$\ln S^*_{mix} = \sum_{j=1}^{a} X^*_j \ln S^*_j \tag{3.3}$$

where S^* is the optimal salinity (wt%), j is each individual component of the mixture, and a is the total number of components.

Baran *et al.* (1994) conducted salinity scans on various hydrocarbons and chlorocarbons using a 2 wt% surfactant solution with Aerosol MA-80. They found the following linear relationship between the natural logarithm of the optimal salinity and the EACN of the chemical compounds,

$$\ln S^{*}\ (\mathrm{wt\%}) = 0.17\ (\mathrm{EACN} + 5.4) \tag{3.4}$$

Note that the slope of the line is 0.17 and agrees quite well with the value of 0.16 previously reported. Using a defined standard state of 1 wt% for the system, the value of 5.4 used in the equation is specific to the type of surfactant used.

3.2 Experimental Description

3.2.1 Materials

Two surfactant solutions were used to investigate the relationship between optimal salinity and the EACN of specific contaminants. The specific properties of the surfactant solutions are shown in Table 3.1. The properties of the eight common groundwater contaminants used in this study are shown in Table 3.2. The surfactant solutions were prepared with de-ionized water and sodium chloride from Fisher Scientific. Iso-butanol (a light alcohol) and *n*-hexanol (a heavy alcohol), both purchased from Aldrich Chemical, were used as cosolvents. Salinity scan samples were stored in 15-ml glass pipettes (Alltech Associates, Inc.) with screw-top caps and calibrated to 0.1 ml. Mass measurements were made on an analytical balance (Sartorius) with a capacity of 30/160 grams.

Table 3.1: Properties of Surfactants (Source: Shiau, 1995)

Solution	Surfactant[a]	wt%	HLB[b]	MW[c]	Type[d]
1	Sodium Dodecyl Sulfate (SDS)[e]	4	40	288	A
2	Bis-2-Ethylhexyl Sodium Sulfosuccinate[g] (Aerosol OT)	2	NA[g]	445	A
	POE(20) Sorbitan Monooleate[h] (Tween-80)	2	NA[g]	1308	N

[a] Used as received from manufacturer
[b] Hydrophilic-Lipophilic Balance
[c] Molecular Weight (g/mole)
[d] Anionic (A) or Nonionic (N)
[e] Obtained from Fisher Scientific
[f] Obtained from American Cyanamid
[g] Obtained from PPG/Mazer Chemicals
[h] Not Available

Table 3.2: Properties of Contaminants (Source: Verschueren (1983) unless noted otherwise)

Contaminant	Formula	MW[a] (g/mole)	Density (at 20°C)	Solubility[b] (mg/l)	EACN[c]
Toluene[d]	C_7H_8	92.14	0.8660	670	1
o-Xylene[d]	C_8H_{10}	106.17	0.8802	170	2
Hexane[d]	C_6H_{14}	86.18	0.6594	NA[f]	6
Heptane[d]	C_7H_{16}	100.21	0.6838	NA[f]	7
Decane[e]	$C_{10}H_{22}$	142.29	0.7301	700	10
Carbon Tetrachloride (CTET)[d]	CCl_4	153.82	1.5890	800	-0.06
Tetrachloroethylene (PCE)[e]	C_2Cl_4	165.83	1.6230	150[f]	2.90
Trichloroethylene (TCE)[d]	C_2HCl_3	131.39	1.4649	1,000[f]	-3.81

[a] Molecular Weight (g/mole)
[b] In distilled water at 20°C (unless noted otherwise)
[c] Data obtained from Baran *et al.* (1994)
[d] Obtained from Fisher Scientific
[e] Obtained from Aldrich Chemical
[f] Data obtained from Knox *et al.* (1993)

3.2.2 Procedures

The procedures used to determine optimal salinity values were consistent with those found in the literature. The initial series of phase behavior experiments was conducted with a 4 wt% aqueous solution of SDS. This solution was prepared by measuring approximately 20 grams of the surfactant into a 500-ml Erlenmeyer flask containing approximately 250 ml of de-ionized (DI) water and gently mixing the contents to dissolve the SDS. After adding DI water until the total weight of the solution was 500 grams, the flask was placed on a stirrer for 1 hour. Subsequent phase behavior experiments were conducted with a 2 wt% mixture of SDS and either 0.3 grams of iso-butanol or 0.1 grams of *n*-hexanol as a cosolvent. Additionally, a 4 wt% mixture of AOT and Tween-80 (2 wt% each) was used without an alcohol cosolvent. All experiments were performed in the manner described below.

To begin the phase behavior studies, 4 ml of the aqueous surfactant solution were transferred to each glass vial and the mass of the solution was measured. After transferring approximately 0.3 grams of iso-butanol (exact mass was recorded), LNAPL contaminant was added to each vial until the total volume was 8 ml. For DNAPLs, the alcohol was placed in the vials first, followed by the cosolvent and then the aqueous surfactant solution. Volume measurements were determined by using the graduated markings on the vials and mass measurements were taken at appropriate steps in the process. All transfers were accomplished with disposable transfer pipettes and vials were handled carefully to avoid premature mixing of their contents.

The initial boundary between the aqueous surfactant phase and the oil phase was noted for each vial (approximately the 4.3-ml mark for LNAPLs and the 4.0-ml mark for DNAPLs). A measured mass of sodium chloride was added to each glass vial, which was then capped and gently shaken to create an emulsion. The vial was allowed to sit until the system reached equilibrium (this ranged from hours to several days depending on the system) and the boundaries between the phases were recorded. The addition of sodium chloride was continued until the salinity limits of the three-phase system were clearly identified. The salinity values and volume measurements thus recorded served as data points to construct volume fraction diagrams (VFDs) for each contaminant.

3.3 Data Analysis

A common way to represent the phase behavior characteristics of a surfactant system is the volume fraction diagram (VFD). Varying the salinity of a surfactant system in what is often called a salinity scan is the most common type of VFD. The volume fractions of each phase of the surfactant system are plotted as a function of the electrolyte concentration.

The VFDs constructed from the data gathered during this research were used to determine the optimal salinity for the compounds investigated. Various definitions of the optimum state for a surfactant system can be found in the literature. Baran *et al.* (1994) describe it as the point in the three-phase region in which the water-to-oil ratio (WOR) of the middle phase equals unity. Salager *et al.* (1979) define it as the mid-point of the salinity range for which the system exhibits three phases. Reed and Healy (1977) use the criterion that the interfacial tensions between the excess oil, the water, and the middle phase are equal. Despite the differing approaches, the various definitions of the optimum state are essentially the same, they just use different parameters to describe the same state (Salager *et al.*, 1979). For this research, the definition presented by Salager *et al.* (1979) was used to derive the following formula,

$$S^* = (S_1 + S_2) / 2 \tag{3.5}$$

where S^* is the optimal salinity, S_1 is the lower salinity limit of the three-phase region, and S_2 is the upper salinity limit of the three-phase region.

3.4 Experimental Results and Discussion

3.4.1 Experiments with 4 wt% SDS

The salinity values found during the phase behavior experiments conducted with the 4 wt% SDS solution and iso-butanol as a cosolvent were adjusted to account for the partitioning of the iso-butanol (a light alcohol) between the oil and surfactant phases. Static partition coefficient tests were conducted to determine the partition coefficient for iso-butanol for each of the contaminants. The respective volumes of iso-butanol were added to the oil and aqueous phases before salinity values were calculated. This more sophisticated approach to determining salinity values appears to be one of the reasons Salager *et al.* (1979) limited their research to heavy alcohols.

Table 3.3 lists the optimal salinity and the width of the salinity range corresponding to the three-phase region for each of the contaminants, as well as the natural logarithm of the optimal salinity. The results of the phase behavior experiments are presented in the VFDs shown in Figures 3.3 through 3.10. The salinity range over which the three-phase regions exist is shown in Figure 3.11 using the EACN values obtained from Baran *et al.* (1994) and listed in Table 3.2. The figure illustrates that the salinity range narrows as the EACN decreases. This behavior is consistent with the results of Salager *et al.* (1979) and indicates that mixtures with higher EACNs are less sensitive to salinity in terms of forming a middle phase.

If the EACN concept is valid, a linear relationship should exist between the natural logarithms of the optimal salinities and the ACNs of the hydrocarbons. As can be seen from Figure 3.12, a linear relationship exists for the alkanes with a corresponding R^2 value of 0.9968. The resulting k value of 0.106 compares well with the value of 0.10 reported by Baran *et al.* (1994) for sulfated surfactants. However, the data points for toluene and *o*-xylene do not follow the linear trend of the alkanes. One possible explanation for this is that aromatic compounds may not exhibit classical phase behavior, or are more difficult to exhibit classical phase behavior, with the SDS surfactant because of their stronger ring structure and multiple double bonds. Another possible explanation is that the ACN values for the aromatics may be wrong and need adjusting to account for the components' ring structure.

Table 3.3: **Results of Phase Behavior Experiments with 4 wt% SDS and 0.3 grams of Iso-butanol**

Contaminant	Optimum Salinity (grams NaCl)	Salinity Range (grams NaCl)	ln S* (wt %)
Toluene	0.2853	0.2329 - 0.3377	1.99
o-Xylene	0.3001	0.2477 - 0.3524	2.05
Hexane	0.3187	0.2617 - 0.3757	2.16
Heptane	0.3917	0.3009 - 0.4824	2.29
Decane	0.5127	0.3750 - 0.6504	2.59
Tetrachloroethylene	0.2642	0.1957 - 0.3326	1.87
Trichloroethylene	0.2024	0.1722 - 0.2325	1.55
Carbon Tetrachloride	0.1888	0.1692 - 0.2084	1.63

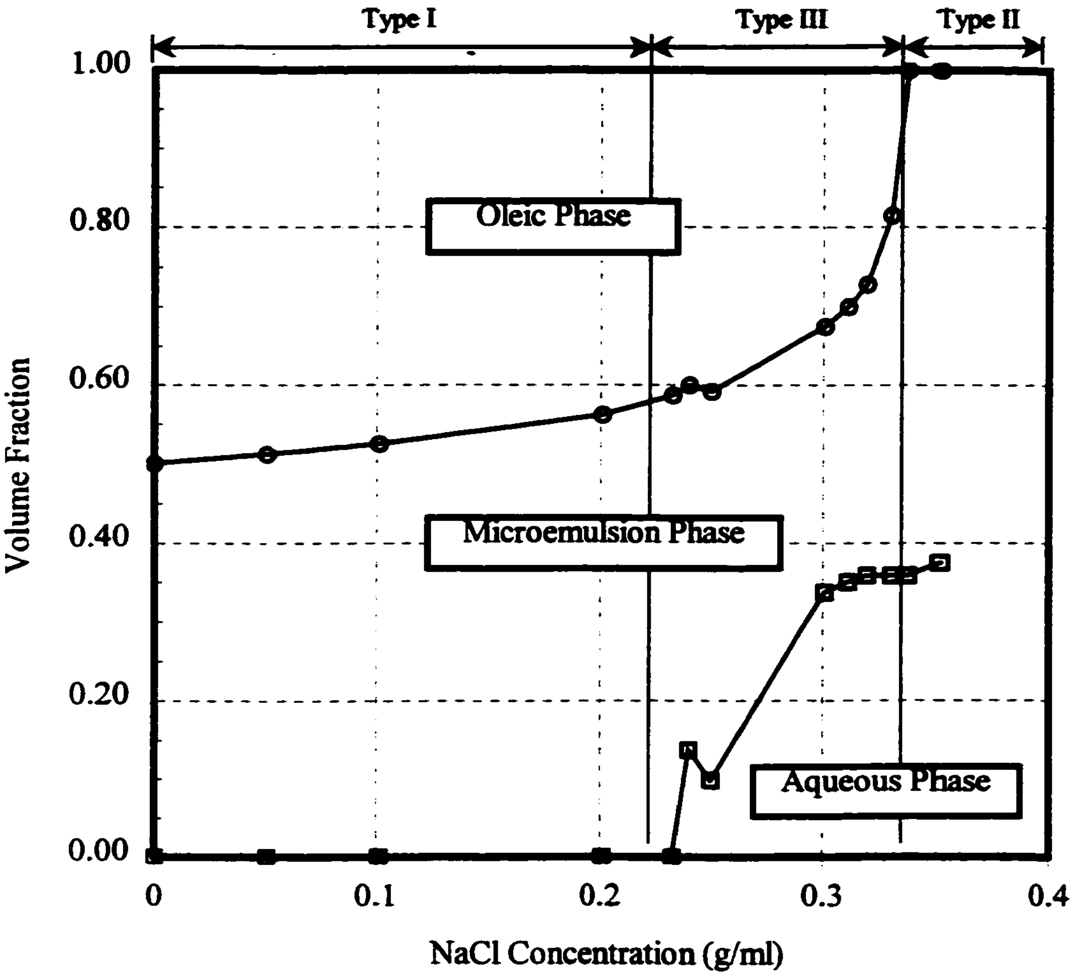

Figure 3.3 Volume Fraction Diagram for Toluene, 4 wt% SDS, and 0.3 grams Iso-butanol

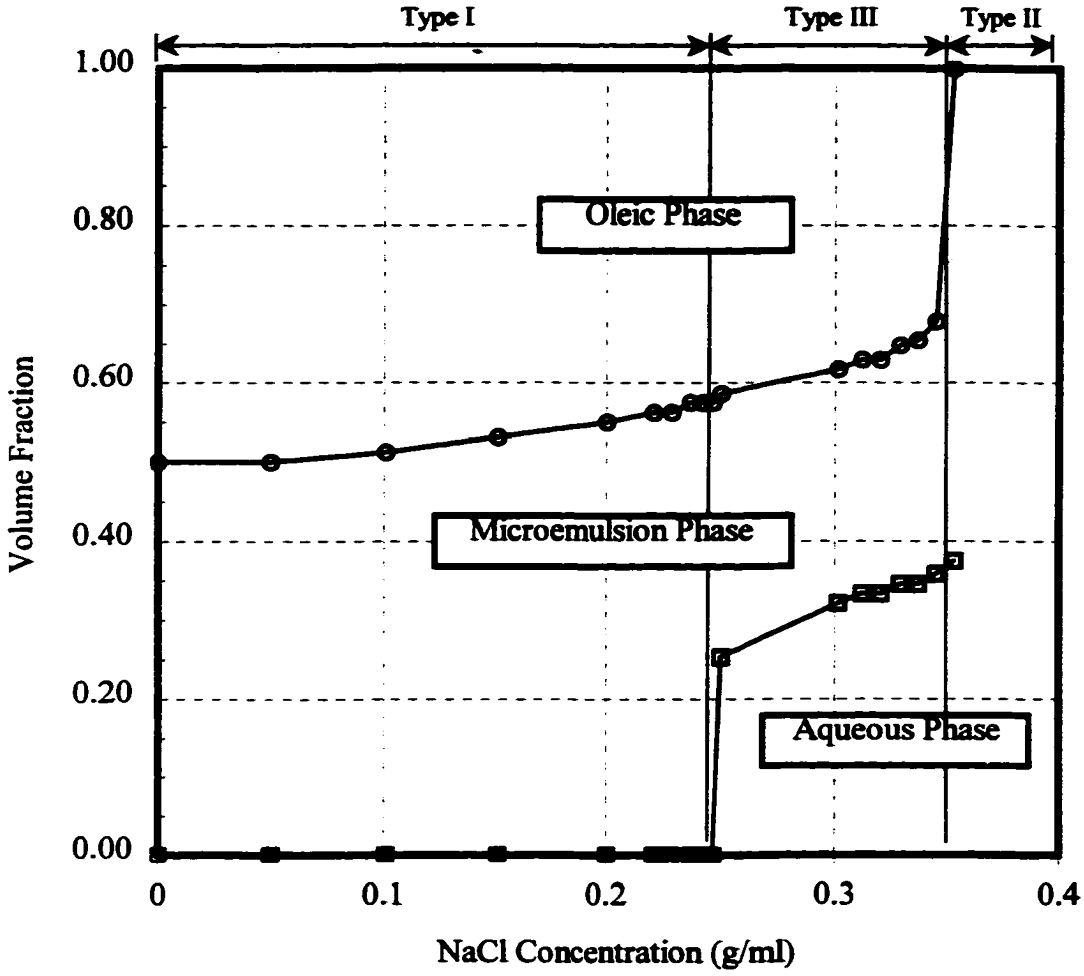

Figure 3.4 Volume Fraction Diagram for *o*-Xylene, 4 wt% SDS, and 0.3 grams Iso-butanol

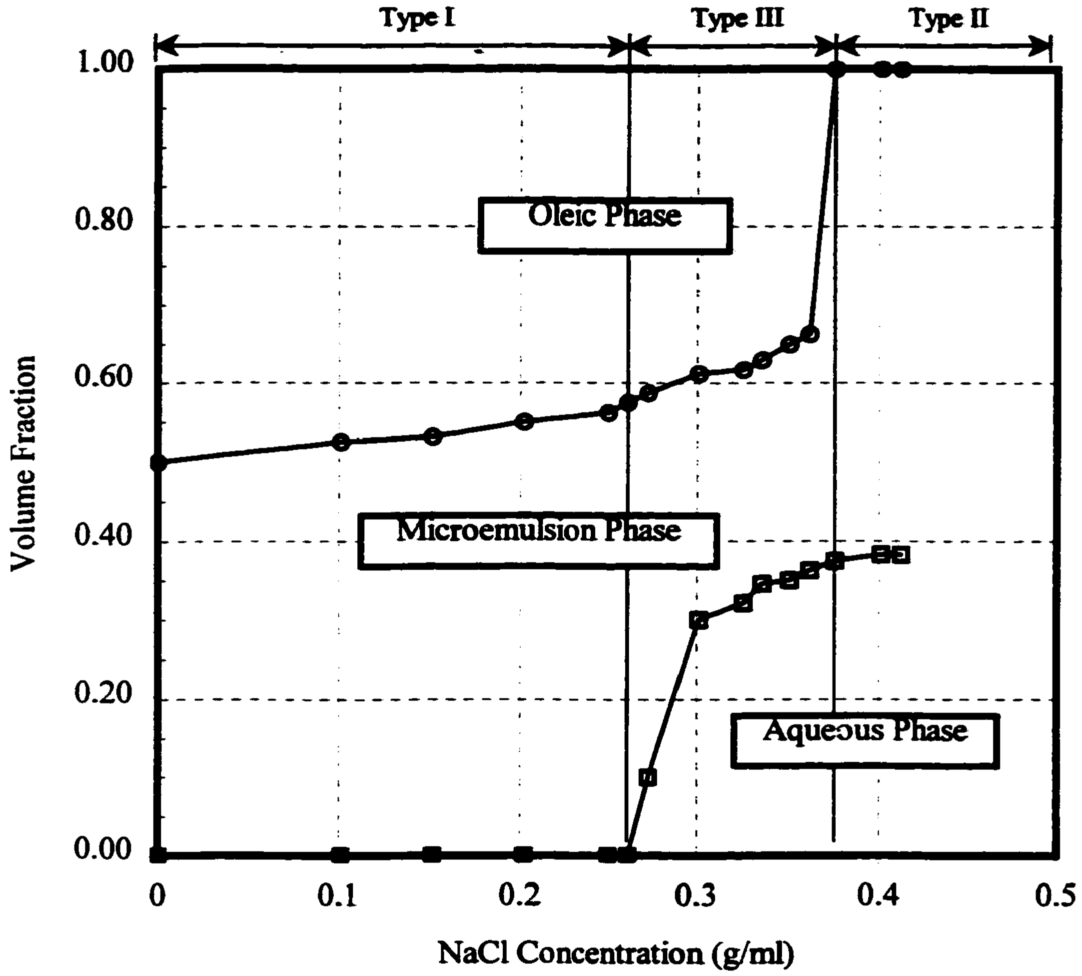

Figure 3.5 Volume Fraction Diagram for Hexane, 4 wt% SDS, and 0.3 grams Iso-butanol

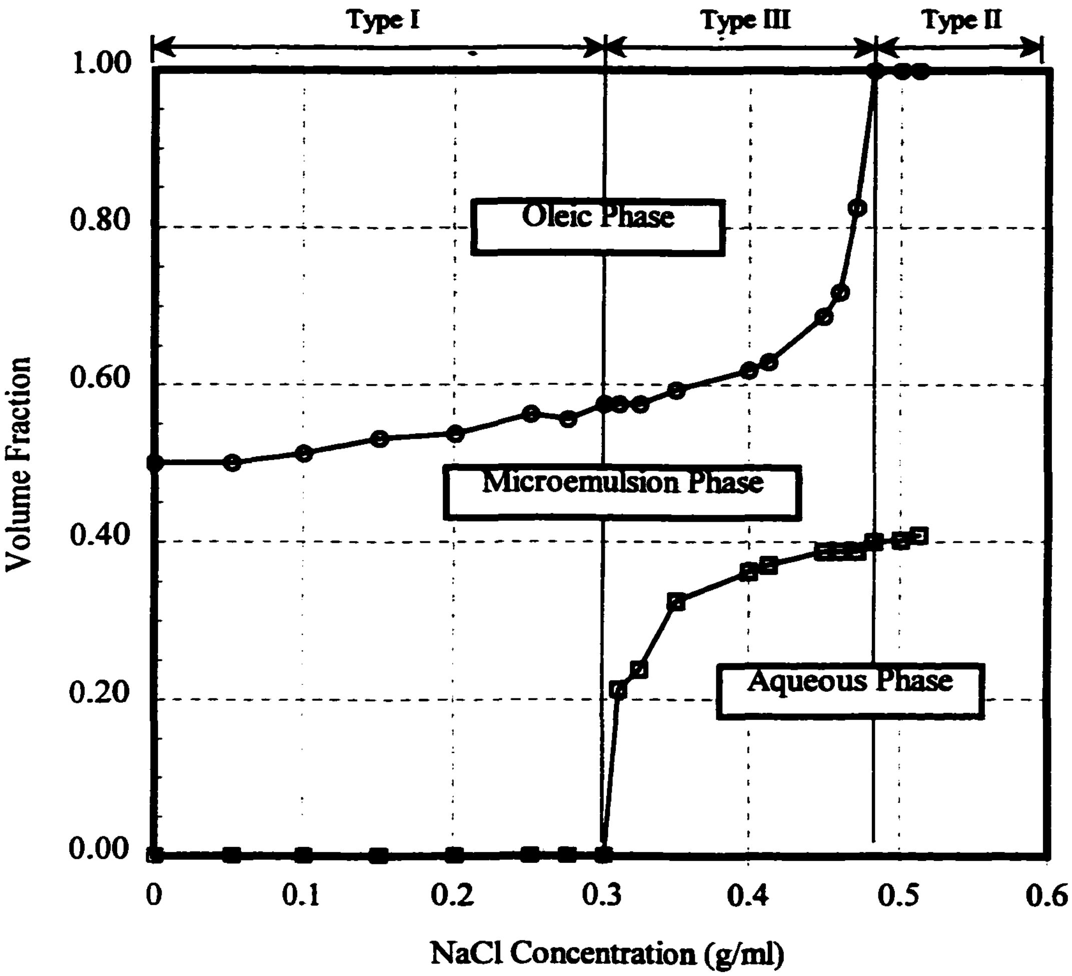

Figure 3.6 Volume Fraction Diagram for Heptane, 4 wt% SDS, and 0.3 grams Iso-butanol

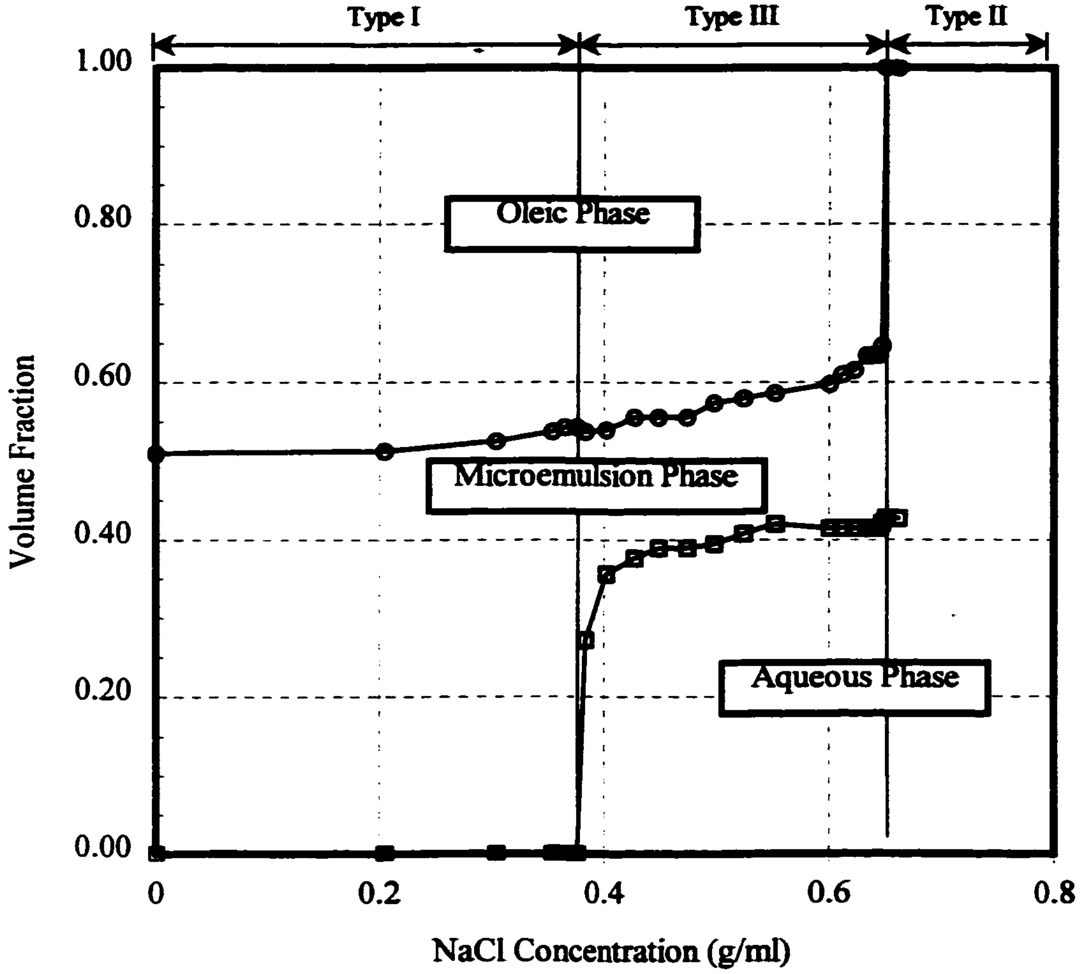

Figure 3.7 Volume Fraction Diagram for Decane, 4 wt% SDS, and 0.3 grams Iso-butanol

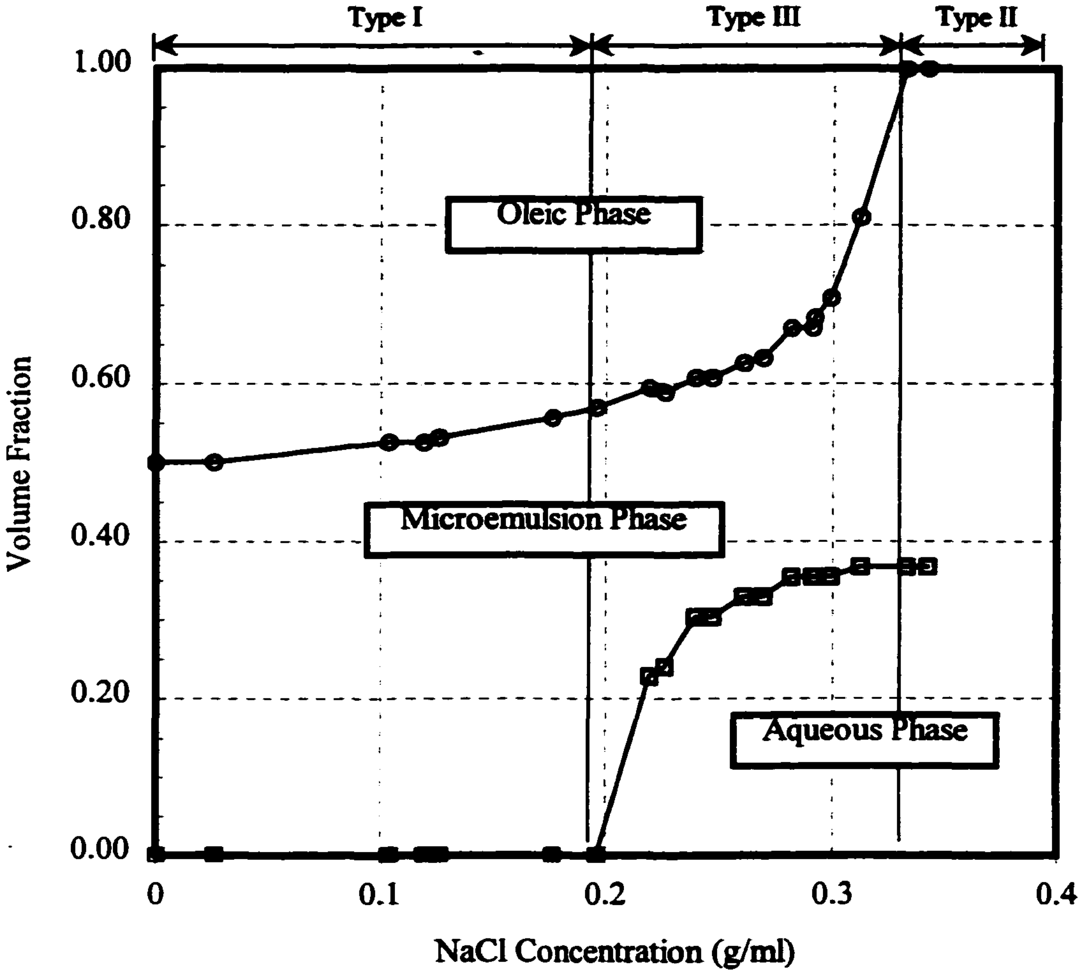

Figure 3.8 Volume Fraction Diagram for PCE,
4 wt% SDS, and 0.3 grams Iso-butanol

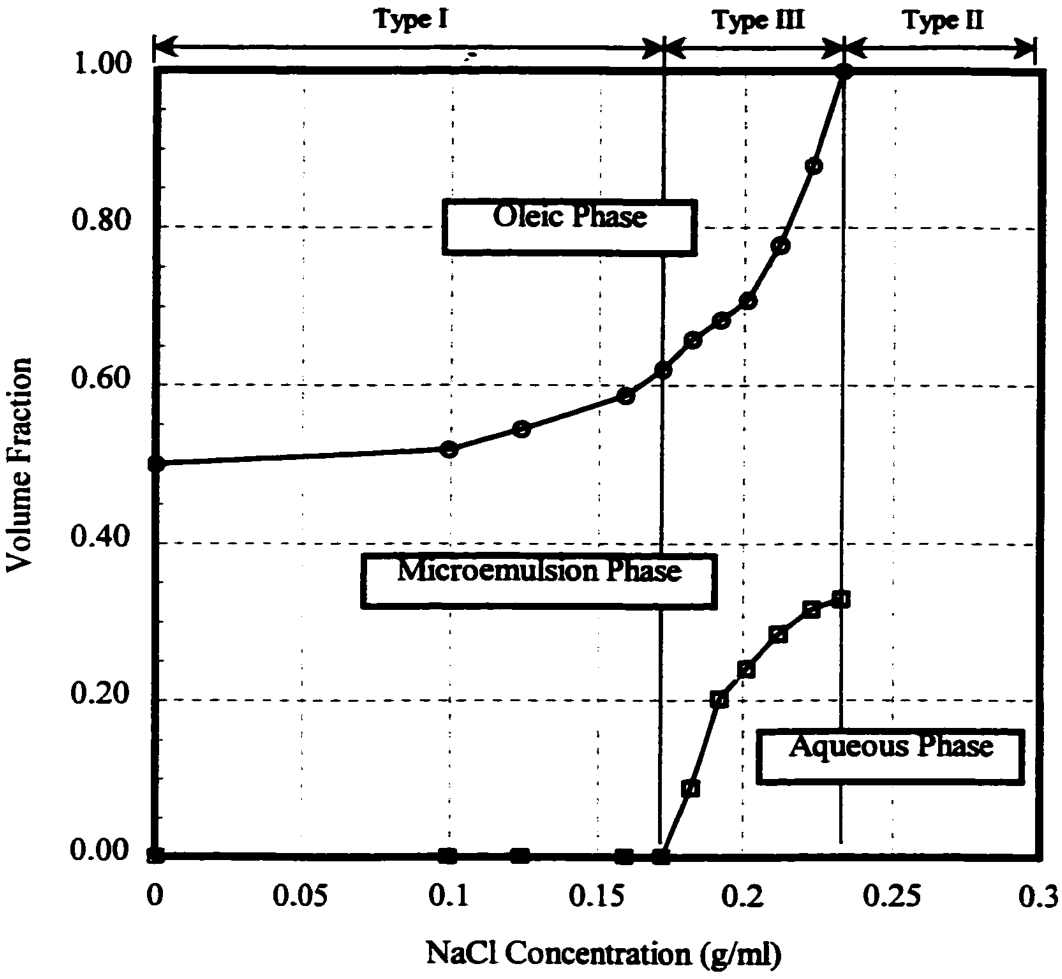

Figure 3.9 Volume Fraction Diagram for CTET, 4 wt% SDS, and 0.3 grams Iso-butanol

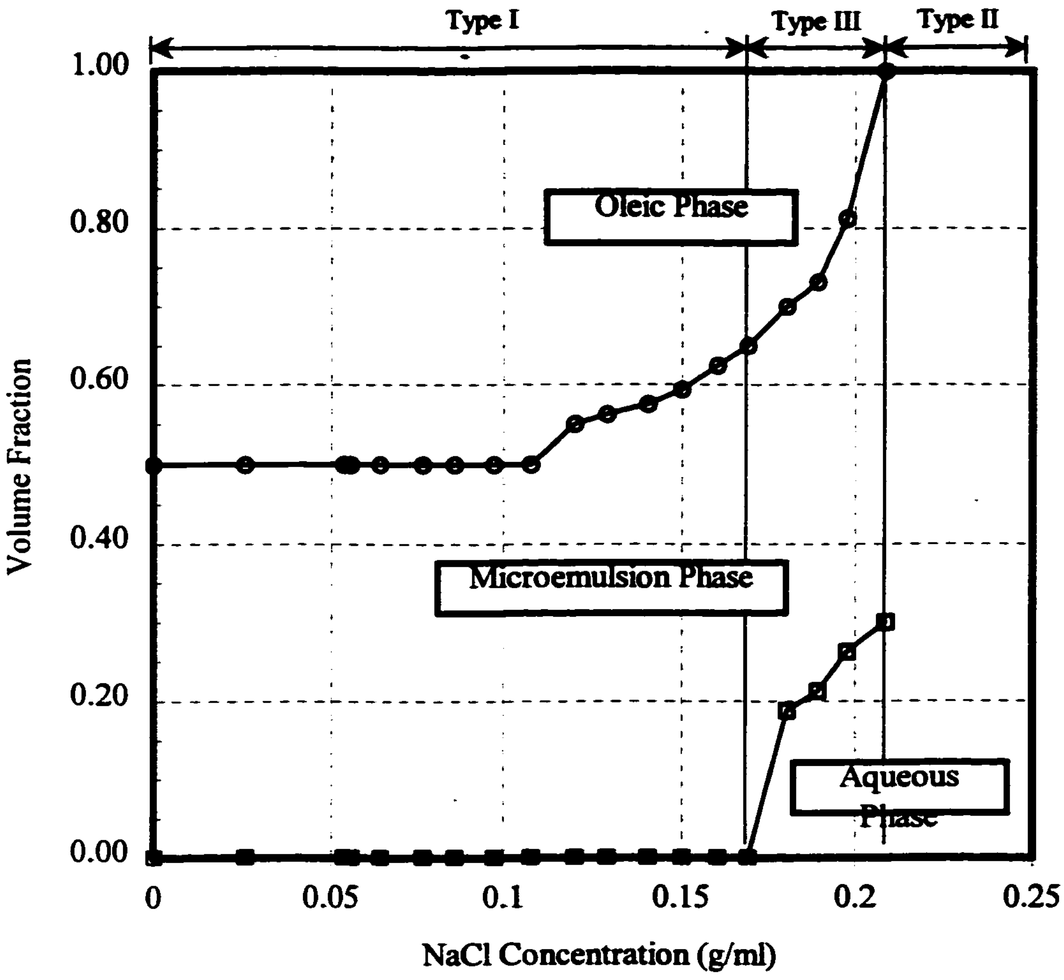

Figure 3.10 Volume Fraction Diagram for TCE, 4 wt% SDS, and 0.3 grams Iso-butanol

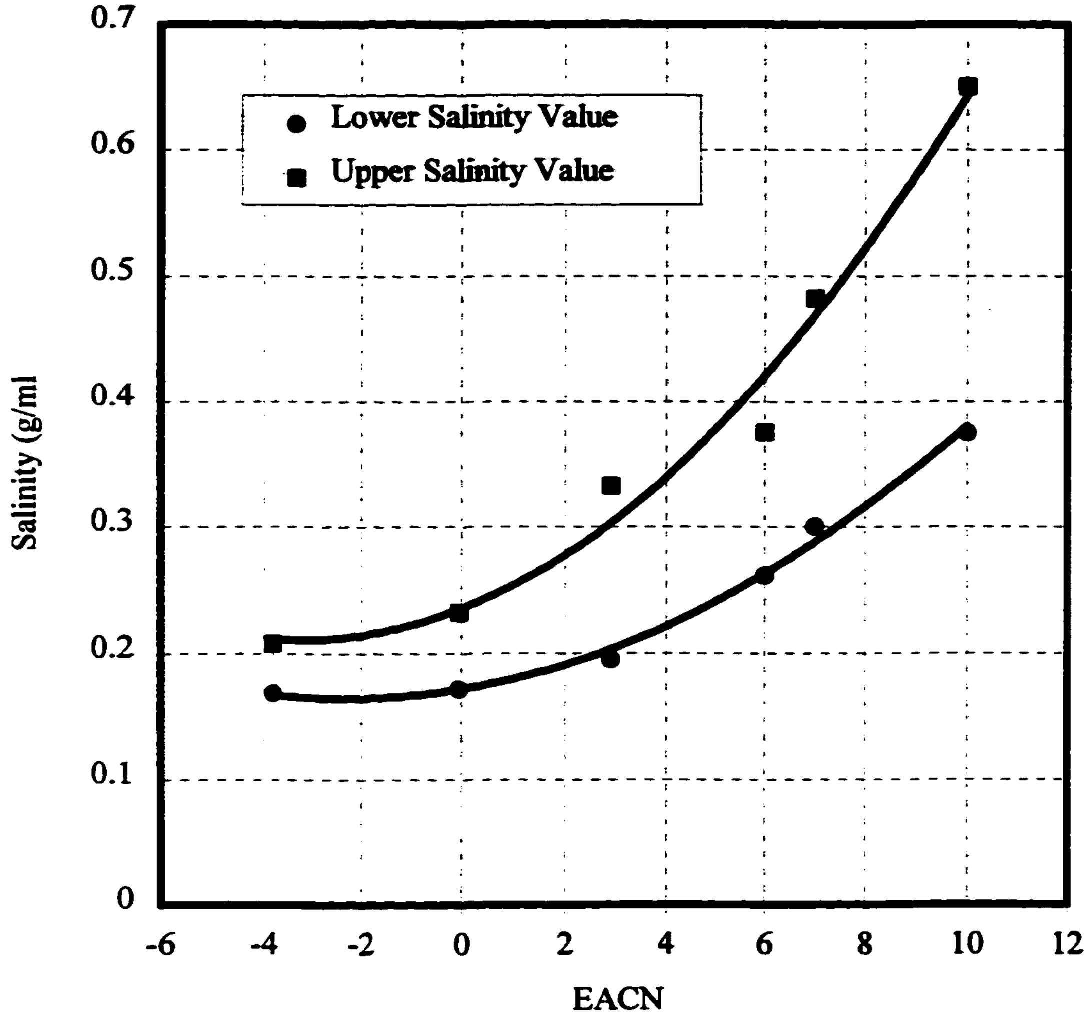

Figure 3.11 Salinity Range Corresponding to Three-Phase Region for 4 wt% SDS with 0.3 grams of Iso-butanol

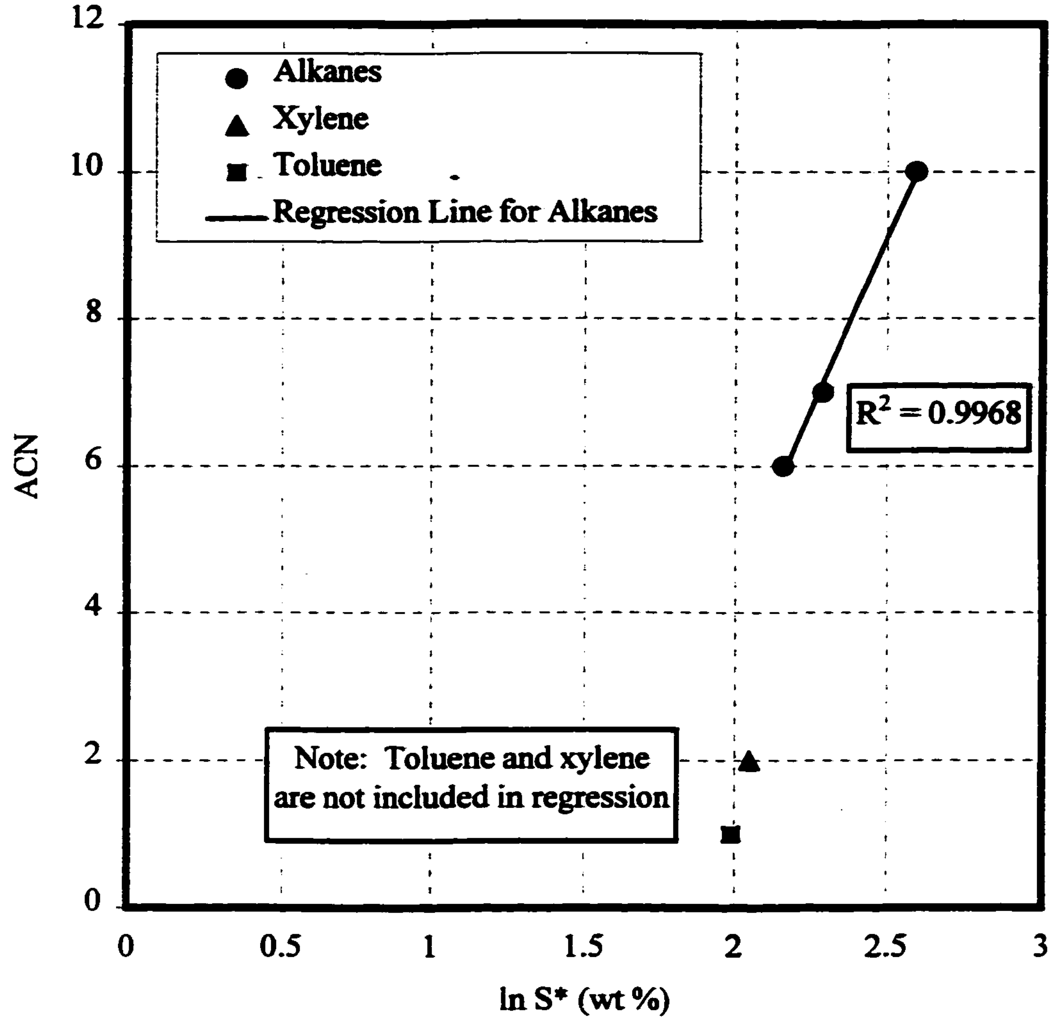

Figure 3.12 ln S* versus ACN for Hydrocarbons using 4 wt% SDS with 0.3 grams of Iso-butanol

For equi-partitioning of a surfactant between the excess oil and aqueous phases, a modified form of the Salager equation (Eq. 3.2) was presented by Baran *et al.* (1994) and can be written as,

$$\ln (S^* / S^{*0}) = k[\mathrm{EACN}^*_{\mathrm{mix}} - N_{\mathrm{min}}] + a(T - 25) + b(A) \qquad (3.6)$$

where S^* is the optimal salinity, S^{*0} is a defined standard state of 1 wt%, $\mathrm{EACN}^*_{\mathrm{mix}}$ is the EACN of the mixture for which an optimum microemulsion was formed, A is the alcohol cosolvent concentration, T is the temperature, and k, a, and b are constants. N_{min} is considered the EACN for which a Winsor Type III system is formed at a standard state of 1 wt% salinity and a temperature of 25°C. If the alcohol concentration is considered a defined standard state, Equation 3.6 reduces to

$$\ln S^* (\mathrm{wt\%}) = k[\mathrm{EACN}^*_{\mathrm{mix}} - N_{\mathrm{min}}] \qquad (3.7)$$

At a standard state of 1 wt% for the salinity, N_{min} must be equal to $\mathrm{EACN}^*_{\mathrm{mix}}$. N_{min} can thus be solved as -14.449 for this particular system and is considered an invariant surfactant property. Equation 3.7 can now be written as

$$\ln S^* (\mathrm{wt\%}) = 0.106[\mathrm{EACN} + 14.449] \qquad (3.8)$$

With this equation, EACN values for the chlorocarbons can be calculated (see Table 3.4). Nearly identical values can be obtained graphically by plotting the ln S* values on the abscissa, determining the intersection with the regression line from the alkanes, and reading the corresponding value on the ordinate (as shown in Figure 3.13).

Table 3.4: Chlorocarbon EACN Values

Chlorocarbon	S*	EACN (Calculated)	EACN (Baran *et al.*, 1994)
Tetrachloroethylene	1.87	3.17	2.90
Carbon Tetrachloride	1.63	0.91	-0.06
Trichloroethylene	1.55	0.16	-3.81

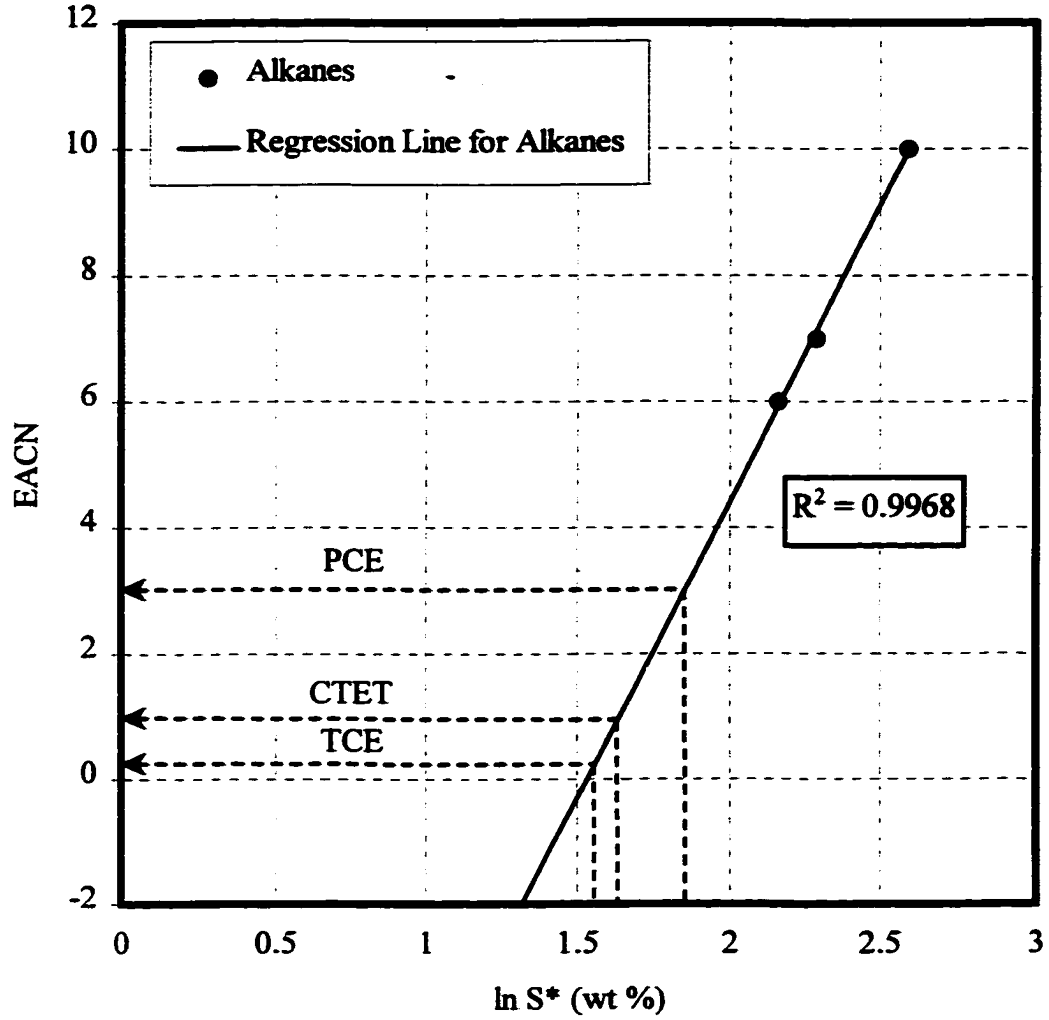

Figure 3.13 Graphical Determination of Chlorocarbon EACNs

Before discussing the values in Table 3.4, it should be noted that negative EACN values have no physical meaning. They are an artifact of the concept and are used to help calculate mixture properties and optimal salinities. The negative values reflect the fact that factors other then molecular weight influence a NAPL's relationship between EACN and ln S* (Baran *et al.*, 1994).

As can be seen from Table 3.4, the EACN for PCE compares favorably with the value determined by Baran *et al.* (1994). The agreement is not as favorable for the other two compounds. A possible explanation for this discrepancy is that SDS may not be a suitable surfactant for chlorocarbons possessing relatively high degrees of polarity. To determine the impact of polarity, the chlorocarbon EACN values from Baran *et al.* (1994) were used to produce Figure 3.14. Note that the least polar of the chlorocarbons, PCE, falls on the regression line for the alkanes. For the other two chlorocarbons, it appears as though the greater the polarity, the greater the deviation from the regression line. This is consistent with findings from Baran *et al.* (1994) who reported that less-polar DNAPLs are more likely to follow classical Winsor-type behavior. Baran *et al.* (1994) concluded that polarity is an important factor, but probably not the only factor, in determining whether a microemulsion can be formed. Further work is needed on the influence of contaminant polarity on microemulsion formation.

Another explanation is that the light alcohol used as the cosolvent may have skewed the salinity values. This was further explored with a subsequent phase behavior experiment using a 4 wt% SDS solution with 0.3 grams of *n*-hexanol (a

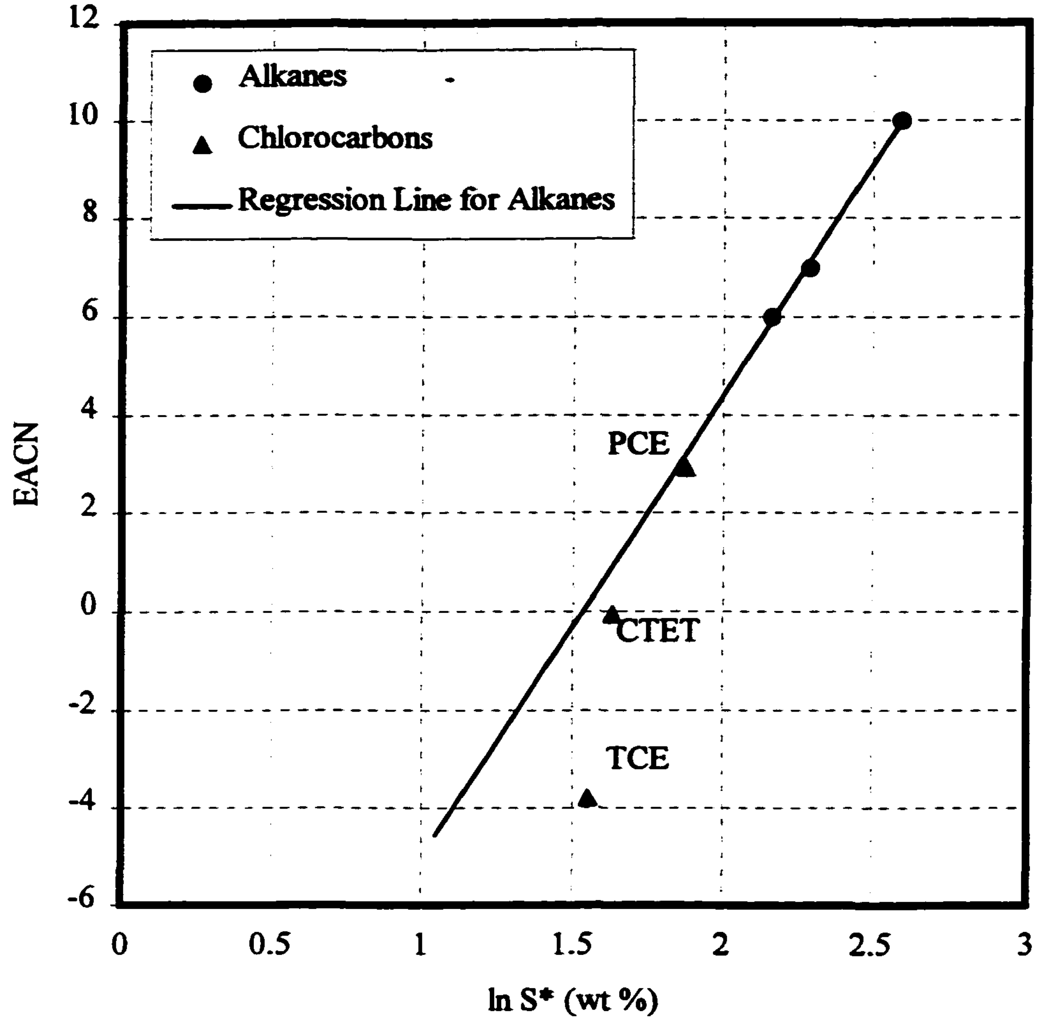

Figure 3.14 ln S* versus EACN for 4 wt% SDS with 0.3 grams of Iso-butanol (using chlorocarbon EACN values from Baran *et al*., 1994)

heavy alcohol) as the cosolvent. However, it was difficult to determine the salinity range for the three-phase region for these systems as they appeared to transition from Type I to Type II very quickly. When present, the three-phase region was relatively thick and the salinity range over which it existed was very small.

3.4.2 Experiments with 2 wt% SDS

The problems encountered with the 4 wt% SDS solution and 0.3 grams of *n*-hexanol may have been caused by high concentrations of the surfactant and the cosolvent. Therefore, a third phase behavior experiment was conducted with a 2 wt% SDS solution and only 0.1 grams of *n*-hexanol. Since heavy alcohols tend to partition preferentially into the oil phase (Salager *et al.*, 1979), adjustments were not made to the salinity values as was the case when the iso-butanol was used.

A distinct three-phase region could be identified only for the alkanes. The results are summarized in Table 3.5, which lists the optimal salinity and the width of the salinity range corresponding to the three-phase region, as well as the natural logarithm of the optimal salinity. The plot of the natural logarithm of the optimal salinities versus the EACNs of the contaminants represents a linear relationship and is shown in Figure 3.15. A least squares regression of the corresponding three data points results in a line with an R^2 value of 0.9996. The resulting k value of 0.098 compares very well with the value of 0.10 reported by Baran *et al.* (1994) for sulfates.

Table 3.5: Results of Phase Behavior Experiments with 2 wt% SDS and 0.1 grams of *n*-Hexanol

Contaminant	Optimum Salinity (grams NaCl)	Salinity Range (grams NaCl)	ln S* (wt %)
Hexane	0.3187	0.2617 - 0.3757	2.16
Heptane	0.3917	0.3009 - 0.4824	2.29
Decane	0.5127	0.3750 - 0.6504	2.59

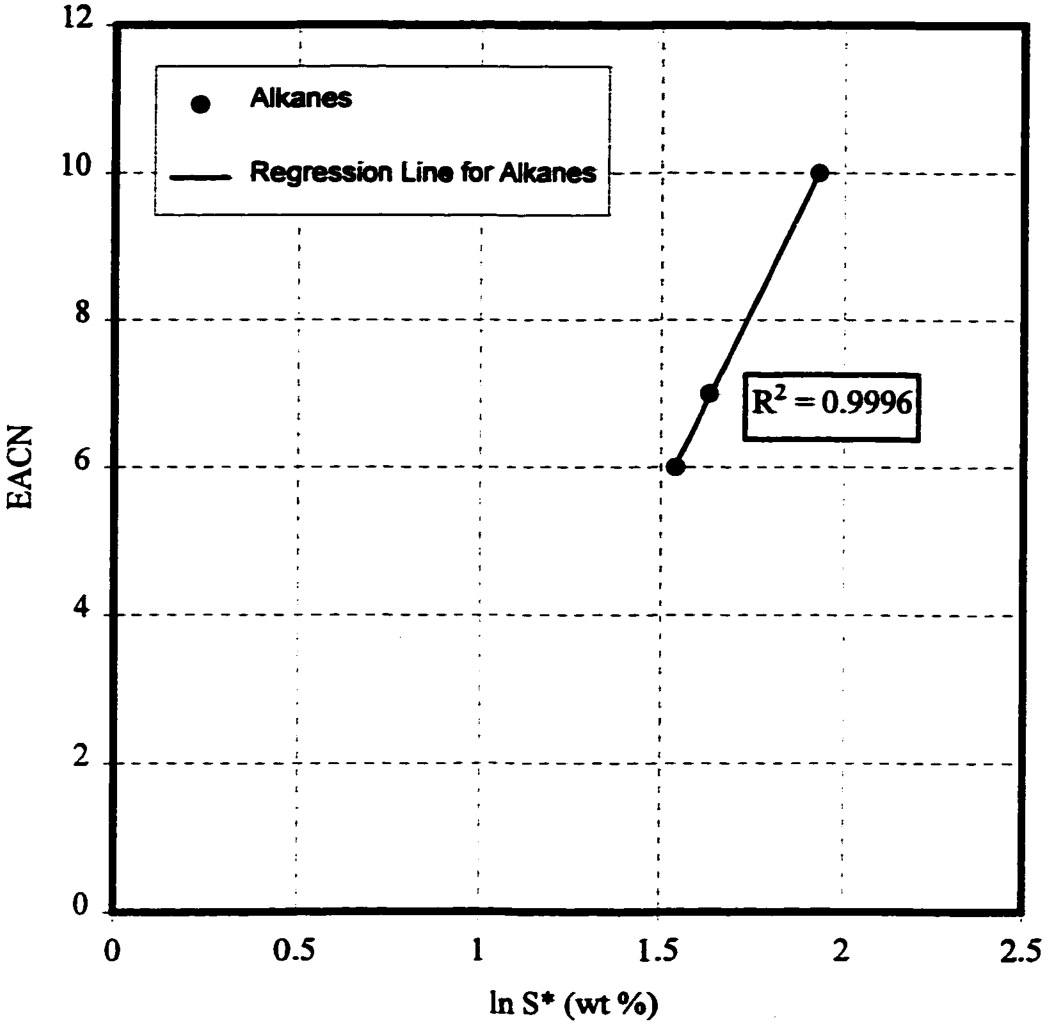

Figure 3.15 ln S* versus EACN for 2 wt% SDS with 0.1 grams of n-Hexanol

During the salinity scans for the alkanes, the lower salinity value for the three-phase region was relatively easy to identify because of the sudden change in the appearance of the contents in the vials. There was also a clear boundary line between the three phases. However, it was more difficult to identify the upper salinity value. The volume of the three-phase region appeared to increase to a certain point at which it remained essentially constant as more sodium chloride was added to the solution. Even when the saturation limit of the system was reached and sodium chloride settled to the bottom of the vials instead of dissolving, the volume of the apparent middle phase remained constant. Therefore, the upper salinity value was chosen as the point at which the middle phase transitioned from a somewhat clear appearance to a cloudy, milky one.

For the aromatics, each compound was mixed with decane with the intention of back-calculating the respective EACN values similar to the method used by Baran *et al.* (1994). However, a middle phase could not be identified from the salinity scans. The systems appeared to transition almost immediately from Type I to Type II. For the same reason, a middle phase could not be determined for the chlorocarbons either.

3.4.3 Experiments with AOT/Tween-80 Mixture

The results of the phase behavior experiments conducted with a 4 wt% surfactant mixture of AOT and Tween-80 (2 wt% each), summarized in Table 3.6, were similar to those for SDS in that a middle phase was achieved only for the

Table 3.6: **Results of Phase Behavior Experiments with 4 wt% AOT/Tween-80**

Contaminant	**Optimum Salinity (grams NaCl)**	**Salinity Range (grams NaCl)**	**ln S* (wt %)**
Hexane	0.1193	0.1102 - 0.1283	1.12
Heptane	0.1452	0.1269 - 0.1635	1.29
Decane	0.2293	0.1854 - 0.2731	1.77

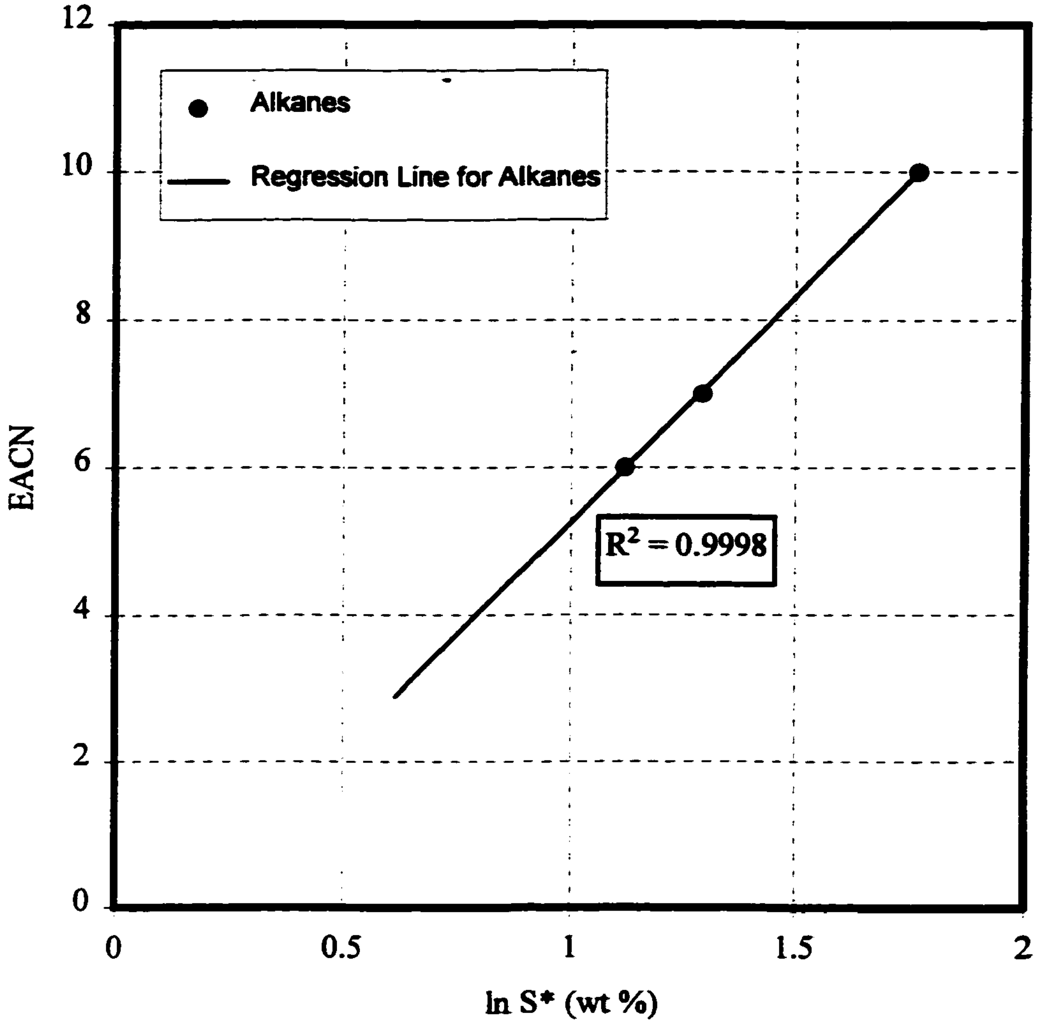

Figure 3.16 ln S* versus EACN for 4 wt% AOT/Tween-80 Mixture

alkanes. The plot of the natural logarithm of the optimal salinities versus the ACNs of the alkanes represents a linear relationship as shown in Figure 3.16. A least squares regression of the corresponding three data points results in a line with an R^2 value of 0.9996. The resulting *k* value of 0.162 compares very well with the value of 0.16 reported by Baran *et al.* (1994) for sulfonated surfactants.

With a *k* value of 0.16, these limited results compare well with previous results reported by other researchers for a sulfonated surfactant. In this particular case, the mixture of the sulfonate with the Tween-80 (a nonionic surfactant) appeared to be dominated by the sulfonate. This is consistent with work by Salager *et al.* (1979) in which they found that the linear relationship occurs over a very limited composition range.

Further research revealed that Shiau (1995) experienced similar difficulties when trying to achieve middle phase microemulsions with edible surfactants (such as Aerosol OT). Instead of the traditional salinity scan to identify an optimal formulation, Shiau (1995) used a surfactant-cosurfactant system. By maintaining a constant Aerosol AOT concentration, and varying the cosurfactant concentration, he was able to achieve a middle phase microemulsion. With surfactant systems considered as the baseline for research involving EACNs, work on surfactant-cosurfactant systems could be considered for the next level of research on the EACN concept.

3.5 Conclusions

The alkanes used in this research were clearly the only compounds for which a three-phase region was identifiable throughout the various surfactant solutions. The linear relationship that existed between the EACNs of the alkanes and the natural logarithm of the system's optimal salinity resulted in *k* values that were in excellent agreement with values previously reported in the literature. Three-phase regions were identifiable for the aromatics and chlorocarbons only with the 4 wt% SDS solution containing 0.3 grams of iso-butanol as a cosolvent. However, the resulting EACNs were inconsistent with values expected from the literature and did not agree with the linear relationship established for the alkanes.

The surfactant solutions appear to be ill-suited for the aromatics and chlorocarbons used in this research for different reasons. It may be more difficult for the aromatics to exhibit classical phase behavior because of their stronger ring structure and multiple double bonds. For the chlorocarbons, it appears as though the more polar the compound, the more difficult it is for the compound to exhibit classical phase behavior. Future research in these areas is necessary to determine causes of the differences and to propose appropriate adjustments to EACN values based on the compounds' respective structures.

CHAPTER 4

RELATIONSHIP BETWEEN ALCOHOL PARTITION COEFFICIENTS AND EACN VALUES

As previously mentioned, one of the objectives of this research was to gain a better understanding of the relationship between the partition coefficient of an alcohol tracer and the composition of the nonaqueous phase liquid (NAPL) with which the tracer is being used. Determining partition coefficients for alcohol tracers used to locate and quantify subsurface NAPL contamination is a reasonably straightforward procedure; the required laboratory work is not extensive and results can be developed in just a few days. However, selecting the appropriate tracers for a given field site usually requires several experiments. A number of tracers are usually evaluated to identify the set of tracers that exhibit the desired partition characteristics. This can be considered time consuming, costly, and difficult to conduct at times (Knaepen *et al.*, 1990; Wang *et al.*, 1998). To improve preliminary planning efforts, the ability to estimate partition coefficients would be useful. The following sections describe the development of an estimation technique that is based upon the equivalent alkane carbon number (EACN) concept.

4.1 Review of Previous Research

This section examines the partition coefficient of an alcohol tracer between the NAPL and groundwater as a function of the EACNs of the NAPL mixture and the alcohol tracer. Similar, yet independent, research was conducted at the University of Texas in which Dwarakanath and Pope (1998) recently reported a bilinear relationship in the form of,

$$\ln K_{i,j} = a + bA_j + cN_i \tag{4.1}$$

where a, b, and c are constants obtained from regression analysis, K is the partition coefficient between alcohol j and NAPL i, A is the EACN of alcohol j, and N is the EACN of NAPL i. The three constants in this equation were determined through linear regression to arrive at the following equation.

$$\log_{10} K_{i,j} = -2.9562 + 0.6548A_j - 0.0505N_i \tag{4.2}$$

The coefficient of determination (R^2) of this regression was reported as 0.984. However, to arrive at this R^2 value, Dwarakanath and Pope (1998) reported that the A_j values of the branched alcohols and the N_i values of the chlorocarbons were adjusted to improve the fit of the original data. No explanation describing what these adjustments were and the rationale for them was provided.

4.2 Experimental Description

4.2.1 Materials

Thirteen alcohol tracers were used with the contaminants previously mentioned to determine partition coefficients under static conditions to ensure equilibrium partitioning. The properties of the alcohols are shown in Table 4.1. Note that the compounds consisted of five linear aliphatic alcohols, four branched alcohols containing one methyl group, and four branched alcohols containing two methyl groups.

Samples were contained in 40-ml glass vials (Fisher Scientific) with screw-top caps and septa. Shaking of the vials was done with a wrist-action shaker manufactured by Burrell Scientific (model 75), while centrifuging was done with an International Clinical Centrifuge (model CL) manufactured by International Equipment Company. A Varian 3300 Gas Chromatograph (GC) was used to analyze the samples. Standard sample bottles from Alltech Associates, Inc., were used for preparing GC samples. Mass measurements were made on an analytical balance (Sartorius) with a capacity of 30/160 grams.

Table 4.1: Properties of Alcohol Tracers (Source: Dean (1992))

Alcohol	Formula	MW[a]	Density[b]
1-propanol[c]	C_3H_8O	60.10	0.8037
1-pentanol[c]	$C_5H_{12}O$	88.15	0.8148
1-hexanol[c]	$C_6H_{14}O$	102.18	0.8186
1-heptanol[c]	$C_7H_{16}O$	116.20	0.8219
2-octanol[c]	$C_8H_{18}O$	130.23	0.8207
4-Methyl-3-Heptanol[c]	$C_8H_{18}O$	130.23	0.8030
6-Methyl-3-Heptanol[c]	$C_8H_{18}O$	130.23	0.8030
2-Methyl-2-Hexanol[c]	$C_7H_{16}O$	116.20	0.8120
2-Methyl-3-Hexanol[c]	$C_7H_{16}O$	116.20	0.8210
2,2-Dimethyl-3-Pentanol[c]	$C_7H_{16}O$	116.20	0.8290
2,4-Dimethyl-3-Pentanol[c]	$C_8H_{18}O$	116.20	0.8290
3,3-Dimethyl-1-Butanol[d]	$C_6H_{14}O$	102.18	0.8147
3,3-Dimethyl-2-Butanol[d]	$C_6H_{14}O$	102.18	0.8185

[a] Molecular Weight (g/mole)
[b] At 20°C for substance relative to water at 4°C
[c] Obtained from Aldrich Chemical
[d] Obtained from Fluka Chemika

4.2.2 Procedures

The procedures used to determine the partition coefficients for the alcohol tracers were consistent with those found in the literature. Tracer stock solutions were prepared by measuring a pre-determined mass of a given alcohol into a 500-ml Erlenmeyer flask containing approximately 100 ml of de-ionized (DI) water. Additional DI water was added to reach the desired concentration levels of approximately 500 mg/l for the less soluble alcohols or 1,000 mg/l for the more soluble ones. Solutions contained either two or three alcohols and were placed on a stirrer for 1 hour.

Approximately 10 grams of each tracer solution were transferred to a 40-ml vial, followed by the addition of 10 grams of LNAPL. Transfers were accomplished with disposable transfer pipettes and mass measurements were taken at each step. The vials were capped with open-topped screw caps containing septa and placed on a wrist-action shaker for 1 hour to equilibrate partitioning of the alcohol between the aqueous and oil phases. Once shaken, vials containing LNAPL were kept inverted. For DNAPLs, the contaminant was placed in the vial first, followed by the tracer solution, and the vial was kept upright. After setting for 24 hours, the vials were placed in a centrifuge for 20 minutes to ensure complete phase separation.

Aqueous aliquots from each vial were then analyzed with a gas chromatograph (GC) to determine the alcohol concentration in the aqueous phase. For DNAPLs, the aliquots were obtained from the middle of the aqueous phase and were transferred to a standard GC sample bottle with a disposable transfer pipette. For inverted LNAPL samples, a syringe was used to puncture the septum and retrieve the aliquots. After each use, the syringe was rinsed twice with de-ionized water to remove trace contaminants. To remove any remaining de-ionized water, the syringe was extracted and plunged down several times. In all cases, triplicate samples were prepared.

The same procedures were used on binary mixtures of compounds to determine if a linear mixing rule was applicable. Complex mixtures, containing three to nine compounds, were then analyzed in a similar fashion. Analysis of all samples was conducted with a Varian GC (model 3300) equipped with a Varian autosampler (model 8100) and a flame ionization detector (FID) using workstation software.

4.3 Data Analysis

The GC results provided the alcohol concentration in the aqueous phase. To determine the alcohol concentration in the oil phase, a mass balance was performed on the mass of tracer initially in the aqueous phase and the mass remaining in the aqueous phase after equilibration. To determine the partition coefficient, the respective masses were converted into concentrations and the following formula used,

$$K = C_{NAPL} / C_{water} \tag{4.3}$$

where K is the partition coefficient, C_{NAPL} is the alcohol concentration in the oil phase, and C_{Water} is the alcohol concentration in the aqueous phase.

4.4 Experimental Results and Discussion

The calibration curves used to determine alcohol concentrations are shown in Figures B.1 through B.13 and summarized in Table B.1 of the Appendix. An implicit assumption in developing the calibration curves was that the partitioning of the alcohols obeyed Raoult's law at dilute concentrations. Determined by a linear regression procedure, the calibration results were based on either five or six data points for each alcohol, and the results were forced to go through the origin. From Table B.1, note that the coefficients of determination range from 0.9938 to 0.9996.

The partition coefficients determined for the alcohols and contaminants used in this research are shown in Table 4.2 (statistical information is shown in Table B.2 of the Appendix). Note that the contaminants are listed from left to right in ascending EACN order. Presented in this manner, a general trend in the data is evident in that the partition coefficients for any given alcohol decrease from left to right. Notable exceptions to this trend include the partition coefficients listed for DCB and CTET and the partition coefficient of 36.01 for 4-methyl-3-heptanol used with PCE. Since triplicate samples were used during the static partition coefficient tests, experimental errors can be safely discounted. These inconsistencies may be related to the chlorine atoms in the contaminants, the molecular structure of the compounds, or inaccurate EACN values. However, until the causes of these inconsistencies are determined in future research, the respective partition coefficients were considered accurate and were included in subsequent analysis efforts.

Table 4.2: Partition Coefficients Between Alcohol Tracers and Various NAPLs

Alcohol	DCB	TCE	CTET	Toluene	*o*-Xylene	PCE	Hexane	Heptane	Decane
Propanol	0.16	0.24	0.08	NA	0.12	0.10	0.04	0.03	0.02
Pentanol	2.10	3.40	1.55	2.54	2.06	0.95	0.57	0.53	0.37
Hexanol	12.11	12.78	5.82	11.62	10.07	6.16	NA	2.86	1.59
Heptanol	NA	55.72	34.19	32.66	28.46	21.06	12.36	NA	8.47
Octanol	165.96	260.38	147.34	144.02	136.73	113.75	57.92	52.86	40.74
2,2-Dimethyl-3-Pentanol	36.95	55.59	30.33	37.16	NA	23.33	14.54	13.62	10.37
2,4-Dimethyl-3-Pentanol	28.15	58.39	30.51	35.13	NA	23.63	15.07	12.60	11.47
2-Methyl-2-Hexanol	16.62	30.75	14.18	17.17	12.11	9.75	NA	8.36	4.45
2-Methyl-3-Hexanol	34.18	55.31	35.43	43.70	32.63	31.28	NA	16.32	10.95
3,3-Dimethyl-1-Butanol	33.07	58.15	NA	36.27	32.63	NA	13.43	11.56	10.91
3,3-Dimethyl-2-Butanol	7.85	13.26	7.85	13.80	8.09	4.19	3.32	4.62	2.60
4-Methyl-3-Heptanol	170.18	326.70	274.24	229.20	201.60	36.01	104.55	NA	51.46
6-Methyl-2-Heptanol	104.96	191.13	147.13	133.82	104.91	71.16	31.78	NA	26.73

4.4.1 Hydrocarbons and Linear Alcohols

Shown in Figure 4.1, a plot of the logarithm of the partition coefficients for the linear alcohols versus the hydrocarbon EACNs revealed a linear relationship. The slopes of the regression lines vary from -0.1538 to -0.2298 with an average of -0.1973 and a standard deviation of 0.0389. From the regression results summarized in Table 4.3, note that the coefficients of determination range from 0.9206 to 0.9968.

The data suggests that a linear relationship may also exist between the type of alcohol and the partitioning coefficients. To explore this possibility, the ACN concept was applied to assign an alcohol carbon number, hereby designated as A_cCN to differentiate it from ACN, to the linear alcohols based on the number of carbon atoms in the alcohol's molecular structure (see Table 4.4). Shown in Figure 4.2, a plot of the logarithm of the partition coefficients versus the alcohol A_cCN s revealed another linear relationship. Similar to Figure 4.1, the slopes range from 1.3147 to 1.5187 with an average of 1.4400 and a standard deviation of 0.0849. The regression results are summarized in Table 4.5; note that the R^2 values are all above 0.99.

The independent linear relationships established above suggest a bilinear relationship. When multiple regression was subsequently performed on the combined data, a strong bilinear relationship ($R^2 = 0.9944$) was discovered of the form,

$$\log_{10} K_{i,j} = -2.7607 + 0.6338A_j - 0.0840N_i \tag{4.4}$$

where A_j is the EACN of alcohol *j* and N_i is the EACN of NAPL *i*.

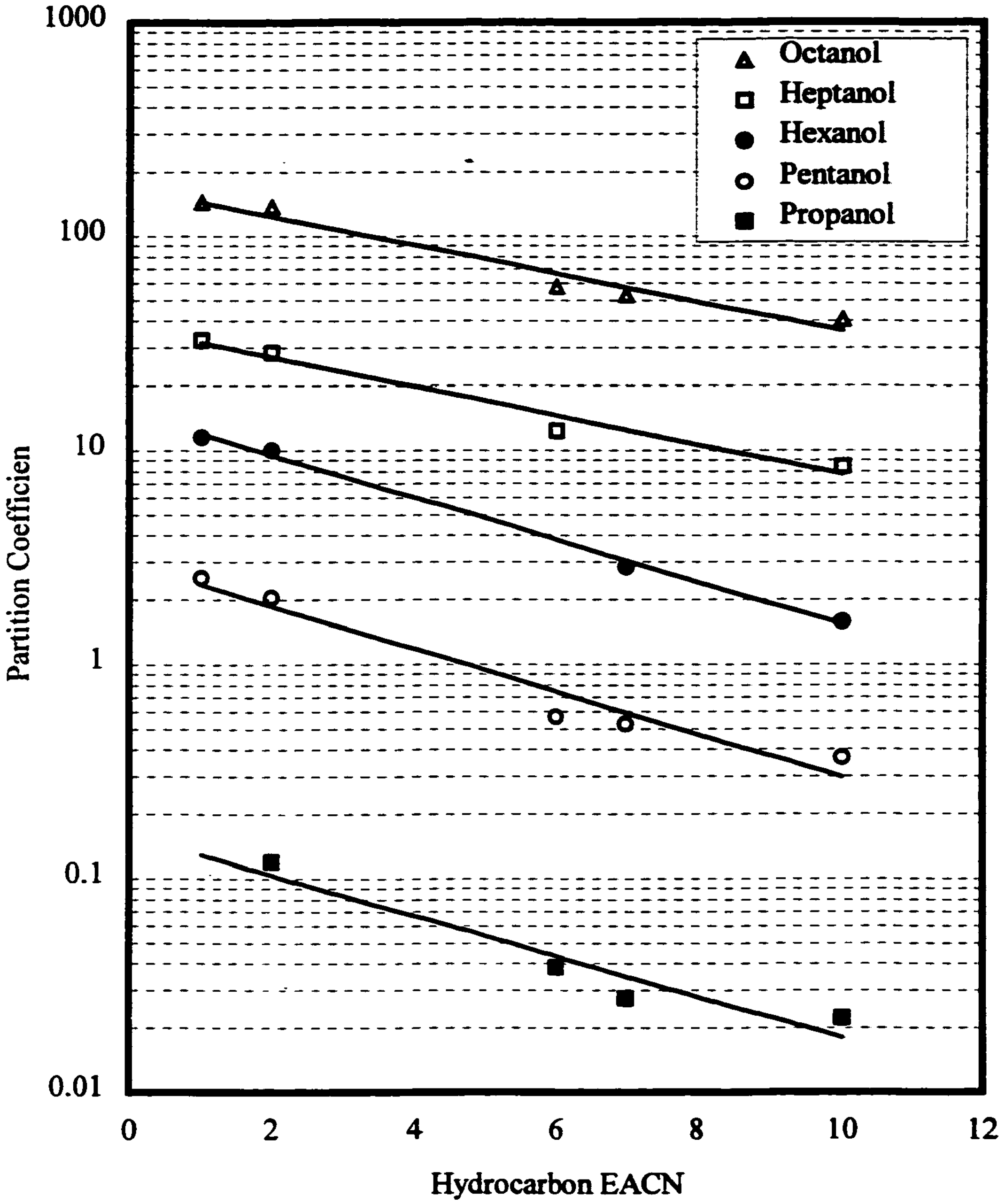

Figure 4.1 Relationship Between Hydrocarbon EACN and Partition Coefficient for the Indicated Linear Alcohols

Table 4.3: **Linear Regression Results for Partition Coefficients and Hydrocarbon EACN Values for the Indicated Linear Alcohols**

Alcohol	**Regression Equation**	R^2
Octanol	$\log_{10} K = 2.2254 - 0.1538N_i$	0.9617
Heptanol	$\log_{10} K = 1.5690 - 0.1561N_i$	0.9713
Hexanol	$\log_{10} K = 1.1769 - 0.2281N_i$	0.9968
Pentanol	$\log_{10} K = 0.4724 - 0.2298N_i$	0.9515
Propanol	$\log_{10} K = -0.7926 - 0.2185N_i$	0.9206

Table 4.4: EA_cCN Values Assigned to Linear Alcohols

Alcohol	Formula	A_cCN
1-Propanol	C_3H_8O	3
1-Pentanol	$C_5H_{12}O$	5
1-Hexanol	$C_6H_{14}O$	6
1-Heptanol	$C_7H_{16}O$	7
1-Octanol	$C_8H_{18}O$	8

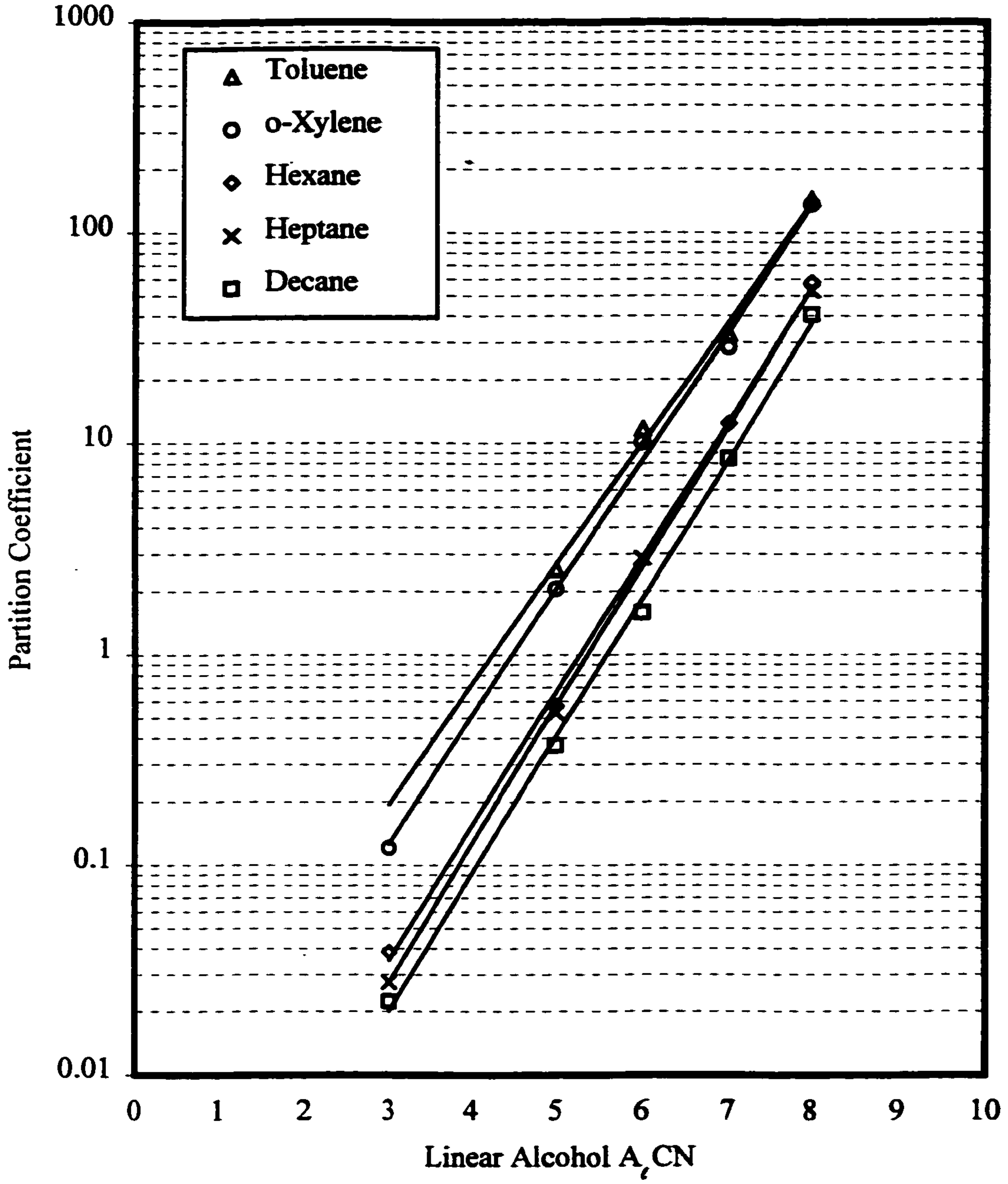

Figure 4.2 Relationship Between Alcohol $A_\ell CN$ and Partition Coefficient for the Indicated Hydrocarbons

Table 4.5: **Linear Regression Results for Partition Coefficients and Linear Alcohol EA$_c$CN Values for the Indicated Hydrocarbons**

Alcohol	Regression Equation	R^2
Toluene	$\log_{10} K = -2.4202 + 1.3147A_j$	0.9949
o-Xylene	$\log_{10} K = -2.7212 + 1.3946A_j$	0.9977
Hexane	$\log_{10} K = -3.3979 + 1.4681A_j$	0.9989
Heptane	$\log_{10} K = -3.5229 + 1.5187A_j$	0.9995
Decane	$\log_{10} K = -3.6990 + 1.5038A_j$	0.9985

4.4.2 Chlorocarbons and Linear Alcohols

Since the bilinear relationship discovered in the previous section includes only hydrocarbons, the analysis was expanded to include chlorocarbons. The chlorocarbon EACN values, shown in Table 4.6, were obtained from Baran *et al.* (1994). As shown in Figure 4.3, a plot of the logarithm of the partition coefficients for the linear alcohols versus the chlorocarbon EACNs revealed a linear relationship similar to that found for the hydrocarbons. The slopes of the lines are similar, ranging from –0.0751 to –0.1444 with an average of –0.1124 and a standard deviation of 0.0268. However, the R^2 values in Table 4.7 range from 0.5722 to 0.9957, indicating more variability of the data about the regression lines. The increased variability could be attributed to the limited number of data points or the inconsistencies noted in the previous section regarding the partition coefficients for alcohols used with DCB and CTET.

When the logarithms of the partition coefficients for the chlorocarbons are plotted against the A_cCNs of the linear alcohols as shown in Figure 4.4 and summarized in Table 4.8, the linear relationship is much stronger. The slopes of the lines range from 1.3911 to 1.5065 with an average of 1.4286 and a standard deviation of 0.0528. Additionally, the coefficients of determination are all above 0.99. When multiple regression was performed on the combined data for chlorocarbons and linear alcohols, the bilinear relationship ($R^2 = 0.9949$) was of the form,

$$\log_{10} K_{i,j} = -2.8660 + 0.6266A_j - 0.0613N_i. \tag{4.5}$$

Table 4.6: Chlorocarbon EACN Values

Compound	EACN Baran *et al.* (1994)
TCE	-3.81
DCB	-4.89
CTET	-0.06
PCE	2.90

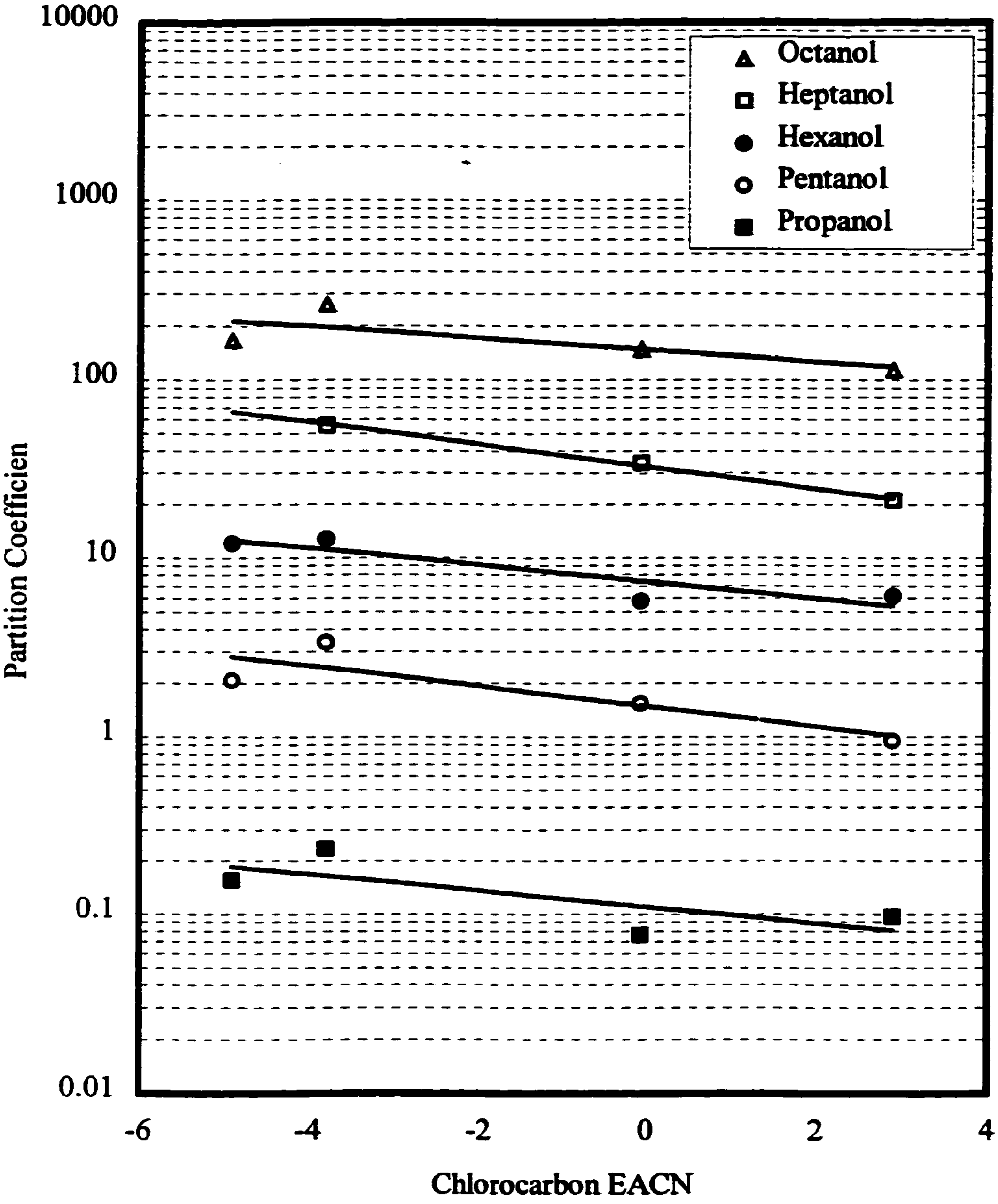

Figure 4.3 Relationship Between Chlorocarbon EACN and Partition Coefficient for the Indicated Linear Alcohols

Table 4.7: **Linear Regression Results for Partition Coefficients and Chlorocarbon EACN Values for the Indicated Linear Alcohols (using EACN values from Baran *et al.* (1994))**

Alcohol	Regression Equation	R^2
Octanol	$\log_{10} K = 2.1672 - 0.0751 N_i$	0.6004
Heptanol	$\log_{10} K = 1.5142 - 0.1444 N_i$	0.9957
Hexanol	$\log_{10} K = 0.8678 - 0.1073 N_i$	0.8195
Pentanol	$\log_{10} K = 0.1720 - 0.1312 N_i$	0.7665
Propanol	$\log_{10} K = -0.9442 - 0.1039 N_i$	0.5722

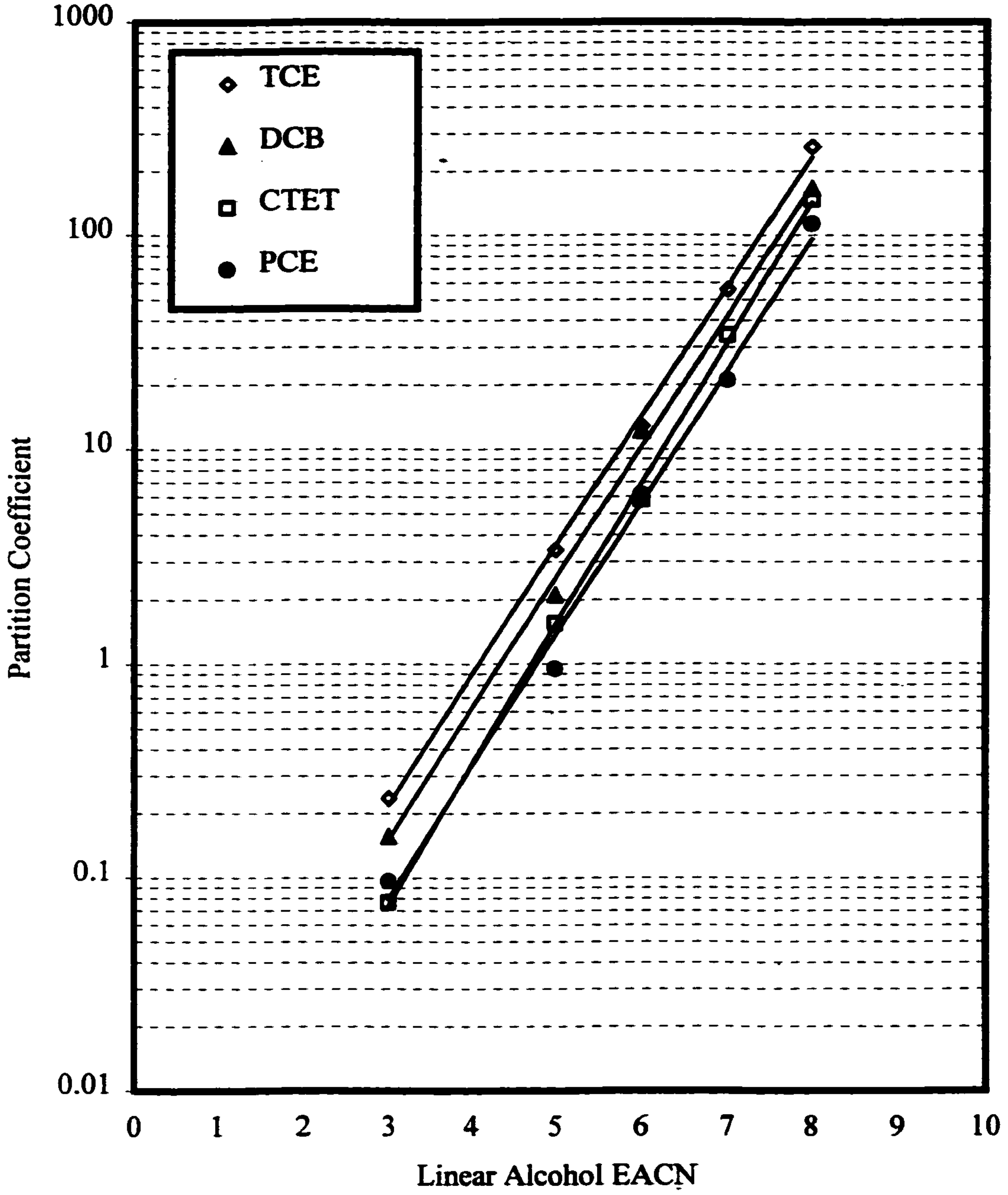

Figure 4.4 Relationship Between Alcohol $EA_{\ell}CN$ and Partition Coefficient for the Indicated Chlorocarbons

Table 4.8: **Linear Regression Results for Partition Coefficients and Linear Alcohol EA$_c$CN Values for the Indicated Chlorocarbons**

Alcohol	**Regression Equation**	R^2
TCE	$\log_{10} K = -2.4685 + 1.3911A_j$	0.9987
DCB	$\log_{10} K = -2.6383 + 1.4028A_j$	0.9975
CTET	$\log_{10} K = -3.0969 + 1.5065A_j$	0.9987
PCE	$\log_{10} K = -2.9208 + 1.4138A_j$	0.9924

4.4.3 Combined Contaminants and Linear Alcohols

Since the hydrocarbons and the chlorocarbons exhibited similar linear relationships, the data was combined. A plot of the partition coefficients versus the EACNs of the nine contaminants is shown in Figure 4.5 with the regression results summarized in Table 4.9. As expected, the linear relationship remained. The slopes of the lines range from –0.1188 to –0.1516 with an average of –0.1393 and a standard deviation of 0.0127. The coefficients of determination range from 0.8102 to 0.9784. This wide range of values can be partially attributed to the inconsistencies previously noted for the partition coefficients relating to DCB and CTET. In fact, if these data points are omitted, the coefficients of determination improve and range from 0.8872 to 0.9768. For the current research, and until further research provides an explanation for the inconsistencies, the data points will be included in the analysis.

After the chlorocarbons were included with the hydrocarbons and linear alcohols, multiple regression was performed on the combined data. This analysis reinforced the strong bilinear relationship represented by Equation 4.2 and resulted in a very similar equation of the form,

$$\log_{10} K_{i,j} = -2.9104 + 0.6339A_j - 0.0604N_i \tag{4.6}$$

The coefficient of determination for this equation is 0.9894.

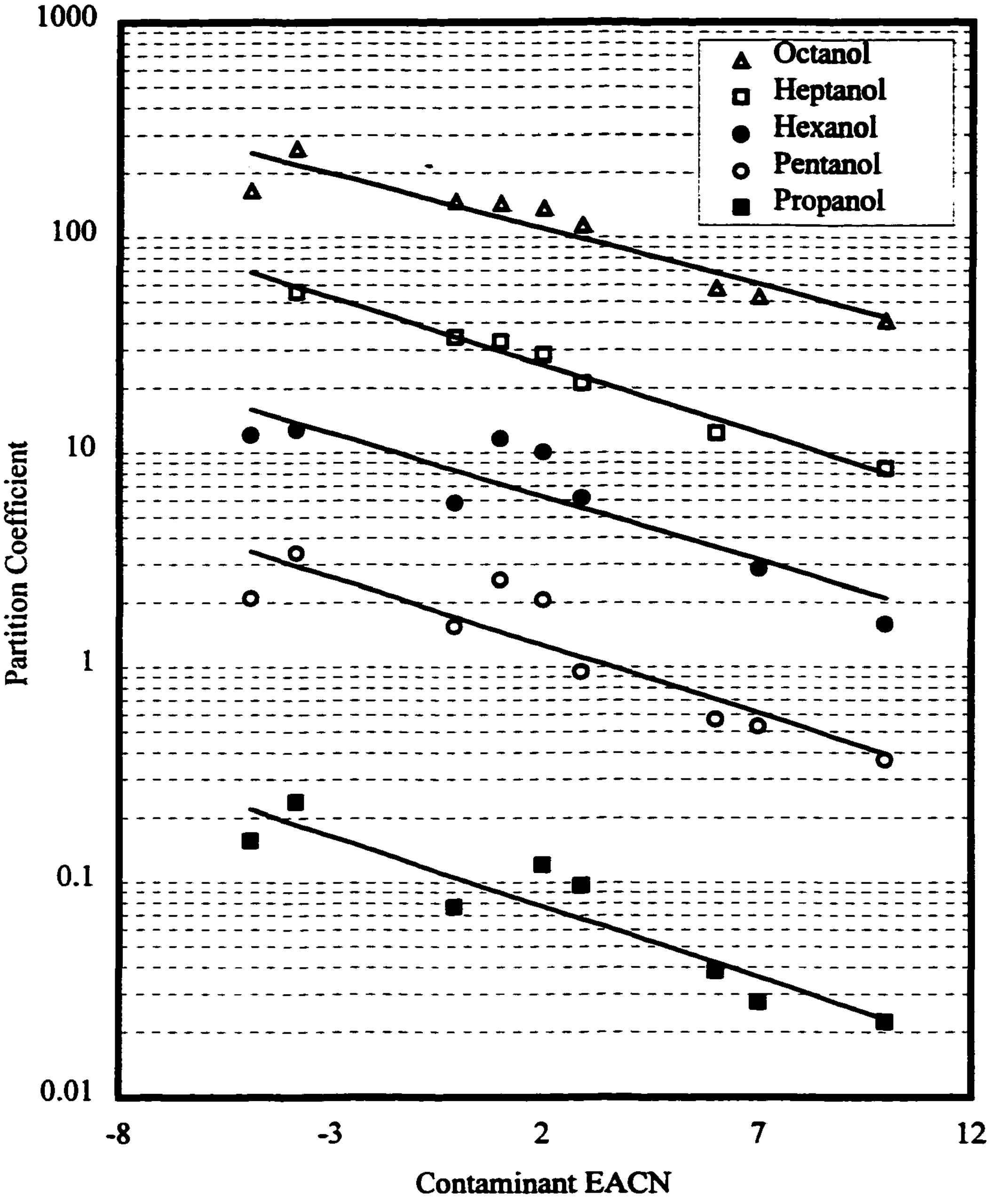

Figure 4.5 Relationship Between Contaminant EACN and Partition Coefficient for the Indicated Linear Alcohols

Table 4.9: **Linear Regression Results for Partition Coefficients and Contaminant EACN Values for the Indicated Linear Alcohols**

Alcohol	Regression Equation	R^2
Octanol	$\log_{10} K = 2.1433 - 0.1188N_i$	0.8897
Heptanol	$\log_{10} K = 1.5315 - 0.1442N_i$	0.9784
Hexanol	$\log_{10} K = 0.9136 - 0.1365N_i$	0.8102
Pentanol	$\log_{10} K = 0.2291 - 0.1455N_i$	0.8166
Propanol	$\log_{10} K = -0.9805 - 0.1516N_i$	0.8644

4.4.4 Determination of EACNs for Branched Alcohols

To incorporate the partition coefficients for the branched alcohols in this analysis, a method must be found to determine their respective EA$_C$N values. If the linear relationship established for the contaminants and linear alcohols is assumed to apply to branched alcohols, then the EA$_C$Ns can be obtained graphically by using the partition coefficients of the branched alcohols with Figures 4.2 and 4.4. The EA$_C$N values for the branched alcohols can also be determined mathematically from the equations shown in Tables 4.5 and 4.8. With either method, a number of EA$_C$N values will be determined for each branched alcohol. These values can be averaged to arrive at an overall EA$_C$N for each respective branched alcohol. Using the equations, the resulting EA$_C$Ns calculated for the branched alcohols are shown in Table 4.10 along with the appropriate statistical data.

The molecular structures of the branched alcohols were examined (see Table 4.11) and compared with the EA$_C$N values shown in Table 4.10. Four of the compounds (2,2-dimethyl-3-pentanol, 2,4-dimethyl-3-pentanol, 2-methyl-3-hexanol, and 3,3-dimethyl-2-butanol) have EA$_C$N values relatively close to their number of carbon atoms. For these compounds, it is interesting to note that the OH groups are near the center of the carbon chain.

The other four alcohols (2-methyl-2-hexanol, 4-methyl-3-heptanol, 3,3-dimethyl-1-butanol, and 6-methyl-2-heptanol) have EA$_C$N values that differ from the number of carbon atoms. For these compounds, the OH groups are located at least

Table 4.10: Calculated EA$_c$CN Values for Branched Alcohols

Alcohol	Number of Data Points	Average EACN	Standard Deviation	95% Interval
2,2-Dimethyl-3-Pentanol	8	7.04	0.01	7.03 – 7.05
2,4-Dimethyl-3-Pentanol	8	7.02	0.17	6.90 – 7.14
2-Methyl-2-Hexanol	8	6.47	0.16	6.36 – 6.58
2-Methyl-3-Hexanol	8	7.08	0.14	6.98 – 7.18
3,3-Dimethyl-1-Butanol	7	7.02	0.13	6.92 – 7.12
3,3-Dimethyl-2-Butanol	8	6.04	0.18	5.92 – 6.16
4-Methyl-3-Heptanol	7	8.30	0.16	8.18 – 8.42
6-Methyl-2-Heptanol	8	7.83	0.12	7.75 – 7.91

Table 4.11: Alcohol Tracer Structures

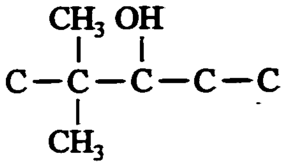 $\mathrm{C-\underset{CH_3}{\overset{CH_3}{C}}-\overset{OH}{C}-C-C}$ 2,2-Dimethyl-3-Pentanol	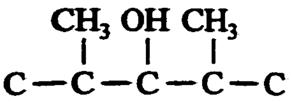 $\mathrm{C-\overset{CH_3}{C}-\overset{OH}{C}-\overset{CH_3}{C}-C}$ 2,4-Dimethyl-3-Pentanol
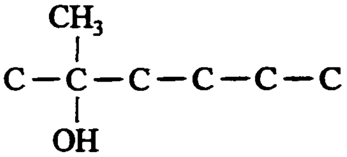 $\mathrm{C-\underset{OH}{\overset{CH_3}{C}}-C-C-C-C}$ 2-Methyl-2-Hexanol	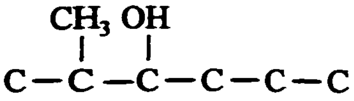 $\mathrm{C-\overset{CH_3}{C}-\overset{OH}{C}-C-C-C}$ 2-Methyl-3-Hexanol
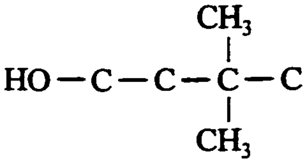 $\mathrm{HO-C-C-\underset{CH_3}{\overset{CH_3}{C}}-C}$ 3,3-Dimethyl-1-Butanol	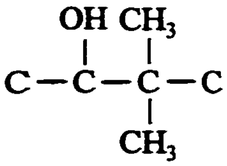 $\mathrm{C-\overset{OH}{C}-\underset{CH_3}{\overset{CH_3}{C}}-C}$ 3,3-Dimethyl-2-Butanol
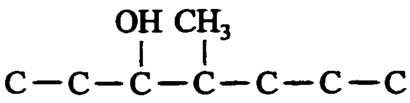 $\mathrm{C-C-\overset{OH}{C}-\overset{CH_3}{C}-C-C-C}$ 4-Methyl-3-Heptanol	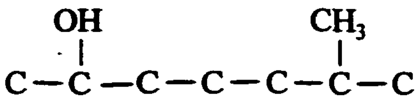 $\mathrm{C-\overset{OH}{C}-C-C-C-\overset{CH_3}{C}-C}$ 6-Methyl-2-Heptanol

one carbon atom from the center of the carbon chain. The OH group is considered to be balanced by a methyl group when both groups are bonded to the same carbon atom or are equi-distant from the center of the carbon chain (i.e., they mirror each other). The EA_cCN values are less than the number of carbons when the OH group is balanced by a methyl group and greater when not balanced. Therefore, the location of the OH group appears to be a critical factor in the EA_cCN value, with its importance possibly diminishing as the carbon chain increases. Future research is needed to determine the implications of OH group locations.

The branched alcohols containing one methyl group and those containing two methyl groups were analyzed separately using linear regression. The results are shown in Table 4.12 (data sets 4 and 5) along with the regression equations developed for the linear alcohols (data sets 1 through 3) for comparison purposes. The high degree of correlation was expected for the branched alcohols as their EACNs were obtained through an "averaged fitting" procedure. A final multiple regression analysis was conducted on the entire data set (all alcohols and all contaminants) and the results are also shown in Table 4.12 (data set 6). The results were nearly identical regardless of which data set was used, an indication of the strong bilinear relationship and the universal nature of the equations.

Table 4.12: **Multiple Regression Analyses Results**

Data Set	Regression Equation	R^2
1	$\log_{10} K_{i,j} = -2.7607 + 0.6338A_j - 0.0840N_i$	0.9944
2	$\log_{10} K_{i,j} = -2.8660 + 0.6266A_j - 0.0613N_i$	0.9949
3	$\log_{10} K_{i,j} = -2.9104 + 0.6339A_j - 0.0604N_i$	0.9894
4	$\log_{10} K_{i,j} = -2.6664 + 0.6135A_j - 0.0683N_i$	0.9703
5	$\log_{10} K_{i,j} = -2.6503 + 0.6070A_j - 0.0664N_i$	0.9558
6	$\log_{10} K_{i,j} = -2.7507 + 0.6271A_j - 0.0746N_i$	0.9910

1 - Linear alcohols / hydrocarbons
2 – Linear alcohols / chlorocarbons
3 - Linear alcohols / all contaminants
4 - Branched alcohols with one methyl group / all contaminants
5 - Branched alcohols with two methyl groups / all contaminants
6 - All alcohols / all contaminants

Figures 4.6 through 4.8 compare the partition coefficients measured during the experiments with those calculated using the final regression equation (data set 6). The excellent agreement between the experimental and calculated values indicated by the figures was expected because of the high degree of correlation of the regression equation ($R^2 = 0.991$). From Figure 4.8, it was interesting to note that the regression equation tended to overestimate the partition coefficient measured experimentally for the chlorocarbons, with the amount of overestimation appearing to increase as the polarity of the contaminant increased (i.e., EACN decreased). Future research is needed to quantify the extent of the impact of polarity and the resulting impact on the determination of EACNs for chlorocarbons.

4.4.5 Mixtures and Partition Coefficients

For the relationship between partition coefficients and EACNs to be useful, it must be applicable to mixtures and follow the linear mixing rule (on a mole fraction basis). Therefore, various binary mixtures of the compounds were prepared and the partition coefficient for respective alcohols was determined. Plots of the alcohol partition coefficients for the mixtures as a function of mole fraction are shown in Figures 4.9 through 4.13. The excellent linear relationship indicated in these plots provides ample evidence that the mixing rule is applicable on a mole fraction basis.

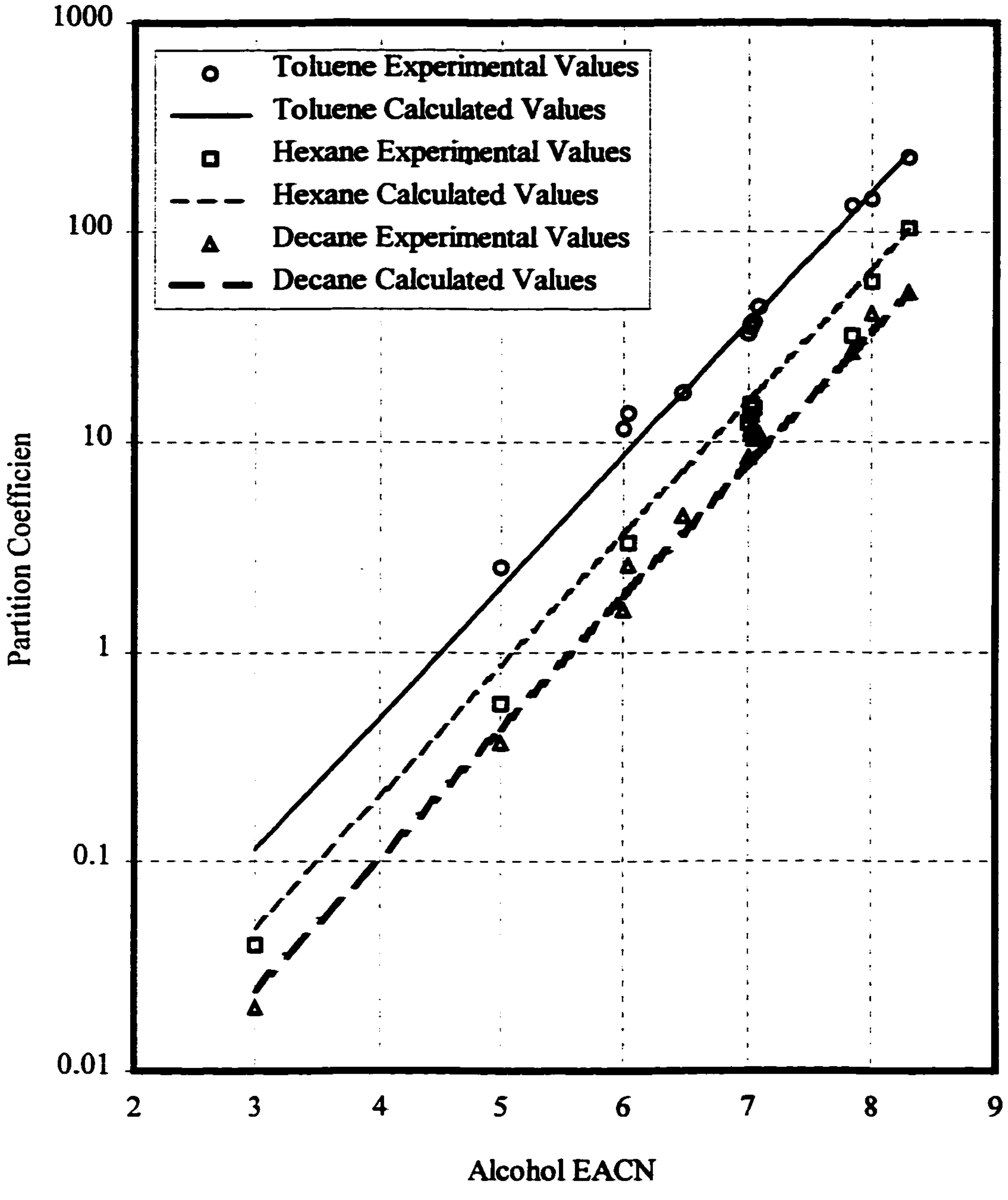

Figure 4.6 Comparison of Experimental and Calculated Partition Coefficients for Toluene, Hexane, and Decane

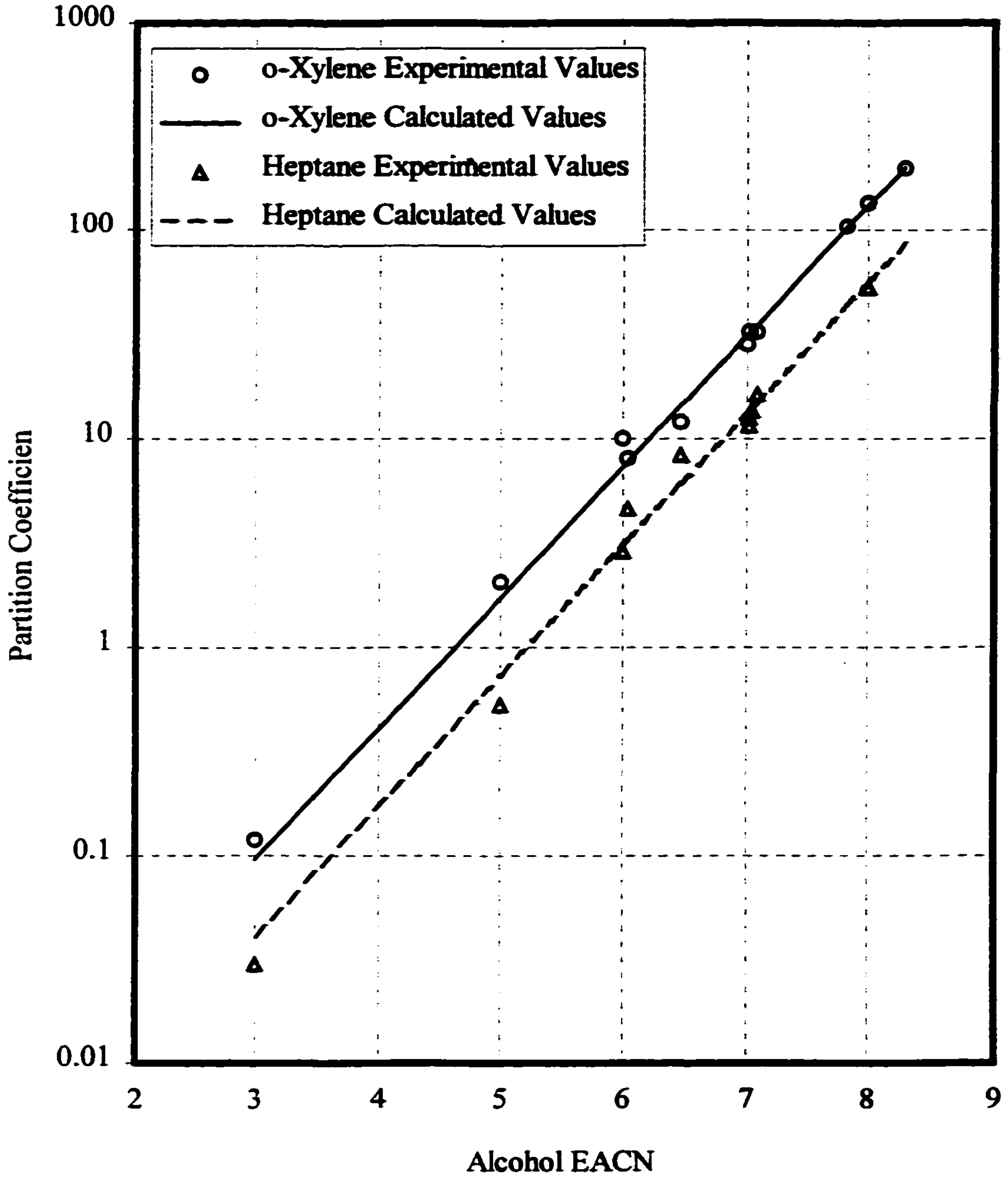

Figure 4.7 Comparison of Experimental and Calculated Partition Coefficients for *o*-Xylene and Heptane

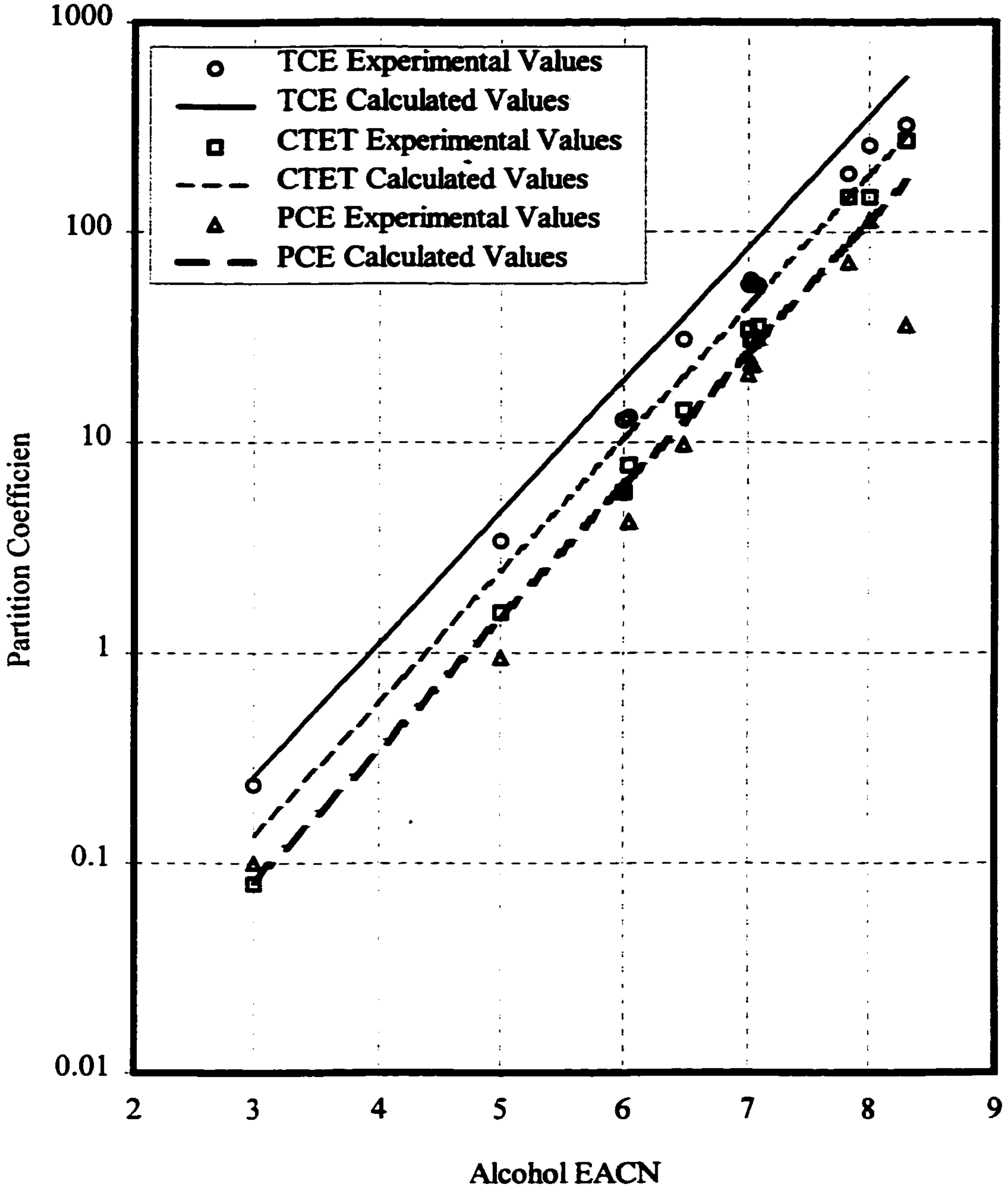

Figure 4.8 Comparison of Experimental and Calculated Partition Coefficients for PCE, CTET, and TCE

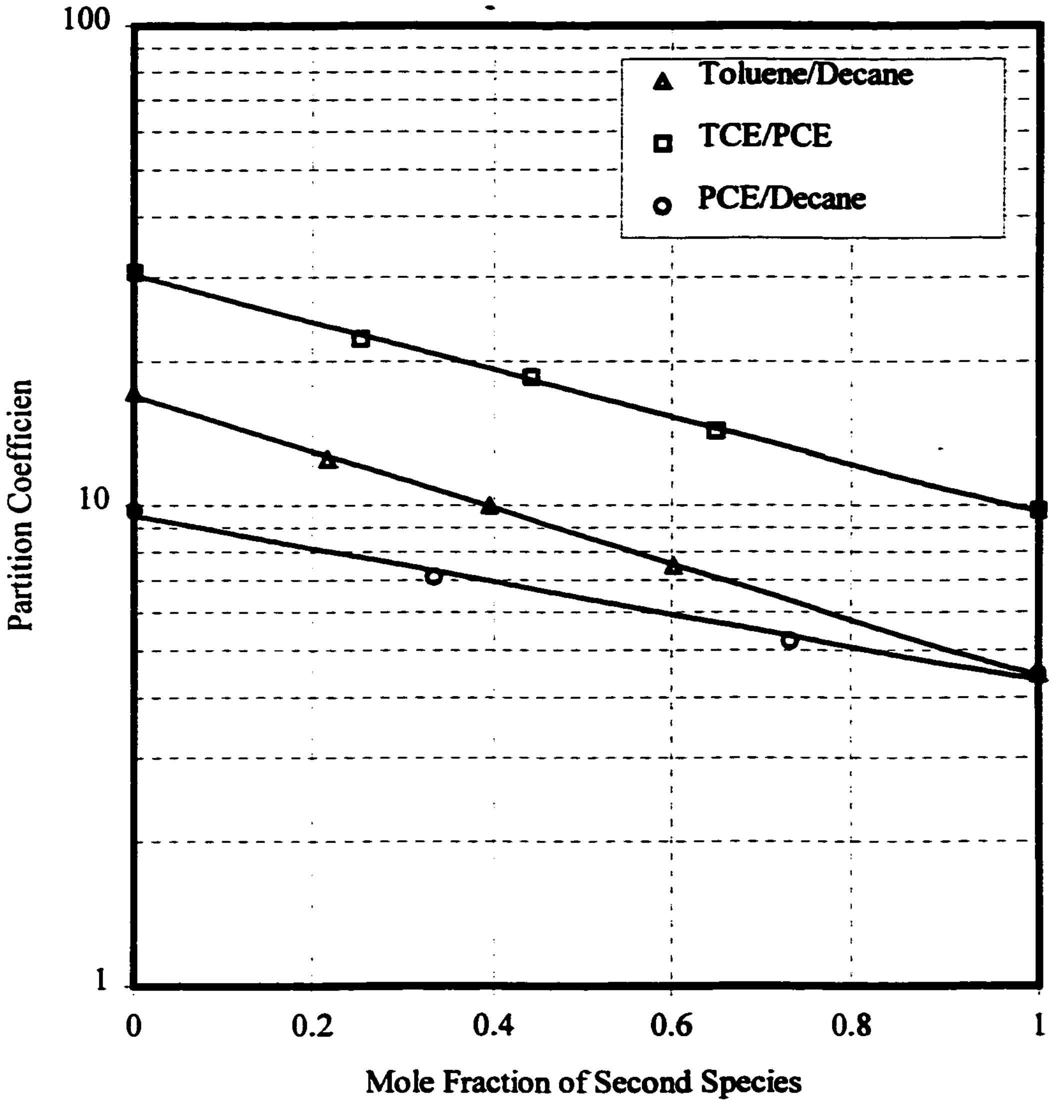

Figure 4.9 Mixing Effect on Partition Coefficient for 2-Methyl-2-Hexanol

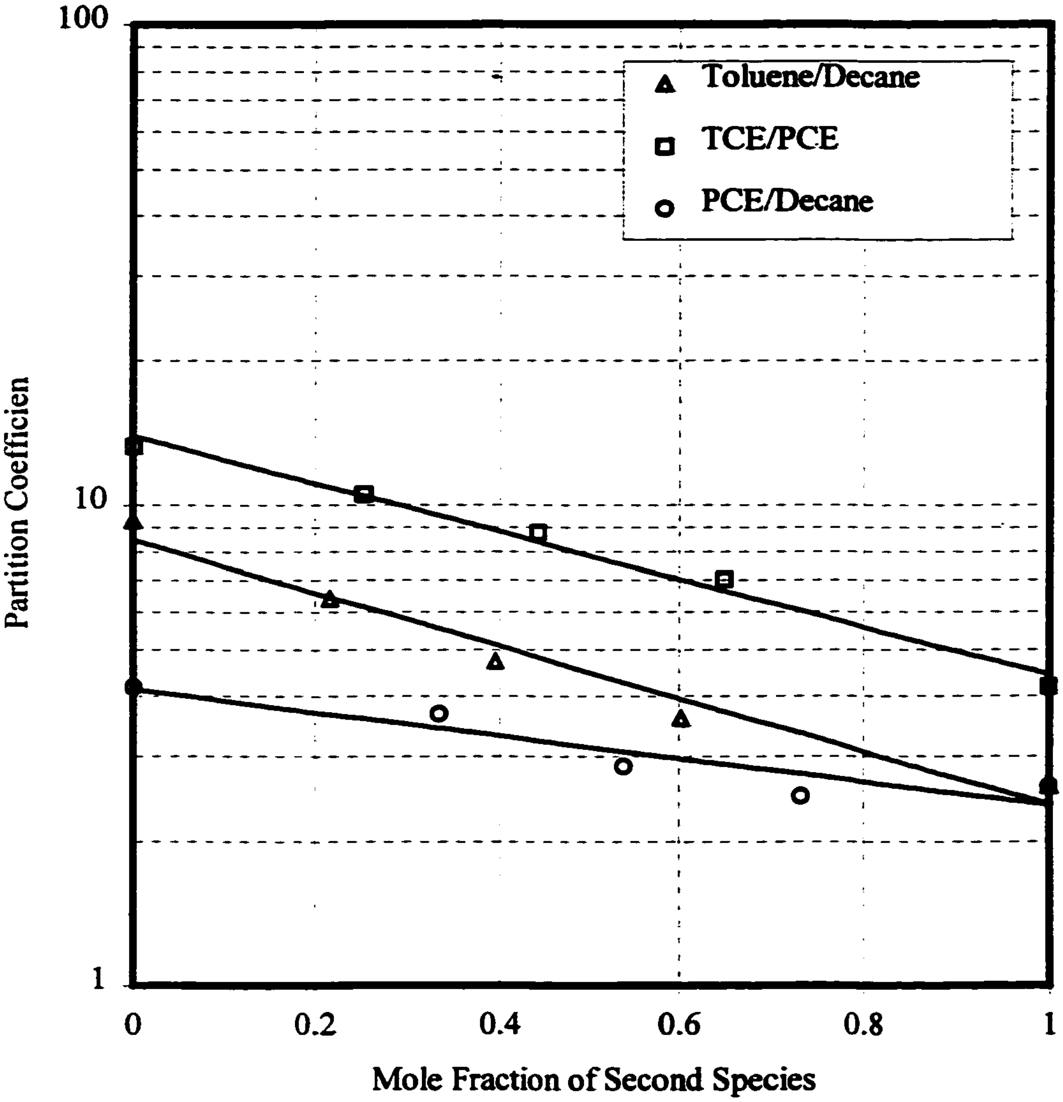

Figure 4.10 Mixing Effect on Partition Coefficient for 3,3-Dimethyl-2-Butanol

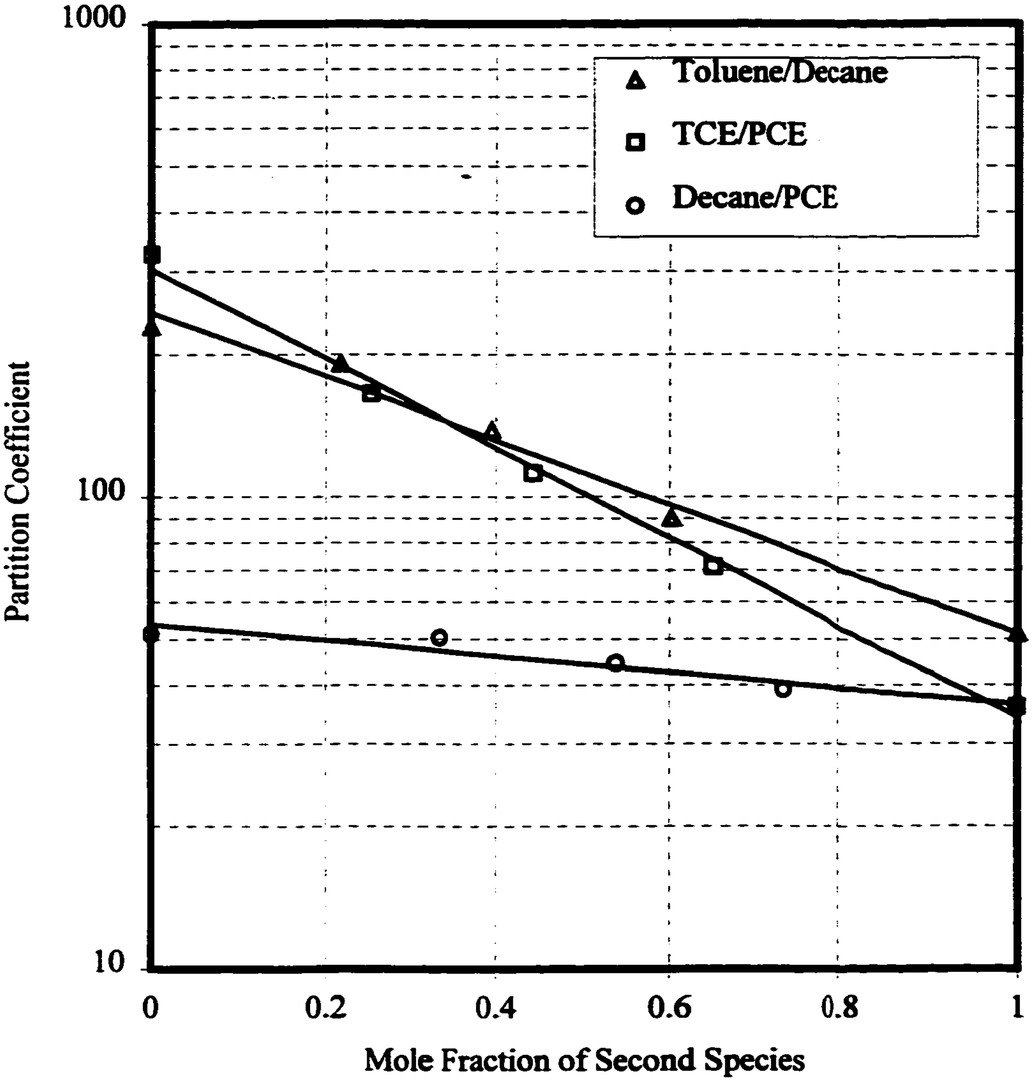

Figure 4.11 Mixing Effect on Partition Coefficient for 4-Methyl-3-Heptanol

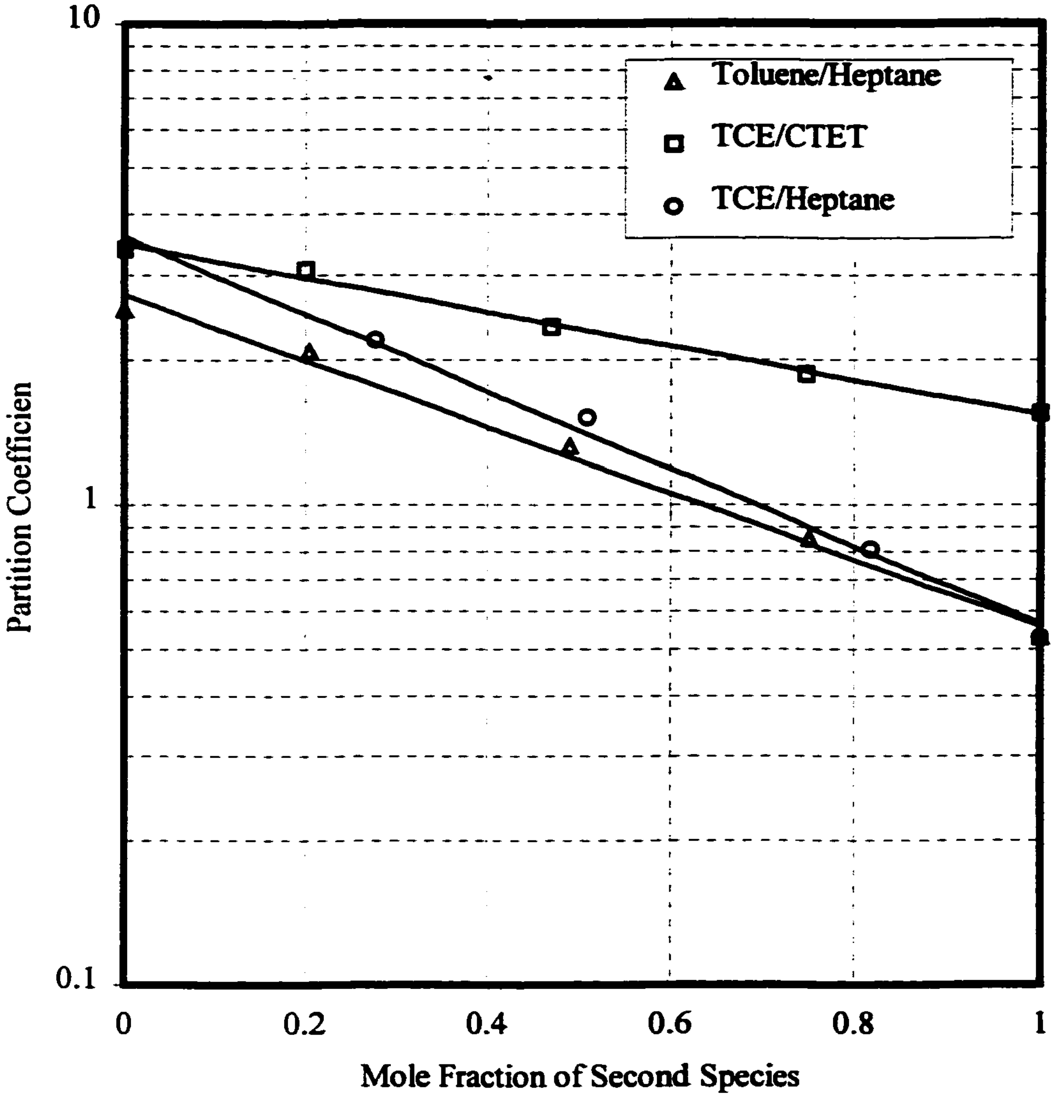

Figure 4.12 Mixing Effect on Partition Coefficient for Pentanol

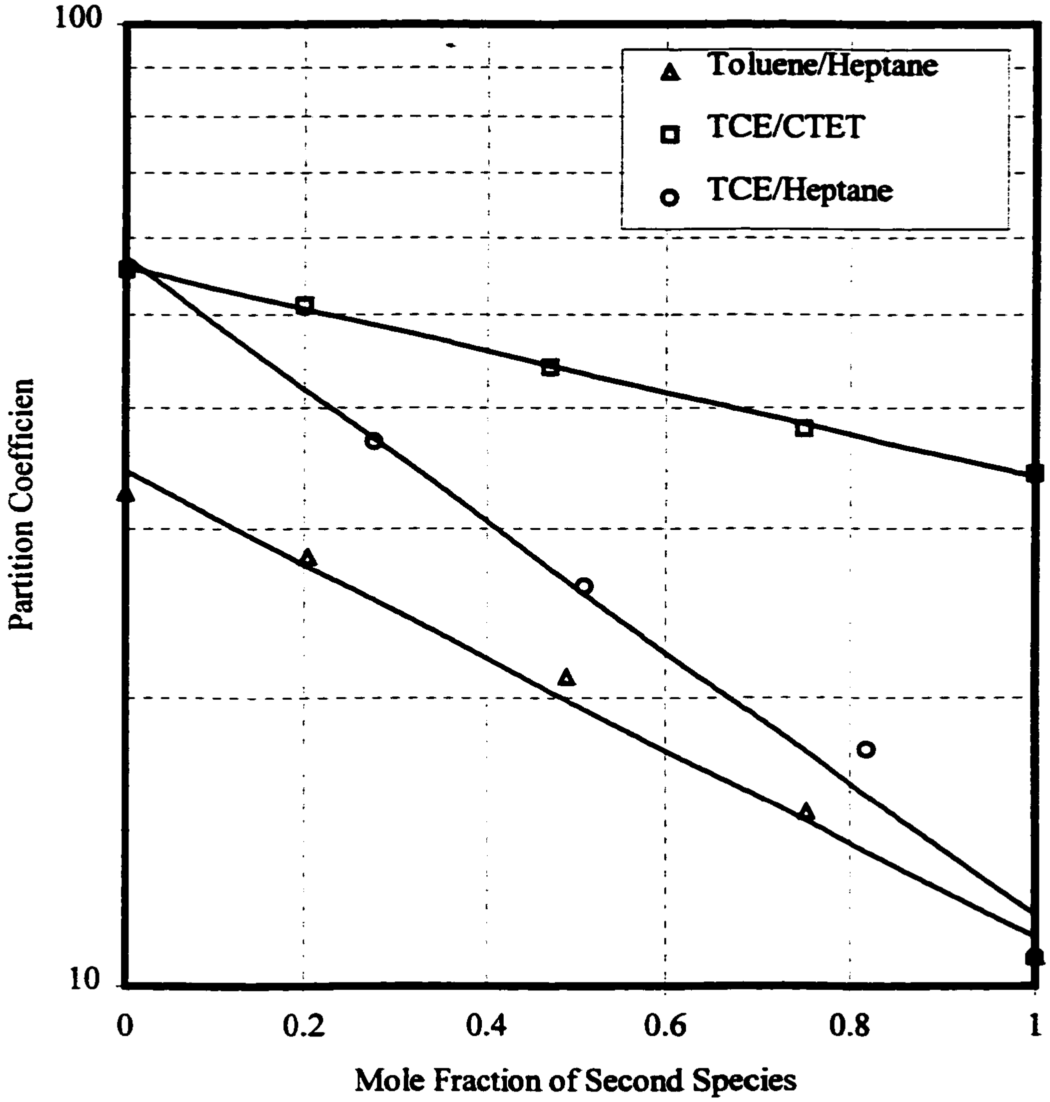

Figure 4.13 Mixing Effect on Partition Coefficient for Heptanol

Since the linear mixing rule is followed, the regression equation developed in this research can be applied to mixtures to calculate partition coefficients. Tables 4.13 through 4.17 list the experimental and calculated values for the binary mixtures shown in Figures 4.9 through 4.13. A review of the tables indicates that the agreement between experimental and calculated values was generally quite good for hydrocarbons and only reasonably good for mixtures containing chlorocarbons. As Table 4.15 indicates, the agreement was rather poor when 4-methyl-3-heptanol was used with chlorocarbons. Future research is needed to validate this observation and provide an explanation for it or determine that the poor agreement is an anomaly due to experimental error.

Table 4.18 lists the experimental and calculated partition coefficients for various complex mixtures (see Appendix C for compositions) and indicates quite good agreement between the values for most of the mixtures. Consistent with the findings from the binary mixtures, there was poor agreement between the values for 4-methyl-3-heptanol. Although octanol was not used with any of the binary mixtures, it also resulted in poor agreement between the experimental and calculated partition coefficients for complex mixtures.

To further analyze the regression equation that was developed, the experimental partition coefficients were plotted against the calculated values as shown in Figures 4.14 and 4.15. Under perfect conditions when the respective values are equal, a regression procedure should result in a straight line with a slope of one. In Figure 4.14, the regression lines for the three alcohols form a straight line with a

Table 4.13: Comparison of Experimental and Calculated Partition Coefficients for 2-Methyl-2-Hexanol in Binary Mixtures

Compound	Mole Fraction of Second Species	EACN of Mixture	Experimental K	Calculated K	Percent Difference
Toluene / Decane	0.0000	1.00	17.17	17.31	-0.82
Toluene / Decane	0.2165	2.95	12.46	12.38	0.64
Toluene / Decane	0.3949	4.55	9.96	9.41	5.52
Toluene / Decane	0.6017	6.42	7.48	6.82	8.82
Toluene / Decane	1.0000	10.00	4.45	3.69	17.08
TCE / PCE	0.0000	-3.81	30.75	39.55	-28.62
TCE / PCE	0.2514	-2.12	22.28	29.58	-32.76
TCE / PCE	0.4428	-0.84	18.50	23.74	-28.32
TCE / PCE	0.6482	0.54	14.28	18.73	-31.16
TCE / PCE	1.0000	2.90	9.75	12.49	-28.10
PCE / Decane	0.3333	5.27	7.13	8.31	-16.55
PCE / Decane	0.7300	8.08	5.24	5.13	2.10

Table 4.14: Comparison of Experimental and Calculated Partition Coefficients for 3,3-Dimethyl-2-Butanol in Binary Mixtures

Compound	Mole Fraction of Second Species	EACN of Mixture	Experimental K	Calculated K	Percent Difference
Toluene / Decane	0.0000	1.00	9.29	9.17	1.29
Toluene / Decane	0.2165	2.95	6.40	6.56	-2.50
Toluene / Decane	0.3949	4.55	4.73	4.98	-5.29
Toluene / Decane	0.6017	6.42	3.60	3.61	-0.28
Toluene / Decane	1.0000	10.00	2.60	1.95	25.00
TCE / PCE	0.0000	-3.81	13.26	20.95	-57.99
TCE / PCE	0.2514	-2.12	10.52	15.67	-48.95
TCE / PCE	0.4428	-0.84	8.76	12.58	-43.61
TCE / PCE	0.6482	0.54	7.03	9.92	-41.11
TCE / PCE	1.0000	2.90	4.19	6.62	-58.00
TCE / PCE	0.3333	5.27	3.69	4.40	-19.24
PCE / Decane	0.5391	6.73	2.86	3.43	-19.93
PCE / Decane	0.7300	8.08	2.48	2.72	-9.68

Table 4.15: Comparison of Experimental and Calculated Partition Coefficients for 4-Methyl-3-Heptanol in Binary Mixtures

Compound	Mole Fraction of Second Species	EACN of Mixture	Experimental K	Calculated K	Percent Difference
Toluene / Decane	0.0000	1.00	229.20	239.68	4.57
Toluene / Decane	0.2165	2.95	191.08	171.46	10.27
Toluene / Decane	0.3949	4.55	138.42	130.26	5.90
Toluene / Decane	0.6017	6.42	90.11	94.47	-4.84
Toluene / Decane	1.0000	10.00	51.46	51.08	0.74
TCE / PCE	0.0000	-3.81	326.70	547.59	-67.61
TCE / PCE	0.2514	-2.12	164.97	409.62	-148.30
TCE / PCE	0.4428	-0.84	112.20	328.77	-193.02
TCE / PCE	0.6482	0.54	71.18	259.39	-264.41
TCE / PCE	1.0000	2.90	36.01	172.94	-380.26
Decane / PCE	0.3333	7.63	50.43	76.74	-52.17
Decane / PCE	0.5391	6.17	44.52	98.62	-121.52
Decane / PCE	0.7300	4.82	39.17	124.35	-217.46

Table 4.16: Comparison of Experimental and Calculated Partition Coefficients for Pentanol in Binary Mixtures

Compound	Mole Fraction of Second Species	EACN of Mixture	Experimental K	Calculated K	Percent Difference
Toluene / Heptane	0.0000	1.00	2.54	2.04	19.69
Toluene / Heptane	0.2040	2.22	2.08	1.66	20.19
Toluene / Heptane	0.4907	3.94	1.32	1.23	6.82
Toluene / Heptane	0.7507	5.50	0.85	0.94	-10.59
Toluene / Heptane	1.0000	7.00	0.53	0.73	-37.74
TCE / CTET	0.0000	-3.81	3.40	4.67	-37.35
TCE / CTET	0.1995	-3.06	3.08	4.10	-33.112
TCE / CTET	0.4708	-2.04	2.34	3.44	-47.01
TCE / CTET	0.7466	-1.01	1.87	2.89	-54.55
TCE / CTET	1.0000	-0.06	1.55	2.45	-58.06
TCE / Heptane	0.2746	-0.84	2.20	2.80	-27.27
TCE / Heptane	0.5100	1.70	1.52	1.81	-19.08
TCE / Heptane	0.8179	5.03	0.81	1.02	-25.93

Table 4.17: Comparison of Experimental and Calculated Partition Coefficients for Heptanol in Binary Mixtures

Compound	Mole Fraction of Second Species	EACN of Mixture	Experimental K	Calculated K	Percent Difference
Toluene / Heptane	0.0000	1.00	32.66	36.68	12.31
Toluene / Heptane	0.2040	2.22	28.04	29.74	6.06
Toluene / Heptane	0.4907	3.94	21.04	22.13	5.18
Toluene / Heptane	0.7507	5.50	15.18	16.93	11.53
Toluene / Heptane	1.0000	7.00	10.73	13.09	21.99
TCE / CTET	0.0000	-3.81	55.72	83.80	50.39
TCE / CTET	0.1995	-3.06	51.09	73.67	44.20
TCE / CTET	0.4708	-2.04	44.12	61.83	40.14
TCE / CTET	0.7466	-1.01	38.09	51.80	35.99
TCE / CTET	1.0000	-0.06	34.19	44.00	28.69
TCE / Heptane	0.2746	-0.84	36.96	50.31	36.12
TCE / Heptane	0.5100	1.70	26.18	32.52	24.22
TCE / Heptane	0.8179	5.03	17.69	18.36	3.79

Table 4.18: Comparison of Experimental and Calculated Partition Coefficients for Complex Mixtures

Mixture	NAPL EACN	Alcohol	Alcohol EACN	Experimental K	Calculated K	Percent Difference
1	1.14	3,3-Dimethyl-2-Butanol	6.04	9.85	8.94	9.24
		4-Methyl-3-Heptanol	8.30	80.03	234.87	-193.48
		6-Methyl-2-Heptanol	7.83	110.35	119.03	-7.87
2	4.27	Octanol	8.00	119.13	88.67	25.57
		Pentanol	5.00	1.31	1.17	10.69
		Heptanol	7.00	24.98	20.92	16.25
3	1.38	Octanol	8.00	211.40	145.67	31.09
		Pentanol	5.00	1.67	1.91	-14.37
		Heptanol	7.00	35.54	34.38	3.26
4	1.21	Octanol	8.00	324.15	149.81	53.78
		Pentanol	5.00	2.19	1.97	10.05
		Heptanol	7.00	38.88	35.35	9.08
5	3.83	2-Methyl-2-Hexanol	6.47	11.84	10.47	11.57
		3,3-Dimethyl-2-Butanol	6.04	5.38	5.63	-4.65
6	1.64	2-Methyl-2-Hexanol	6.47	15.15	15.26	-0.73
		3,3-Dimethyl-2-Butanol	6.04	7.66	8.20	-7.05
7	1.21	2-Methyl-2-Hexanol	6.47	15.27	16.43	-7.60
		3,3-Dimethyl-2-Butanol	6.04	8.57	8.83	-3.03

slope slightly greater than one. The linear relationship is another indication of good agreement between the experimental and calculated values. However, the slope of the line indicates that the regression equation generally overestimates the values. Figure 4.15 is a similar plot for 4-methyl-3-heptanol. As the figure indicates, there was a large difference in the amount of agreement between the partition coefficients. The agreement is nearly perfect for the hydrocarbons and quite disappointing for mixtures including chlorocarbons.

4.5 Conclusions

A bilinear relationship was found to exist in which the partitioning coefficient of an alcohol tracer was related to the EACNs of both the contaminant and the alcohol. This relationship was consistent for hydrocarbons and chlorocarbons, as well as for linear and branched alcohol tracers. Furthermore, the partition coefficient obeyed the linear mixing rule when applied on a mole fraction basis. The resulting bilinear equation, with a coefficient of determination of 0.9910, was found to be applicable to neat compounds, binary mixtures, and complex mixtures. This equation can be quite useful in the preliminary planning stages of a tracer test. The ability to predict partition coefficients, when coupled with modeling efforts, enables the researcher to narrow the list of tracers to those possessing the partition characteristics most suitable for a given field site. Preliminary planning efforts thus require fewer laboratory experiments, which translates into less time and money.

However, there were two critical inconsistencies discovered concerning the use of the equation. First, when the logarithm of the partition coefficients were plotted versus the contaminant EACNs, the data points for dichlorobenzene and carbon tetrachloride were not consistent with the remainder of the data. This discrepancy did not exist when the partition coefficients were plotted versus the alcohol EACNs. Therefore, it appears as though the EACN values for DCB and CTET may not have been accurate. Second, the regression equation greatly overestimated the partition coefficients when 4-methyl-3-heptanol was used with chlorocarbons. In both of these instances, further research is needed so that the regression equation developed in this chapter can be more effectively used.

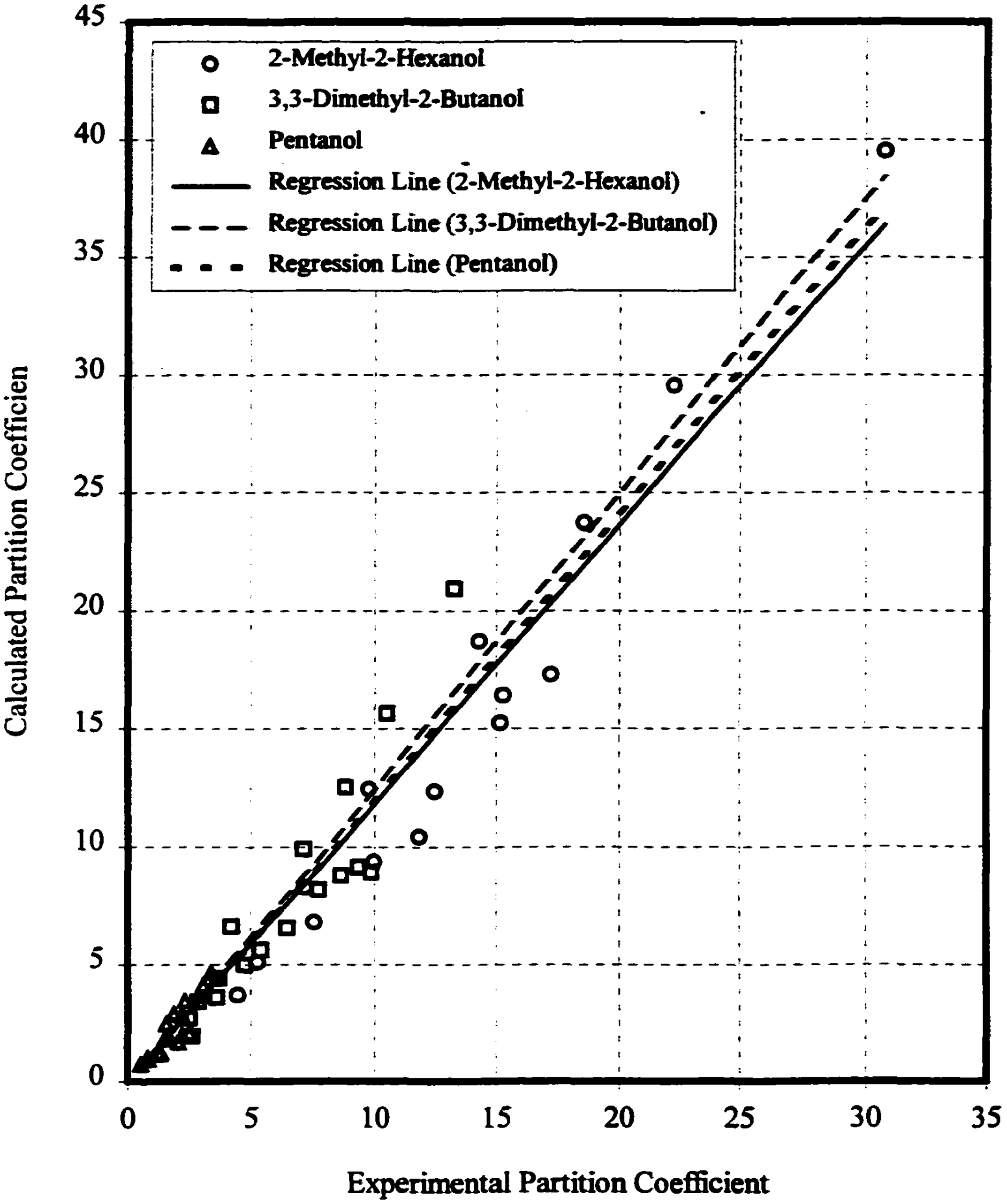

Figure 4.14 Experimental versus Calculated Partition Coefficient Values

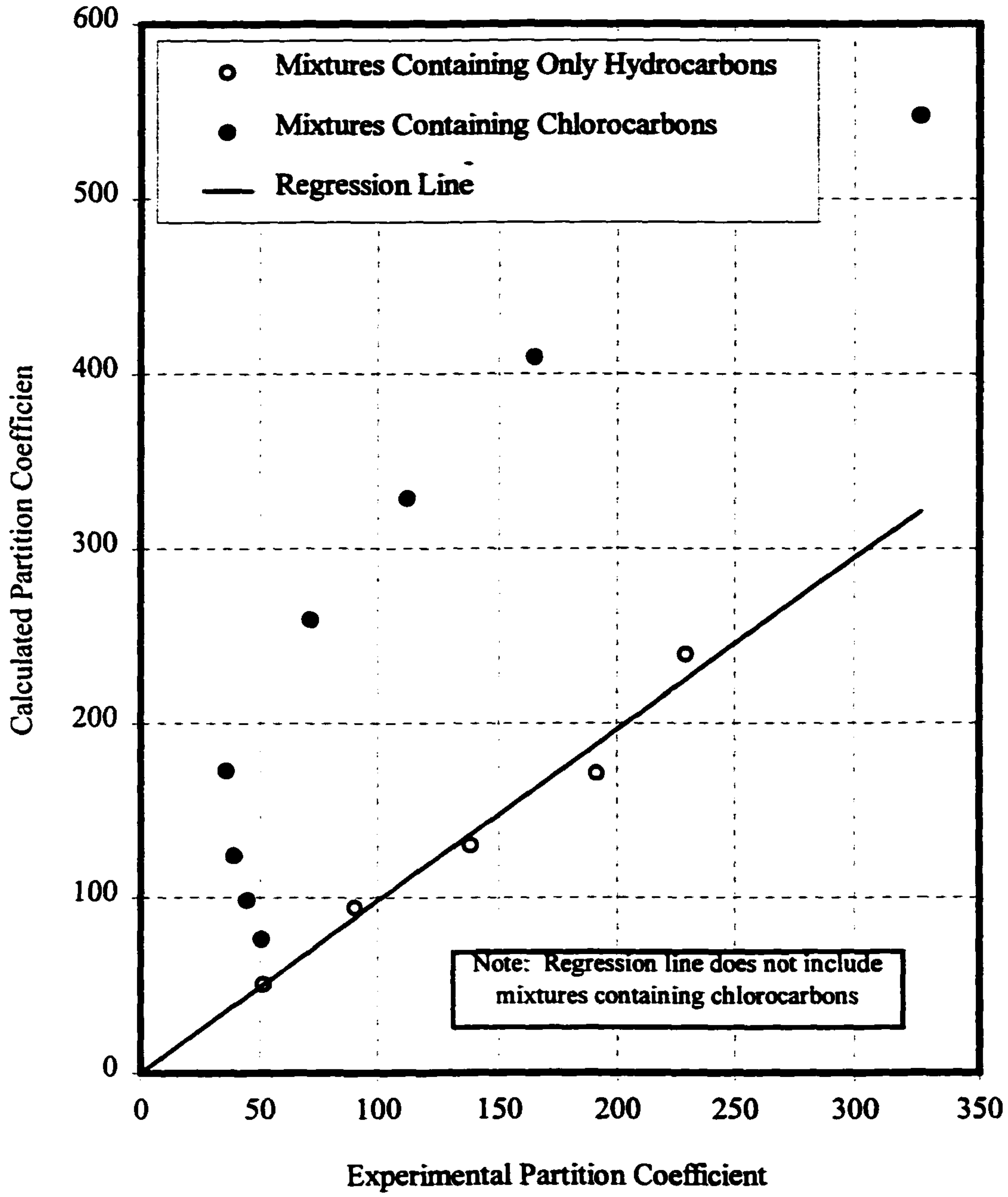

Figure 4.15 Experimental versus Calculated Partition Coefficient Values for 4-Methyl-3-Heptanol

CHAPTER 5

A REVIEW OF TRACER TESTS AND NAPL COMPOSITION ASSOCIATED WITH SURFACTANT-ENHANCED REMEDIATION

Laboratory column studies have been conducted by various researchers to evaluate the effectiveness of surfactant flushing in remediating NAPL contamination. Most of this work has focused on the solubilization aspect of surfactant use and on the overall effectiveness of the contaminant removal process, with the mobilization aspect receiving increased attention in the last few years. From the literature review conducted as part of this research, it did not appear as though the variable nature of NAPL composition during remediation efforts has been investigated.

This chapter provides the results of various experiments performed during a column study to investigate the impact of flow rate on residual saturation calculations and to assess the performance of a surfactant flood. The effluent during the surfactant flooding process was analyzed to evaluate the effects of the surfactant on NAPL composition. These findings were combined with the relationship established in the previous chapter to determine the impact of NAPL composition on tracer test results and alcohol partition coefficients. Throughout the analysis, the regression equation developed in Chapter 4 was used to determine partition coefficients to further demonstrate its usefulness. A similar approach was used on data from a field site to make a meaningful comparison between laboratory and field results.

In the past, many researchers have used the same partition coefficients for pre- and post-remediation NAPL characterization. If the NAPL composition remains reasonably constant throughout the remedial efforts, this may be an adequate approach. However, if preferential solubilization or mobilization of specific components in the NAPL occurs, different partition coefficients should be expected and used for pre- and post-remediation site characterization efforts.

5.1 Experimental Description

5.1.1 Materials

The medium used for the column study was obtained from the Canadian River floodplain near Norman, Oklahoma, and will be referred to as Canadian River Alluvium (CRA). Shiau (1995) reported the composition of CRA (wt% basis) as 72.4 percent sand and 27.6 percent silts and clays, with the fraction organic content (f_{oc}) being 0.07 percent. The column study was performed with a synthetic NAPL mixture prepared in the laboratory (see Table 5.1), Dowfax 8390 as the surfactant, and the tracer combinations listed in Table 5.2. All tracer solutions were prepared on a weight basis and placed on a stirrer for 1 hour. Although the tracers were selected arbitrarily, they were chosen such that the resulting retardation factor (R_f) was within an acceptable range ($1.2 < R_f < 4.0$). If the retardation factor were less than 1.2, there would not be enough separation in breakthrough curves to differentiate it from the non-conservative tracer. If the retardation factor were greater than 4.0, generation of a full breakthrough curve would require too much time.

Table 5.1: Synthetic NAPL Composition

Component	Mass (g)	Volume (ml)	Moles	Mole Fraction
Decane	9.9113	13.5771	0.0696	0.1276
Heptane	4.8766	7.1327	0.0487	0.0892
Hexane	5.0915	7.7109	0.0591	0.1082
o-Xylene	14.7524	16.7622	0.1390	0.2546
Toluene	15.0954	17.4312	0.1638	0.3001
TCE	4.9028	3.3468	0.0373	0.0684
PCE	4.7044	2.8986	0.0284	0.0520

Table 5.2: Tracer Combinations

Compound		Combinations		
		1	2	3
Ethanol	Mass (g)	0.1002	0.0952	0.1077
	Concentration (mg/l)	1282.39	801.35	1027.67
1-Pentanol	Mass (g)	0.1069	0.0936	0.0875
	Concentration (mg/l)	1768.14	787.88	834.92
1-Hexanol	Mass (g)	NA	0.1246	NA
	Concentration (mg/l)	NA	1048.82	NA
2-Methyl-2-Hexanol	Mass (g)	NA	0.0973	0.0637
	Concentration (mg/l)	NA	819.20	607.82
6-Methyl-2-Heptanol	Mass (g)	0.0623	NA	NA
	Concentration (mg/l)	797.33	NA	NA

NA - Not Applicable

Solutions were introduced to a Kontes™ glass liquid chromatography column through a Cole-Palmer™ Masterflex peristaltic pump. Associated tubing connected to the column was either PTFE or Masterflex "14" tubing. Effluent samples were obtained with an Eldex™ universal time-controlled fraction collector and were prepared in standard 5-ml or 20-ml glass bottles (Alltech Associates, Inc.).

5.1.2 Procedures

The procedures used to conduct the column studies were consistent with those found in the literature. The CRA was air-dried, ground in a mixing bowl, and sieved five times with a U.S. Standard Sieve #2000 (openings of 2000 microns) from Fisher Scientific Company. The column was packed in incremental layers, with each layer being manually stirred before the addition of the next layer. The column was prepared in this manner to achieve homogeneity; however, some degree of heterogeneity is expected. The column was weighed before and after packing to determine bulk density.

The column was saturated with de-ionized water in an upflow mode and weighed. The porosity and pore volume were determined from mass balance measurements. With the soil column saturated, the first tracer solution (Combination #1 in Table 5.2) was injected for two hours at a flow rate of 0.3 ml/min, followed by de-ionized water for 4.38 hours. The resulting breakthrough curves were used to analyze the pore volume and longitudinal dispersivity of the soil column.

NAPL saturation was accomplished by pumping two pore volumes of a synthetic NAPL mixture (see Table 5.1) into the column at a rate of 0.3 ml/min in a downflow mode. The downflow mode was chosen to ensure stable displacement of the water. To establish residual saturation levels, the column was flushed with de-ionized water in an upflow mode at a flow rate of 1.0 ml/min for 6 hours. Further flushing was accomplished at a flow rate of 0.3 ml/min for 18 hours. The residual saturation was determined gravimetrically be using the difference in weights between the uncontaminated and contaminated soil columns and the density of the NAPL.

The second tracer solution (Combination #2 in Table 5.2) was then injected into the soil column in a downflow mode. Breakthrough curves of the effluent concentration and the method of moments was used to determine residual saturation values. To evaluate the effects of flow rate on residual saturation value calculations, tracer tests were conducted with a constant tracer solution volume of 6 ml at flow rates of 0.3, 0.5, and 0.8 ml/min. After tracer injection, de-ionized water was flushed through the column for about 7, 5, and 4 hours, respectively. The flushing times were based on the expected retardation of the tracers and were selected to ensure that complete breakthrough curves could be developed from the experimental data.

The contaminated soil column was then flushed in a downflow mode at a rate of 0.3 ml/min with an aqueous surfactant solution containing 4 wt% Dowfax 8390 for 6.57 hours. To achieve a 4 wt% mixture, the Dowfax surfactant (36 percent active as received from the manufacturer) and was mixed with de-ionized water on a 1:8 ratio. The downflow mode for the surfactant flooding process was chosen to minimize the mobilization of any separate phase NAPL in the column and to focus more on the preferential solubilization of NAPL components. Following the injection of surfactant solution, de-ionized water was flushed through the column for 6 hours to remove trace amounts of the surfactant. During the surfactant and water flooding processes, effluent samples were collected and analyzed for surfactant, as well as NAPL component, concentrations.

After the soil column was flushed with several pore volumes of water at a flow rate of 0.3 ml/min, the post-remediation residual saturation value was determined using the final set of tracers (Combination #3 in Table 5.2). The tracer solution was injected into the soil column in a downward mode for 20 minutes at a flow rate of 0.3 ml/min, followed by de-ionized water for 6.58 hours.

Alcohol tracer analysis was conducted with a Varian gas chromatograph (model 3300) equipped with a Varian autosampler (model 8100) and a flame ionization detector (FID). Surfactant concentrations were determined with a Shimadzu HPLC (model LC-10AD) equipped with an autoinjector (model SIL-10A) and system controller (model SCL-10A). Contaminant concentrations were determined with a Tekmar 7000 Headspace Autosampler, which was connected to a Shimadzu GC (model GC-17A) through a cryofocusing capillary interface. Varian Star Chromatography software was used to interpret the respective results.

5.2 Data Analysis

The residual NAPL saturation can be calculated on a mass balance basis by using the difference in weight of the contaminated soil column after water flushing and the weight of the soil column saturated only with water. The volume of NAPL remaining in the soil column after the water flushing can thus be determined from,

$$V_{NAPL} = (W_N - W_W) / (\rho_N - \rho_W) \tag{5.1}$$

where W_N is the weight of the contaminated soil column after water flushing, W_W is the weight of the soil column saturated only with water, ρ_N is the density of the NAPL mixture, and ρ_W is the density of water. The porosity can be calculated from,

$$\eta = (W_{sat} - W_{dry}) / V_c \tag{5.2}$$

where η is the porosity, W_{sat} is the weight of the water-saturated soil column, W_{dry} is the weight of the soil column before water was injected, and V_c is the volume of the column. The pore volume (PV) can be calculated from,

$$PV = (W_{sat} - W_{dry}) / \rho \tag{5.3}$$

where ρ is the density of the water. The residual NAPL saturation can then be calculated from,

$$S_N = V_{NAPL} / PV \tag{5.4}$$

where S_N is the residual NAPL saturation, V_{NAPL} is as described by Equation 5.1, and

PV is the pore volume. The pore volume and residual NAPL saturation can also be determined from the tracer breakthrough curves using the method of moments (Jin, 1995).

Longitudinal dispersivity of a soil column can be determined from the one-dimensional advection-dispersion equation,

$$\frac{\partial C}{\partial t} = -V_{pw}\left(\frac{\partial C}{\partial x}\right) + D_h\left(\frac{\partial^2 C}{\partial x^2}\right) \tag{5.5}$$

where C is the effluent concentration (mg/l) at the end of the column, t is the time in minutes, x is the length of the column in centimeters, V_{pw} is the pore water velocity in cm/min, and D_h is the hydrodynamic dispersion coefficient in cm^2/min. D_h represents the tortuosity of the flow path within the soil column and is defined as,

$$D_h = \alpha\, V_{pw} + D_d \tag{5.6}$$

where α is the dispersivity of the soil in centimeters and D_d is the molecular diffusion of the fluid with units of cm^2/min. The corresponding analytical solution to Equation 5.5 with appropriate initial and boundary conditions is represented by,

$$\frac{C}{C_o} = 0.5\left[erfc\left(\frac{x - V_{pw}\,t}{2\sqrt{D_h\,t}}\right) + \left\{\exp\left(\frac{V_{pw}\,x}{D_h}\right)\right\} erfc\left(\frac{x - V_{pw}\,t}{2\sqrt{D_h\,t}}\right)\right] \tag{5.7}$$

where *erfc* is the complementary error function and *exp* is the Napierian logarithm. In the above equation, all values are known except for the hydrodynamic dispersion coefficient (D_h). Equation 5.7 can be solved for various values of D_h through an iterative process (using linear least squares regression) until the resulting breakthrough curve matches the breakthrough curve for the column data. Equation 5.6 can then be used to solve for the dispersivity.

5.3 Experimental Results and Discussion

5.3.1 Calibration Curves

The calibration curves for the alcohol tracers were previously established as described in Chapter 4. The calibration curves used to determine the surfactant and contaminant concentrations in the effluent samples are shown in Figures B.14 through B.20 and summarized in Table B.2 of the Appendix. An implicit assumption in developing the contaminant calibration curves was that Henry's law applied; i.e., the partial pressure of a contaminant above a liquid was related to the concentration of the contaminant in the liquid phase by the Henry's constant. Furthermore, a linear relationship was assumed between the partial pressure of a contaminant and its mole fraction (i.e., Raoult's law for dilute solutions was obeyed). Determined through a linear regression procedure, the calibration results were based on up to seven data points and were forced to go through the origin. For some of the contaminants, the linear relationship described by Raoult's law for dilute solutions was violated at higher concentrations. In those instances, the data points were not included in the regression analysis. From Table B.2, note that the coefficients of determination range from 0.9939 to 0.9995.

During the calibration process, the retention times for TCE and heptane were nearly identical, and the headspace autosampler was not able to distinguish between the two components. Therefore, a combined calibration curve was used to analyze column effluent samples for combined concentrations of TCE and heptane. This process obviously introduces a source of error and makes interpretation of the data more subjective.

5.3.2 Uncontaminated Column

Volume and mass measurements for the column study are shown in Table 5.3. The bulk density, porosity, and pore volume were calculated as 1.62 g/cm^3, 0.35, and 25.3 cm^3, respectively. The breakthrough curves for the tracers injected into the uncontaminated column are shown in Figure 5.1 with the results summarized in Table 5.4. If residual NAPL does not exist, tracer breakthrough curves should be identical regardless of the types of tracers. However, the breakthrough curves shown in Figure 5.1 show clear signs of separation, an indication that the alcohols were adsorbing to organic matter in the soil. This was expected since Shiau (1995) reported the fraction organic content (f_{oc}) of CRA as 0.07 percent (weight basis). To analyze the breakthrough curves using the method of moments, it must be assumed that the tracer partitions into the organic material, which represents 0.33 percent (volume basis). If the organic material is assumed to have an EACN of zero, the regression equation developed in Chapter 4 can be used to calculate the tracers' partition coefficients.

Table 5.3: Volume and Mass Measurements Associated with Column Study

	Inside Diameter (cm)	Length (cm)	Volume (cm^3)	Mass (g)
Empty Column	2.5	14.8	72.65	225.0
Tubing				
Masterflex	0.1524	48.1	0.88	NA
PTFE	0.1575	192.5	3.75	
Combined			4.63	
Column with Dry Soil	NA	NA	NA	342.8
Water-Saturated Column	NA	NA	NA	368.1
Column at Residual Saturation	NA	NA	NA	367.4

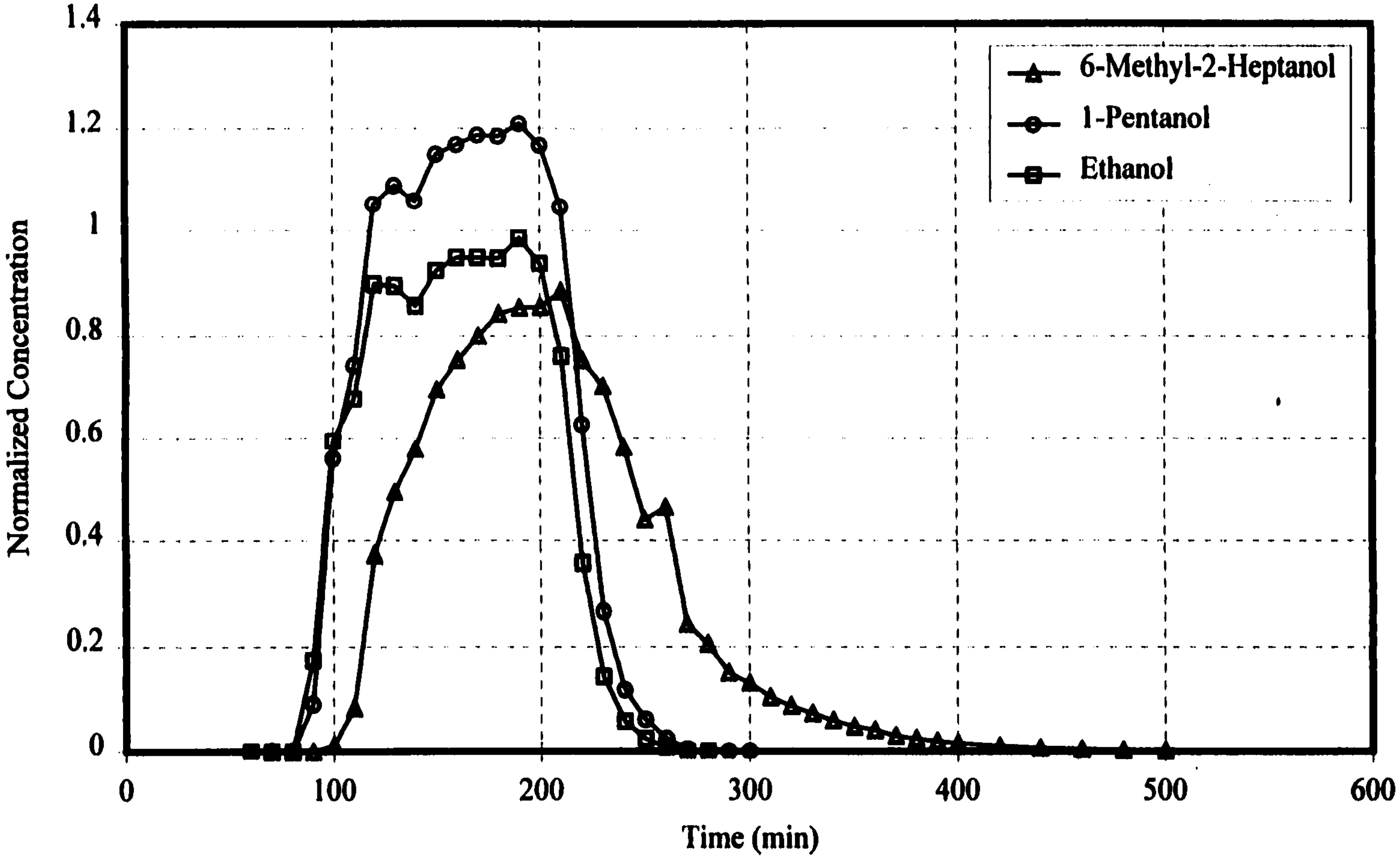

Figure 5.1 Breakthrough Curve for Uncontaminated Column

Table 5.4: Tracer Test Results for Uncontaminated Column

				Method of Moments Calculations			
Tracer	Residence Time (mins)	Mass Recovery	K^a	R	S_N^b (%)	S_N^c (%)	PV (cm^3)
6-Methyl-2-Heptanol	143.72	0.959	144.38	1.43	0.30	0.26	30.19
1-Pentanol	104.28	1.403	2.43	1.04	1.60	NA[e]	30.59
Ethanol	100.32	0.938	0.00[d]	1.00	NA[e]	NA[e]	NA[e]

[a] Calculated
[b] Relative to ethanol
[c] Relative to 1-pentanol
[d] Non-partitioning
[e] Not Applicable

The results from using the method of moments are presented in Table 5.4. The calculated pore volumes agree well with the pore volume of 25.3 cm^3 determined from the mass balance calculations. Two of the three calculated residual saturation values agree well with the 0.33 percent value calculated from Shiau's (1995) data. However, these results must be regarded cautiously for a number of reasons. Assuming that the organic material in the soil can be converted to an equivalent liquid form with an EACN of zero may not be appropriate. Furthermore, the pentanol data may not be reliable since its maximum concentration values were near 1.2 and its mass recovery was 140 percent during the tracer test. Assuming these high values are attributable to experimental errors during the calibration process, there would be no impact on calculations using the method of moments.

If the organic matter is not treated as an equivalent liquid, the tracer partition coefficients are assumed to equal zero and the retardation of the respective tracers is the result of adsorption. Since mass recovery was relatively high for ethanol and 6-methyl-2-heptanol (93.8 and 95.9 percent, respectively), the adsorption process was considered reversible. The amount of adsorption for ethanol and pentanol was considered negligible because their respective breakthrough points for 0.5 C/C_0 occurred slightly before one pore volume of the tracer solution had been injected (about 84 minutes). For adsorption to be considered significant, solute transport would have been delayed and the 0.5 C/C_0 breakpoint would have occurred after one pore volume of the tracer solution had been injected.

The asymmetry depicted by the curves in Figure 5.1 may be attributed to desorption hysteresis, chemical non-equilibrium, physical non-equilibrium, or a combination of chemical and physical non-equilibrium. This is consistent with results reported in the literature that equilibrium adsorption is often not observed in column studies conducted at higher pore water velocities (Knox *et al.*, 1993). Because of the mass recovery rates encountered during the column studies and the general shapes of the breakthrough curves, hysteresis was not considered. As for non-equilibrium, many researchers have found it difficult to distinguish between the two processes from laboratory data and have reported similar results from respective models (Knox *et al.*, 1993). Therefore, the physical non-equilibrium explanation will be assumed so that UTCHEM's capacitance model can be used (discussed in more detail in Chapter 6).

The pore water velocity for the soil column was 0.175 cm/min. This was calculated from the flow rate of 0.3 ml/min, a cross-sectional area of 4.91 cm^2, and a porosity of 0.35. Using Equation 5.7 in the iterative manner previously described with the ethanol breakthrough data, the hydrodynamic dispersion coefficient for the uncontaminated soil column was estimated as 0.045 cm^2/min. Substituting this value into Equation 5.6 resulted in a dispersivity calculation of 0.26 cm.

5.3.3 Column at Residual Saturation

The volume of residual NAPL was determined gravimetrically from Equation 5.1 as 5.0615 cm^3, and the residual saturation was calculated from Equation 5.4 as 19.76 percent. Tracer breakthrough curves at flow rates of 0.3, 0.5, and 0.8 ml/min are shown in Figures 5.2 through 5.4, respectively. The breakthrough curves exhibit varying degrees of tailing and asymmetry, consistent with the breakthrough curves for the uncontaminated column. As previously mentioned, the presence of dead-end pore space and non-equilibrium transport will be investigated in Chapter 6 as a cause for the asymmetry. In each figure, the separation of curves clearly indicates the presence of residual saturation. To quantify the amount of residual NAPL, as well as the pore volume and retardation factor, the method of moments was applied to each flow rate. The results are shown in Tables 5.5 through 5.7. A summary of the results, along with other properties of the soil column, is shown in Table 5.8.

The respective tracer retardation factors and mass recovery rates at each flow rate are reasonably consistent, indicating that the values appear to be independent of flow rate. The residual NAPL amounts are also reasonably consistent, except for those values, which included the 2-methyl-2-hexanol data in their calculations. If the inconsistent values were limited to one flow rate, experimental error could be attributed as the cause. Since the inconsistent values exist across all flow rates though, a more systemic factor is suspected and deserves further research. The mass recovery rates range from 0.887 to 1.454 and are highest for hexanol instead of 2-methyl-2-hexanol, another indication that further research is warranted.

If calculations involving 2-methyl-2-hexanol are excluded, the average residual saturations are in good agreement with each other (as shown in Table 5.8). Although about 10 percent higher, the values are also in good agreement with the residual saturation amount determined gravimetrically (19.76 percent). Similarly, the calculated pore volumes are in good agreement with each other. However, they are about 20 percent higher than the initial value determined gravimetrically (25.30 cm^3). One possible explanation is that the partition coefficients used in the method of moments calculations were based on the regression equation developed in Chapter 4. Considering the intent of developing the regression equation was only to provide estimates though, the results appear to be within an acceptable range.

Using an effective porosity of 0.28, Equation 5.7 was used in an iterative manner to estimate the hydrodynamic dispersion coefficient for each flow condition. The results were then used in Equation 5.6 to determine the respective dispersivity values. As shown in Table 5.8, the hydrodynamic dispersion coefficient and dispersivity values did not change appreciably in the presence of residual NAPL under flow conditions of 0.3 ml/min. The slight increase in dispersivity was expected due to the presence of residual NAPL. For higher flow rates, the hydrodynamic dispersion coefficients increased in direct proportion to the fluid velocity while the dispersivity values remained reasonably constant. Since dispersivity is a function of the soil medium, the constant values were expected. A decreasing trend in the dispersivity values appears to exist as velocities are increased. However, three data points are not sufficient to provide conclusive evidence of the trend.

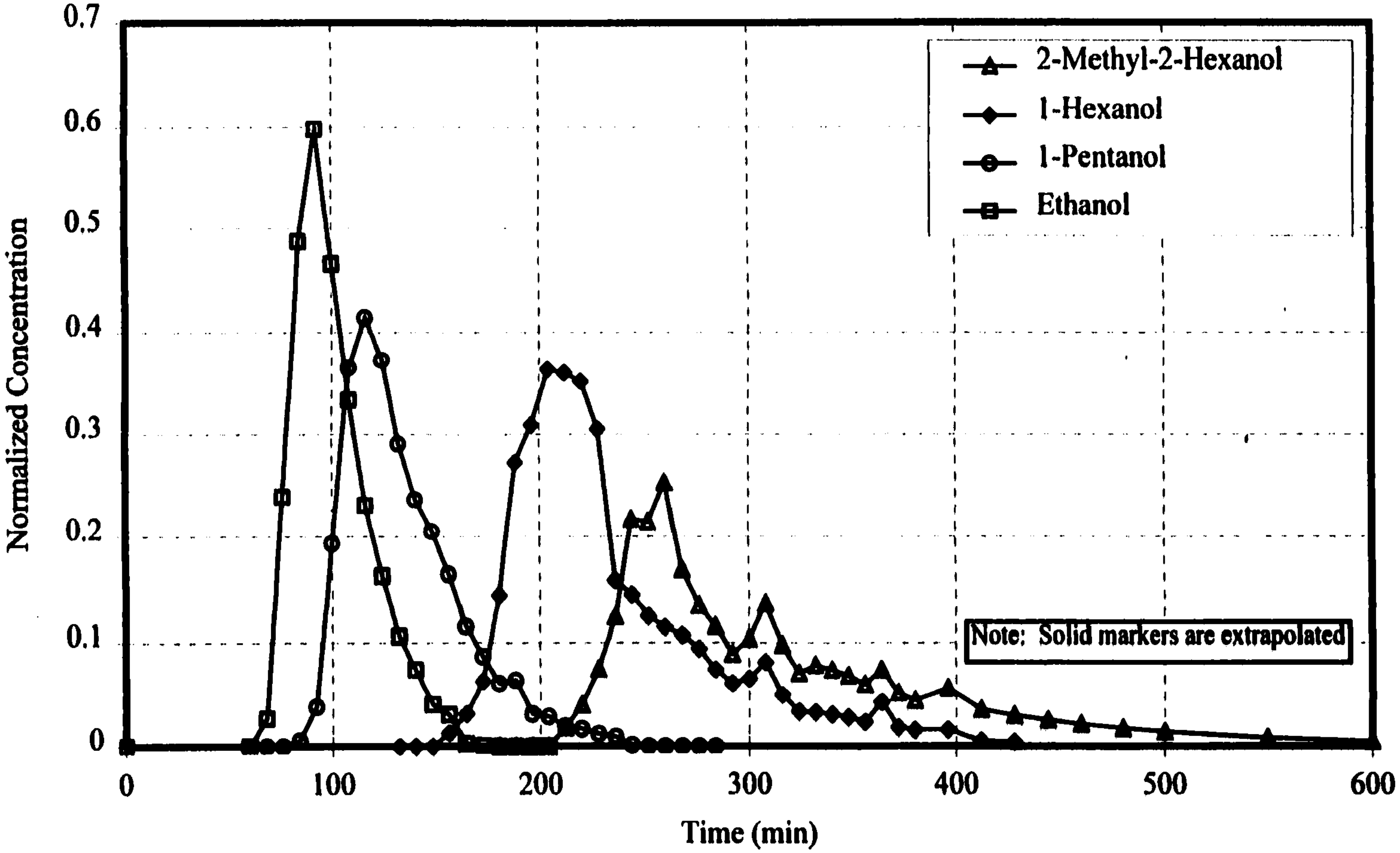

Figure 5.2 Breakthrough Curves for Column at Residual Saturation (flow rate = 0.3 ml/min)

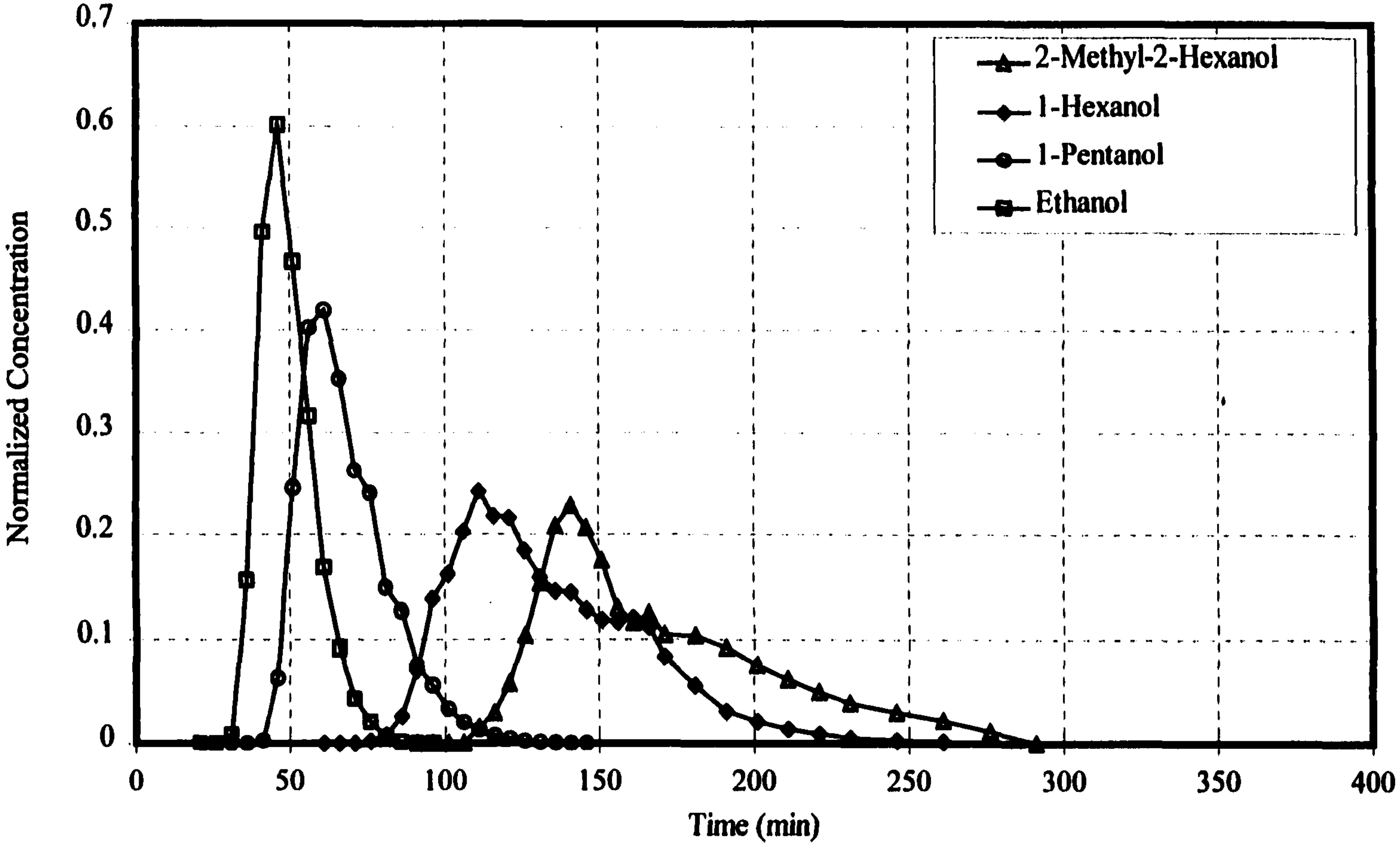

Figure 5.3 Breakthrough Curves for Column at Residual Saturation (flow rate = 0.5 ml/min)

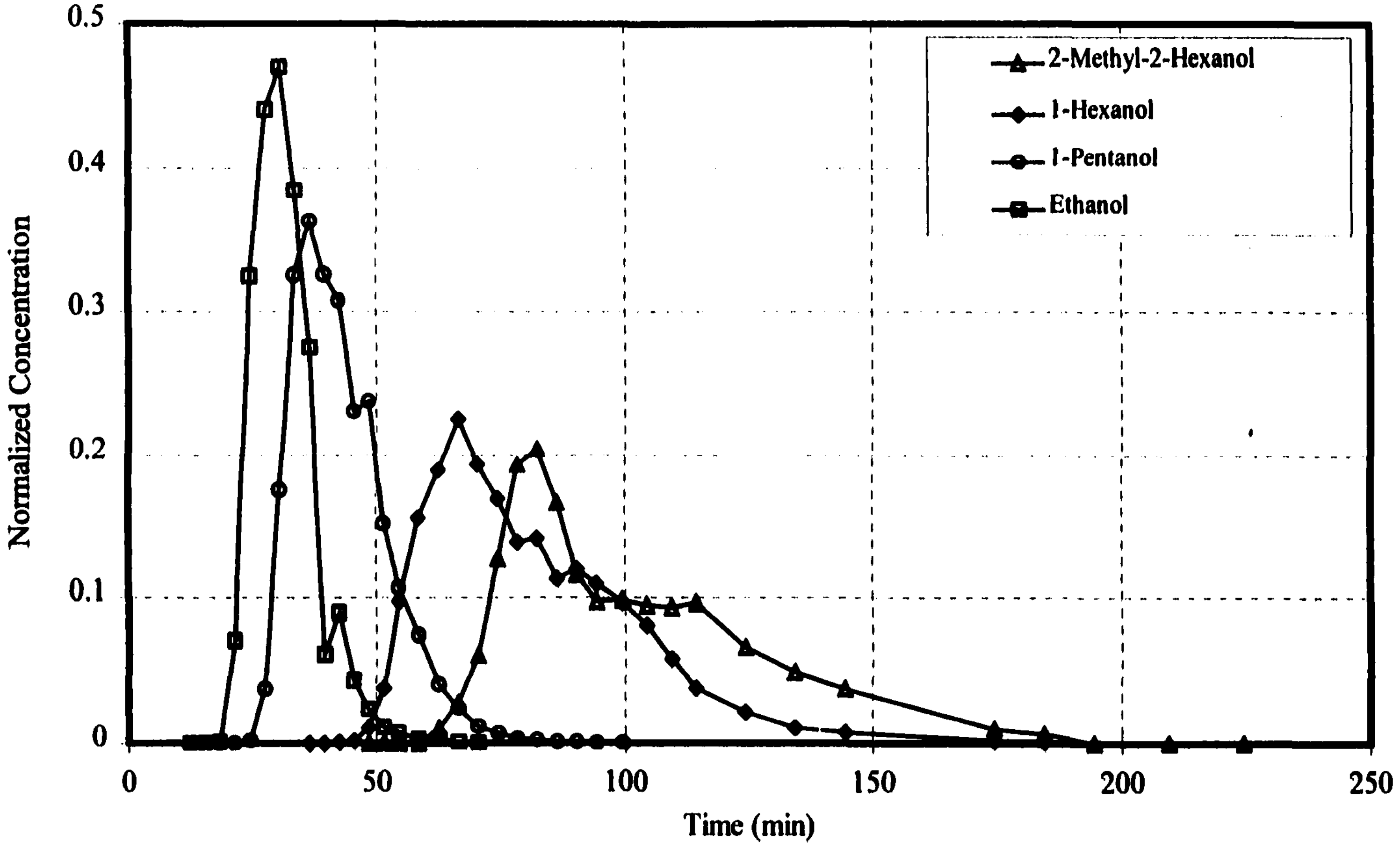

Figure 5.4 Breakthrough Curves for Column at Residual Saturation (flow rate = 0.8 ml/min)

Table 5.5: Tracer Test Results for Column at Residual Saturation (flow rate = 0.3 ml/min)

Tracer	Residence Time (mins)	Mass Recovery	K	Method of Moments Calculations				
				R	S_N[a] (%)	S_N[b] (%)	S_N[c] (%)	PV (cm^3)
2-Methyl-2-Hexanol	298.46	1.106	11.20	3.30	17.03	14.98	7.37	32.71
1-Hexanol	229.13	1.454	5.68	2.53	21.72	20.90	NA[d]	34.66
1-Pentanol	124.08	1.093	1.34	1.37	21.25	NA[d]	NA[d]	34.46
Ethanol	90.45	1.119	1.00	1.00	NA[d]	NA[d]	NA[d]	NA[d]

[a] Relative to ethanol
[b] Relative to 1-pentanol
[c] Relative to 1-hexanol
[d] Not Applicable

Table 5.6: Tracer Test Results for Column at Residual Saturation (flow rate = 0.5 ml/min)

Tracer	Residence Time (mins)	Mass Recovery	K	Method of Moments Calculations				
				R	S_N[a] (%)	S_N[b] (%)	S_N[c] (%)	PV (cm^3)
2-Methyl-2-Hexanol	174.13	1.149	11.20	3.33	17.25	15.60	5.92'	31.55
1-Hexanol	138.64	1.227	5.68	2.66	22.56	23.90	NA[d]	33.72
1-Pentanol	70.76	1.033	1.34	1.36	20.95	NA[d]	NA[d]	33.03
Ethanol	52.22	0.989	1.00	1.00	NA[d]	NA[d]	NA[d]	NA[d]

[a] Relative to ethanol
[b] Relative to 1-pentanol
[c] Relative to 1-hexanol
[d] Not Applicable

Table 5.7: Tracer Test Results for Column at Residual Saturation (flow rate = 0.8 ml/min)

Tracer	Residence Time (mins)	Mass Recovery	K	Method of Moments Calculations				
				R	S_N[a] (%)	S_N[b] (%)	S_N[c] (%)	PV (cm^3)
2-Methyl-2-Hexanol	106.60	1.120	11.20	3.20	16.43	14.82	5.99	31.87
1-Hexanol	84.72	1.172	5.68	2.54	21.38	22.32	NA[d]	33.88
1-Pentanol	44.58	1.002	1.34	1.34	20.20	NA[d]	NA[d]	33.38
Ethanol	33.29	0.887	1.00	1.00	NA[d]	NA[d]	NA[d]	NA[d]

[a] Relative to ethanol
[b] Relative to 1-pentanol
[c] Relative to 1-hexanol
[d] Not Applicable

Table 5.8: Summary of Column Study Results

Condition	Flow Rate (ml/min)	Average S_N (%)	Average PV (cm^3)	Pore Water Velocity (cm/min)	Hydrodynamic Dispersion Coefficient (cm^2/min)	Dispersivity (cm)
Uncontaminated	0.3	NA	25.76	0.175	0.045	0.26
NAPL Residual	0.3	21.29	29.95	0.219	0.064	0.29
NAPL Residual	0.5	22.47	28.75	0.366	0.091	0.25
NAPL Residual	0.8	21.30	28.96	0.586	0.138	0.24

NA – Not Applicable

5.3.4 Effluent Concentrations During Surfactant Flooding

During the surfactant flooding process, the effluent began to show a slight change in color after 105 minutes. The color became progressively darker, yet remained clear, until the 210-minute mark. At that point, the color remained constant. Since the synthetic NAPL and surfactant solution were colorless liquids, it was hypothesized that there was some mobilization of fine sediments from the soil column. This was confirmed when the effluent began to become cloudy after 450 minutes. Mobilization of fines was not unexpected as phase behavior studies were not conducted to optimize the Dowfax solution and the surfactant flooding process was conducted in a downflow mode.

The contaminant and surfactant concentration histories during the surfactant flooding process are shown in Figure 5.5. The most striking observations about Figure 5.5 are the slightly higher concentration levels just before the 150-minute mark and the much higher values prior to the 500-minute mark. For column studies conducted in an upflow mode involving LNAPLs, a large spike in concentration levels representing mobilized contaminant usually coincides with or slightly precedes the surfactant breakthrough. The first, although relatively small peak, fits this description. However, since the experiment was conducted in a downflow mode, the peak is dampened by buoyancy forces acting in an upward direction on the LNAPL. The larger peak, occurring after surfactant concentration levels near zero, was unexpected because Dowfax does not mobilize contaminants without the presence of a cosolvent. The later peaks could be due to NAPL adsorbed to colloids mobilized

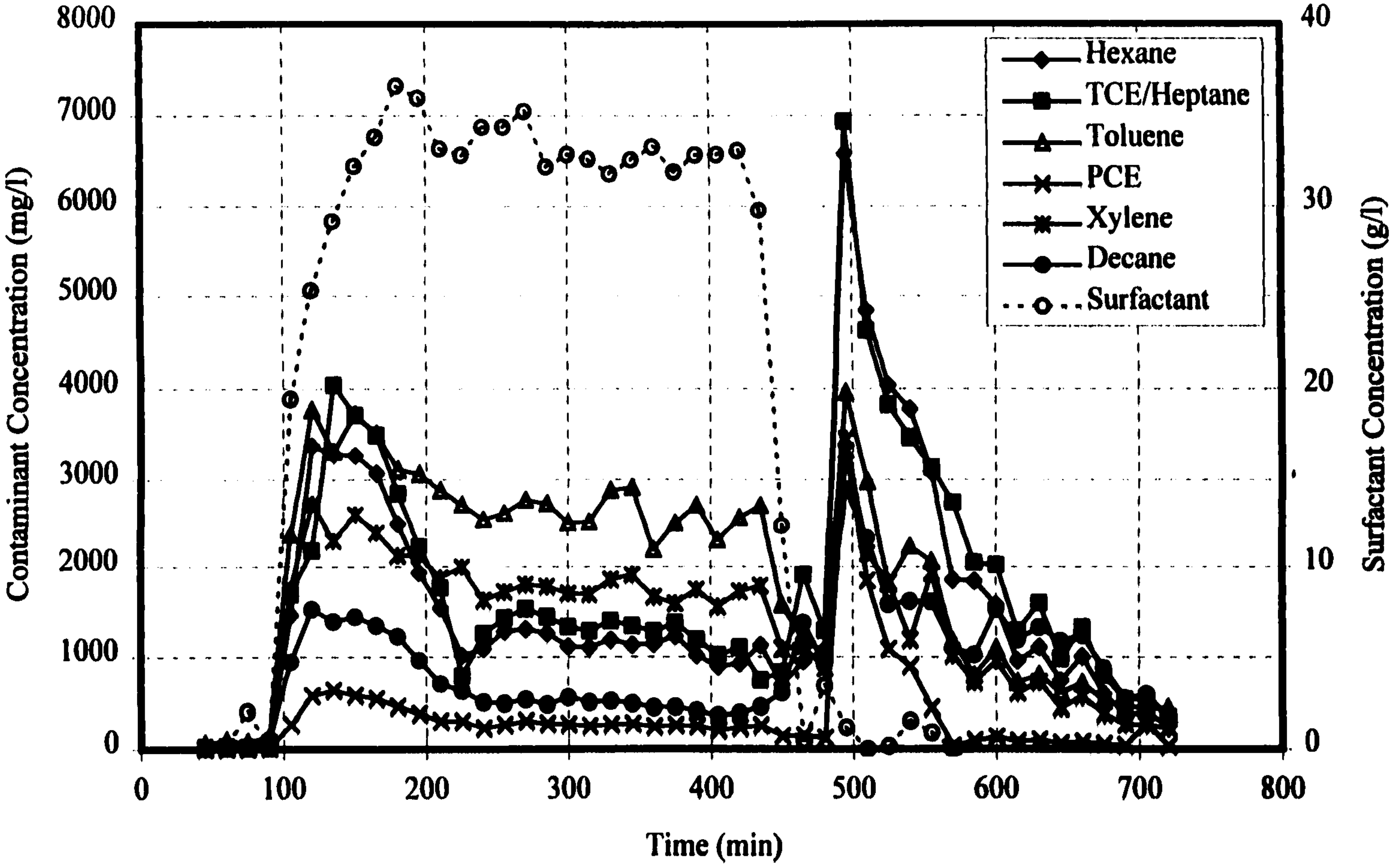

Figure 5.5 Contaminant and Surfactant Concentration Histories During Surfactant Flooding Process and Subsequent Water Flush (PV = 85 mins)

during the experiment and/or small amounts of separate phase NAPL remaining in the column after the emplacement process. Since the focus of this portion of the experiment was on the difference between the pre- and post-remediation tracer tests, the later peaks are intriguing but not critical to this research.

Another observation from Figure 5.5 is the similarity in the plots for components within the same homologous series. Consider toluene and *o*-xylene, both aromatic hydrocarbons, for example. Except for the difference in concentration levels, the overall patterns of the respective plots are similar. The plots for hexane and the TCE/heptane combination are also analogous, with slight differences being due to the presence of the TCE. It is difficult to match the plots of decane and PCE with any of the other compounds because of their low solubility and low polarity, respectively. However, the overall trends for both compounds are similar to the other plots.

Figure 5.6 is a plot of the mole fraction of each component in the effluent as a function of time. Definite changes in the component mole fractions are evident during the transition zones in which the surfactant concentrations either increase or decrease. Referring to the figure and moving left to right, a number of observations can be made. However, relying on the relative order of the respective plots to make generalizations can be misleading because the initial aqueous solubility and amount of increase in solubility are not readily discernible. Important features are the pattern of each respective plot, general trends, and relative magnitude of changes in the plots.

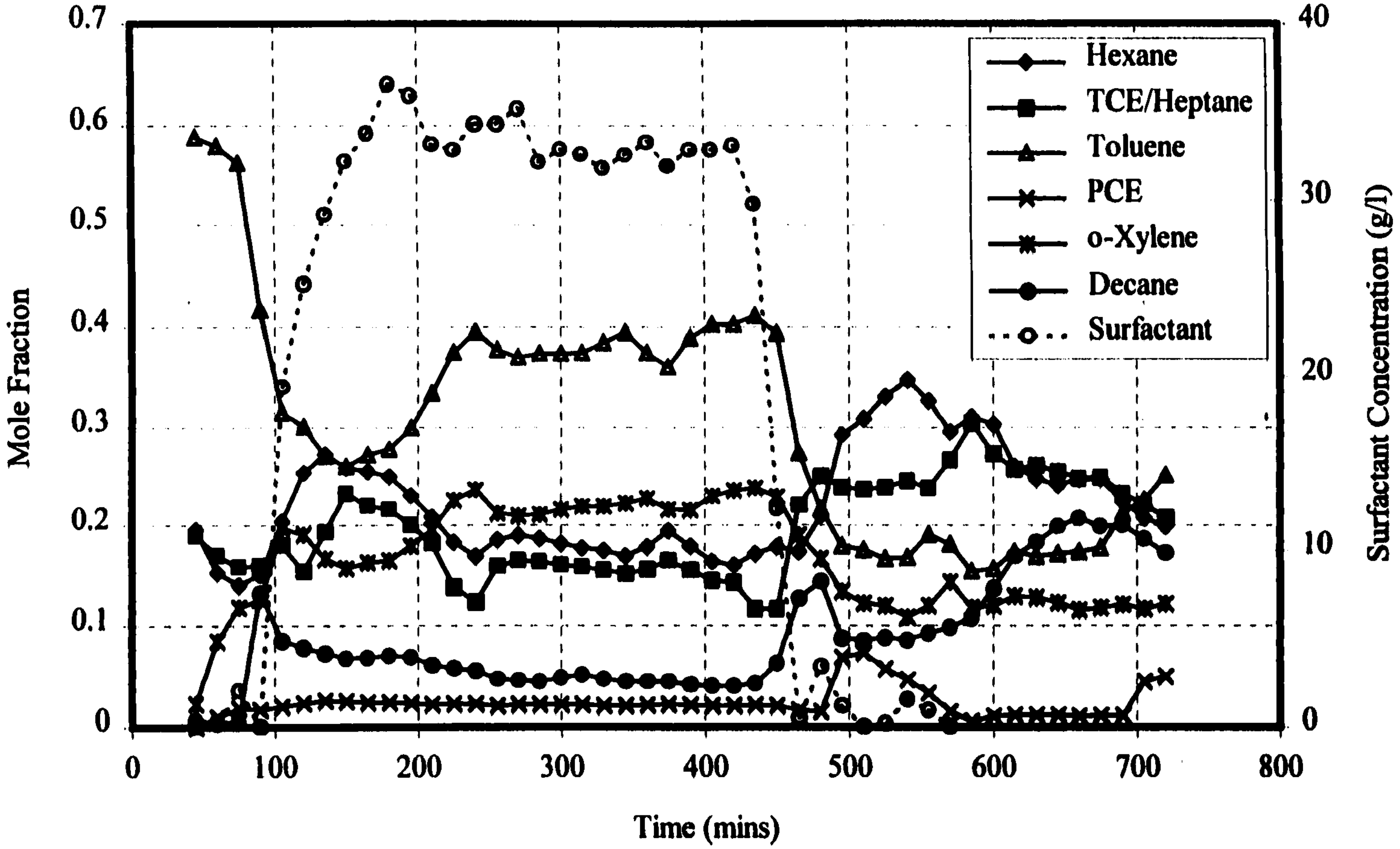

Figure 5.6 Effluent Contaminant Mole Fraction Histories During Surfactant Flooding Process and Subsequent Water Flush

The change in initial mole fraction values prior to surfactant breakthrough is the result of going from a static condition to a dynamic one in which the system is attempting to equilibrate itself. As the surfactant breaks through, there is a change in the mole fraction values corresponding to the first peak in Figure 5.5, which is represented in a slightly different way in Figure 5.6. Note that the mole fractions of hexane and TCE/heptane increase, while the values for toluene, *o*-xylene, and decane decrease. The PCE plot remains fairly constant, indicating the effect of the surfactant might be minimal. The fact that decane does not appear to follow the same trend as the other alkanes is deceiving because its aqueous solubility is 3-4 orders of magnitude smaller. A preliminary conclusion from these observations is that the surfactant seems to cause preferential solubilization of the alkanes.

From approximately 140 to 230 minutes, there is a sharp rise in mole fraction values for toluene and *o*-xylene, accompanied by a drop in values for hexane and TCE/heptane. Note that the decreases in hexane and TCE/heptane values are much greater than the increases in toluene and *o*-xylene mole fractions. During this timeframe (see Figure 5.5), the initial peak of solubilized NAPL is dissipating and concentration values are becoming more representative. The result is a change in mole fraction values as indicated in Figure 5.6. From 230 to 450 minutes, the mole fractions of the contaminant components are reasonably constant. The relative order of contaminant components, and the higher mole fraction values for *o*-xylene and toluene, seem to indicate that the aromatic compounds are undergoing preferential solubilization, contradicting the preliminary conclusion from the previous paragraph.

The large peak in concentration levels after the surfactant concentrations have dissipated (Figure 5.5) is also reflected in a rather abrupt change in the mole fraction values of the effluent as shown in Figure 5.6. The increases in mole fraction values for hexane, TCE/heptane, and decane appear to indicate preferential mobilization for the alkanes. The sharp reductions in values for the aromatics seem to indicate that the surfactant did not have a significant mobilization effect on them. The increase in PCE mole fraction values can probably be attributed more to its greater density than to the surfactant.

Figure 5.7 was prepared to compare the cumulative mole fraction of each component in the effluent as a function of time. The cumulative mole fraction can be defined as the mole fraction of a given component in the accumulated column effluent. As previously identified, the plots for toluene and *o*-xylene are very similar, as are the plot for hexane and TCE/heptane. Once surfactant concentrations begin to peak, there is a slight increasing trend for toluene and *o*-xylene. The other components show slight decreasing trends. As the surfactant concentrations approach zero, these trends reverse themselves. The exception is PCE, which remains essentially constant. A preliminary conclusion from this figure would again seem to indicate that the aromatics are undergoing preferential solubilization.

Figure 5.8 was prepared to compare the cumulative number of moles for each contaminant component as a function of time. Three distinct zones are evident in the figure. From 100 to 200 minutes, the respective slopes for each component represent the initial peak in Figure 5.5. After the peak has dissipated, the slopes decrease and

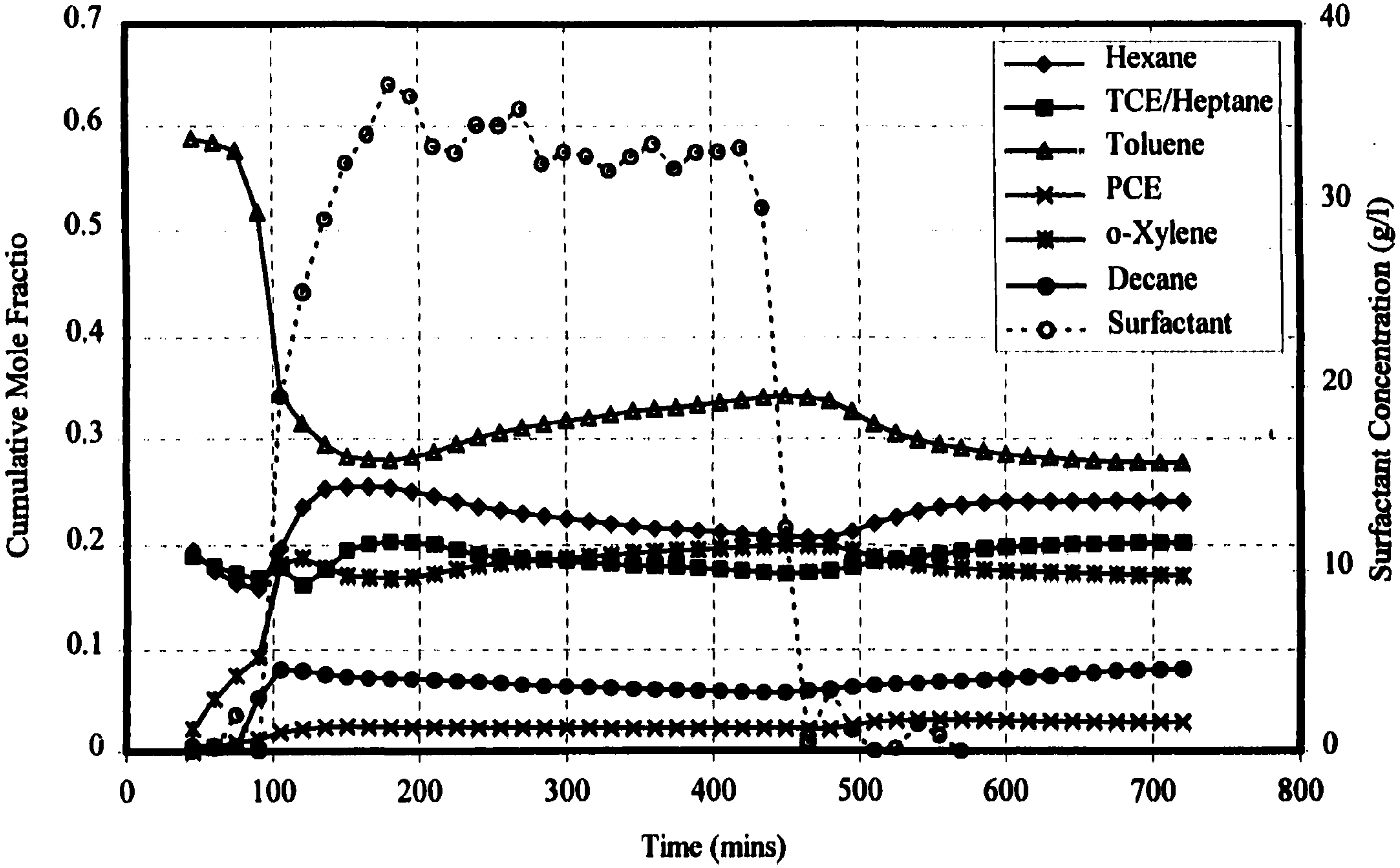

Figure 5.7 Effluent Cumulative Contaminant Mole Fraction Histories During Surfactant Flooding Process and Subsequent Water Flush

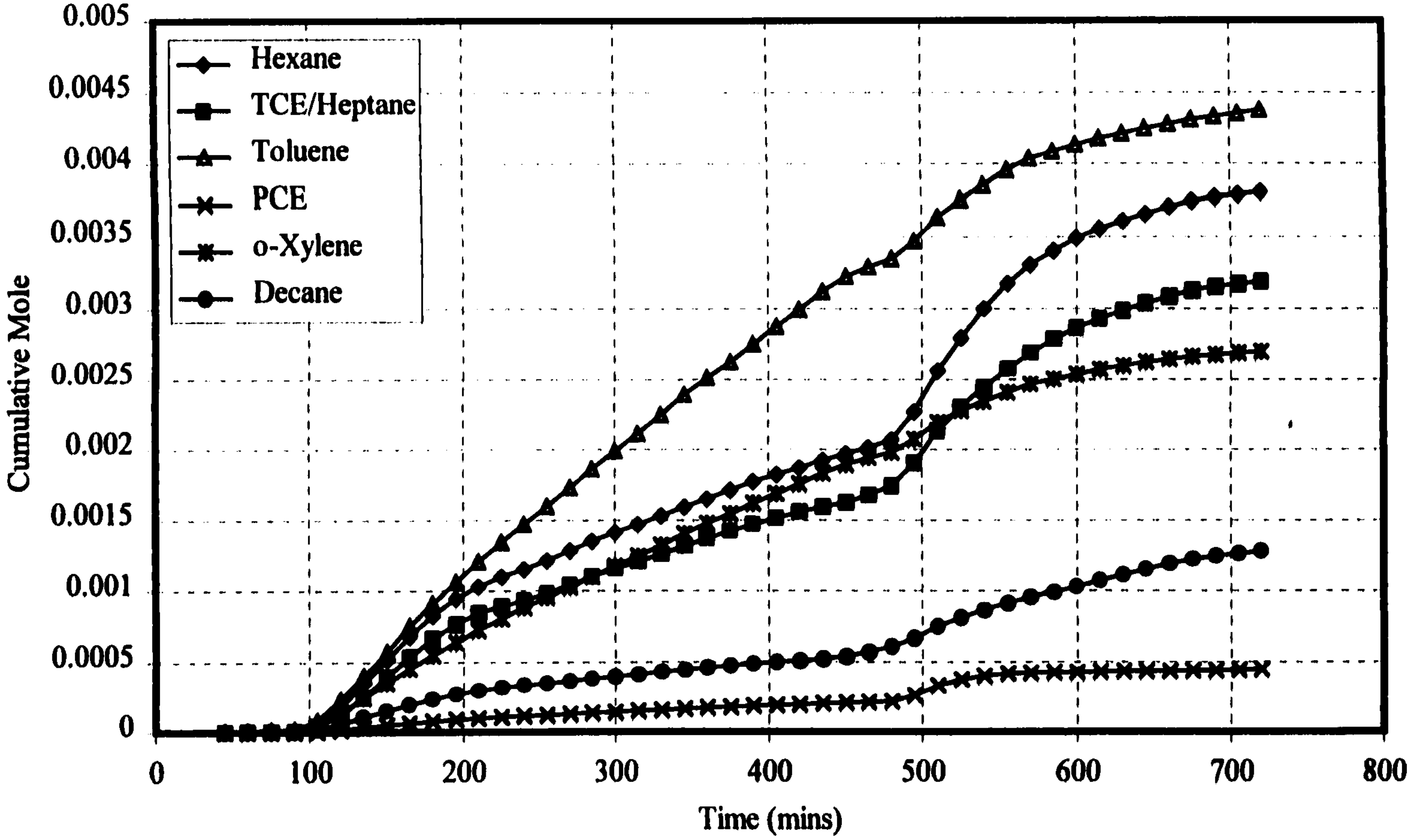

Figure 5.8 Effluent Cumulative Contaminant Mole Histories During Surfactant Flooding Process and Subsequent Water Flush

reflect the accumulation of solubilized components. At the 500-minute mark, the respective slopes increase and reflect the mobilized components in the second peak of Figure 5.5. As the mobilized contaminants dissipate and the water flush is occurring, the slopes again decrease and begin to approach zero. Since the contaminant mole fractions are accumulating at a higher rate during the mobilization peaks, the slopes of the respective plots were greater during these timeframes. If the slopes of the plots during the solubilization process are considered, it appears as though toluene and *o*-xylene are being preferentially solubilized because of their steeper slopes.

Interpreting plots such as Figures 5.5 through 5.8 can be a challenging task. To make it easier to identify preferential solubilization/mobilization, the increase in solubility levels due to the addition of surfactant can be evaluated. A Solubility Ratio Index (SRI) was thus devised as part of this research and defined as,

$$\mathrm{SRI} = C / S \tag{5.8}$$

where, for a given contaminant, C is the measured concentration during the solubilization process and S is the component's aqueous solubility (adjusted according to Raoult's Law).

The SRI values for the contaminant components used during the column study are shown in Table 5.9. The increased solubilities of some of the contaminants were not as significant as those typically found in the literature, many of which are 5 to 7 orders of magnitude greater than their aqueous solubilities. However, the values reported by other researchers were for single-component NAPLs. Therefore, one

Table 5.9: Concentration Levels in Effluent (mg/l) and SRI Values

Component	Aqueous Solubility (mg/l)[a]	Average Levels in Surfactant Zone[b]	SRI	log SRI	Rank[c]
Hexane	1.36	1580	1159	3.06	2
TCE/Heptane	69.88	1720	24.6	1.39	5
Toluene	136.3	2766	20.3	1.31	6
PCE	10.37	320	30.9	1.49	4
o-Xylene	51.97	1877	36.1	1.56	3
Decane	0.0052	720	13,800	5.14	1

[a] Adjusted according to Raoult's Law
[b] From 105 to 450 minutes
[c] Order of preferential solubilization magnitude

possible explanation for smaller solubility increases may be the preferential solubilization of certain components in the multi-component NAPL. This agrees with the observations made about the previous figures. Another possible explanation may be the non-optimized surfactant solution, which was a 4 wt% mixture of de-ionized water and Dowfax 8390, and the resulting inefficient remediation process.

Given the non-optimized conditions and multi-component nature of the NAPL, the variability in SRI values was interesting. The solubility of toluene was increased by a factor of about 20, the SRI was increased by over 5 orders of magnitude for decane, and the other components had increases between these two extremes. For the TCE/heptane combination, it was hypothesized that the solubility of the TCE (69.5 mg/l) was not significantly enhanced by the addition of the surfactant since the TCE is highly polar. Therefore, the observed solubility increase for the TCE/heptane combination was attributed primarily to an increase in the solubility of heptane. If the aqueous solubility of TCE is subtracted from the TCE/Heptane value in Table 5.9, an SRI of almost 4,400 can be calculated for the heptane (with a log SRI value of 3.64).

A trend is evident if the SRI values are considered for each series of components (i.e., hydrocarbons and chlorocarbons). The lower the aqueous solubility of a component within a particular series, the greater the increase in solubility due to the addition of the surfactant. Given the extremely small sample size for each series of components (only two or three samples), this trend should be considered somewhat tenuous. However, it is apparent from Figures 5.5 through 5.8, and the results shown in Table 5.9, that preferential solubilization occurred. Furthermore, the SRI concept provides values that also correspond to a relative ranking of the order in which the process occurred (i.e., the decane and toluene are the most and least preferentially solubilized, respectively).

Figure 5.9 is a plot of log SRI values as a function of time and clearly shows the effect of the surfactant. If it is assumed that all contaminant components respond to the surfactant in a consistent manner, the respective plots in Figure 5.9 should not intersect except during transition periods (beginning and end of surfactant breakthrough). The TCE/heptane plot violates this principle because of the large difference in respective aqueous solubilities (1,100 mg/l versus 2.4 mg/l).

Figure 5.10 is a plot of log SRI values as a function of aqueous solubility for each component. The result is an inverse linear relationship for the hydrocarbon compounds. Note that the data point for the TCE/heptane mixture in Figure 5.10 lies close to the regression line, an indication that the surfactant had relatively little impact on TCE. Assuming that to be the case, a log SRI value of 3.64 can be calculated for heptane. If this value and the heptane solubility of 0.38 mg/l were plotted in Figure 5.10, the data point would lie close to the regression line. The TCE data point would then be offset from the hydrocarbon regression line by a distance similar to that of the PCE data point (and the slope of the resulting line would be similar to that of the hydrocarbon regression line). Further research is needed to determine if these observations represent a universal relationship that can be used to predict solubility increases.

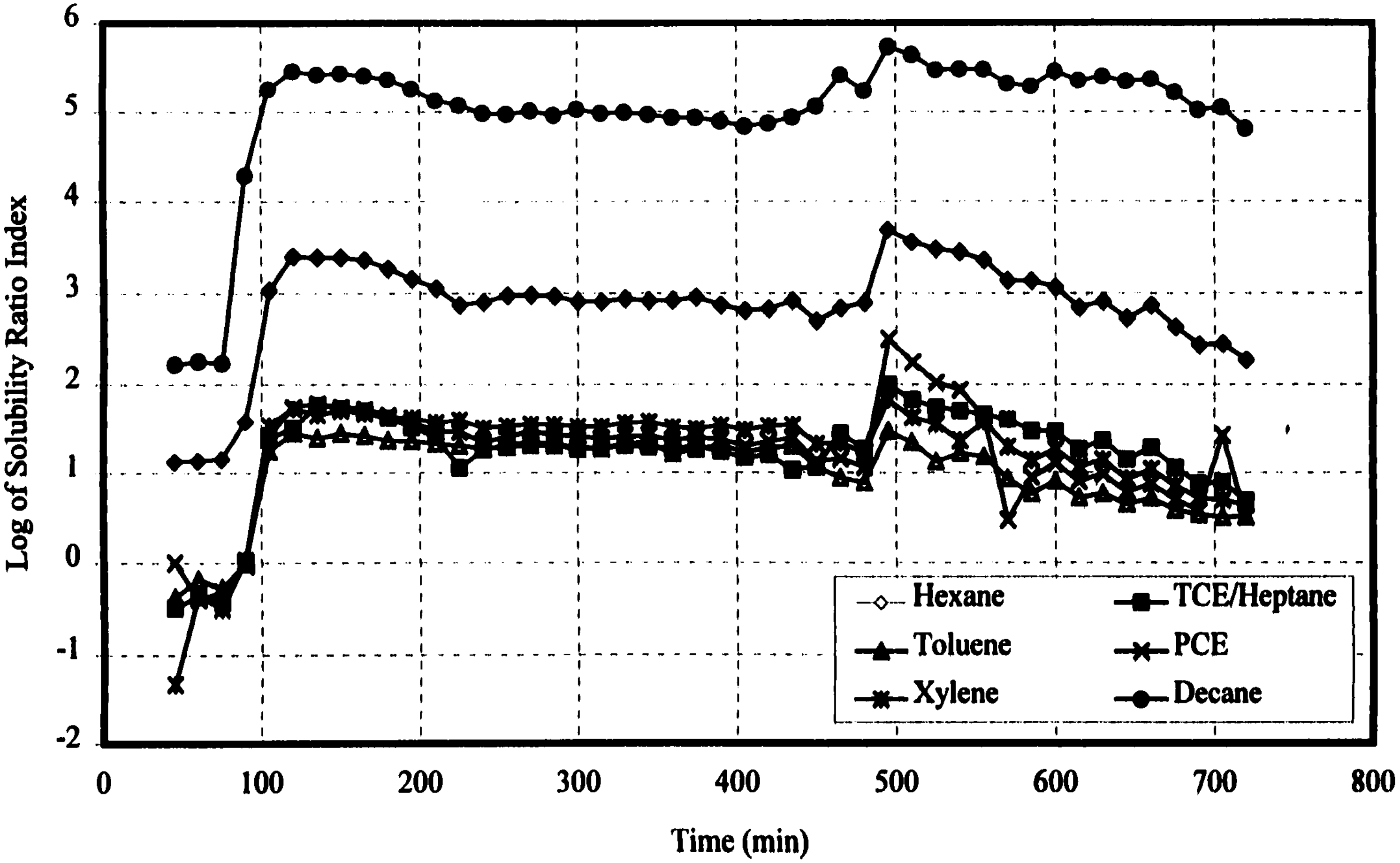

Figure 5.9 Solubility Ratio Index Histories During Surfactant Flooding Process and Subsequent Water Flush

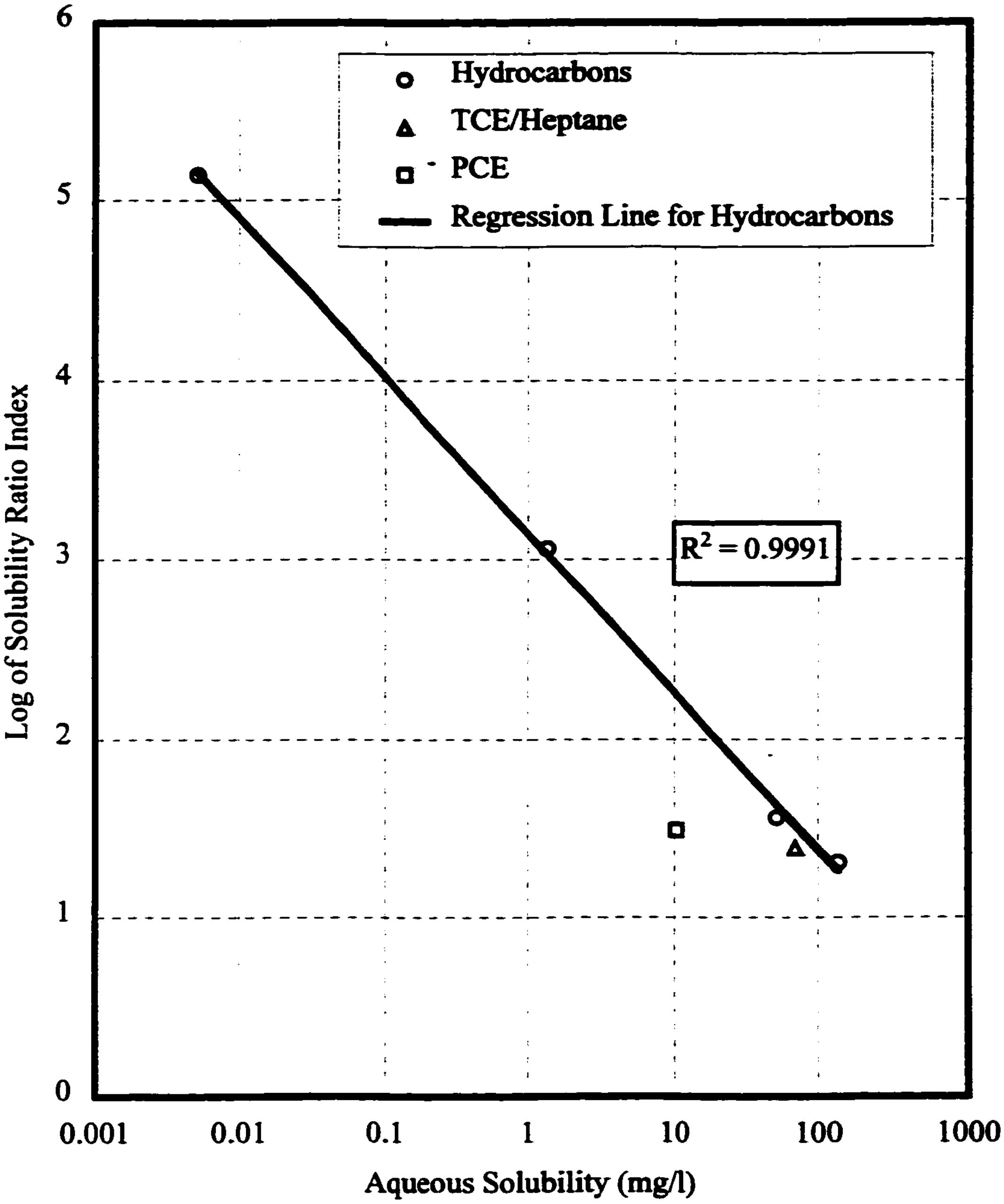

Figure 5.10 Relationship Between Solubility Ratio Index and Aqueous Solubility

The discussion to this point has centered on effluent composition. Crucial to this research though, is the composition of residual NAPL remaining in the column. Recall that the original synthetic NAPL composition was given in Table 5.1. It was assumed that the composition of the NAPL was not altered significantly by the emplacement and flushing processes. Furthermore, it was assumed the composition remained constant during the initial series of tracer tests. To determine the mass of each component present in the soil column before remediation, mass ratios were determined from the data shown in Table 5.1 and the volume of residual NAPL was calculated as 6.48 cm^3 (21.7 percent) from the method of moments,

$$V_{NAPL} = S_N * PV \tag{5.9}$$

Using the mole fractions to determine a density of 0.86, the corresponding mass of the residual NAPL was calculated as 5.5872 grams. For each contaminant component, the corresponding mass is shown in Table 5.10 along with the cumulative mass in the effluent and the mass remaining after remediation (with mole fraction calculations). Assuming no change in the pore volume, the residual NAPL mass of 3.9594 grams remaining after surfactant flooding represents a mass reduction of 29.1 percent and a residual saturation of 15.37 percent.

Using the same mass balance approach, Figure 5.11 illustrates the mole fraction composition of the remaining residual NAPL. From the figure, it is apparent that the composition of the residual NAPL did not appear to change appreciably during the remediation process. The largest change was the mole fraction decrease

Table 5.10: Mass Balance Analysis

Component	Decane	TCE/Heptane	Hexane	*o*-Xylene	Toluene	PCE
Mass Ratio	0.1670	0.1648	0.0858	0.2486	0.2544	0.0793
Residual NAPL Mass (g)	0.9331	0.9208	0.4794	1.3890	1.4214	0.4431
Effluent Mass (g)	0.1799	0.3608	0.3268	0.2854	0.4010	0.0735
Mass Remaining (g)	0.7532	0.5600	0.1526	1.1036	1.0204	0.3696
Moles (x 10^{-3}) Remaining	5.2934	4.9235	1.7707	10.3947	11.0745	2.2288
Mole Fraction Remaining	0.1483	0.1380	0.0496	0.2913	0.3103	0.0625

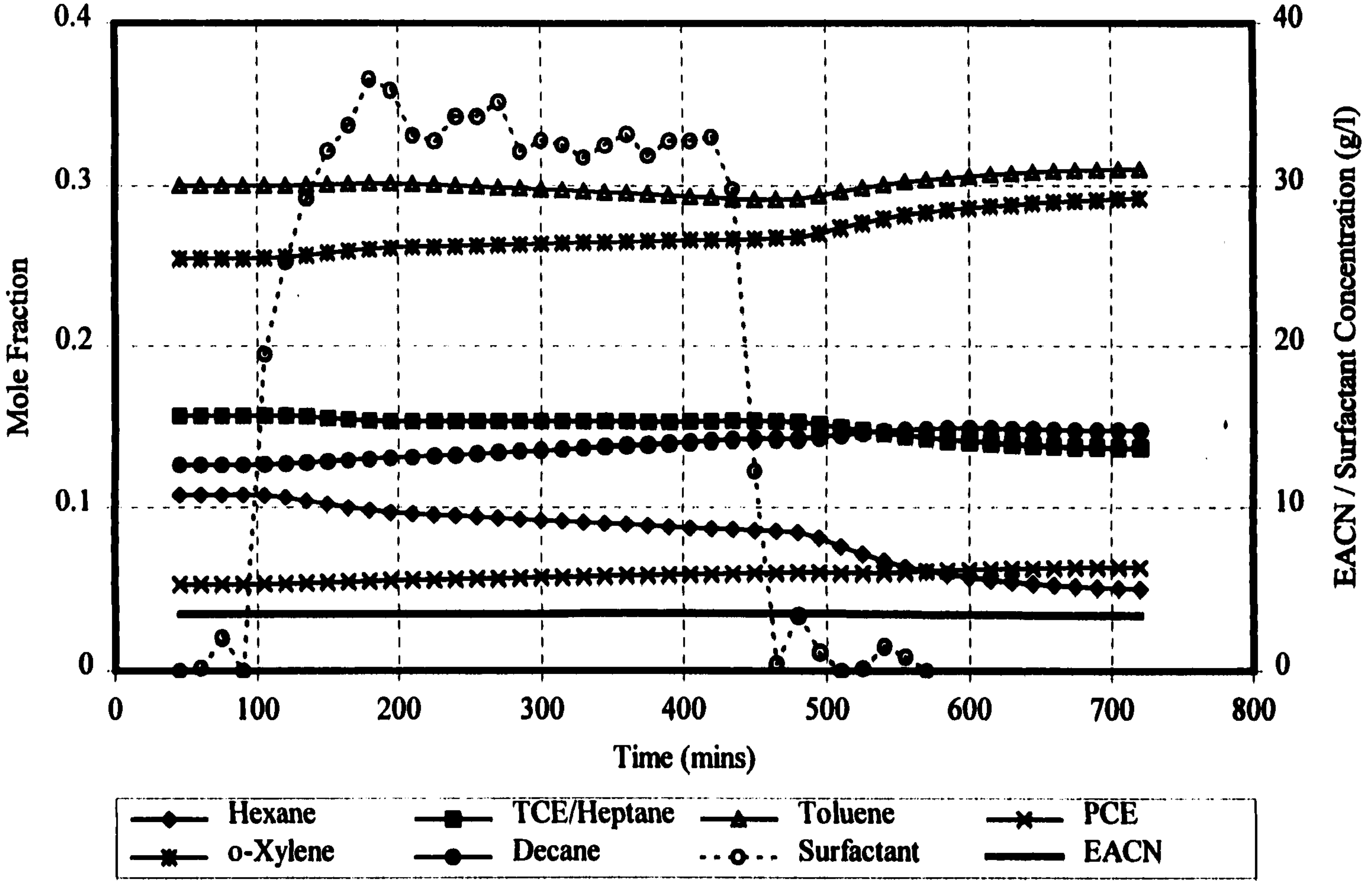

Figure 5.11 Contaminant Mole Fraction of Residual NAPL in Column During Surfactant Flooding Process and Subsequent Water Flush

from 0.11 to 0.05 for hexane. The other components had only slight changes and were reasonably constant. To determine if these differences affected the EACN of the NAPL, the EACN value was calculated at each time step throughout the process and plotted on the figure as well. As can be seen from the figure, the EACN values were remarkably constant and varied by less than 3 percent. The lack of change in composition and EACN were unexpected. However, only about 25 percent of the residual NAPL was removed during the surfactant flushing process. Extended flushing with greater mass removal might cause changes in the NAPL composition and EACN.

5.3.5 NAPL Composition and Partition Coefficients

The relationships previously developed and represented by the equations in Table 4.11 clearly show that the partition coefficient of an alcohol tracer is a function of both the NAPL and alcohol EACN values. Implicit in these equations is the fact that a change in NAPL composition results in a change in the partition coefficient. Using the effluent concentration histories from the column study, the EACN of residual NAPL remaining after remediation was calculated as 3.36. This was slightly lower than the EACN of 3.46 for the original synthetic NAPL. Recall from Figure 5.11 that EACN values were relatively constant throughout the remediation process. Using the new EACN value, the partition coefficient was calculated as 11.376 for 2-methyl-2-hexanol and 1.362 for pentanol. These values differ from the original partition coefficients (11.182 and 1.339, respectively) by only 1.7 percent.

5.3.6 Final Tracer Test Results

After the surfactant flushing process, several pore volumes of water were flushed through the column and a final tracer test was conducted to determine the remaining residual saturation. The breakthrough curves for the tracers injected into the column at a flow rate of 0.3 ml/min are shown in Figure 5.12 and summarized in Table 5.11. The separation of curves indicates that a significant amount of NAPL remained in the soil column after the surfactant flooding process. Using the method of moments, the remaining residual saturation was determined to be 13.39 percent, which is lower than, but still in good agreement with, the value of 15.37 percent determined from the mass balance analysis.

Using the method of moments to calculate the pore volume resulted in an average value of 39.04 cm^3. Subtracting the volume of tubing (4.63 cm^3) provided a final pore volume estimate of 34.41 cm^3. This is approximately 34 percent higher than the initial pore volume calculated gravimetrically and 20 percent higher than previous values calculated using the method of moments. A possible explanation for the increase is the mobilization of fines during the surfactant flushing process. If the remaining residual mass of 3.9594 grams is assumed to exist in the original pore volume of 25.3 cm^3, the corresponding residual saturation is 15.65 percent, which is in excellent agreement with the value of 15.37 percent determined from the mass balance analysis.

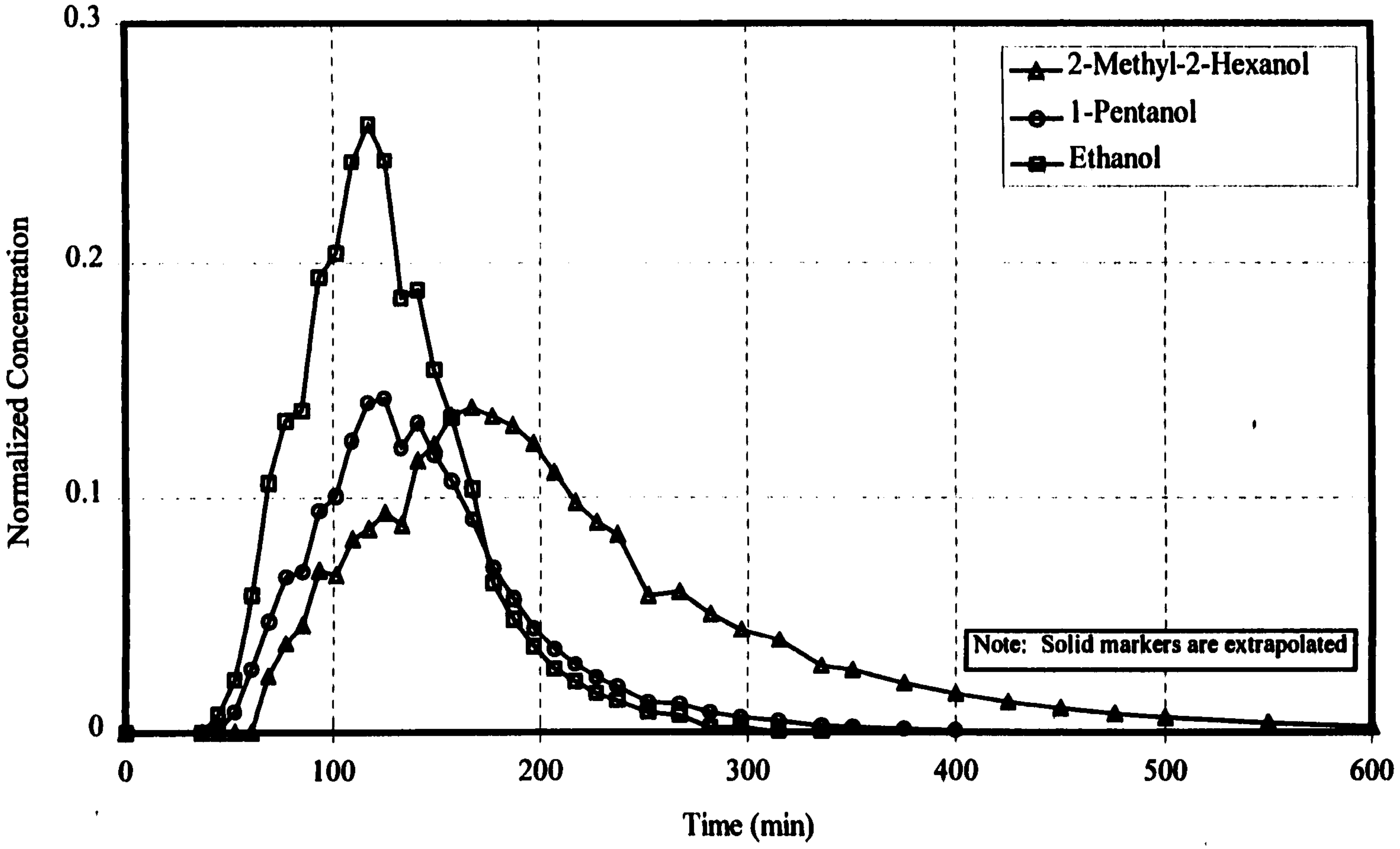

Note: Solid markers are extrapolated

Figure 5.12 Breakthrough Curves for Column after Surfactant Flood (flow rate = 0.3 ml/min)

Table 5.11: Tracer Test Results for Column after Surfactant Flooding

Tracer	Residence Time (mins)	Mass Recovery	K	R	S_N[a] (%)	S_N[b] (%)	PV (cm^3)
2-Methyl-2-Hexanol	199.53	1.044	11.38	1.72	13.46	9.65	38.84
1-Pentanol	135.49	1.151	1.36	1.16	13.32	NA[c]	39.20
Ethanol	116.49	1.096	1.00	NA[c]	NA[c]	NA[c]	NA[c]

[a] Relative to ethanol
[b] Relative to 1-pentanol
[c] Not Applicable

If the pore water velocity is 0.22 cm/min, as calculated in Section 5.4.3, Equation 5.7 can be used iteratively with the ethanol breakthrough data to estimate a hydrodynamic dispersion coefficient of 2.69 cm^2/min. Substituting this value into Equation 5.6 resulted in a dispersivity calculation of 12.23 cm. This value is significantly larger than the 0.26-cm value calculated previously and reflects the increased "spreading" observed for the ethanol data in Figure 5.12 (compared with Figure 5.2).

For comparison purposes, the pre- and post-remediation ethanol breakthrough curves are shown in Figure 5.13. Since there is an indication of increased void space caused by the mobilization of fines during the surfactant flushing, pore volumes were used for the *x-axis* to make comparisons more meaningful. The mean travel times are expected to be nearly equal for the pre- and post-remediation tracer tests since ethanol is a non-partitioning tracer. For this research, the values were 1.01 and 0.96 pore volumes, respectively, which are in good agreement with each other. The 5 percent difference is considered to be within an acceptable range for experimental error. Plotted as a function of pore volume, the increased spreading is still illustrated and serves as validation that fine sediments were mobilized during the surfactant flushing process.

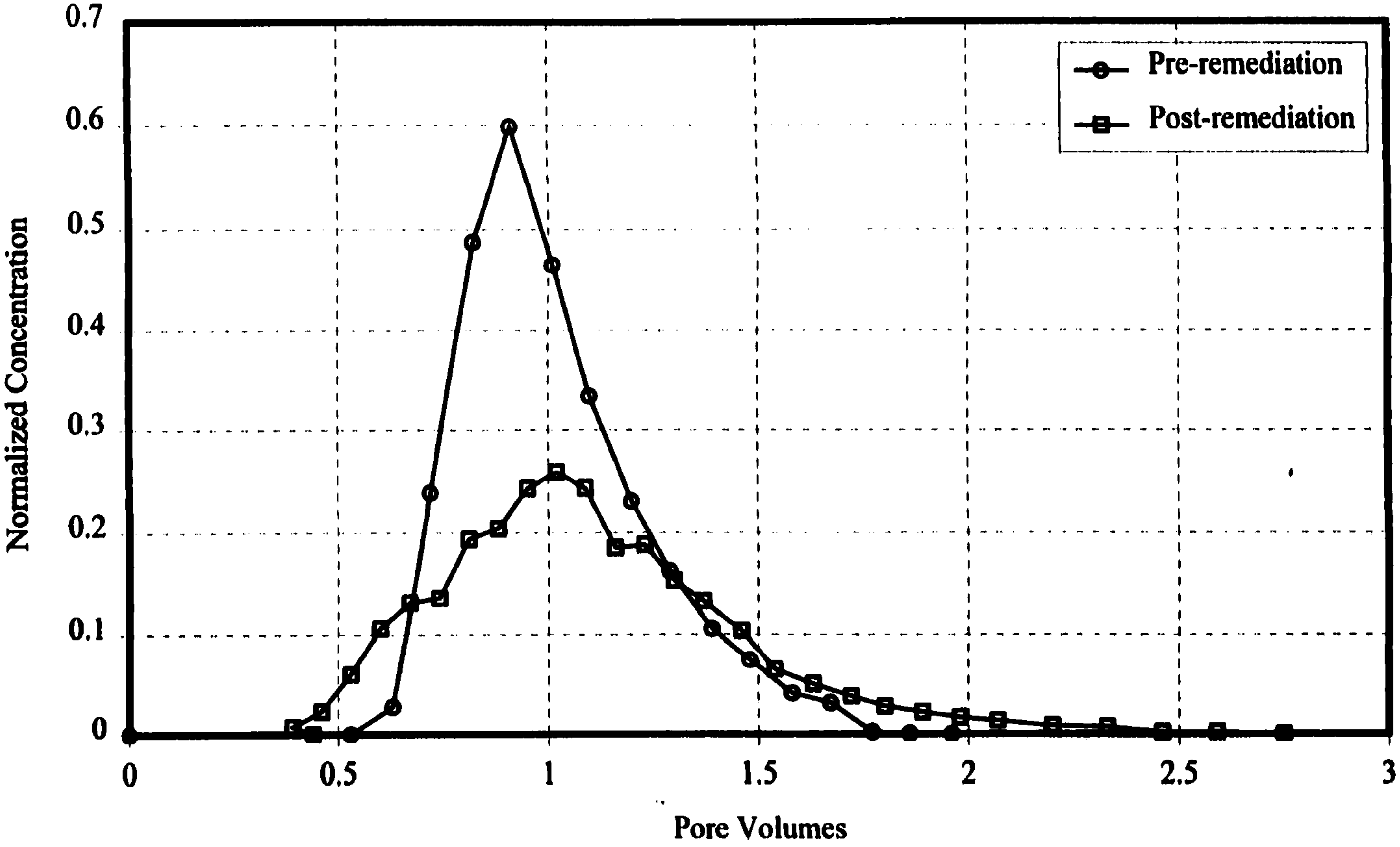

Figure 5.13 Comparison of Pre- and Post-Remediation Breakthrough Curves for Ethanol

5.4 Comparison with Test Cell Results

A similar mass balance analysis was conducted with data from a test cell at Hill Air Force Base (AFB), Utah. The purpose of this analysis was to determine if the trends identified in the column study were consistent on a larger scale. A site plan for the test cell is shown in Figure 5.14 and background material regarding the site can be obtained from the draft Phase I Work Plan prepared by Montgomery Watson (1995). The aqueous solubilities of the contaminants investigated at the site are shown in Table 5.12. These values were adjusted according to Raoult's Law with the mole fraction of each contaminant being based on the results from core samples.

The effluent concentration histories for each of the three extraction wells used during the surfactant flooding process are shown in Figures 5.15 through 5.17. Note the concentration levels in all three figures are relatively low in comparison with the column study concentrations. One possible explanation for this is that the contaminants were chosen as target analytes, with their concentrations assumed to be indicative of the amount of overall NAPL in the subsurface.

In all three figures, there was an initial peak coinciding with the surfactant breakthrough that represented the initial amount of mobilized NAPL. The concentrations slowly decreased and then remained fairly constant after the 125-hour mark. As the surfactant began to dissipate after 250 hours, the contaminant concentrations decreased significantly, evidence that the surfactant solution enhanced solubilization of the contaminants.

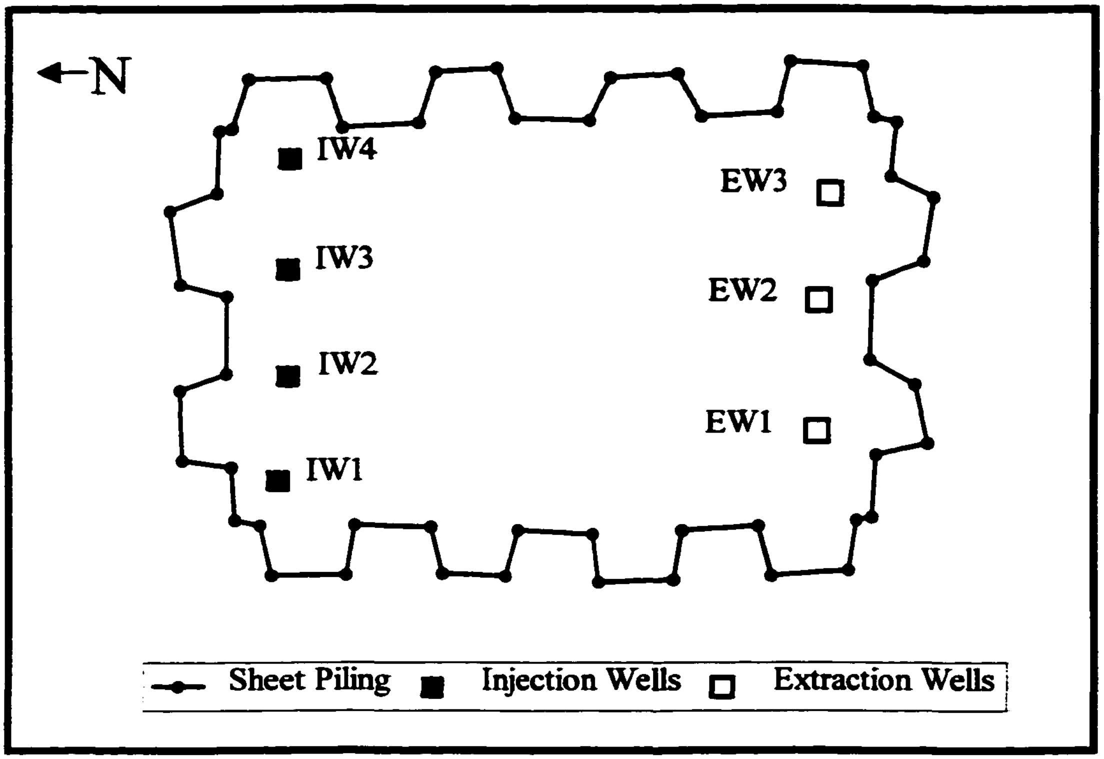

Figure 5.14 Site Plan for Hill AFB Test Cell

Table 5.12: Aqueous Solubilities for HILL AFB Contaminants

Contaminant	Aqueous Solubility (mg/l)
Decane	0.0025
Dichlorobenzene	0.7096
Naphthalene	0.7521
o-Xylene	2.6556
Toluene	0.6383
Trimethylbenzene	1.6509
Undecane	0.0032[a]

Data from Verschueren (1983)
[a] Estimated

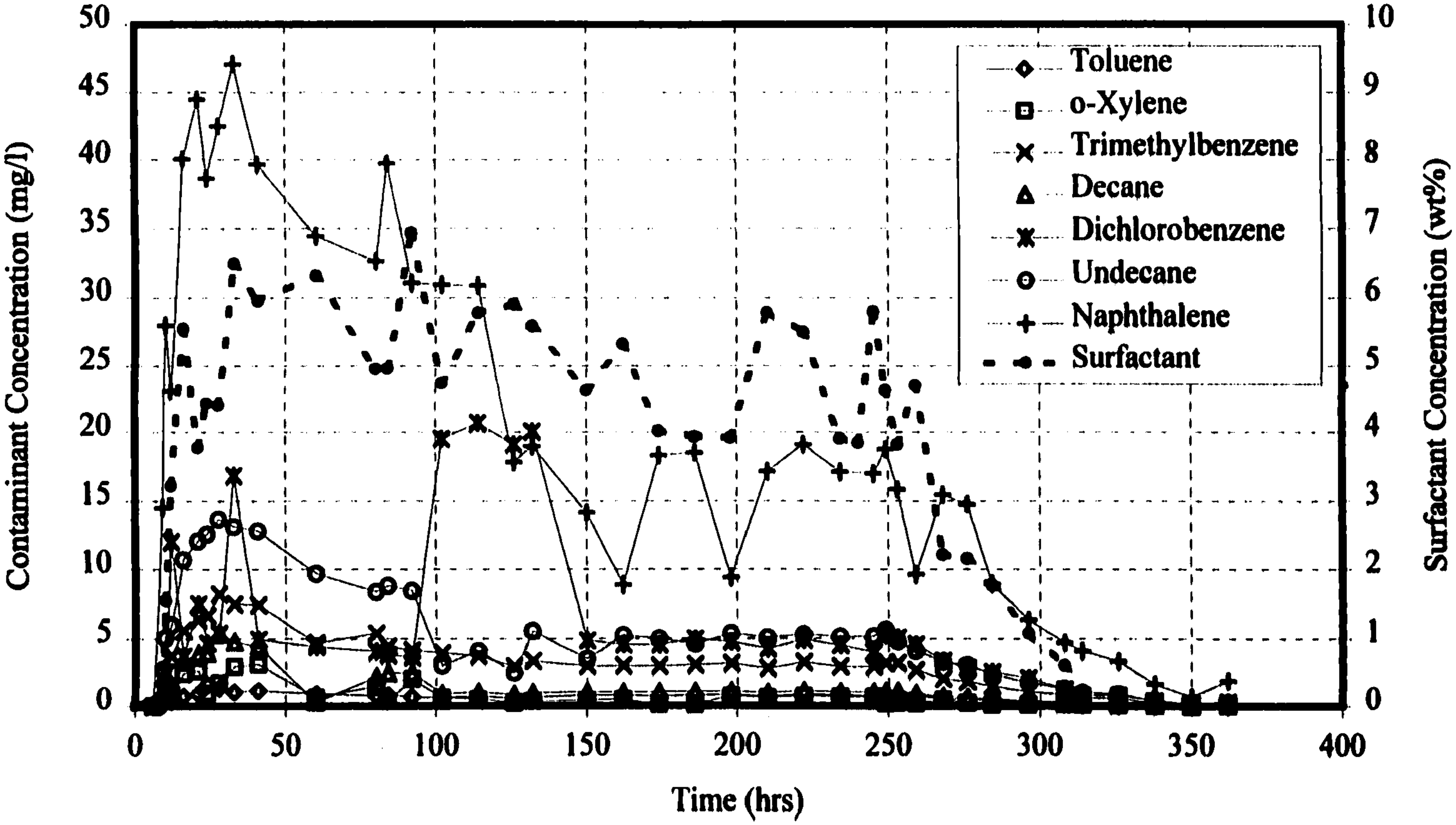

Figure 5.15 Effluent Concentration Histories During Surfactant Flooding Process for Extraction Well 1 at Hill AFB Test Cell

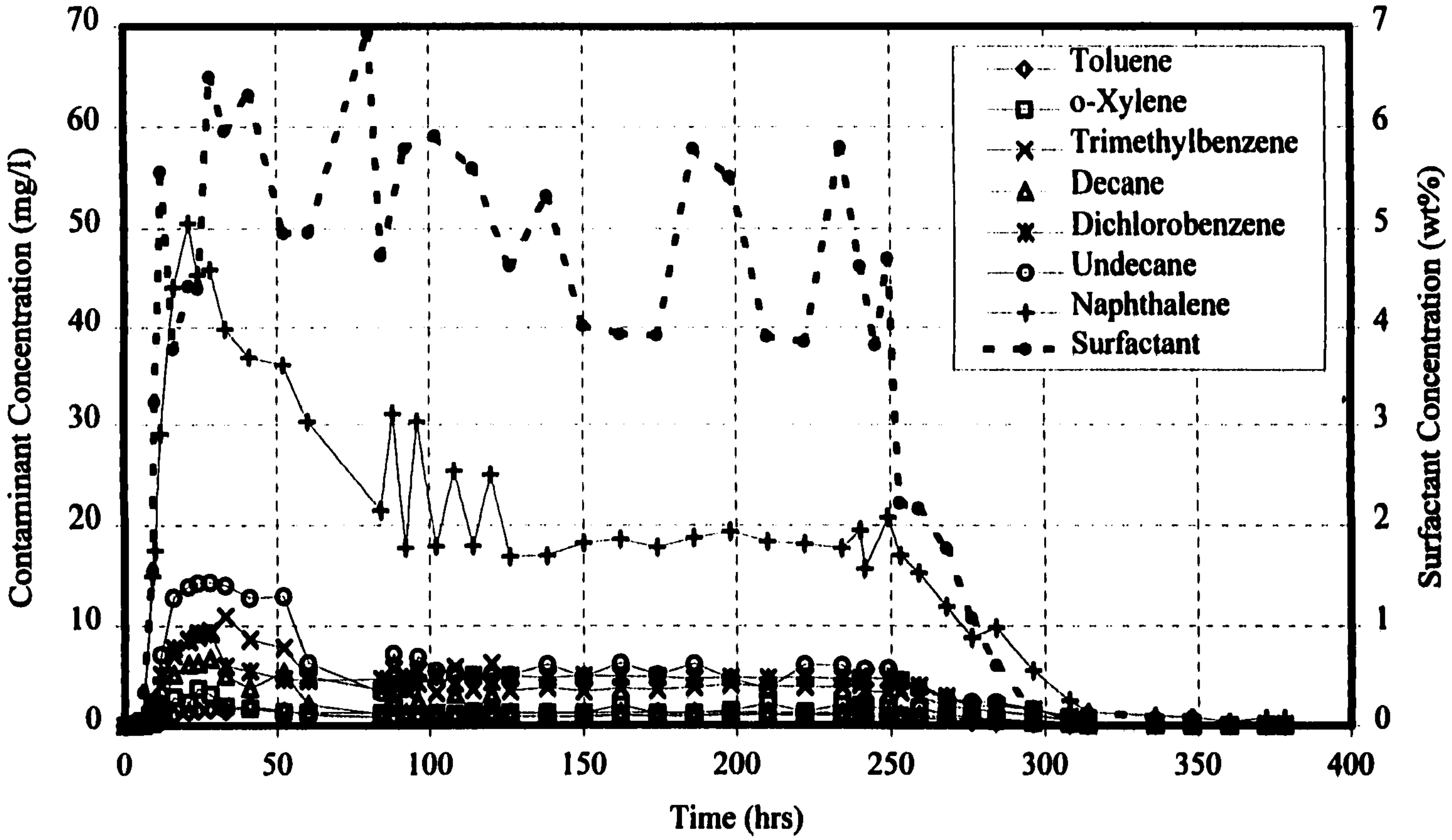

Figure 5.16 Effluent Concentration Histories During Surfactant Flooding Process for Extraction Well 2 at Hill AFB Test Cell

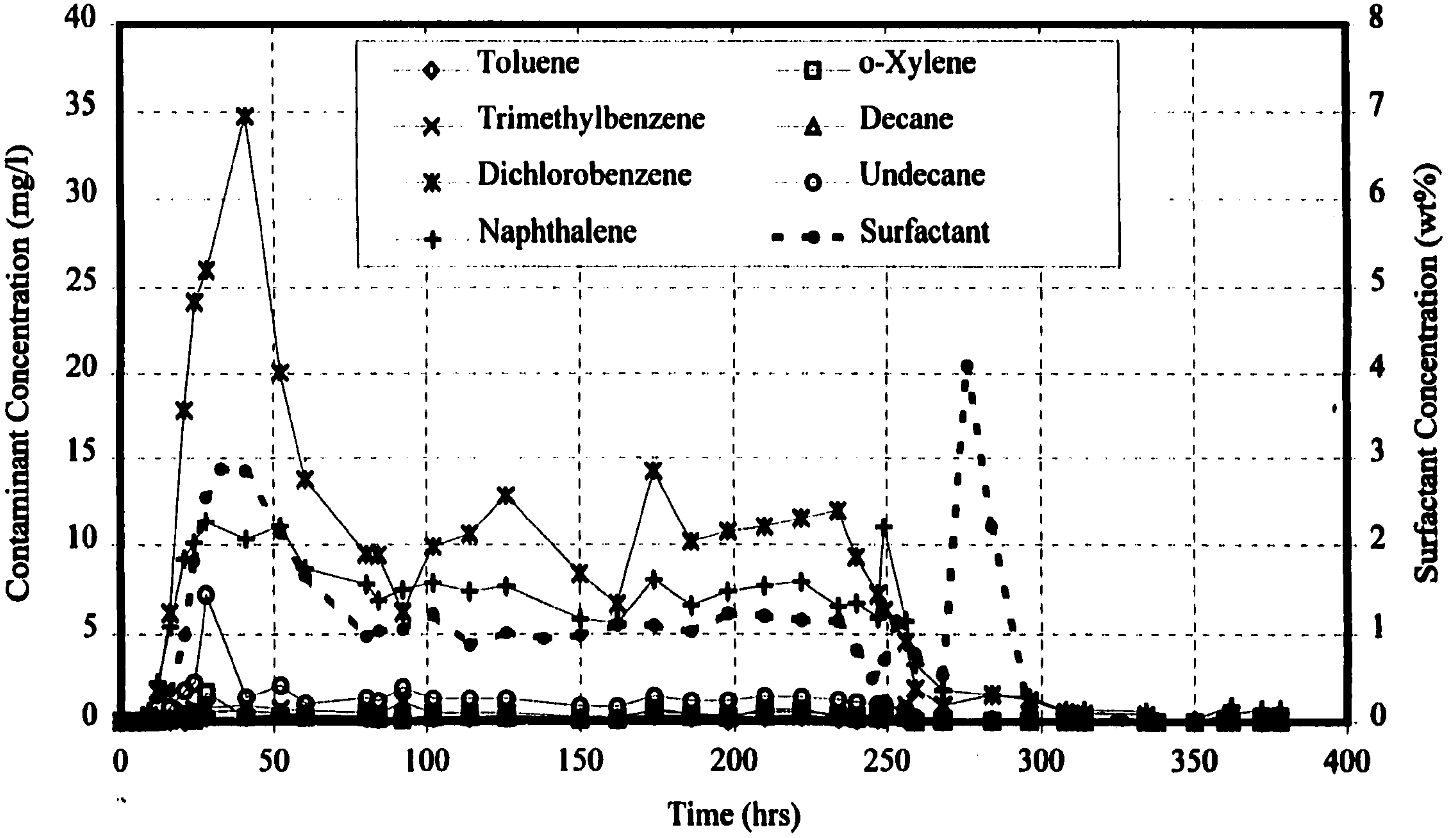

Figure 5.17 Effluent Concentration Histories During Surfactant Flooding Process for Extraction Well 3 at Hill AFB Test Cell

The concentration histories for extraction wells 1 and 2 were noticeably different than that for well 3. Part of the reason for this is because surfactant was only injected in the first three injection wells; the fourth injection well received only water. This is reflected in the lower average surfactant concentrations for extraction well 3 (0.927 wt% versus 3.4 wt% for extraction wells 1 and 2). The variable surfactant concentrations illustrate the effects of surfactant concentration on contaminant concentration levels and the relative order of contaminant concentration levels. The initial hump in surfactant concentrations indicated for all three extraction wells can be attributed to settling of the surfactant solution in the mixing tank.

The concentration histories for extraction wells 1 and 2 are similar. The primary difference is the 4-fold increase in dichlorobenzene (DCB) concentrations in extraction well 1 between 100 and 130 hours. As a DNAPL constituent, the late arrival of the DCB peak is not unexpected. However, the increase is present only in extraction well 1 and seems to indicate that a pocket of concentrated DCB exists along the western edge of the test cell.

Naphthalene exhibited significantly higher concentrations in extraction wells 1 and 2, while dichlorobenzene was present in significantly higher concentrations in extraction well 3. This appears to indicate that naphthalene existed in higher amounts in the western half of the test cell and that DCB existed in higher amounts along the eastern edge of the cell (as well as the concentrated area along the western edge noted above).

Figures 5.18 through 5.20, the effluent concentration histories for the extraction wells on a mole fraction basis, reinforce the observations made from the concentration histories (Figures 5.15 through 5.17). There was a sharp increase in the mole fraction of DCB between 100 and 160 hours, agreeing with the concentration increase observed in Figure 5.15. It was interesting to note that the mole fraction of naphthalene, for all three extraction wells, began to increase as the surfactant concentration approached zero and appeared to continue to rise as the surfactant dissipated.

To help draw meaningful conclusions from the test cell data, the SRI concept was applied to the effluent histories. Figures 5.21 through 5.23 are plots of the logarithm of SRI as a function of time for the respective extraction wells. The order of contaminants and range of SRI values (1 to -3) are similar in all three figures. The negative SRI values represent concentrations less than aqueous solubility levels. This was expected since the contaminants were target analytes in low concentrations and were estimated to represent only 1 to 2 percent of the total contaminant volume. The order of contaminants for extraction wells 1 and 2 are identical and clearly show that undecane and decane are preferentially solubilized. The plot for extraction well 3 indicates preferential solubilization for undecane and decane. The difference in the order of the contaminants from that of the first two extraction wells is due to the lower surfactant concentrations.

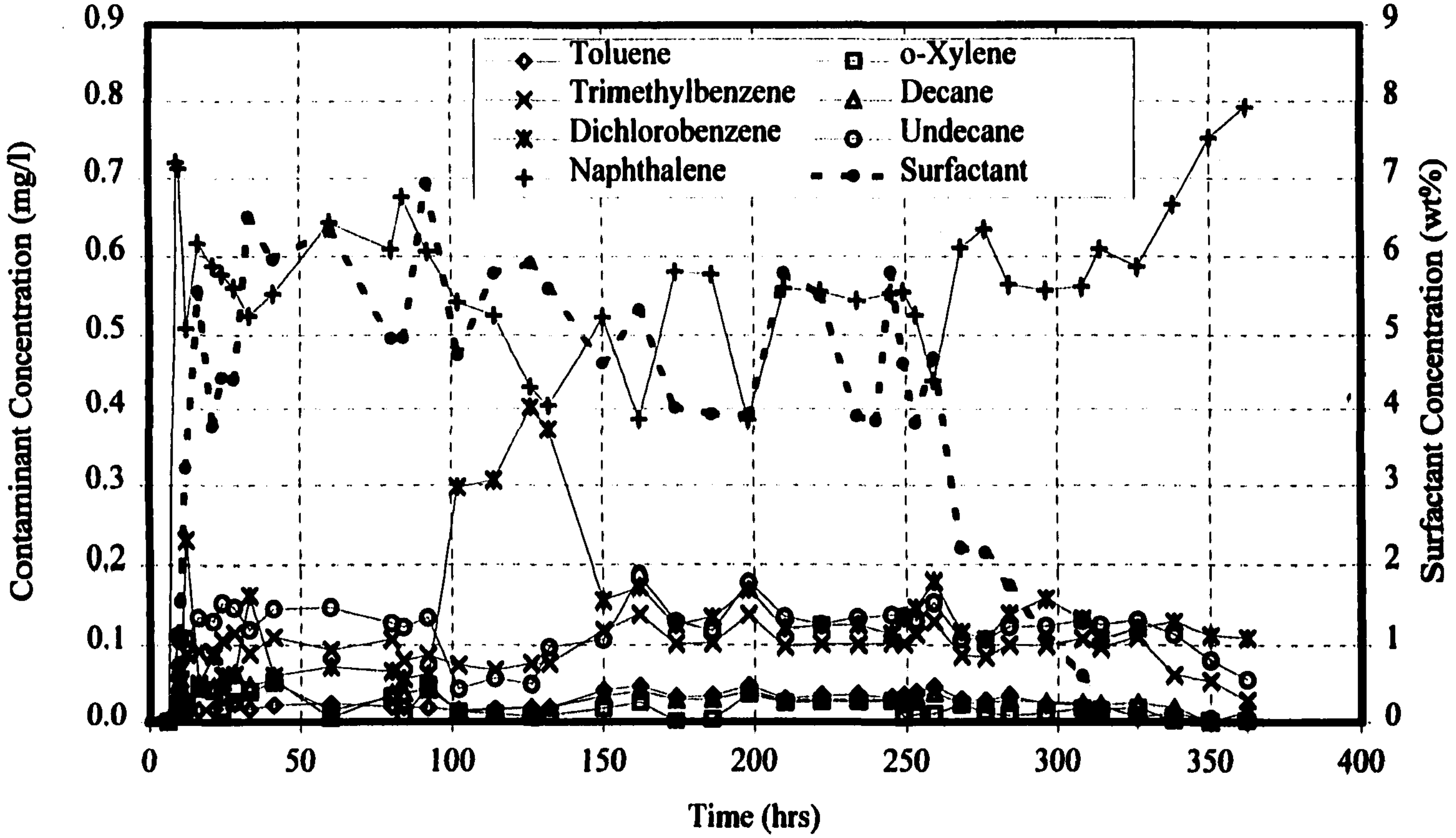

Figure 5.18 Effluent Mole Fraction Histories During Surfactant Flooding Process for Extraction Well 1 at Hill AFB Test Cell

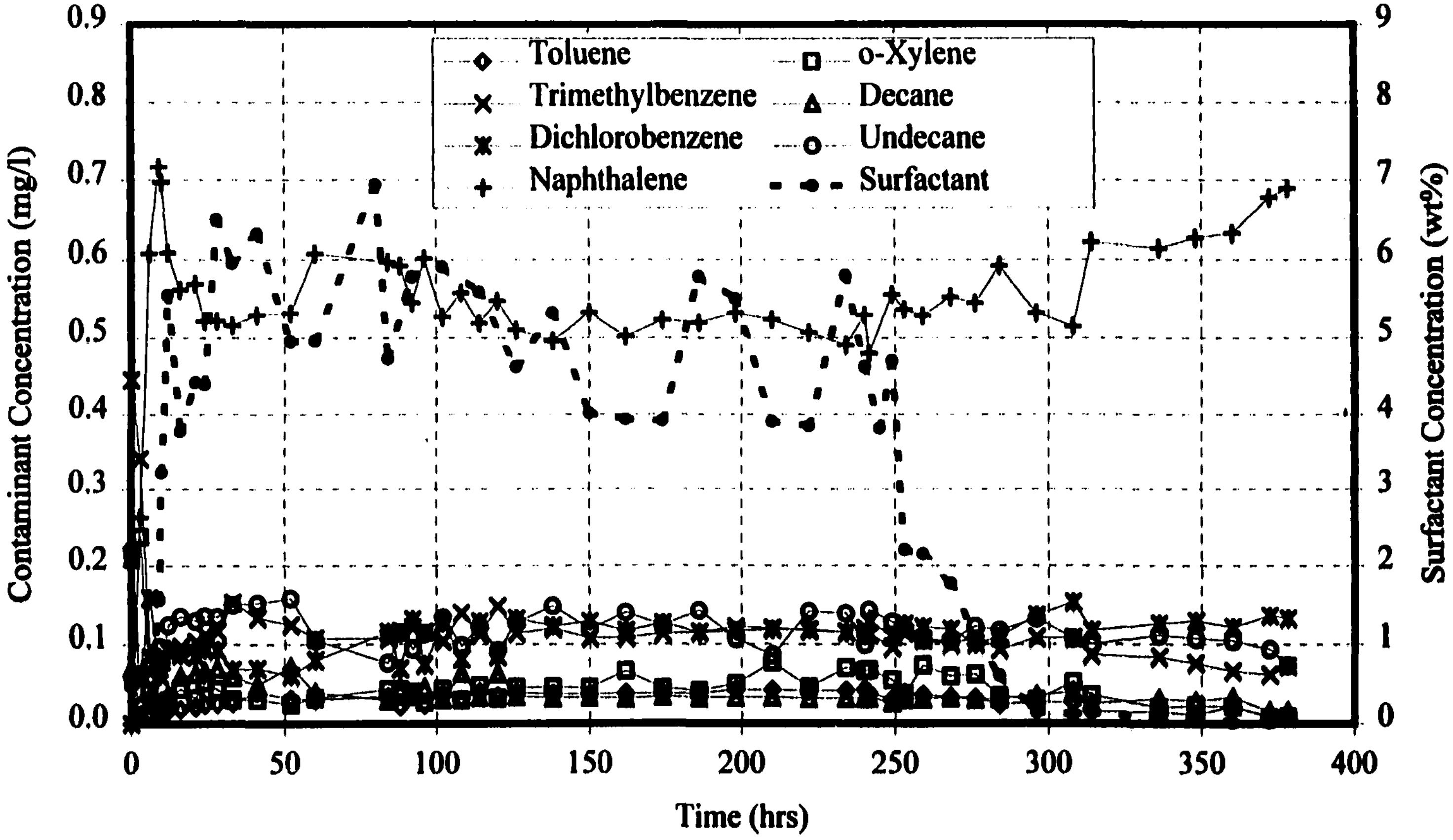

Figure 5.19 Effluent Mole Fraction Histories During Surfactant Flooding Process for Extraction Well 2 at Hill AFB Test Cell

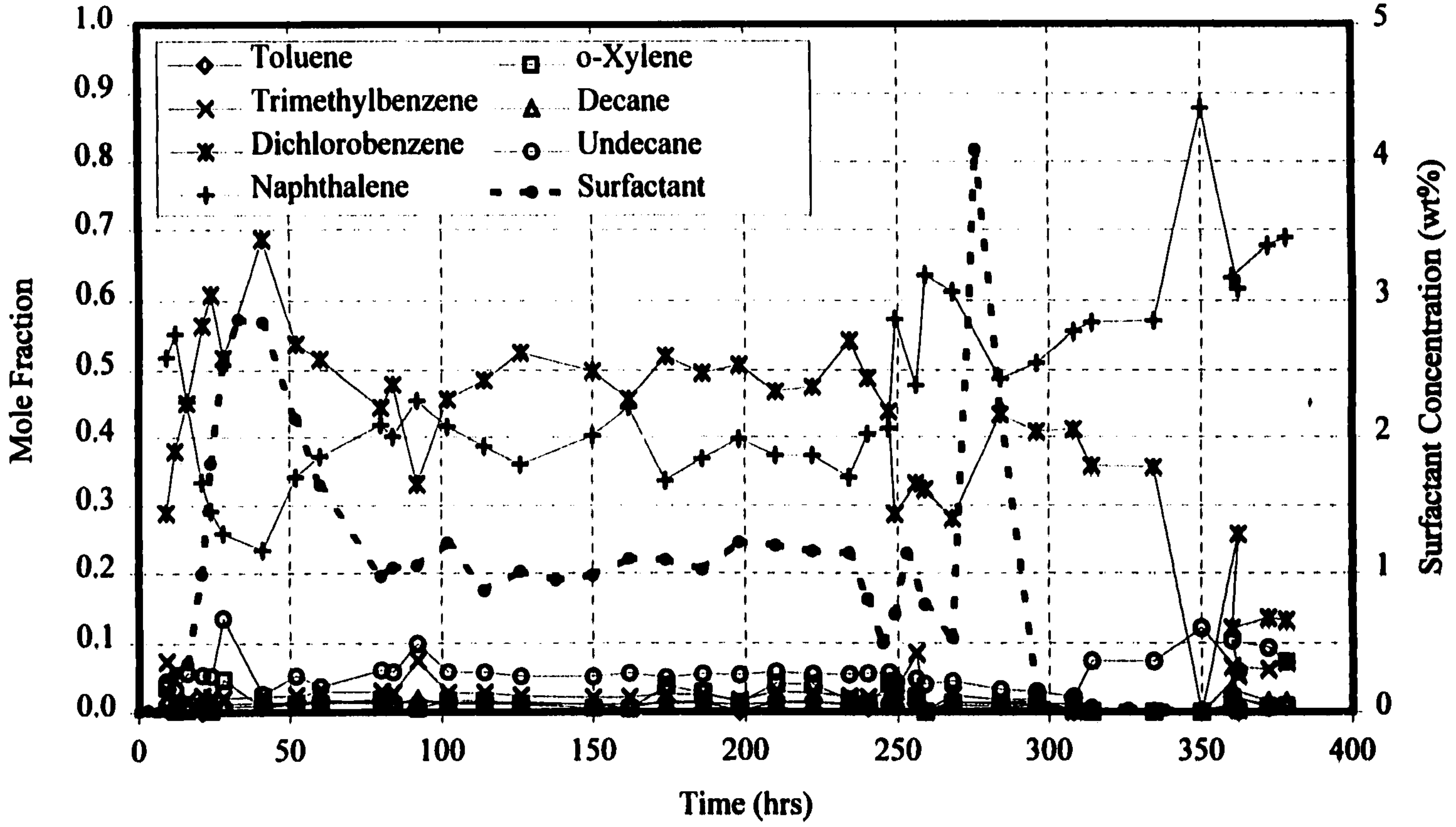

Figure 5.20 Effluent Mole Fraction Histories During Surfactant Flooding Process for Extraction Well 3 at Hill AFB Test Cell

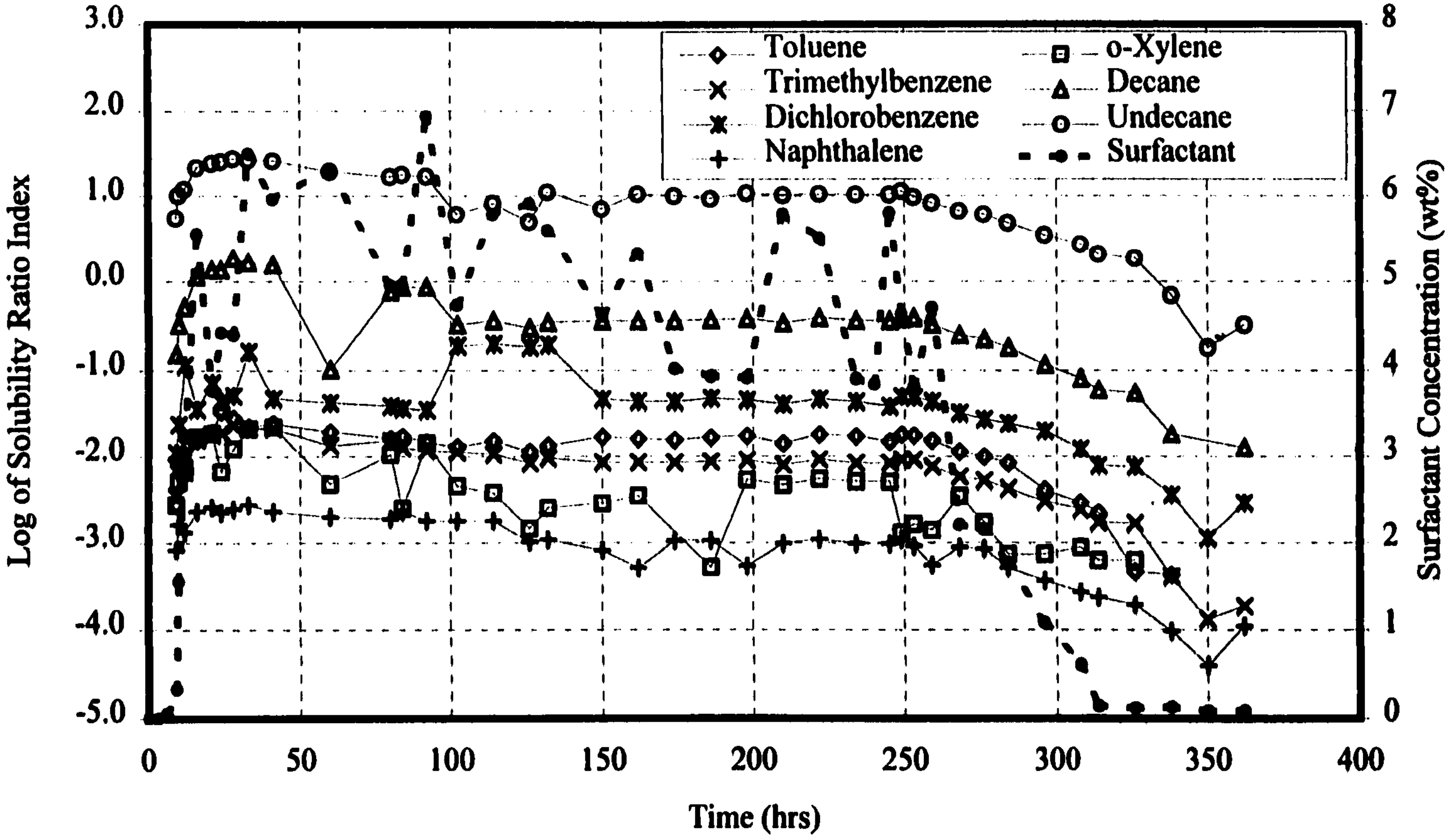

Figure 5.21 SRI Histories During Surfactant Flooding Process for Extraction Well 1 at Hill AFB Test Cell

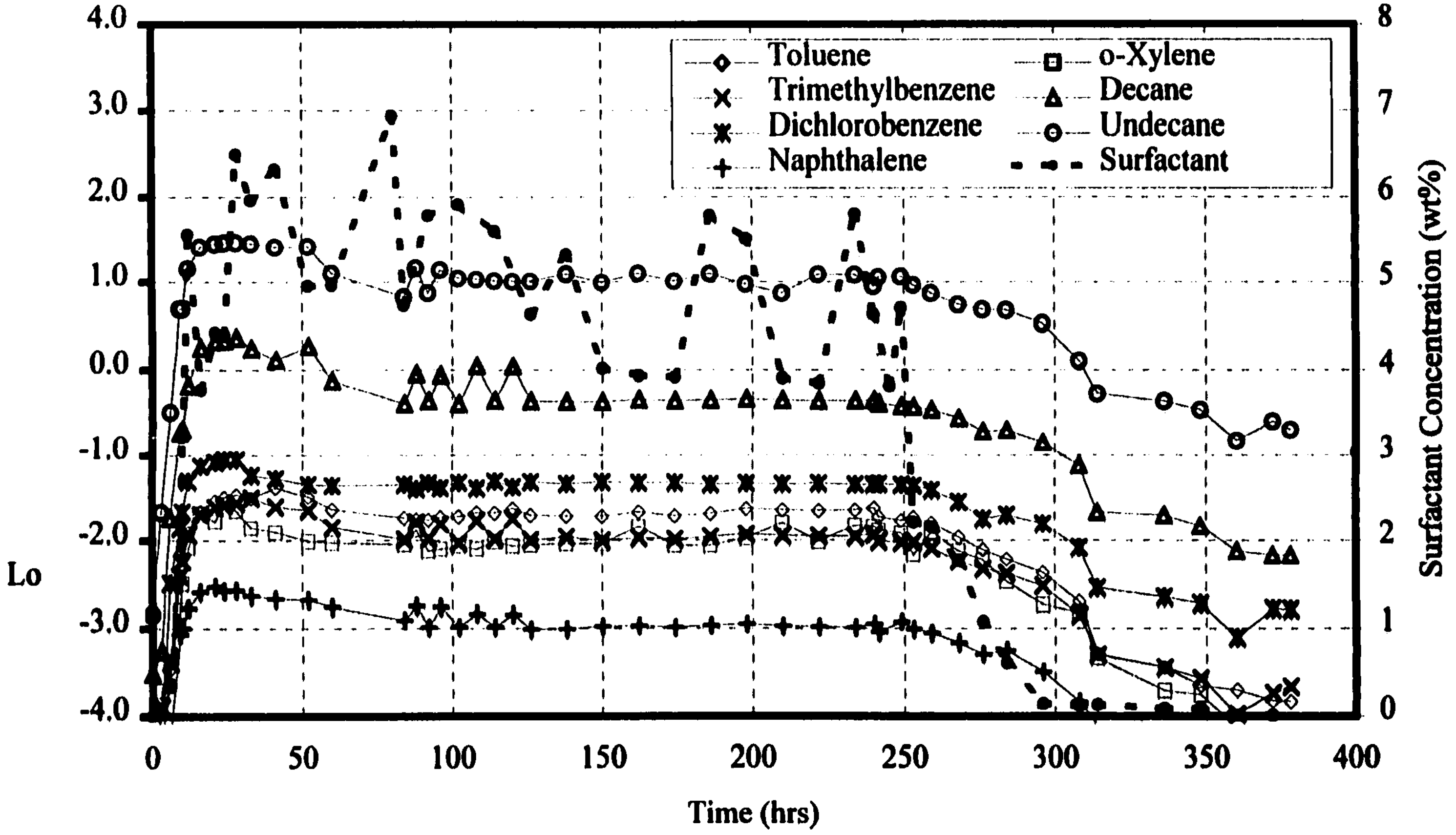

Figure 5.22 SRI Histories During Surfactant Flooding Process for Extraction Well 2 at Hill AFB Test Cell

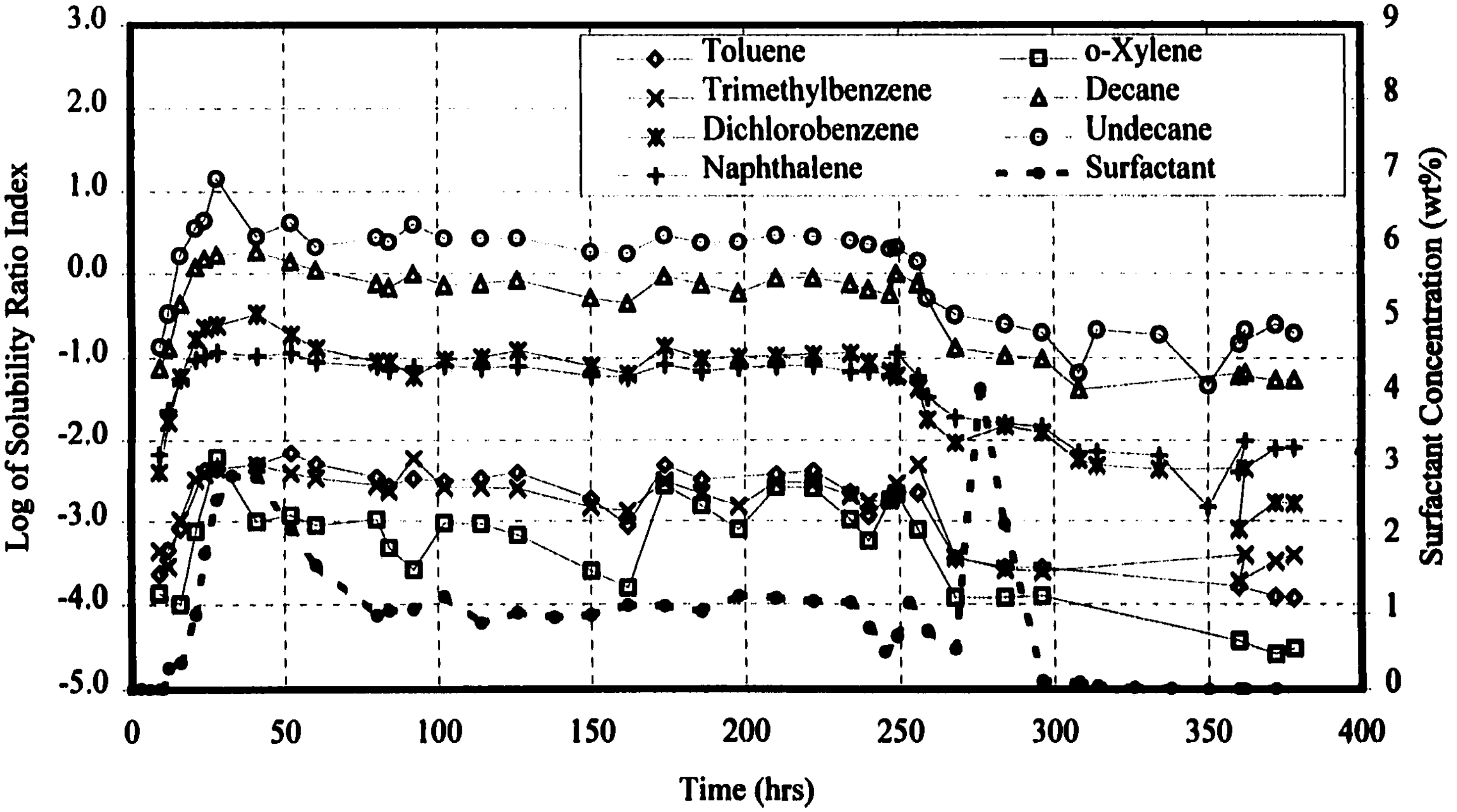

Figure 5.23 SRI Histories During Surfactant Flooding Process for Extraction Well 3 at Hill AFB Test Cell

Figure 5.24 is a plot of the logarithm of average SRI values versus contaminant aqueous solubilities (adjusted according to Raoult's Law) for the extraction wells. A least-squares linear regression of the data resulted in the lines shown in the figure. The R^2 values for extraction wells 1, 2, and 3 were 0.858, 0.872, and 0.774, respectively. Since the column study results showed that PCE did not fit the linear relationship, the relatively low R^2 values were expected because of the presence of the chlorocarbon (dichlorobenzene). Given the relatively low R^2 values, the similarity in slopes of the lines was interesting. This may indicate that a subset of the data possesses a strong linear relationship with a common effect being caused by one or more of the other contaminants.

When dichlorobenzene was omitted from the regression, the R^2 values improved only slightly and the lines remained nearly parallel. Since the naphthalene data points appeared to be outliers, they were omitted from the regression and the R^2 values improved to 0.958, 0.967, and 0.977, respectively. The strong linear relationship between the logarithm of SRI values and aqueous solubilities, shown in Figure 5.25, was consistent with the one discovered during the column experiment. The separation of the lines is an indication of the effect surfactant concentration has on solubilization, while the similar slopes illustrate that the linear relationship is independent of surfactant concentration. The naphthalene data may not fit the linear relationship because of its double-ring structure. Further research is necessary to determine if other polyaromatic hydrocarbons (PAHs) solubilize in the presence of surfactants in a similar manner.

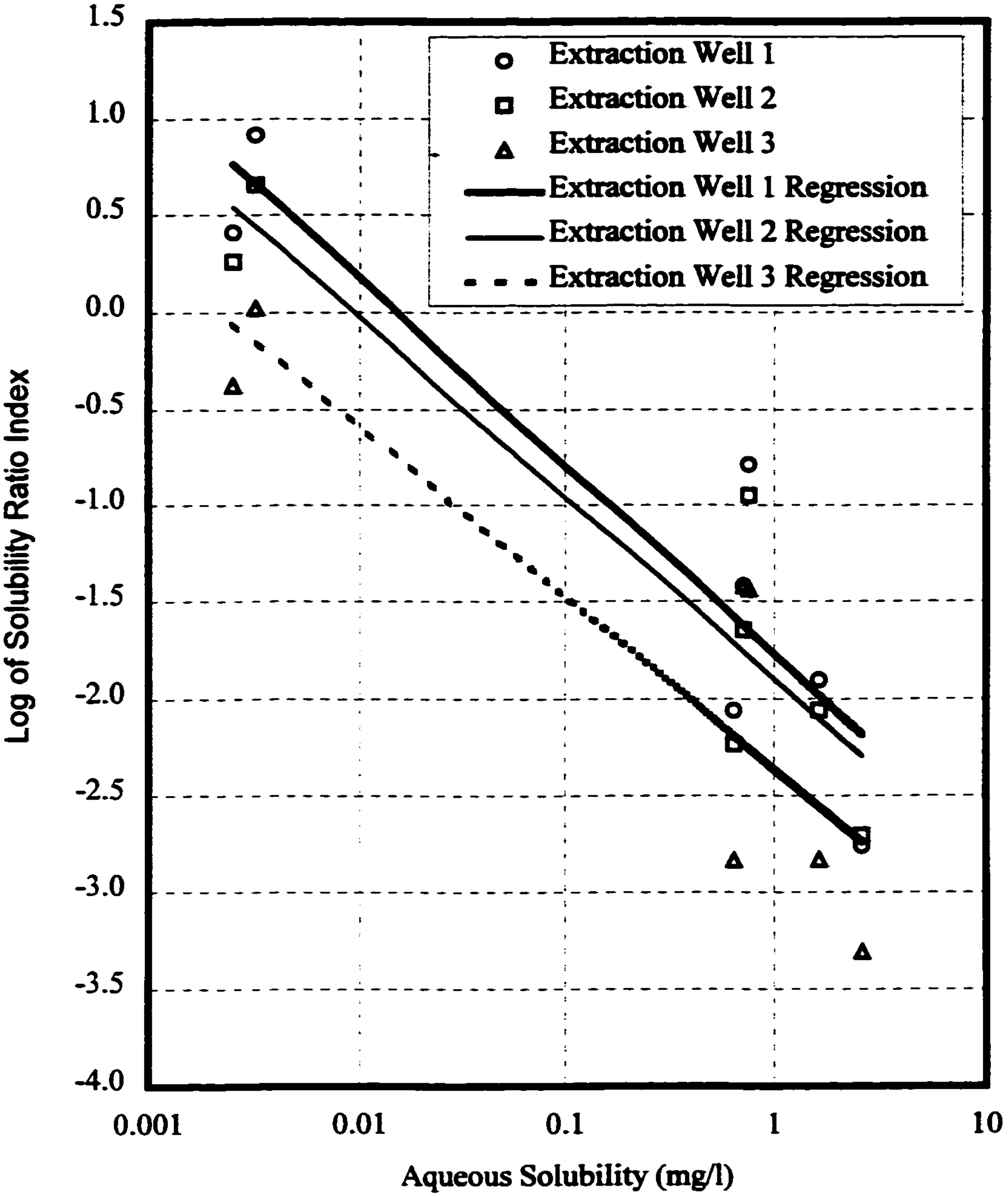

Figure 5.24 Relationship Between Solubility Ratio Index and Aqueous Solubility for Hill AFB Extraction Wells with All Contaminants Included

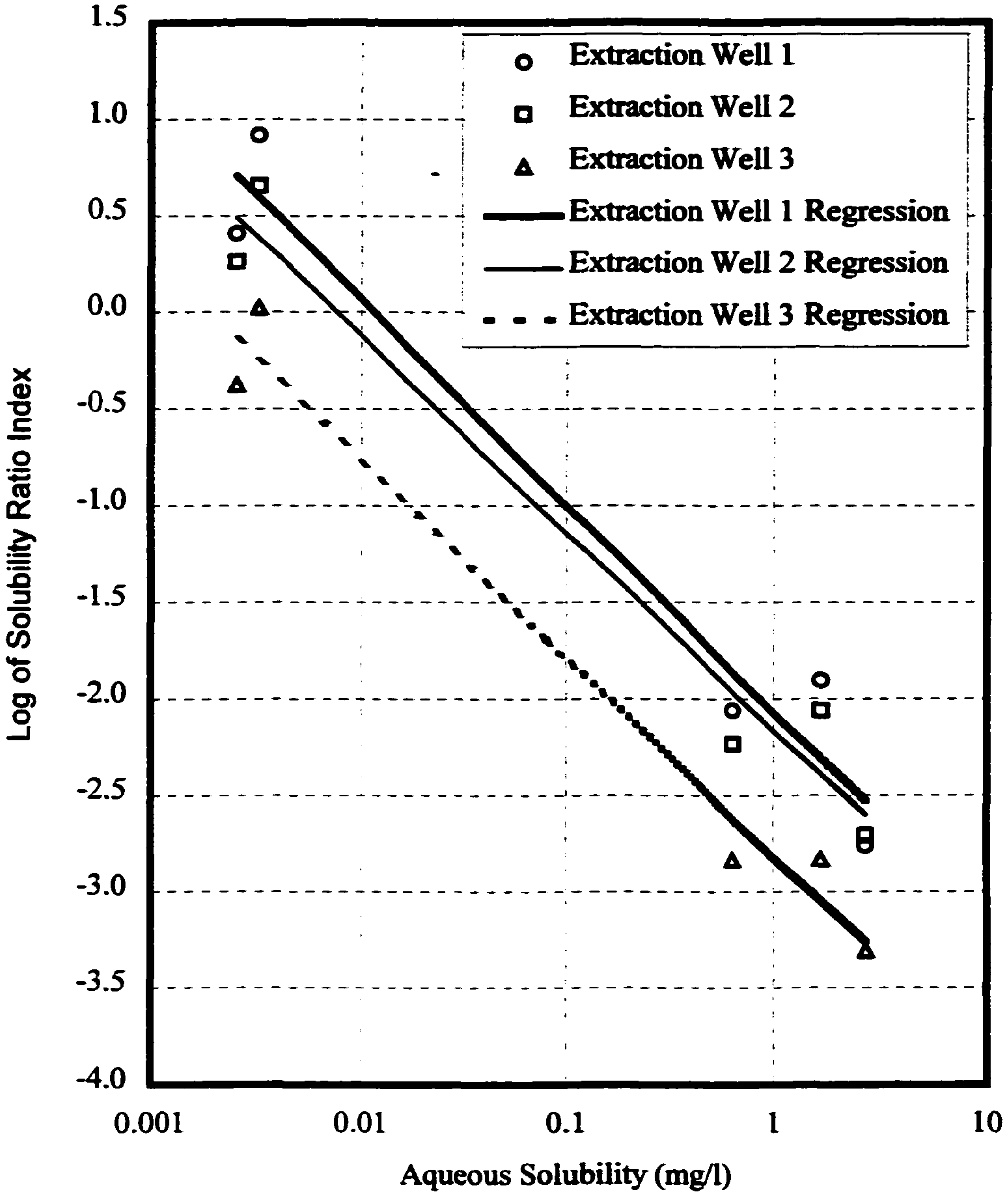

Figure 5.25 Relationship Between Solubility Ratio Index and Aqueous Solubility for Hill AFB Extraction Wells without Dichlorobenzene or Naphthalene

The mole fraction of residual NAPL remaining in the test cell as a function of time could not be calculated due to inconsistent field sample results. Using the results of pre- and post remediation tracer tests, it was estimated that there was a 39 percent reduction in residual saturation levels due to surfactant flushing. From the analysis of soil cores, the reduction was estimated at 57 percent. However, the post-remediation levels for decane and undecane were almost 30 percent greater than pre-remediation levels. Furthermore, the apparent heterogeneity in residual saturation levels was not conducive to the mass balance approach.

5.6 Conclusions

During tracer studies conducted in the laboratory, it was discovered that the partitioning tracers appeared to be adsorbing to the organic content of the Canadian River alluvium. The respective breakthrough curves also exhibited slight tailing and asymmetry. The relatively high mass recovery rates for the tracers indicated that the adsorption process was reversible. Since the general shape of the curves did not appear to indicate that hysteresis was a significant factor, the tailing and asymmetry of the curves was attributed to either chemical or physical non-equilibrium transport. Since many researchers have found it difficult to distinguish between the two processes from laboratory data (Knox *et al.*, 1993), the physical non-equilibrium explanation will be assumed so that UTCHEM's capacitance model can be used.

After residual NAPL was established in the soil column, the dispersivity increased by about 11.5 percent. As tracer flow rates increased, a slight decreasing trend in dispersivity values was found. Excluding 2-methyl-2-hexanol, the calculated values for pore volume, residual saturation, and tracer retardation factors were reasonably consistent. This is an indication that these properties are independent of tracer flow rate. The flow rates used during the column studies were artificially elevated though. The flow rates of 0.3, 0.5, and 0.8 ml/min translate into linear velocities of 2.52, 4.20, and 6.72 m/day, respectively. Lower flow rates that better represent groundwater conditions should be investigated before a final conclusion can be made. The inconsistencies involving 2-methyl-2-hexanol are an area requiring further research as well.

During the surfactant flooding process, plots of effluent concentration and effluent mole fraction histories helped identify trends for similar components. From the plots, identifying enhanced solubilization/mobilization was relatively easy. However, identifying preferential solubilization was difficult and often misleading because the plots do not adequately reflect the wide range in initial aqueous solubilities of the respective components.

The development of the Solubility Ratio Index (SRI) appeared to provide the best indicator of preferential solubility. If SRI values are considered for each series of components (i.e., hydrocarbons and chlorocarbons), a trend is evident. The lower the aqueous solubility of a component within a particular series (and the lower the EACN), the greater the increase in solubility due to the surfactant. When the SRI values were plotted against the aqueous solubility for each component, a strong linear relationship was found for the hydrocarbon compounds. Given the limited number of data points, further research is needed to determine if this is a universal relationship that can be used to predict solubility increases for hydrocarbons. Research to determine if a similar relationship exists for chlorocarbons is also needed.

The composition of NAPL remaining in the soil column was relatively constant on a mole fraction basis throughout the surfactant flooding process. When mole fraction changes were observed, they appeared to be more influenced by mobilization. In either case though, the impact on the NAPL EACN was minimal and the calculated partition coefficients were constant.

Performing the same analysis on field data reinforced the observations and conclusions made from the laboratory data. While plots of the effluent concentration histories were not very helpful in identifying preferential solubilization, the SRI concept was clearly more effective. The linear relationship between initial aqueous solubility and SRI was also demonstrated. The differing results from extraction well 3 are a strong indicator that the surfactant formulation needs to be closely monitored during the remediation process.

CHAPTER 6

A COMPARISON OF COLUMN STUDY AND SIMULATION RESULTS

In Chapter 5, tracer breakthrough curves and effluent concentration histories of the surfactant flooding process from column studies conducted in the laboratory were introduced. This chapter presents the results of respective simulation studies and compares those results with the laboratory data. All simulations were conducted with UTCHEM (a three-dimensional chemical flooding simulator developed at the University of Texas at Austin).

6.1 Simulation Model

The purpose of this section is to describe the development of the model used to simulate the tracer tests and the surfactant flooding process during the laboratory experiments. Specific properties of the soil column and fluids used in the model are presented in the discussion related to each simulation, while more general properties are discussed in the physical properties section. If specific data were not available concerning medium and fluid properties, representative values were selected based upon values cited in the literature. For the reader's benefit, a sample input file for UTCHEM is included in Appendix D.

6.1.1 Simulation Domain

The simulation domain was considered to be one-dimensional in the vertical direction and was based upon the Cartesian coordinate system. The column was assumed to be completely saturated with no-flow conditions along the vertical boundaries. The boundary conditions were constant pressure at the base of the domain and constant flux at the top. The 1.25-cm radius of the column was represented by a square of equal area ($\Delta x = \Delta y = 2.2156$ cm), with no further subdivision for grid blocks. The 14.8-cm length of the column was arbitrarily divided into 50 grid blocks of equal size ($\Delta z = 0.296$ cm).

6.1.2 Physical Properties

The soil column was considered to be isotropic and homogenous. Furthermore, column properties were considered to be constant throughout the process being modeled. It was also assumed that biotic and abiotic processes, tracer reactions, and temperature variations did not occur. Initially dead-end pore space was ignored; however, subsequent use of the capacitance model provided better results.

The porosity, initial water saturation, and longitudinal dispersivity were based upon data obtained during the experiments. Transverse dispersivity was not considered because of the one-dimensional nature of the soil column. Fluid compressibility, molecular diffusion, hysteresis, organic adsorption, and aqueous solubility of NAPL components in the absence of surfactant were considered negligible and were not included in the simulations. The initial pressure within the column was assumed to be at atmospheric levels and subsequent pressure readings were not monitored. Since the column was assumed to be fully saturated, the gas phase was not considered. During tracer simulations, the organic phase was considered to be comprised of a single component because only one partition coefficient for each tracer is allowed by UTCHEM; whereas during the surfactant flooding simulations, it was considered to consist of the seven individual components contained in the original synthetic NAPL. The water used throughout the saturation and flooding processes was de-ionized; therefore brine salinity values were considered to be zero. The partition coefficients for the alcohol tracers were determined from the equation developed in Chapter 4.

Residual saturation and relative permeability values were considered to be dependent on the capillary number, with changes in respective values being calculated with Parker and Lenhard's model. This model requires that endpoint and exponent parameters be determined through a fitting procedure based on experimental data. Since capillary pressure experiments are time-consuming, the values determined by Brown (1993) for the Borden site were used. Subsequent sensitivity analyses showed that changes in permeability and capillary pressure values did not affect simulation results. During the surfactant flooding process, phase behavior was assumed to be independent of organic composition and was modeled using UTCHEM's input solubilization ratio option. As phase behavior properties change in response to the surfactant, interfacial tension calculations were accomplished using Huh's correlation.

6.1.3 Injection and Extraction Wells

One injection and one extraction well, each of the same diameter as the column, were used for the simulations. The injection well penetrates to the center of the first gridblock of the soil column, is considered to be fully completed, and is rate constrained (0.3, 0.5, or 0.8 ml/min). The extraction well penetrates to the center of the last gridblock, is considered to be completed only in the last gridblock, and is pressure constrained (101.325 kPa). Since normalized concentration is used as the ordinate axis for the breakthrough curves, all concentration values were input as unity in a dimensionless format.

6.2 Tracer Test Simulations

Results of the tracer tests conducted in the laboratory were presented in the previous chapter. UTCHEM was subsequently used to simulate the tracer tests in an attempt to duplicate the laboratory results. Therefore, this section compares the simulation results with the experimental results for the tracer tests.

6.2.1 Uncontaminated Column

The more significant UTCHEM input values for the initial simulation are listed in Table 6.1. From Chapter 5, it was observed that the breakthrough curves obtained from the laboratory data showed clear signs of separation, an indication that the alcohols were adsorbing to organic matter in the soil. The subsequent retardation

Table 6.1: Column and Fluid Properties for Initial Simulation

Property	Value
Porosity[a]	0.35
Permeability[b]	5,000 milli-Darcies (0.005 cm/sec)
Water Saturation[b]	1.0
Longitudinal Dispersivity[a]	0.0026 m
Tracer Partition Coefficients[a]	
Ethanol	0.0
Pentanol	0.0
6-Methyl-2-Heptanol	0.0
Water Viscosity[b]	1.0 cp
Water Density[b]	1.0 g/cm^3
Tracer Retardation Factors[a]	
Ethanol	0.0
Pentanol	0.04
6-Methyl-2-Heptanol	0.43

[a] Calculated (see Chapter 5)
[b] Representative

factors were calculated as 1.0, 1.04, and 1.43 for the ethanol, pentanol, and 6-methyl-2-heptanol tracers, respectively. Since UTCHEM defines the tracer retardation factor as the ratio of the adsorbed tracer concentration to the aqueous tracer concentration, the calculated values were reduced by one to determine the appropriate input values.

The breakthrough curves for the initial simulation are shown in Figure 6.1. The ethanol and pentanol plots are reasonably close to the ones obtained from the laboratory data (compare with Figure 5.1). However, the base of both plots is slightly wider, an indication that the dispersivity value used in the simulation was too large. The 6-methyl-2-heptanol plot is more symmetrical and exhibits less tailing than the plot obtained from the laboratory. There are a number of possible reasons for this difference.

One potential explanation is that UTCHEM assumes the adsorption of any type of tracer to be a linear, equilibrium process. However, it is reasonable to expect that different types of tracers may react differently with soil particles. Further research may reveal that the adsorption process for some tracers can be described more accurately with a Freundlich or Langmuir model. Another possible explanation is that there may be a hysteretic effect regarding the desorption of tracers from organic material. UTCHEM does not have the capability of modeling either of these processes (non-linear or hysteretic).

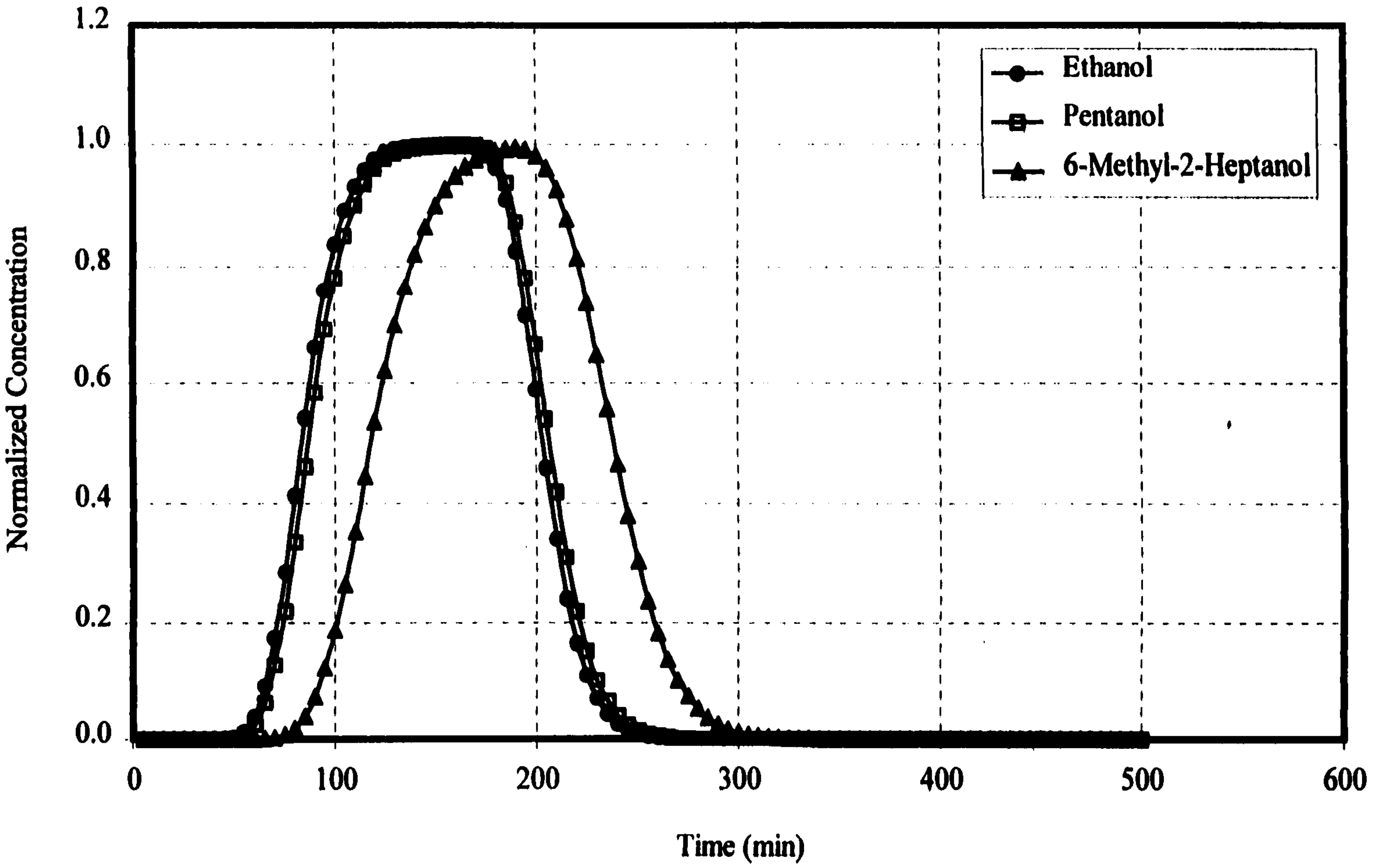

Figure 6.1 Initial UTCHEM Simulation in Uncontaminated Soil Column

Another possible explanation for the poor match between the laboratory data and the simulation results is the presence of chemical and physical non-equilibrium. The general shape of the plot in Figure 5.1 resembles those reported by other researchers investigating the impact of dead-end pore space. Coats and Smith (1964) developed a two-region model (mobile and immobile regions) to address asymmetrical effluent profiles attributed to stagnant regions of pore spaces. Li *et al.* (1994) also used the two-region model to report on nonideal chemical transport.

The behavior of two-region systems may be influenced by factors such as those listed in Table 6.2. The most influential factors are the dispersion coefficient, flowing fraction of pore volume, and mass transfer coefficient (Bai *et al.*, 1999). The flowing fraction of pore volume can be interpreted as the fraction of the pore volume for each phase in which the respective fluid is accessible by the flowing tracers. The researchers referenced above also reported that asymmetrical effluent profiles are observed more often at high Peclet numbers. The Peclet number for the experiments conducted as part of this research was calculated as 56.9 (using the dispersivity value of 0.26 cm), which fits into the transitional transport category. The dispersivity value of 0.1 cm subsequently used in the simulations results in a Peclet number of 148.

Many researchers claim it is difficult to differentiate between physical and chemical non-equilibrium. Physical non-equilibrium is due to film transport and/or the steps in intraparticle diffusion, while chemical non-equilibrium is due to the time-dependent nature of the adsorption process (Knox *et al.*, 1993). Physical non-equilibrium was used in the simulations and was assumed to be the result of dead-end

Table 6.2: Factors Influencing the Capacitance Effect

Wettability
Phase Saturation
Porous Medium Type
Flow Velocity and Contrast
Mass Transfer Rate
Sample Scale
Macroscopic Heterogeneity
Anisotropy
Sorption/Adsorption
Chemical Reaction Morphology
Pore Connectivity
Initial and Boundary Conditions

Source: Bai *et al.* (1999)

pore space, which UTCHEM models with a capacitance model adapted from Coats and Smith (1964). For each phase, UTCHEM requires an estimation of the flowing and dendritic fractions, as well as the mass transfer coefficient for each tracer in each phase. The respective values were determined in an iterative manner to determine the best matches. To simplify the process, mass transfer coefficients for a given tracer was assumed to be constant regardless of the phase in which the tracer was located. The dispersivity providing the best match was 0.1 cm, which was about 60 percent lower than the value calculated from the laboratory data (0.26 cm). This agrees with the conclusion of Coats and Smith (1964) that dispersion coefficients determined with a diffusion-type model may be several times too large. The retardation factors also needed to be adjusted to obtain better agreement between the simulations and laboratory data. The revised values for various parameters providing the best agreement between the simulated and laboratory results are shown in Table 6.3.

The simulated breakthrough curves are compared with the curves from the laboratory data in Figure 6.2. The breakthrough curve for pentanol is not shown because it is very similar to the one for ethanol. The excellent agreement between the curves and their respective experimental data is clearly evident. However, obtaining such a close match was not possible without a labor-intensive, trial-and-error fitting procedure. Validation of the results was not attempted because of the need for multiple columns and the inherent variability of dead-end pore space in the respective columns. Future efforts should include the use of an optimization program to more accurately and efficiently determine appropriate parameter values.

Table 6.3: Revised Parameter Values Providing Best Agreement Between Simulated and Laboratory Results

Property	Value
Longitudinal Dispersivity	0.0010 m
Water/Oil Flowing Fraction	0.84
Mass Transfer Coefficients	
Ethanol	4×10^{-6}
Pentanol	6×10^{-6}
6-Methyl-2-Heptanol	5×10^{-6}
Tracer Retardation Factors	
Ethanol	0.16
Pentanol	0.22
6-Methyl-2-Heptanol	0.45

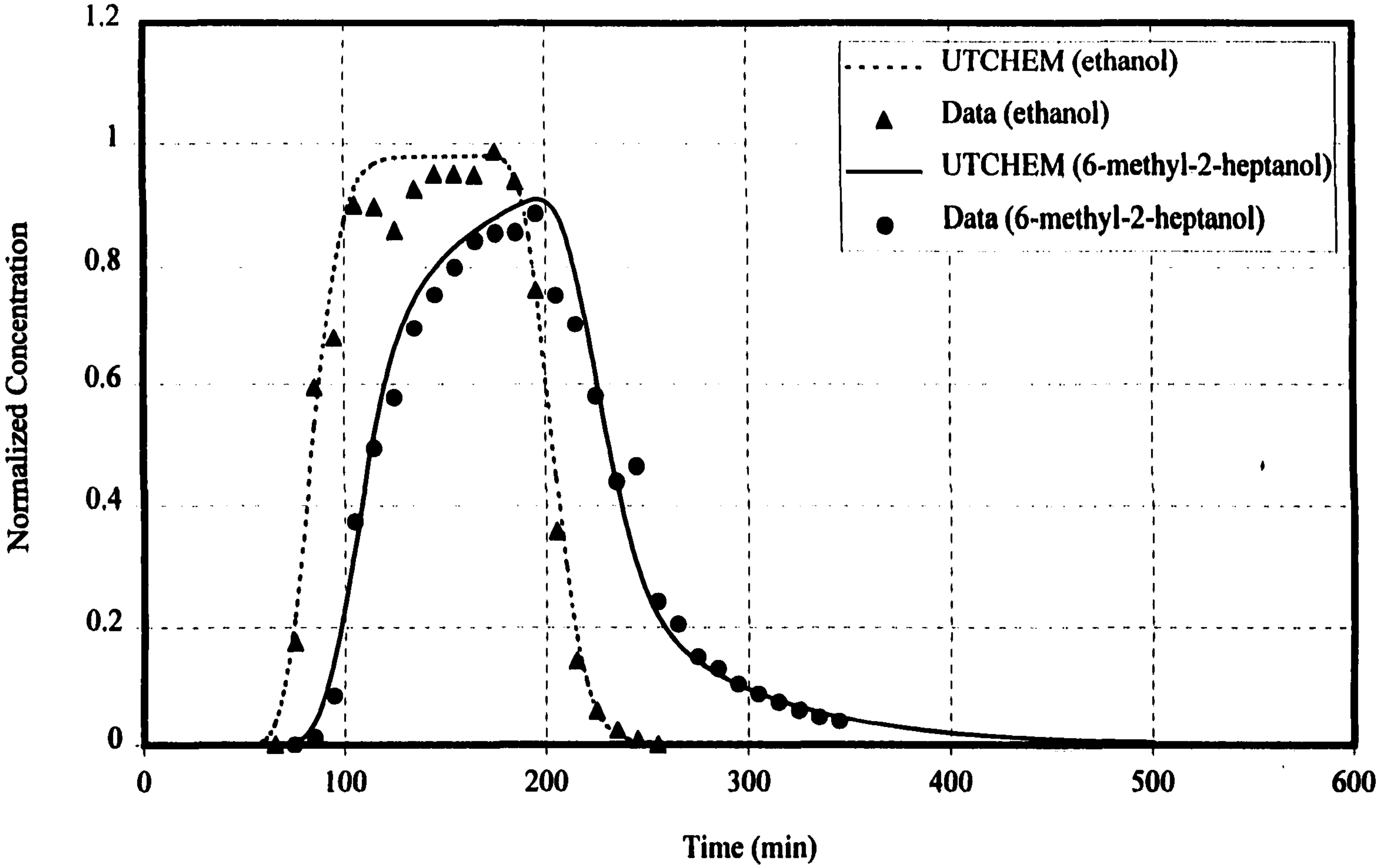

Figure 6.2 Comparison of Breakthrough Curves from Simulation and Laboratory Data

6.2.2 Column at Residual Saturation and Lower Flow Rate

As discussed in Chapter 5, there was clear separation of the breakthrough curves for the tracer tests conducted with the soil column in the laboratory, thereby confirming the presence and amount of residual NAPL. To simulate the tracer tests, it was initially assumed that the amount of tracer adsorption under contaminated conditions was consistent with the amount adsorbed under uncontaminated conditions. Therefore, the retardation factor for ethanol and pentanol were assumed to remain the same (0.16 and 0.22, respectively). The retardation factors for hexanol and 2-methyl-2-hexanol were initially estimated to be 0.30 and 0.35, respectively, and were subsequently modified.

The results of the initial simulation, which assumed dead-end pore space (i.e., capacitance) did not exist, are shown in Figure 6.3. Although the general shapes of the curves, and the separation between them, are typical of tracer tests conducted in contaminated medium, the curves are quite different from those obtained from the laboratory data (see Figure 5.2). The retardation of the respective tracers is greater in the simulations, with the amount of increase appearing to be proportional to the partition coefficient. Additionally, the symmetrical nature of the simulated curves contradicts the asymmetry associated with the laboratory data. Furthermore, the simulated curves do not exhibit the same signs of extended tailing.

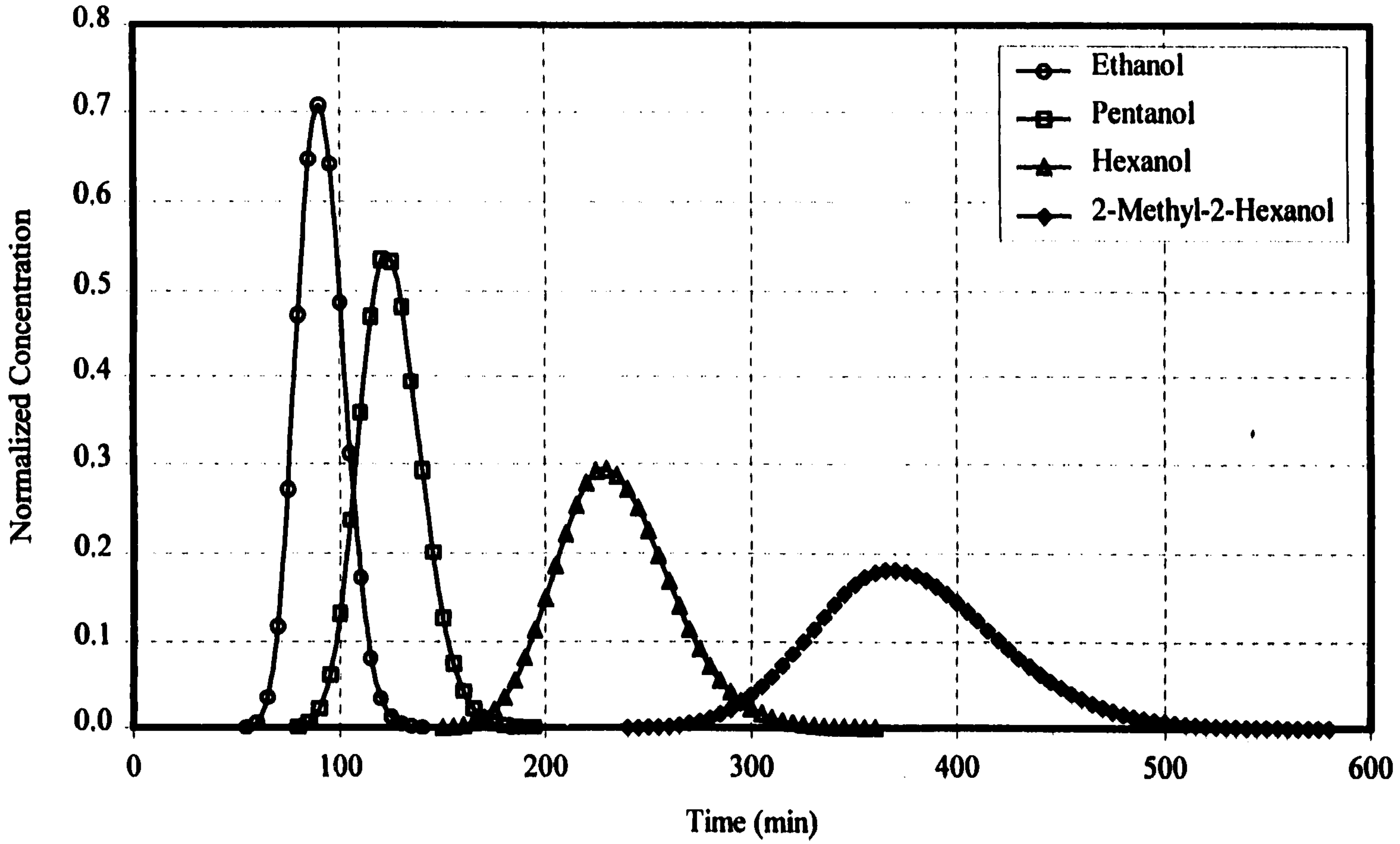

Figure 6.3 Initial Simulation of Column under Residual Saturation Conditions at a Flow Rate of 0.3 ml/min

To obtain better results, the capacitance model was included in the simulations. Initially, it was assumed that the flow rates used during the emplacement process for the residual NAPL did not appreciably alter the amount of dead-end pore space and the flowing fraction for the aqueous phase was considered unchanged. However, the results using this approach were rather poor. Therefore, to determine the flowing fraction for the oil and water phases, as well as the associated mass transfer coefficients, numerous simulations were conducted. The values providing the best agreement between the simulated and laboratory results are shown in Table 6.4. Although some of the values do not appear realistic, they provide the best agreement between the simulations and the laboratory data.

The simulated breakthrough curves are compared with the laboratory-produced curves in Figures 6.4 and 6.5. While the overall shape of each curve is in good agreement with its respective laboratory data, the simulations appear to underestimate the peak concentration values. However, this was expected to some degree because the mass recovery rates were about 145 percent for hexanol and 110 percent for the remaining alcohols during the tracer tests conducted in the laboratory (see Chapter 5). In fact, the curve representing the poorest agreement with the laboratory data was for the tracer with the greatest mass recovery rate (i.e., experimental measurement error). As tracer retardation increases, the plots appear to indicate that simulating the laboratory results may be more difficult.

Table 6.4: Parameter Values Providing Best Agreement Between Simulated and Laboratory Results at 0.3 ml/min

Property	Value
Longitudinal Dispersivity	0.0005 m
Water Flowing Fraction	0.72
Oil Flowing Fraction	0.40
Mass Transfer Coefficients	
Ethanol	4×10^{-4}
Pentanol	3×10^{-4}
Hexanol	8×10^{-5}
2-Methyl-2-Hexanol	1×10^{-4}
Tracer Retardation Factors	
Ethanol	0.09
Pentanol	0.25
Hexanol	0.60
2-Methyl-2-Hexanol	0.45

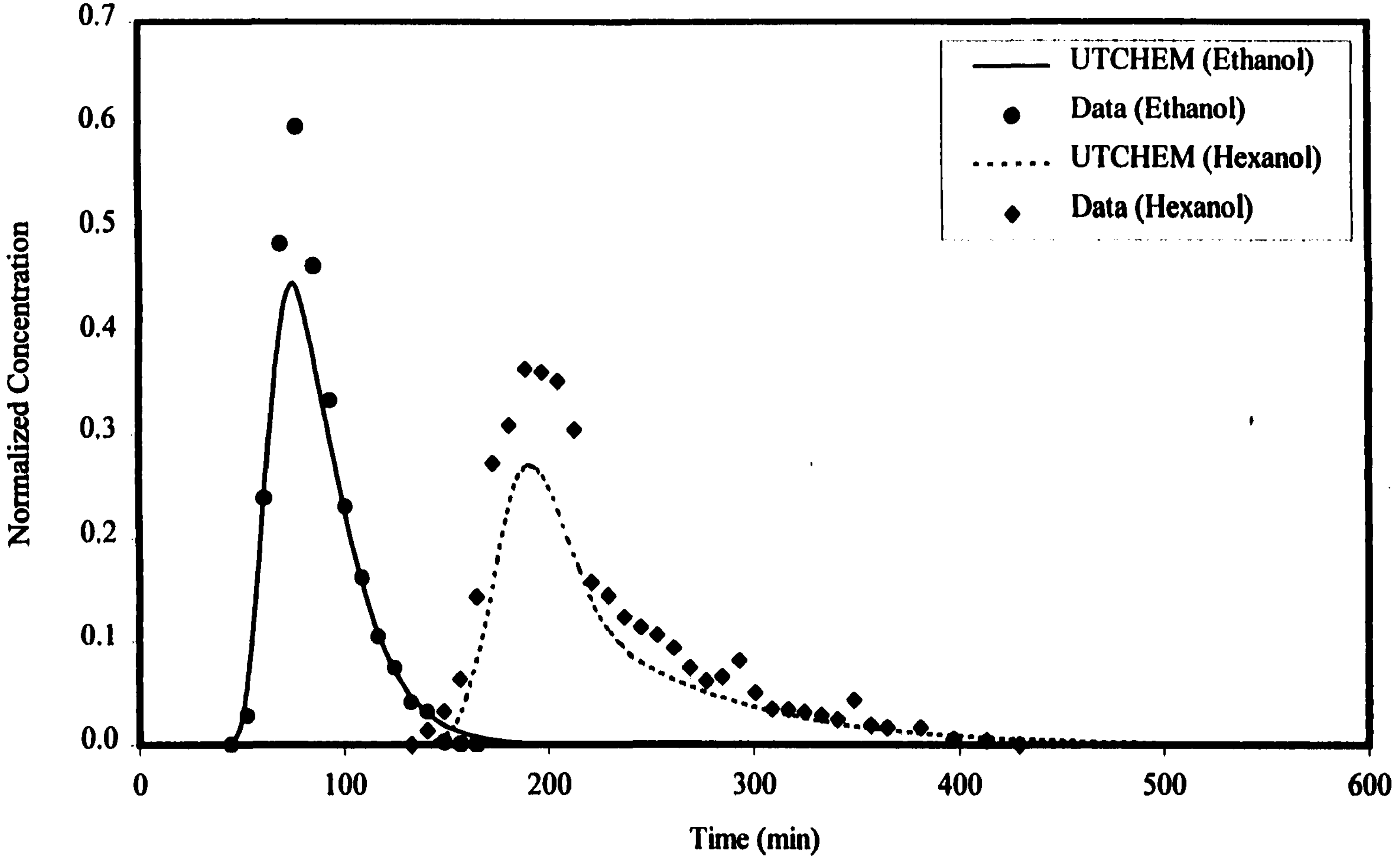

Figure 6.4 Comparison of Breakthrough Curves under Residual Saturation Conditions for Ethanol and Hexanol at a Flow Rate of 0.3 ml/min

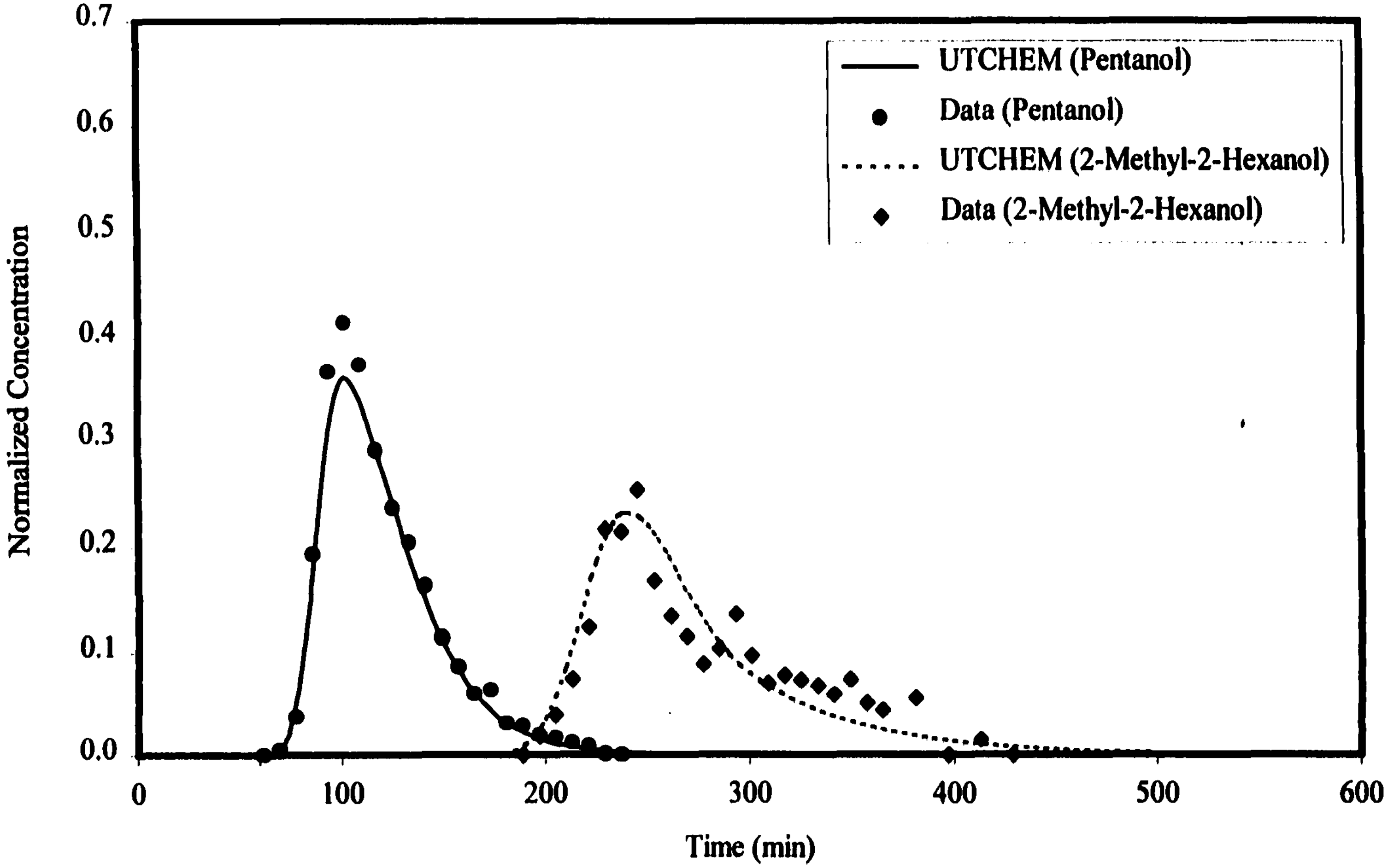

Figure 6.5 Comparison of Breakthrough Curves under Residual Saturation Conditions for Pentanol and 2-Methyl-2-Hexanol at a Flow Rate of 0.3 ml/min

6.2.3 Column at Residual Saturation and Higher Flow Rates

The parameter values providing the best agreement between the simulated and laboratory results for the flow rates of 0.5 and 0.8 ml/min are shown in Table 6.5. The corresponding breakthrough curves are compared with the laboratory-produced curves for the flow rate of 0.5 ml/min in Figures 6.6 and 6.7. For the flow rate of 0.8 ml/min, a similar comparison between simulated breakthrough curves and laboratory-produced are shown in Figures 6.8 and 6.9. As the figures indicate, there is good agreement between the actual and simulated breakthrough curves. However, as in the cases before, the close match was not possible without a labor-intensive, trial-and-error fitting procedure.

Comparing the values in Table 6.5 with those in Table 6.4, three observations can be made. As the flow rate increases, (1) the water flowing fraction values decrease, (2) the mass transfer coefficients increase, and (3) the retardation factors for hexanol and 2-methyl-2-hexanol decrease. This was expected as the increased flow rates create more preferential flow paths and provide less time for mass transfer. It was interesting to note that a plateau region appeared to exist on the tailing side of the breakthrough curves for hexanol and 2-methyl-2-hexanol at all three flow rates. This could possibly be an indication of a hysteretic effect regarding the desorption of tracers from the organic material in the soil or an indication of non-equilibrium transport. Further research regarding both of these phenomena should be conducted to better explain the observations.

Table 6.5: Parameter Values Providing Best Agreement Between Simulated and Laboratory Results at Higher Flow Rates

Property	Value	
	0.5 ml/min	0.8 ml/min
Longitudinal Dispersivity	0.0005 m	0.0005 m
Water Flowing Fraction	0.68	0.56
Oil Flowing Fraction	0.40	0.40
Mass Transfer Coefficients		
Ethanol	5×10^{-4}	1×10^{-3}
Pentanol	3×10^{-4}	2×10^{-3}
Hexanol	3×10^{-4}	8×10^{-4}
2-Methyl-2-Hexanol	2×10^{-4}	5×10^{-4}
Tracer Retardation Factors		
Ethanol	0.09	0.09
Pentanol	0.22	0.22
Hexanol	0.50	0.40
2-Methyl-2-Hexanol	0.40	0.30

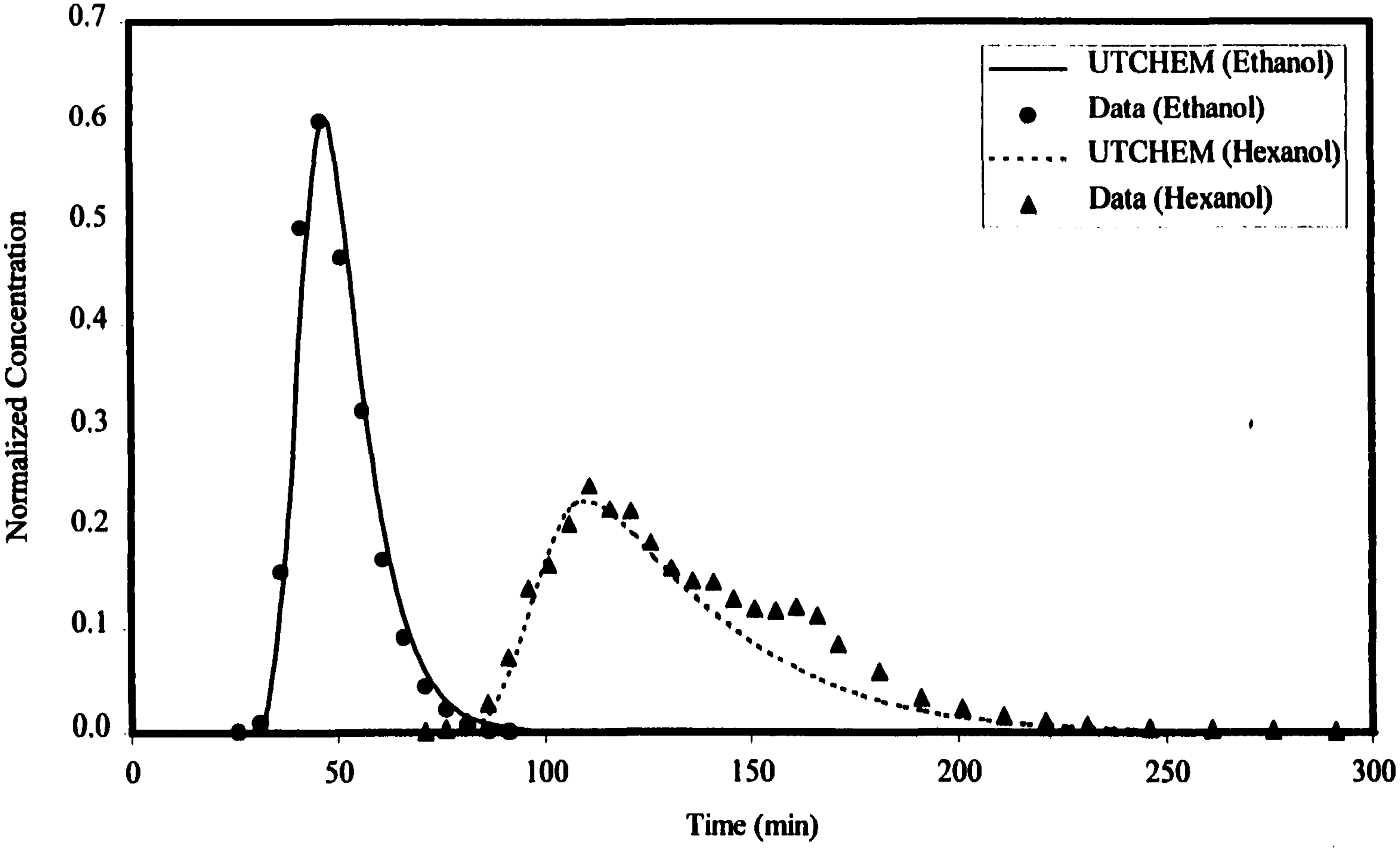

Figure 6.6 Comparison of Breakthrough Curves under Residual Saturation Conditions for Ethanol and Hexanol at a Flow Rate of 0.5 ml/min

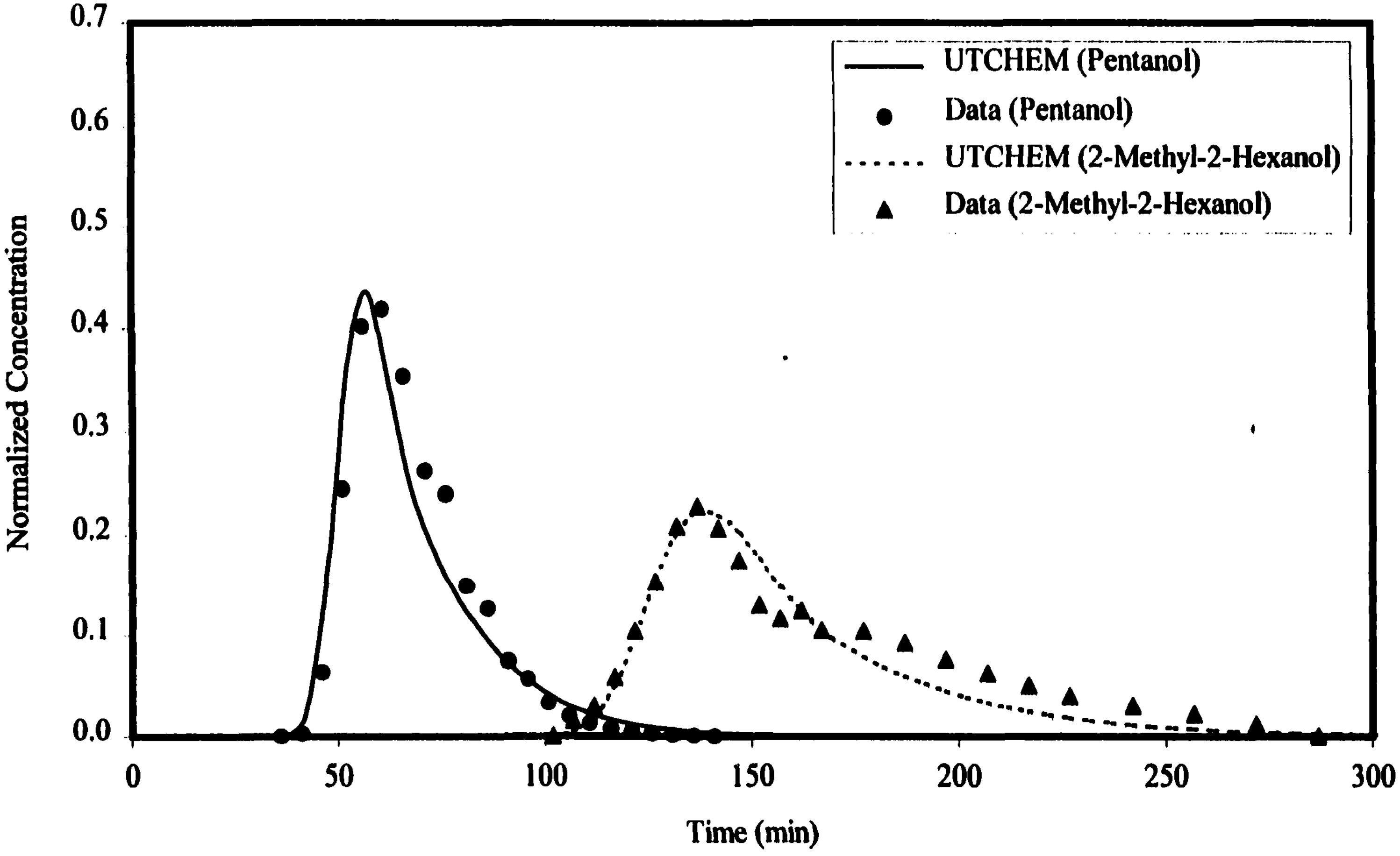

Figure 6.7 Comparison of Breakthrough Curves under Residual Saturation Conditions for Pentanol and 2-Methyl-2-Hexanol at a Flow Rate of 0.5 ml/min

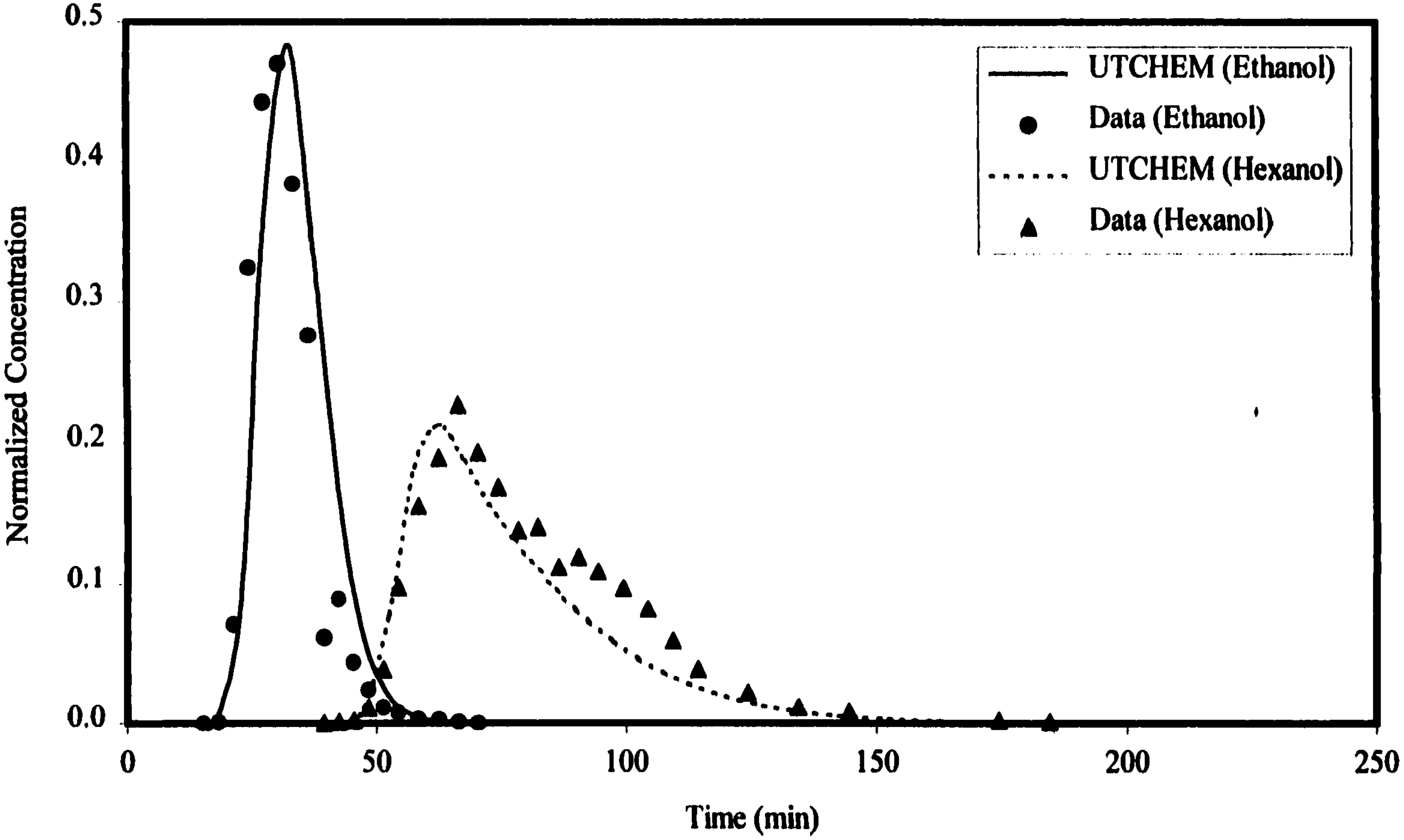

Figure 6.8 Comparison of Breakthrough Curves under Residual Saturation Conditions for Ethanol and Hexanol at a Flow Rate of 0.8 ml/min

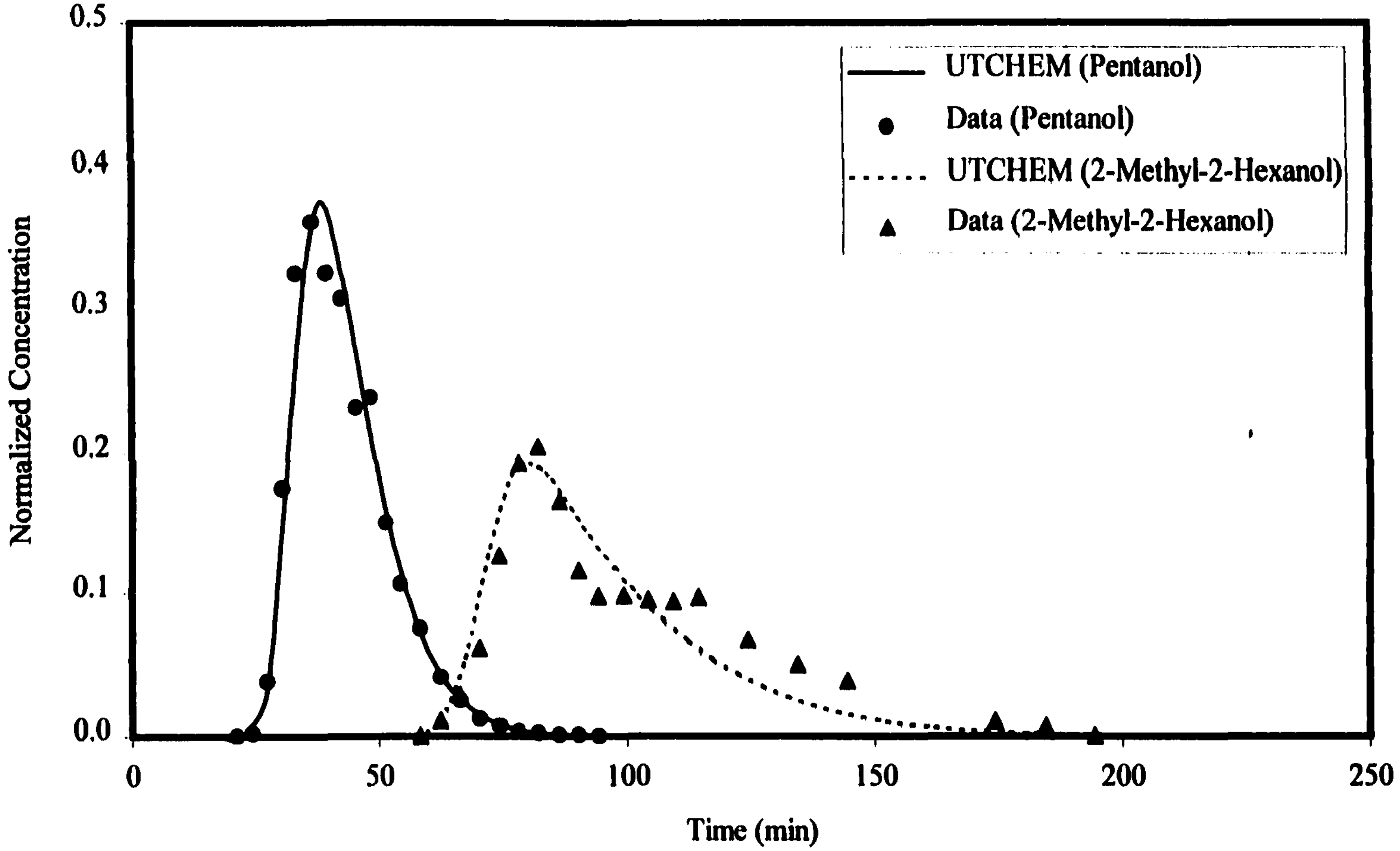

Figure 6.9 Comparison of Breakthrough Curves under Residual Saturation Conditions for Pentanol and 2-Methyl-2-Hexanol at a Flow Rate of 0.8 ml/min

6.3 Surfactant-Enhanced Remediation Simulations

Results of the surfactant flooding experiment conducted in the laboratory were presented in the previous chapter. UTCHEM was subsequently used to simulate the surfactant flooding process in an attempt to duplicate the laboratory results. Therefore, this section compares the simulation results with the experimental results.

The more significant UTCHEM input values are listed in Table 6.6, with more specific information regarding the oil mixture being shown in Table 6.7. The simulations discussed in this section were conducted assuming that properties influencing phase behavior were independent of organic mixture, a common assumption for surfactant-enhanced remediation. Using the solubilization ratio input option, UTCHEM requires three input values for salinity and their associated solubility values for a Type III phase region. The first set of values is for a salinity which is between the lower and optimal effective salinity limits, the second set of values is for the optimal effective salinity, and the third set of values is for a salinity which is between the optimal and upper effective salinity limits. However, Dowfax 8390 does not readily form a microemulsion phase unless a cosurfactant is used. Therefore, values were not available for the required input variables. Of the six required variables, only the solubility value for the salinity, which is between the lower and optimal effective salinity limits, had any impact on the results. This input variable was determined using a trial-and-error matching procedure to produce simulated results that most closely matched the laboratory results. The resulting effluent history plots are shown in Figure 6.10.

Table 6.6: Column and Fluid Properties for Surfactant Flooding Simulation

Property	Value
Porosity	0.35
Permeability	5,000 milli-Darcies
Water Saturation	0.7871
Surfactant CMC	0.00321 (volume fraction)
Enhanced Solubility	2.5 (volume fraction)
Interfacial Tension ($\log_{10}$)	1.61
Density (g/cm^3)	
Water	1.0
Oil	0.859
Surfactant	1.150

Table 6.7: Oil Component Properties

Oil Component	Volume Fraction	Aqueous Solubility (Volume Fraction)	Viscosity (cp)	Density (g/cm^3)	Molecular Wt (g/mole)	EACN
Toluene	0.2531	6×10^{-4}	0.590	0.8660	92.14	1
o-Xylene	0.2434	2×10^{-4}	0.810	0.8802	106.17	2
Hexane	0.1120	2×10^{-5}	0.326	0.6594	86.18	6
Heptane	0.1036	3.5×10^{-6}	0.418	0.6838	100.21	7
Decane	0.1972	1×10^{-8}	0.920	0.7301	142.29	10
TCE	0.0486	7.5×10^{-4}	1.200	1.4649	131.39	-3.81
PCE	0.0421	9×10^{-5}	1.840	1.6230	165.83	2.90

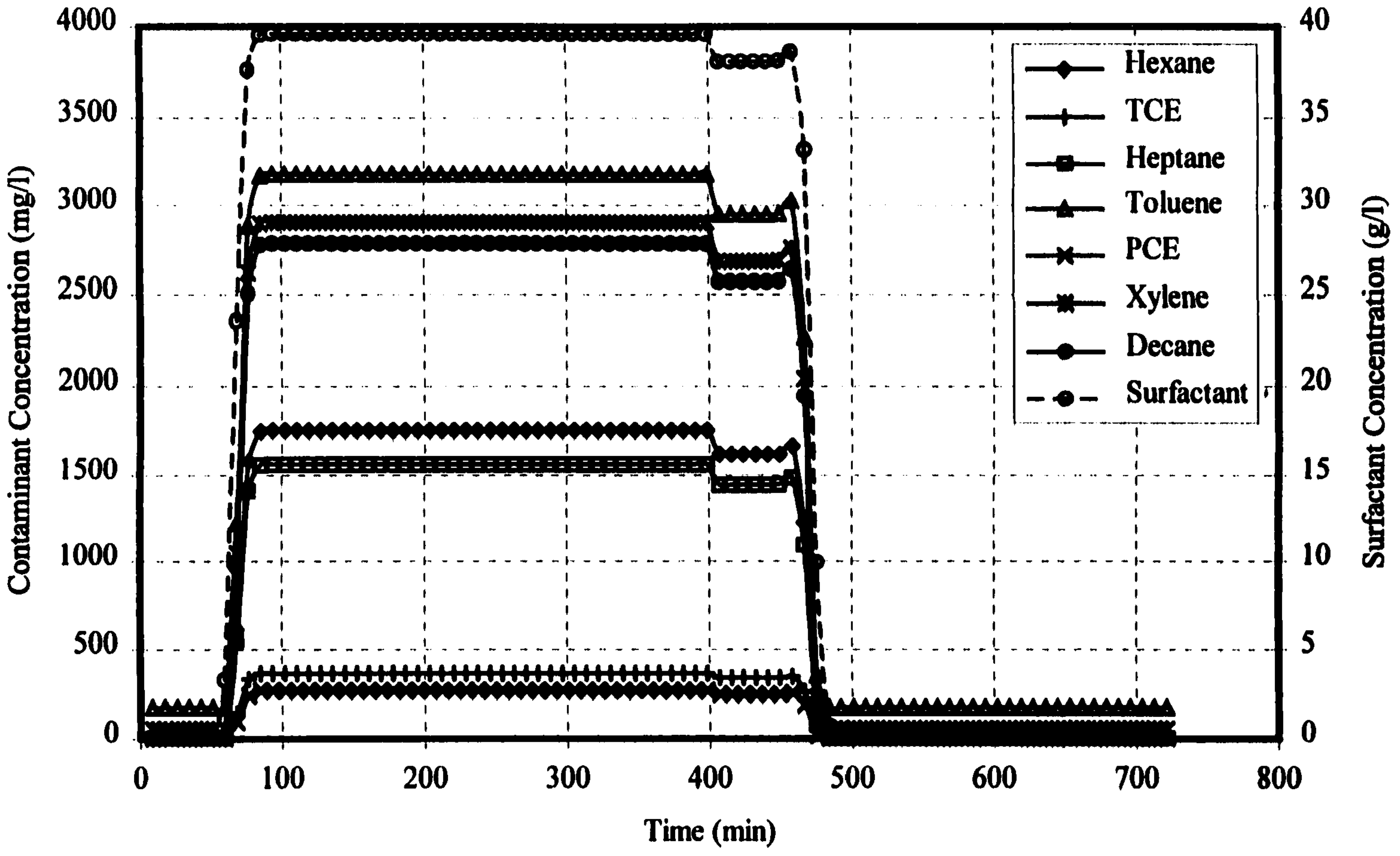

Figure 6.10 Contaminant and Surfactant Concentration Histories During Simulated Surfactant Flooding Process

The simulated results in Figure 6.10 are quite different than the laboratory results shown in Figure 5.5. The laboratory results indicate a slight peak in contaminant concentrations coinciding with the surfactant breakthrough followed by relatively consistent values. However, the simulated results indicate constant concentration values for the respective contaminants. The slight peak in values is not represented in the simulations because of the assumption of homogeneous soil conditions. Therefore, variations in porosity and permeability were not reflected. In the laboratory experiment, it is hypothesized that the surfactant solution would flow through the more permeable areas of the soil column first and solubilize residual saturation from those areas relatively quickly. As less permeable areas are encountered, the contaminant solubilization process is slightly less efficient and results in a decrease in effluent concentration values. Furthermore, variability of laboratory effluent histories may reflect inconsistent surfactant concentrations during the flushing process.

The large peaks in contaminant concentrations after the surfactant dissipated in the soil column are not reflected in the simulation results. Despite numerous simulations as part of the sensitivity analysis, mobilization of the contaminants could not be simulated. Since Dowfax 8390 does not readily form a microemulsion, mobilization of the contaminants was not expected. The presence of the large peaks after the surfactant dissipated and the likely cause were previously discussed in Chapter 5.

The order of the contaminants in Figure 6.10 is slightly different from that shown in Figure 5.5. During the timeframe of relatively consistent concentration values, toluene and *o*-xylene are present in the greatest concentrations for both the laboratory and simulated results. Similarly, PCE exists in the smallest concentrations for both results. During the laboratory experiment, hexane is present in greater concentrations than decane. Conversely, decane exists in greater concentrations than hexane during the simulations. Since TCE and heptane were considered as a mixture during the laboratory experiment, comparisons cannot be made concerning the simulated results for those two components.

The slight discrepancies discussed above can be primarily attributed to two factors. The first, which has already been mentioned, is the fact that comparisons are being made between a real situation (which is heterogeneous and anisotropic) and an idealized situation (which is assumed to be homogeneous and isotropic). There will undoubtedly be minor differences when comparisons of this type are made. The second factor concerns the assumption that the composition of the residual oil in the column did not change appreciably during the emplacement process and the subsequent tracer tests. Despite this assumption though, the composition may have indeed been altered during the emplacement process, during the course of the tracer tests, and possibly throughout the entire experiment due to volatilization. Therefore, slight variations between laboratory and simulated results are expected.

As discussed in Chapter 5, drawing any conclusions from the effluent concentration histories is difficult because they do not take into account the initial aqueous solubility of the contaminants and their increase in solubility due to the presence of the surfactant. A plot of the Solubility Ratio Index (SRI) versus aqueous solubility for the simulated results is shown in Figure 6.11. Consistent with the results presented in Chapter 5, there is a linear relationship between the SRI and the aqueous solubility of a component for the hydrocarbons. This shows that enhanced solubilization is occurring and that the more hydrophobic components are realizing the greatest enhancement. In other words, Figure 6.11 clearly indicates the presence and order of preferential solubilization. Although further research would be necessary to verify it, it also appears as though a similar linear relationship exists for the chlorocarbons with a similar slope.

Despite the difference in the order of contaminants between the simulated and laboratory results for some of the components, it is interesting to note that the linear relationship remains intact in Figure 6.11. This is easily explained by observing that the respective concentration values in Figures 5.5 and 6.10 differ by a factor of less than two. However, the respective increases in solubility (i.e., SRI values) range over two orders of magnitude. The wide difference in scales thus negates the effect of small differences in concentration values and further emphasizes that point that simulation results are only estimates that must be interpreted and used carefully.

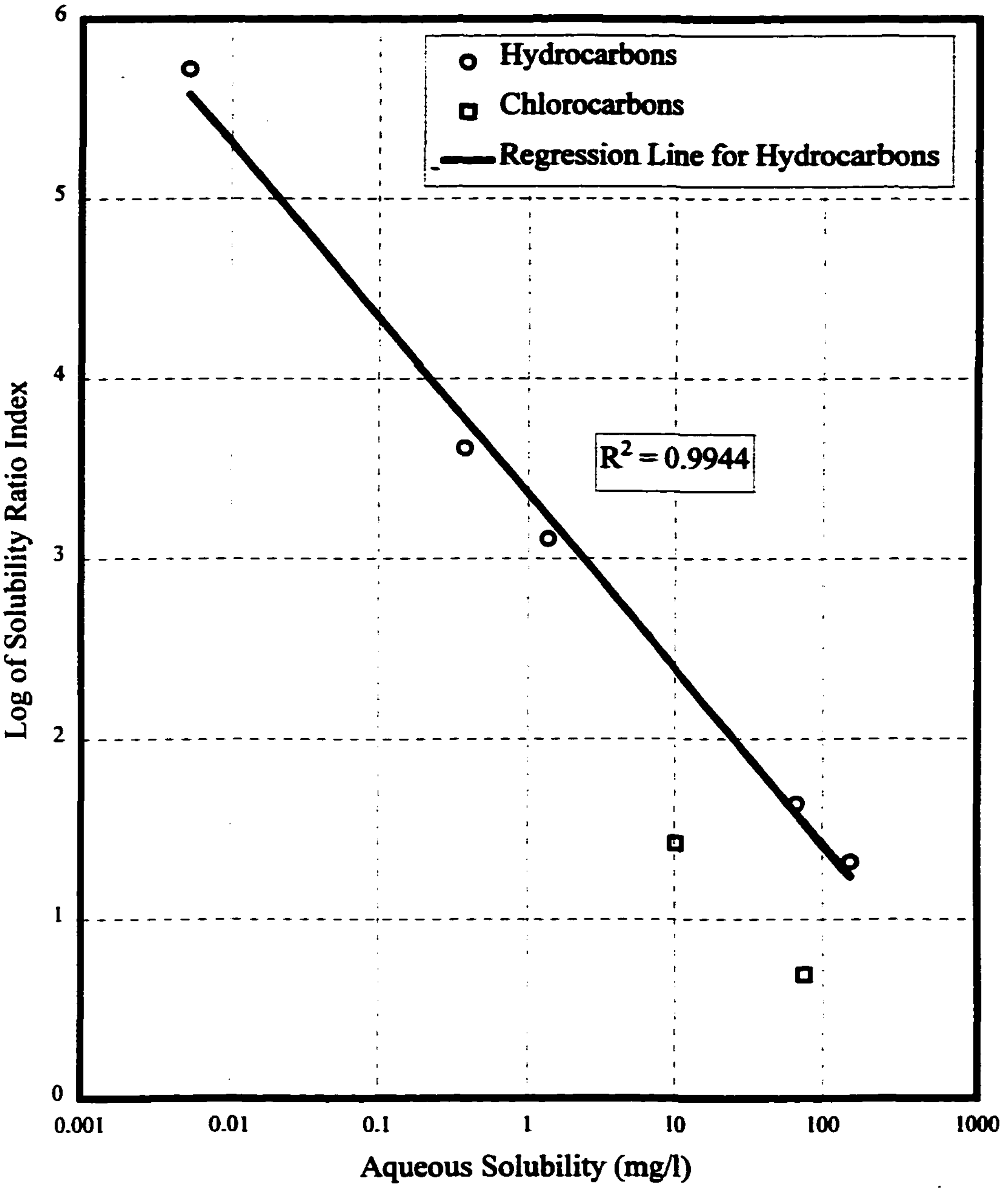

Figure 6.11 Relationship Between Solubility Ratio Index and Aquesous Solubility Based on Simulated Results

6.4 Sensitivity Analysis

A sensitivity analysis was conducted with the tracer simulations to determine how sensitive the overall results were to changes in some of the input parameters. This analysis was conducted at a flow rate of 0.3 ml/min, with the base case being represented by Figures 6.4 and 6.5. In all cases, the general simulation conditions were the same as those described in Section 6.2.2 except for the changes made to an individual input parameter.

Figures 6.12 through 6.18 show the sensitivity of the tracer test results to variations in individual parameters. In each figure, the base case is shown as the solid line and the respective input value is increased and decreased by either 10 percent or a factor of two (these values were arbitrarily selected to provide a reasonable range). The tracers shown in each figure are representative of the trend indicated by all four tracers included in the simulations. Before discussing individual results, it should be noted that altering the permeability, capillary pressure, and residual saturation (i.e., drainage) values did not have any affect on the simulation results. This was expected because of the assumed homogeneous and isotropic nature of the soil column and the forced-flow conditions used during the experiments. The relatively high flow rates may have also contributed to this observation.

From Figures 6.12, 6.14, and 6.18, it appears as though increases in porosity values, retardation factors, and partition coefficients have similar effects on the tracer test results. Breakthrough times were later and peak concentration values were reduced and shifted to the right. Additionally, the tailing was slightly less pronounced and ended at about the same time. There are two primary conclusions to draw from these observations. First, the required duration of the tracer test can be easily determined and is independent of small variations in the three referenced parameters. Second, the mass of each tracer must be sufficient to ensure that detection limits are not violated during the last part of the tail.

Figure 6.13 shows the sensitivity of the tracer test results to variations in the dispersivity value. Although breakthrough times are earlier with increased dispersivity, there does not appear to be any effect on the tailing portion of the curves. The peak concentration values are reduced but occur at essentially the same time. Therefore, the design of the tracer test (duration and tracer mass) is relatively independent of dispersivity.

As shown in Figure 6.15, the primary implication of increasing the water flowing fraction is that any tailing is more pronounced. Therefore, the duration of the tracer test as well as the required mass of each tracer will be very sensitive to the fraction of the aqueous phase that is considered accessible to the tracers. Conversely, increases in the oil flowing fraction (see Figure 6.16) do not affect the tail and thus have minimal effect on the tracer test design. There is a slight reduction and shift to the right in peak concentration values; however, these have little impact on the overall tracer test design.

If non-equilibrium conditions are anticipated, Figure 6.17 indicates that slight changes in mass transfer coefficients can have a definite effect on tracer test results. The peak concentration values are impacted, but more important are the rather dramatic changes in the shape of the respective tails for both partitioning and non-partitioning tracers. It is evident that the accurate determination of mass transfer coefficients is critical to an effective tracer test design.

If non-equilibrium processes are not anticipated, the design of an effective tracer test is rather simple to accomplish using UTCHEM simulation results. The duration of the test and the required mass of each tracer can be determined such that concentrations in the timeframe of interest are above the detection limit of the analytical equipment being used. Using the method of moments with the simulated tracer tests will provide a means of selecting which types of tracers to use to ensure adequate separation of the curves and to ensure retardation factors are within an acceptable range. These results also provide a sound basis for the development of a sampling plan.

Although not applicable to tracers used in a column in the laboratory, tracer test designs for the field can be further improved by using an optimization program to evaluate the placement and flow rates of injection and extraction wells. If complete characterization of a site is the goal, UTCHEM simulations can also be used to help determine the location of observation wells and the screening intervals within those wells (i.e., the use of multi-level samplers).

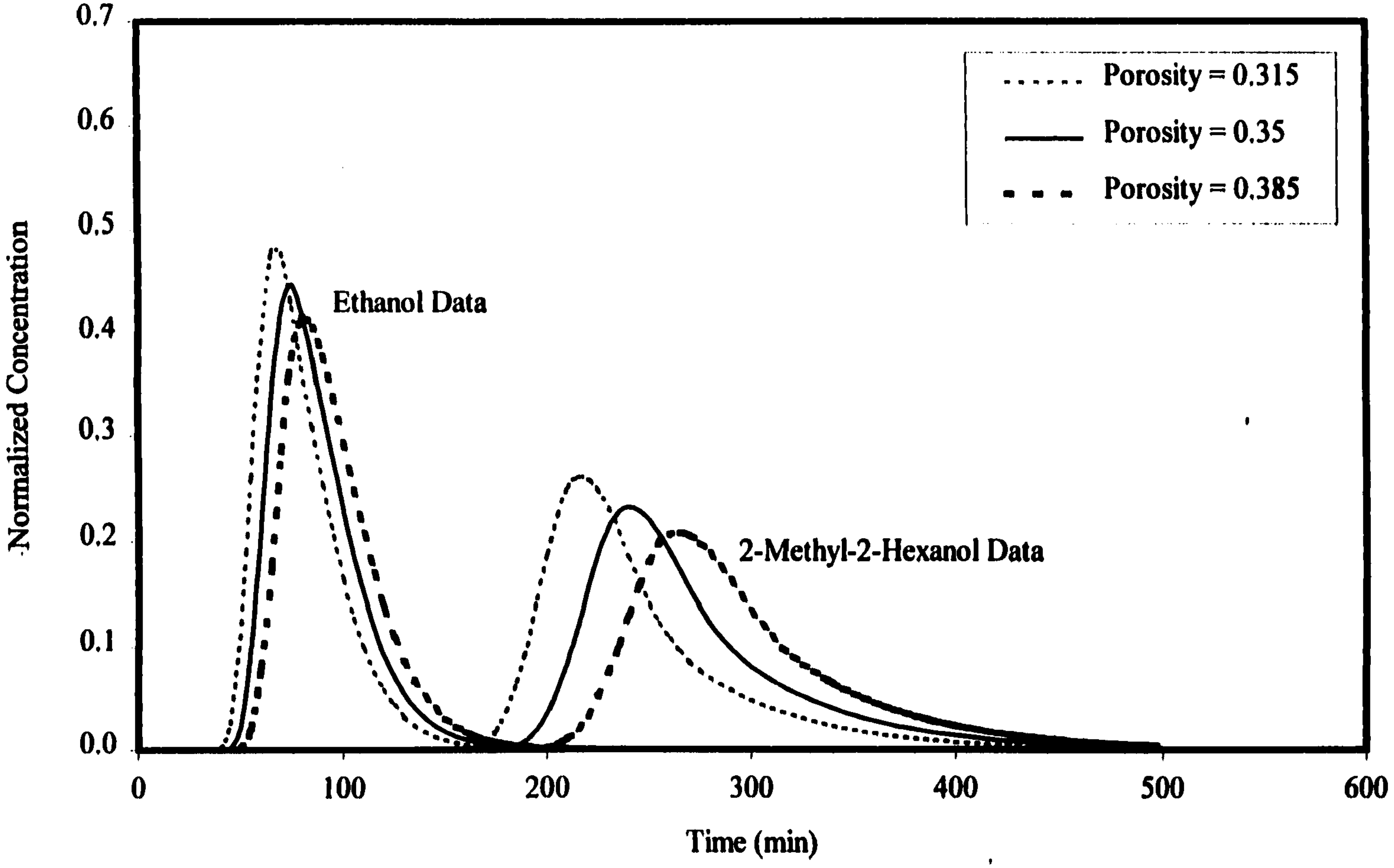

Figure 6.12 Impact of Porosity on Simulated Breakthrough Curves for Ethanol and 2-Methyl-2-Hexanol at a Flow Rate of 0.3 ml/min

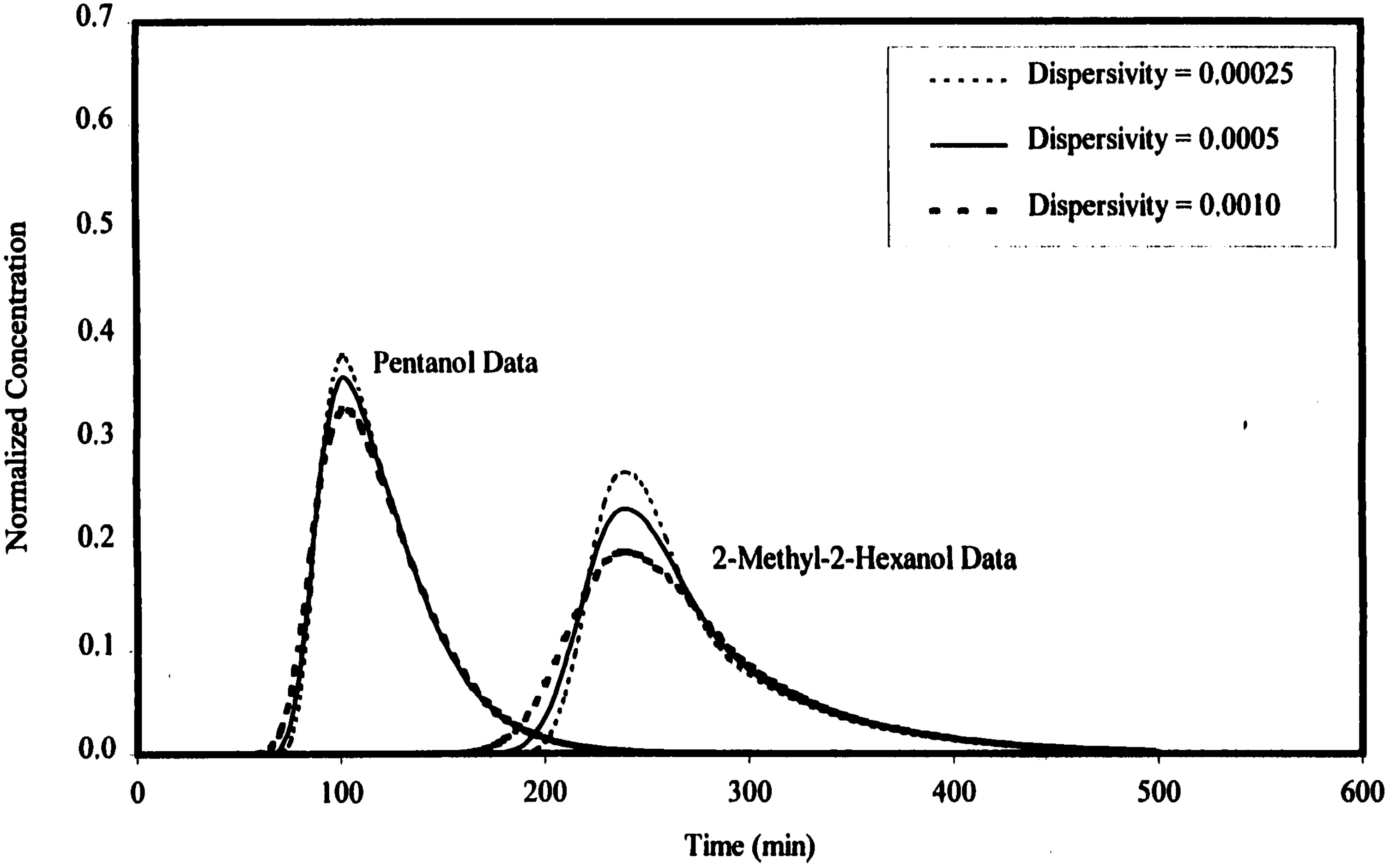

Figure 6.13 Impact of Dispersivity on Simulated Breakthrough Curves for Pentanol and 2-Methyl-2-Hexanol at a Flow Rate of 0.3 ml/min

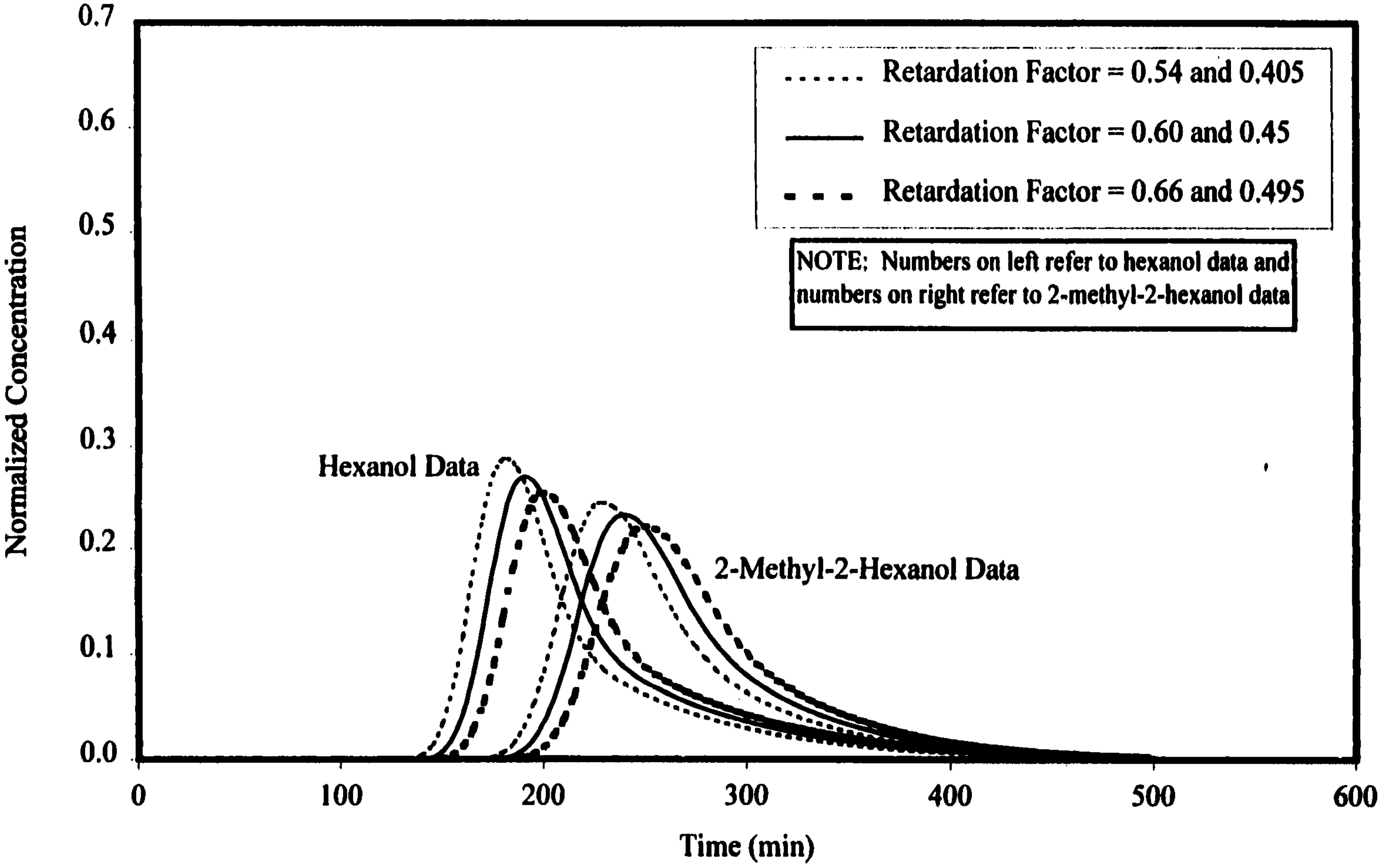

Figure 6.14 Impact of Retardation Factor on Simulated Breakthrough Curves for Pentanol and 2-Methyl-2-Hexanol at a Flow Rate of 0.3 ml/min

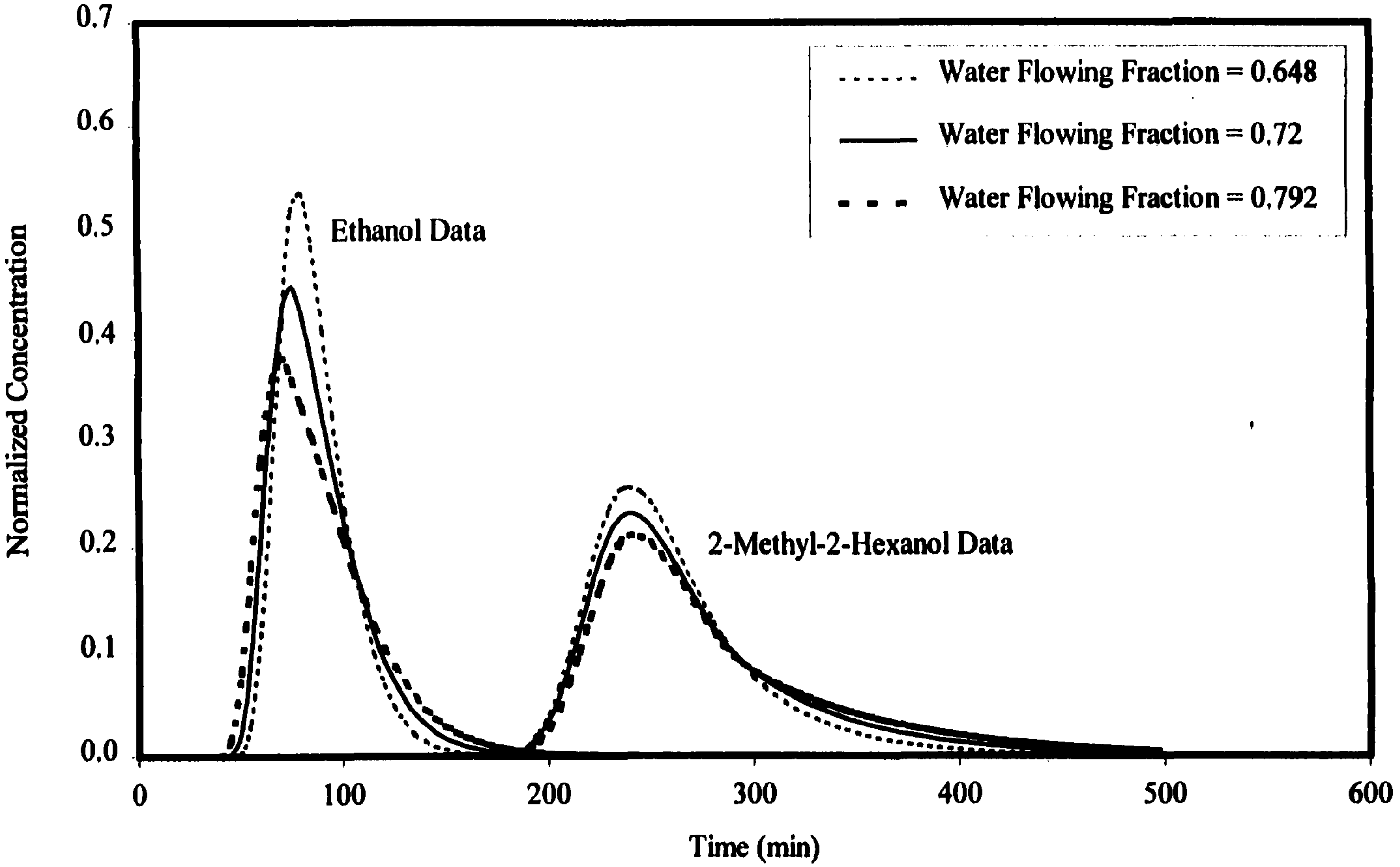

Figure 6.15 Impact of Water Flowing Fraction on Simulated Breakthrough Curves for Pentanol and 2-Methyl-2-Hexanol at a Flow Rate of 0.3 ml/min

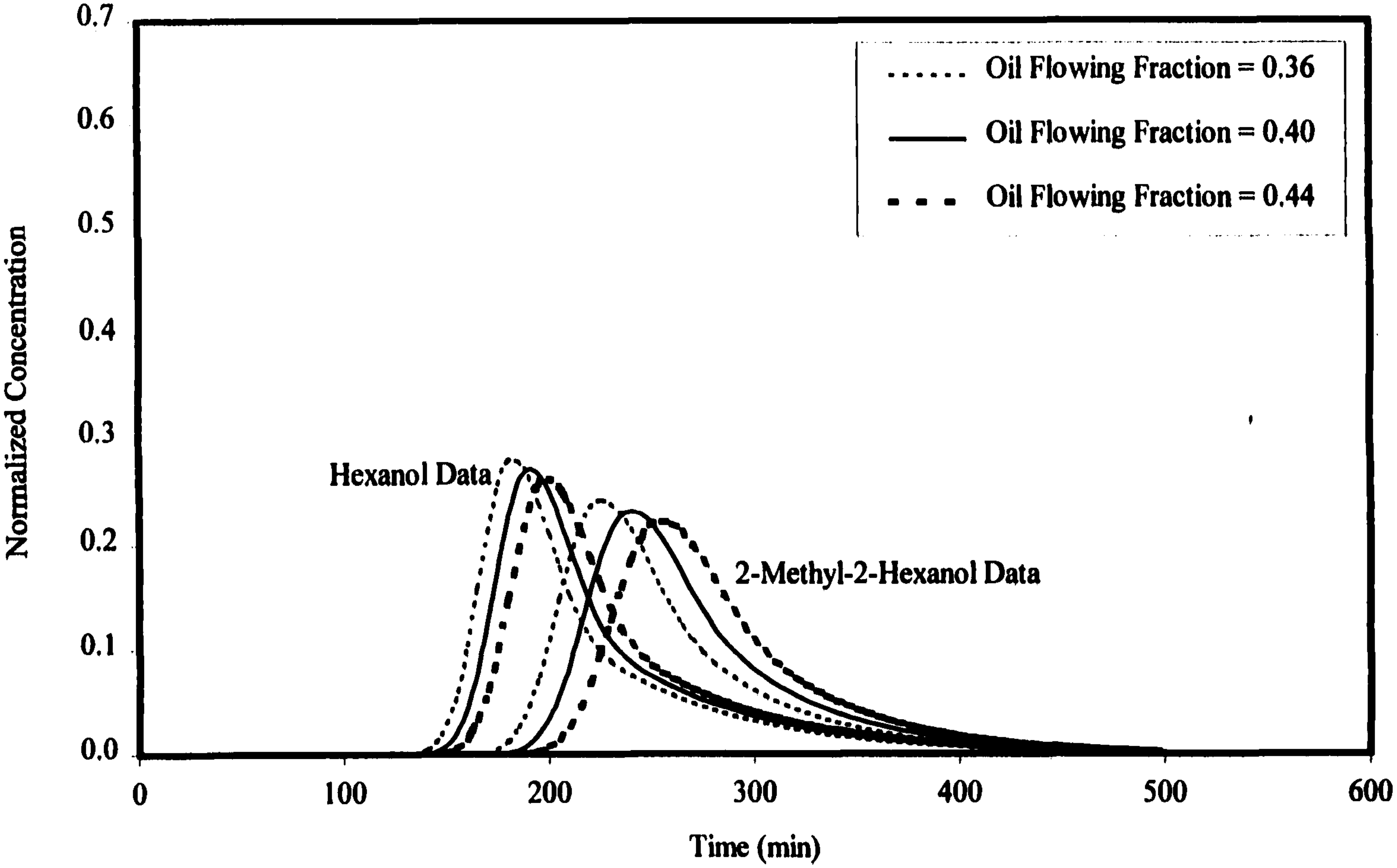

Figure 6.16 Impact of Oil Flowing Fraction on Simulated Breakthrough Curves for Pentanol and 2-Methyl-2-Hexanol at a Flow Rate of 0.3 ml/min

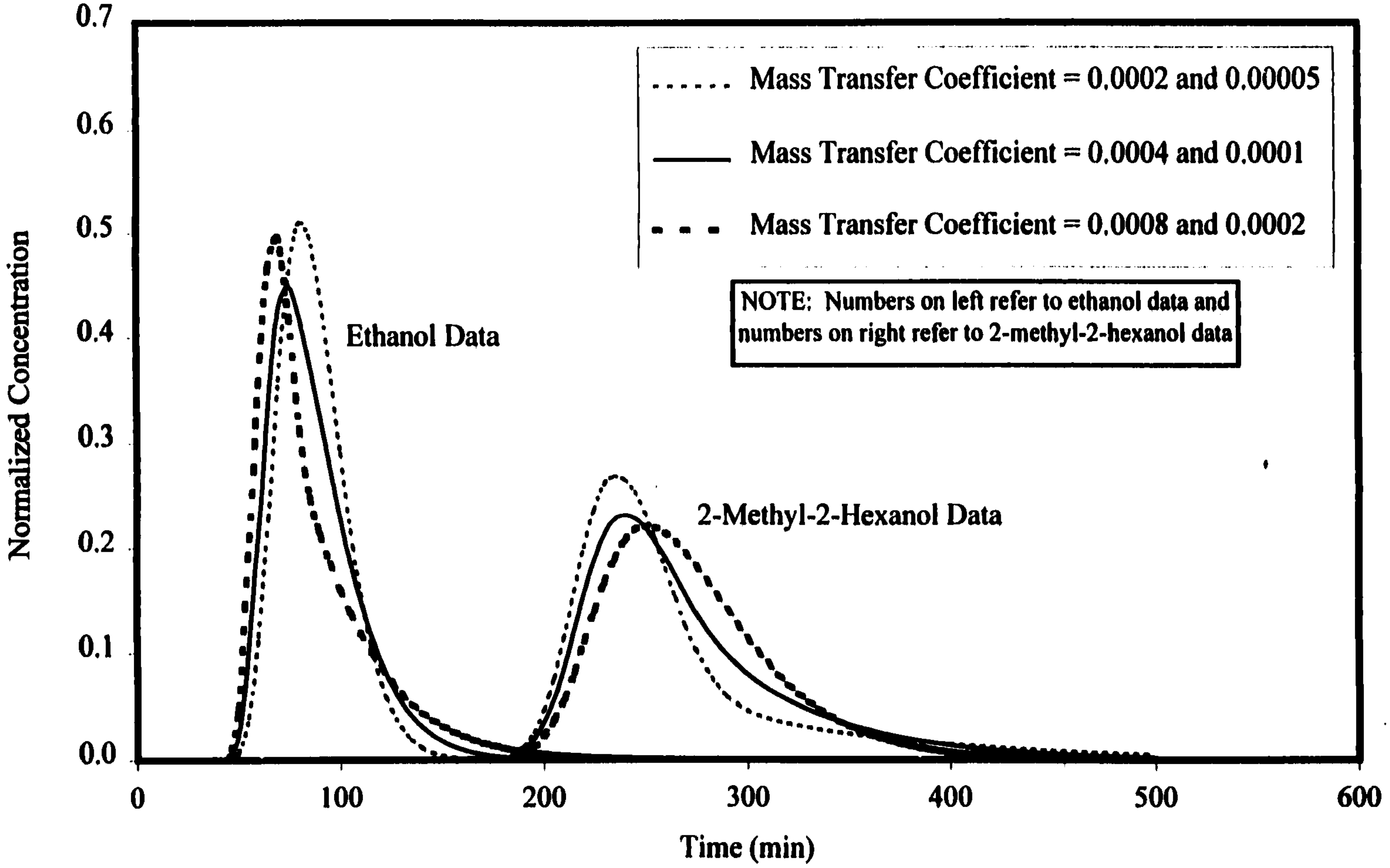

Figure 6.17 Impact of Mass Transfer Coefficient on Simulated Breakthrough Curves

for Pentanol and 2-Methyl-2-Hexanol at a Flow Rate of 0.3 ml/min

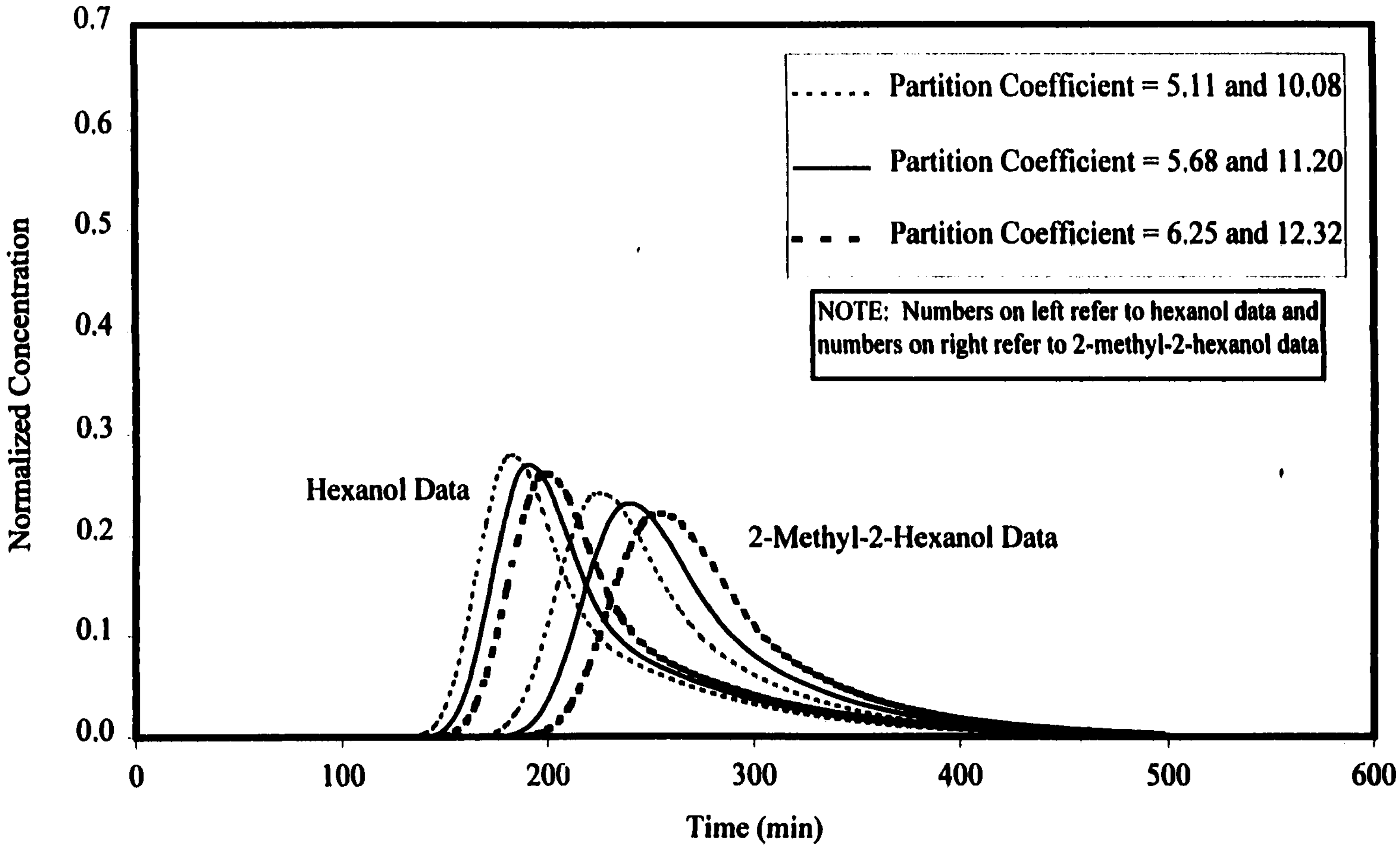

Figure 6.18 Impact of Partition Coefficient on Simulated Breakthrough Curves for Hexanol and 2-Methyl-2-Hexanol at a Flow Rate of 0.3 ml/min

6.5 Conclusions

Simulating the column experiments was possible only if dead-end pore space and physical non-equilibrium conditions were assumed. However, other explanations are possible for the difference between the laboratory and simulation results. Further research may reveal that the adsorption process for some tracers can be described more accurately with a Freundlich or Langmuir model instead of the linear process used in UTCHEM. There may also be a hysteretic effect associated with the desorption of tracers from organic material in the soil. These explanations may be more pronounced in the column experiments because of the relatively small scale of the column and the relatively high flow rates.

By using the capacitance model in UTCHEM, good agreement was obtained between the laboratory data and the simulation results. Using a trial-and-error fitting procedure for certain parameters in the simulations, it was discovered that increasing flow rates caused (1) water flowing fraction values to decrease, (2) mass transfer coefficients to increase, and (3) retardation factors for hexanol and 2-methyl-2-hexanol to decrease. These observations can be attributed to the creation of preferential flow paths and reduced retention times at high flow rates. The presence of a plateau region on the tailing side of the breakthrough curves for hexanol and 2-methyl-2-hexanol is a possible indication of a hysteretic effect regarding the desorption of tracers from organic soil material or non-equilibrium transport. Additional research is recommended to better explain these phenomena.

Given the heterogeneous and anisotropic conditions of the laboratory surfactant flooding experiment and the homogeneous and isotropic assumptions used in the simulations, there was reasonably good agreement between the respective results. In the laboratory experiment, it is hypothesized that the surfactant solution would flow through the more permeable areas of the soil column first and solubilize residual areas from those areas relatively quickly. As less permeable areas are encountered, the solubilization process becomes increasingly less efficient. The one-dimensional nature of the simulations did not account for this variability. Furthermore, since Dowfax 8390 does not readily form a microemulsion without a co-surfactant, mobilization of the contaminants was not possible during the simulations. It is hypothesized that the large peaks in the contaminant concentration histories after the surfactant dissipated represent contaminants adsorbed to colloids mobilized during the surfactant flooding process. A linear relationship existed between the Solubility Ratio Index (SRI) and the aqueous solubility of hydrocarbons for both the laboratory data and the simulations (the slopes and *x*-intercepts varied by 10 and 7 percent, respectively). This concept proved useful in identifying the presence of preferential solubilization and the respective order of contaminants. Further research is necessary to verify the appearance of a similar linear relationship for the chlorocarbons.

A sensitivity analysis helped identify the parameters, which appeared to be the most critical to the effective design of a tracer test (i.e., duration and respective tracer masses). For the column experiment, altering the permeability, capillary pressure, and residual saturation (i.e., drainage) values did not have any effect on the simulation results. The most influential factors were the water flowing fraction, mass transfer coefficients, and porosity. Although changes in dispersivity and oil flowing fraction values had minor effects on breakthrough curves, there was virtually no effect on the tailing portion of the curves. Therefore, the tracer test design is relatively independent of these parameters. A similar sensitivity analysis can be performed to determine the required duration of any tracer test and the required mass of individual tracers such that tracer concentrations in the timeframe of interest are above the detection limit of the analytical equipment being used. The method of moments described in earlier chapters can also be used to further refine the tracer test design by helping ensure adequate separation of breakthrough curves and helping determine appropriate sampling times.

CHAPTER 7

A COMPARISON OF FIELD AND SIMULATION RESULTS

In Chapter 5, the effluent concentration histories from three extraction wells used during a treatability study for surfactant-enhanced remediation at Hill Air Force Base (AFB), Utah, were introduced. This chapter provides the results of simulation studies of both the remediation effort and tracer tests conducted within the test cell. The simulations were conducted with UTCHEM (a three-dimensional chemical flooding simulator developed at the University of Texas at Austin) and were compared with the field data. Background data concerning the test cell can be obtained from Montgomery Watson (1995).

7.1 Simulation Model

The purpose of this section is to describe the development of the model used to simulate the tracer tests and the surfactant flooding process performed within the test cell at Hill AFB. Specific site properties were used when available for more accurate simulations. If site-specific data were not available, representative properties were selected based upon values cited in the literature.

7.1.1 Simulation Domain and Grid

The simulation domain was determined primarily by the dimensions of the test cell (see Figure 5.1). The area to be simulated was about 107 ft^2 and was represented by an 18 x 12 grid ($\Delta x = 0.6722$ ft and $\Delta y = 0.7375$ ft). The horizontal and transverse grid spacings were arbitrarily selected to accommodate uniform spacing in each respective direction while attempting to place wells near the center of a grid block. The depth of the test cell was 29 feet below ground surface (bgs) with a clay layer forming the bottom boundary (25 to 29 feet bgs).

During the pre-remediation tracer study, the fluid level within the test cell was measured at 16.41 feet bgs. To simulate the tracer test, the resulting saturated zone thickness of 8.59 feet was arbitrarily divided into 12 equal layers ($\Delta z = 0.7158$ ft). The fluid level was at 15.85 feet bgs during the surfactant remediation demonstration and the saturated zone thickness of 9.15 feet was divided into 10 equal layers ($\Delta z = 0.7625$ ft) for the subsequent simulations. The grid for the test cell was assumed to be perfectly horizontal and constant in terms of grid sizes. All boundary conditions were considered to be no-flow, with the saturated zone being the only portion of the test cell that was modeled.

7.1.2 Physical Properties

Bastasch (1996) performed 68 slug tests at 10 locations in the area of the test cell and determined the average hydraulic conductivity of the underlying aquifer was 6.3×10^{-4} ft/sec. Using measured flow rates during research conducted in the test cell, Shiau *et al.* (1997) determined cell-specific hydraulic conductivities to be 5.75×10^{-4} ft/sec during the pre-remediation tracer test and 2.53×10^{-4} ft/sec during the surfactant demonstration. A slight decrease in hydraulic conductivity was expected because of the higher viscosity of the surfactant solution. The cell-specific values were considered more representative of the hydraulically-controlled environment of the test cell and were used as inputs in UTCHEM.

The effective porosity within the test cell was determined from the results of the conservative tracer test. During the test, measured flow rates averaged 0.0922 ft^3/min. The cross-sectional area of the treatment zone was 76.11 ft^2 and the distance between the injection and extraction wells was 12.1 feet. The corresponding velocity was calculated as 0.0012 ft/min and the travel time between the injection and extraction wells was calculated as 10,083 minutes. From the effluent concentration history for the conservative tracer, the method of moments was used to calculate a mean travel time of 2,097 minutes. The ratio of the two travel times represents the porosity, which equals 0.21 in this case.

Dispersivity values for the test cell were not available. Values of longitudinal dispersivity have been reported in the literature to range from 0.01 to 170 meters over distances of 0.7 to 43,000 meters (Brown, 1993). In modeling efforts at a nearby test cell, Jin (1995) used a longitudinal dispersivity of 2.6 feet and a transverse dispersivity in the horizontal direction of 0.9 feet. Jin's values are considered more representative and were used as inputs in UTCHEM. Transverse dispersivity in the vertical direction was assumed to be negligible because of the relatively small scale of the test cell.

Site properties were initially considered to be constant (invariant with time) throughout the test cell and were subsequently modified during the sensitivity analysis. To simplify the simulations, it was also assumed that biotic and abiotic processes, tracer reactions, and temperature variations did not occur. Fluid compressibility, molecular diffusion, hysteresis, organic adsorption, and aqueous solubility of NAPL components in the absence of surfactant were considered negligible and were not included in the simulations. The initial pressure within the test cell was assumed to be at atmospheric levels and the gas phase was not considered. During tracer test simulations, the organic phase was considered to be comprised of a single component because only one partition coefficient for each tracer is allowed by UTCHEM; whereas during the surfactant flooding simulations, it was considered to consist of the seven individual components identified as target analytes. Assumptions regarding residual saturation and relative permeability are the same as those discussed for the column experiment in Chapter 6.

The surfactant used in the test cell solubilization study was Dowfax 8390, a hexadecyl diphenyl oxide disulfonate ($C_{16}H_{33}C_{12}H_7O(SO_3Na)_2$) with a molecular weight of 642 atomic mass units (amu). The initial electrolyte concentration of the groundwater was assumed to be 500 mg/l $CaCl_2$. Since electrolyte concentrations n UTCHEM are expressed in milli-equivalents per milliliter (meq/ml), 500 mg/l $CaCl_2$ was converted to 0.009 meq/ml for both the cation and anion concentrations.

7.1.3 Injection and Extraction Wells

Four injection and three extraction wells, each with a diameter of 2 inches, were used for the simulations. All wells penetrate to the center of the last gridblock and are considered to be fully completed. The injection wells are rate constrained (38.5 ft^3/day) and the extraction wells are pressure constrained (14.7 psia). The injection time for the tracers and surfactant were 234 minutes and 10 days, respectively, with all concentration values being input as unity in a dimensionless format. During the remediation simulation, surfactant was used in the first three injection wells and water was the only fluid injected through injection well 4.

7.2 Tracer Test Simulations

The more significant UTCHEM input values used to simulate the field tracer test are listed in Table 7.1. Residual NAPL saturation, determined by applying the method of moments to field data and averaging the results from the extraction wells, was initially assumed to be constant throughout the test cell. Subsequent values were determined for each gridblock through statistical interpolation of soil core data for the seven target analytes (listed in Table 5.12). Soil cores were obtained from eight separate locations and data was collected over 2-foot depth intervals. Kriging of the

Table 7.1: Test Cell Properties for Simulation of Field Tracer Test

Property	Value
Porosity[a]	0.21
Permeability	
Longitudinal[a]	11,787 milli-Darcies
Transverse Horizontal[b]	11,787 milli-Darcies
Water Saturation[a]	0.9151
Water Viscosity[b]	1.0 cp
Oil Viscosity[b]	0.89 cp
Water Density[b]	0.4334 lb/ft^3
Oil Density[b]	0.3467 lb/ft^3
Dispersivity[b]	
Longitudinal	2.6 ft
Transverse	0.9 ft
Tracer Partition Coefficients[a]	
Bromide	0.0
Hexanol	4.0
2,2-Dimethyl-3-Pentanol	13.0

[a] Calculated from laboratory data
[b] Representative

data was accomplished with SURFER® using a linear variogram in the horizontal direction with a scale of 1. Kriging with a linear variogram is the statistical technique recommended by the SURFER® software when dealing with a limited number of data points. Furthermore, the concentration data in a given layer were assumed to be independent of data in over- and underlying layers.

Simulated breakthrough curves are shown in Figures 7.1 through 7.3. During the field tracer test, the hexanol breakthrough curve was not consistent with expected behavior and the data was considered unreliable. Breakthrough curves for the other tracers were incomplete due to either the curtailed sampling period or dilution below detectable limits. Modified breakthrough curves, reflecting exponential extrapolation of the data, are shown when comparisons are made to simulations.

If Figures 7.1 through 7.3 are overlain, the breakthrough curves for the respective tracers are almost identical. This is expected because of the relative symmetry between the injection and extraction wells and the assumption of homogeneous and isotropic conditions. Given the generalized conditions, visual inspection of the figures seems to indicate reasonably good agreement between the laboratory data and the simulations. This is confirmed by comparing method of moments calculations for both the field data and the simulations as shown in Table 7.2. The residual saturation calculated from the simulation results differs from the input value (i.e., the average of the field results) by only 6.9 percent. The mean travel times are in good agreement for two of the extraction wells. However, the field mean travel times for extraction well 1 are more then double the simulated results. The

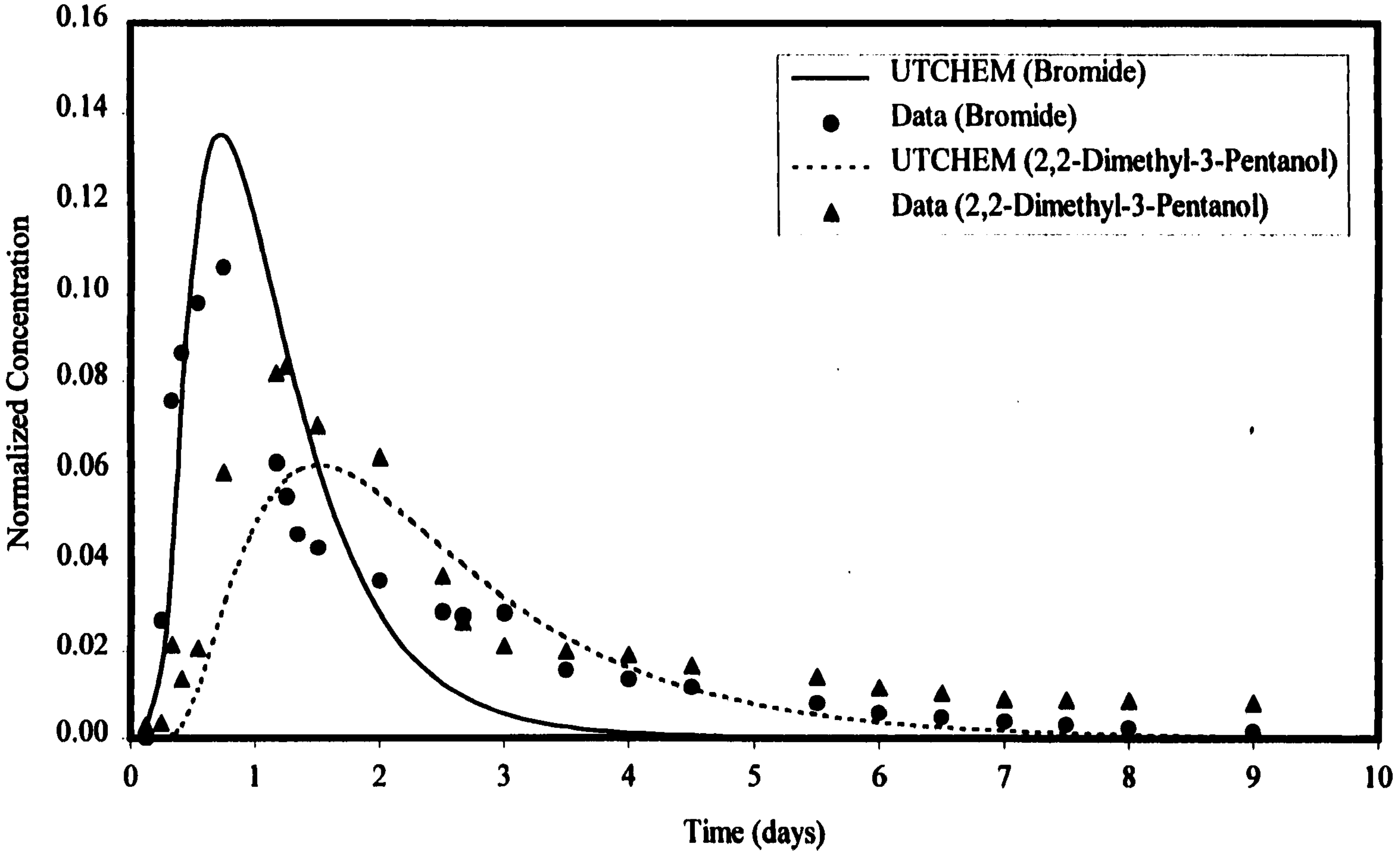

Figure 7.1 Comparison of Breakthrough Curves from Simulated and Field Data for Extraction Well 1 at Hill AFB Test Cell

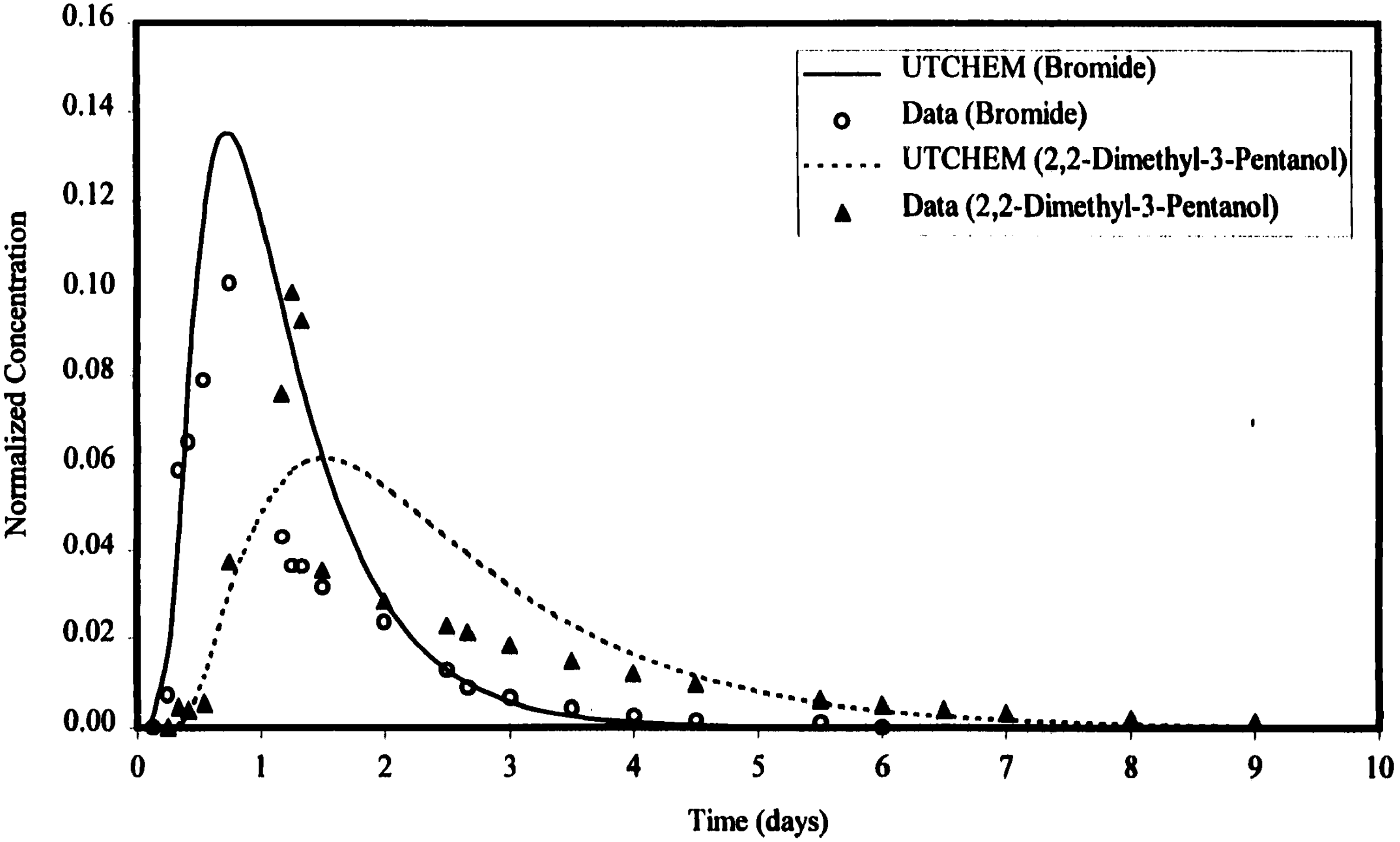

Figure 7.2 Comparison of Breakthrough Curves from Simulated and Field Data for Extraction Well 2 at Hill AFB Test Cell

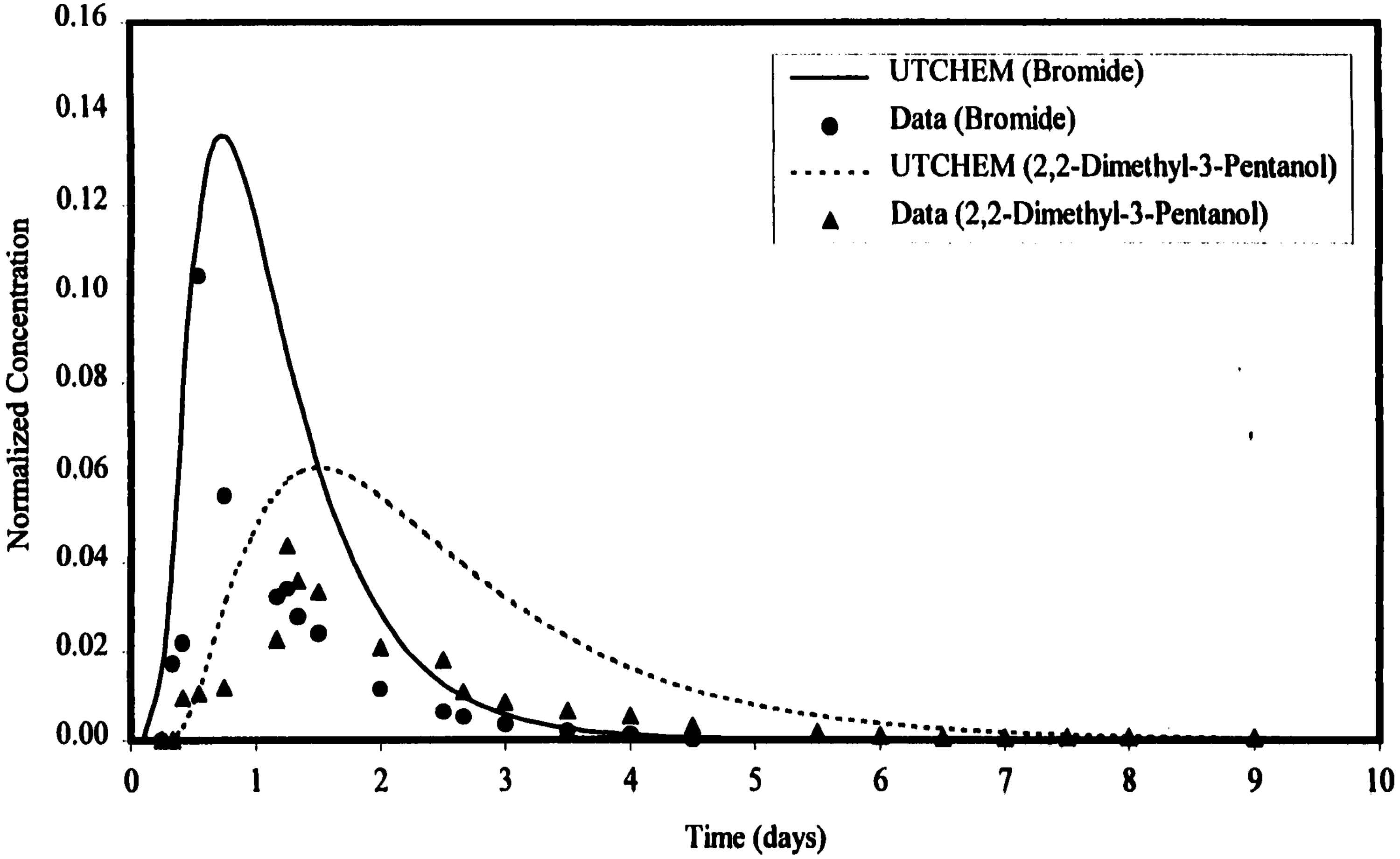

Figure 7.3 Comparison of Breakthrough Curves from Simulated and Field Data for Extraction Well 3 at Hill AFB Test Cell

Table 7.2: **Comparison of Travel Times and Residual Saturation Values Determined from the Method of Moments**

Case	Mean Travel Time (mins)		Residual Saturation (%)
	Bromide	2,2-Dimethyl-3-Pentanol	
Simulation	1453	3339	9.08
Field Data (EW1)	1553	3062	6.96
Field Data (EW2)	1730	3313	8.79
Field Data (EW3)	3009	7218	9.72

most likely explanation for this difference is that the simulation did not account for higher residual saturation levels and reduced permeability in the respective portion of the test cell. In fact, the overall differences between the field and simulated breakthrough curves can probably be attributed to the homogeneous and isotropic conditions assumed in the simulations.

Instead of assuming homogeneous conditions, residual saturation and permeability values were also input as heterogeneous values. For residual saturation, kriged values determined from the soil core data were input for each gridblock, and also averaged and input for each layer. However, the tracer breakthrough curves from the simulations were nearly identical to the results obtained when constant residual saturation was assumed.

Random permeability values were also input for individual layers and gridblocks. The results were useful in that they helped illustrate the effects of heterogeneity and allowed for better conceptualization of the subsurface. However, varying values in this type of "curve fitting" procedure to match the field data is not an effective way of analyzing the site. Even if a good match is found, there are no guarantees that the permeability values truly represent site conditions; the values certainly do not represent a unique solution. Without any statistical data regarding permeability values, no attempt was made to generate a stochastic permeability field. Future research can explore this option in more detail and possibly incorporate a porosity-permeability function to create a stochastic porosity field.

A sensitivity analysis was conducted to determine how sensitive the overall results were to changes in some of the input parameters. The objective was to determine which parameters require the most accurate estimation to ensure good simulation results. In all cases, the base case is represented by Figures 7.1 through 7.3. The general simulation conditions are the same as those described in Table 7.3 and Section 7.1 except for the changes made to an individual input parameter.

Sensitivity analysis showed that an order of magnitude increase or decrease in permeability (when permeability was assumed constant throughout the test cell) did not have any effect on the simulated tracer tests. Additionally, assuming a capillary pressure of zero did not have any effect on the simulation results. These findings, consistent with observations from the column study, were expected because of the forced-flow conditions of the experiment and the fact that the respective property values were assumed to be constant throughout the test cell.

Figures 7.4 and 7.5 show the sensitivity of field tracer test simulations to variations in porosity and dispersivity, respectively. In each figure, the base case is shown as the solid line and the respective input value is increased and decreased by an appropriate factor. The changes in the breakthrough curves were consistent with those observed for the column studies. Table 7.2 compares the mean travel times and residual saturation values determined using the method of moments for both the simulations and the laboratory data. Varying the porosity by ±10 percent causes the mean travel times and residual saturation values to vary by about 11 and 1.5 percent, respectively. Varying the dispersivity by a factor of 2 does not appear to cause any

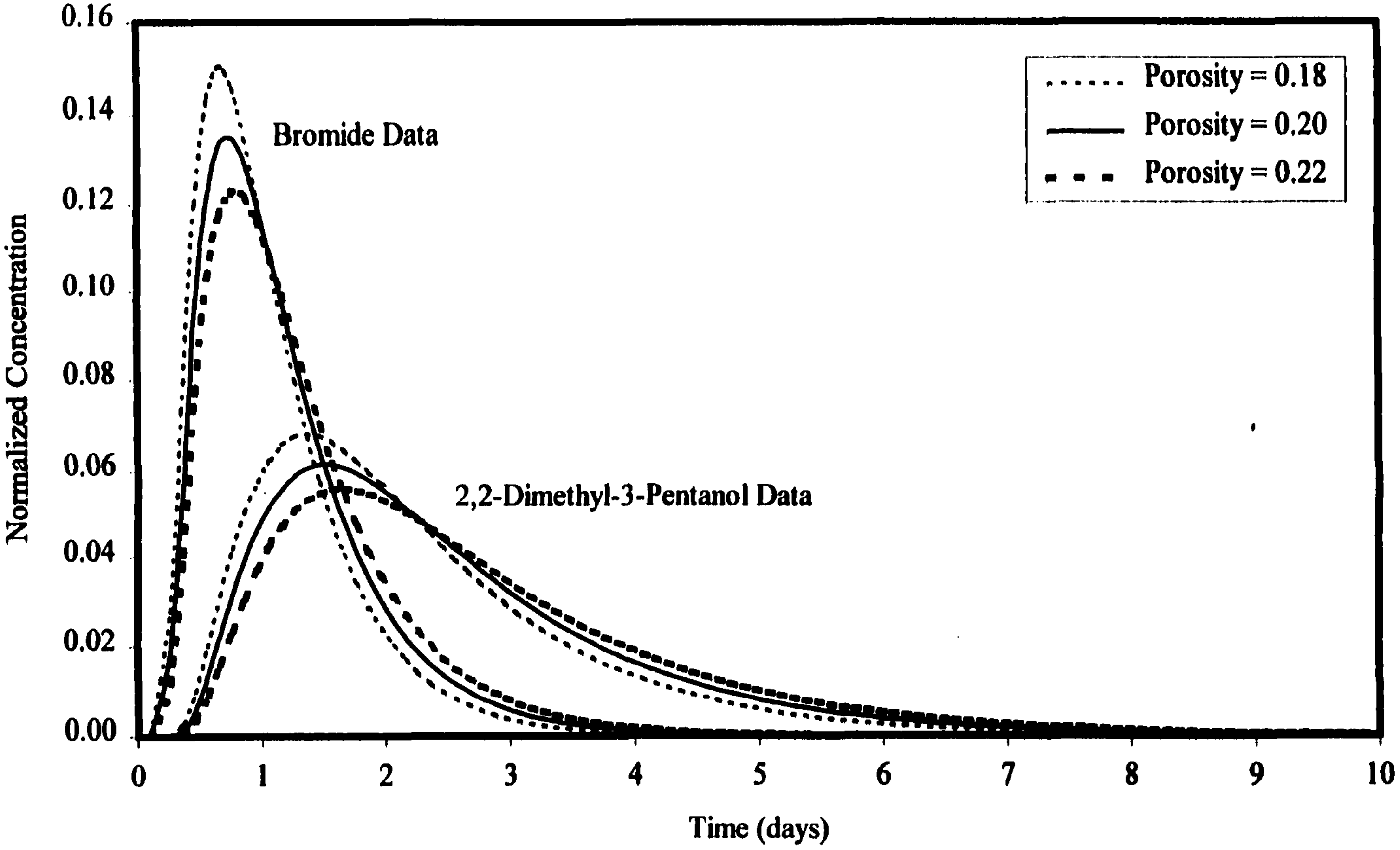

Figure 7.4 Impact of Porosity on Simulated Field Tracer Test for Bromide and 2,2-Dimethyl-3-Pentanol

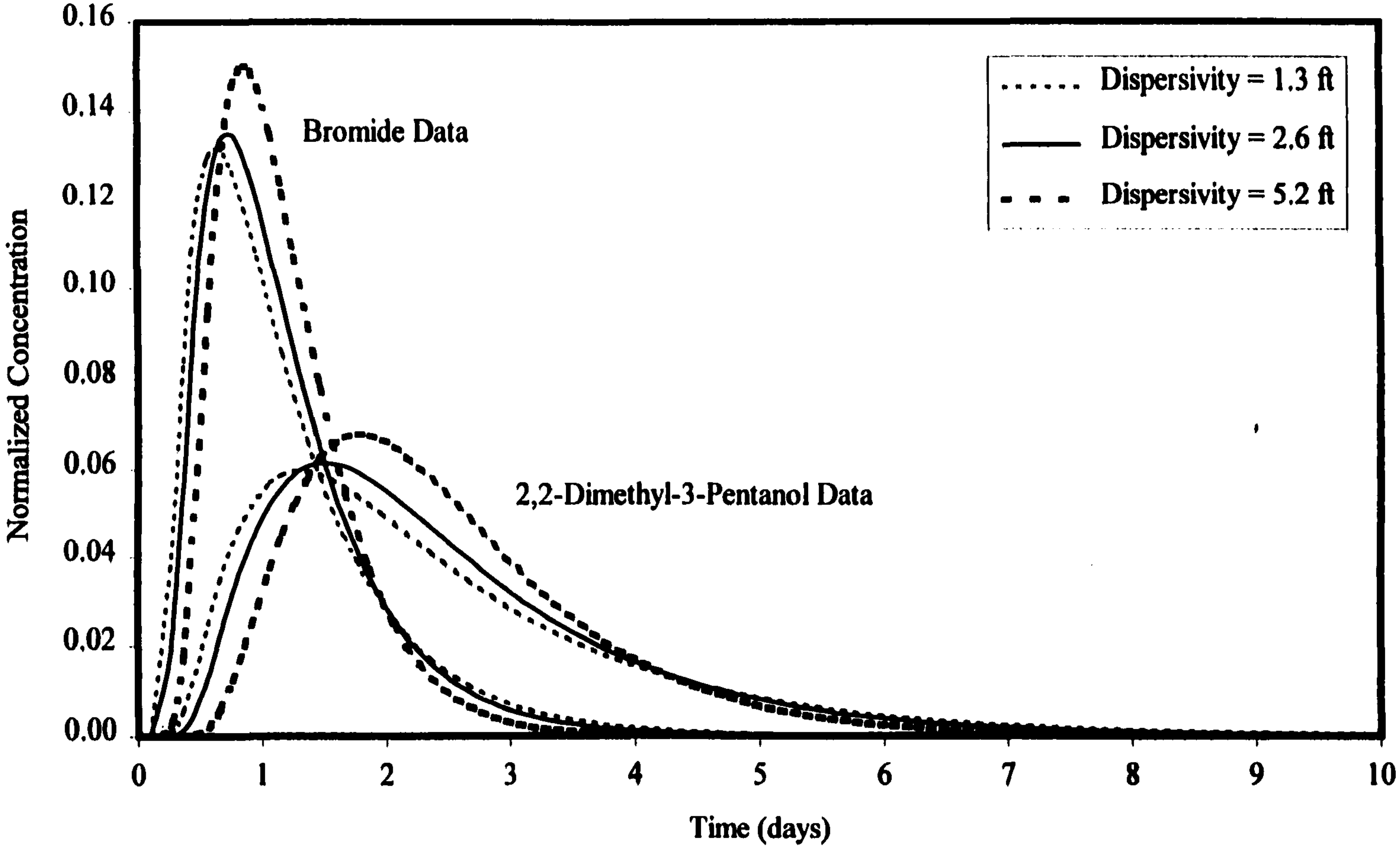

Figure 7.5 Impact of Dispersivity on Simulated Field Tracer Test for Bromide and 2,2-Dimethyl-3-Pentanol

significant differences in the calculations (< 1 percent difference). These results are helpful in determining the required duration, the mass of each tracer, and an appropriate sampling strategy for the tracer test design. The results also help identify which aquifer parameters have the greatest effect on the simulations and, therefore, require more accurate estimation.

7.3 Surfactant Remediation Simulations

Results of the surfactant flooding experiment conducted in the test cell were presented in the Chapter 5. UTCHEM was subsequently used to simulate the surfactant flooding process in an attempt to duplicate the results from the test cell. Therefore, this section compares the simulation results with the field results.

In addition to the test cell properties shown in Table 7.1, surfactant properties were assumed to be the same as those used during the column study (see Table 6.6). Because of the homogeneous conditions assumed for the test cell and the symmetry of the injection/extraction wells, the plots for the respective extraction wells were similar. Figures 7.6 and 7.7 show the simulated concentration histories for the surfactant and undecane, respectively. The decreasing trend in both figures is a reflection of the unbalanced surfactant injection pattern caused by using only water in injection well 4. Comparisons of plots for the remaining six contaminant components are not shown because they exhibit similar behavior.

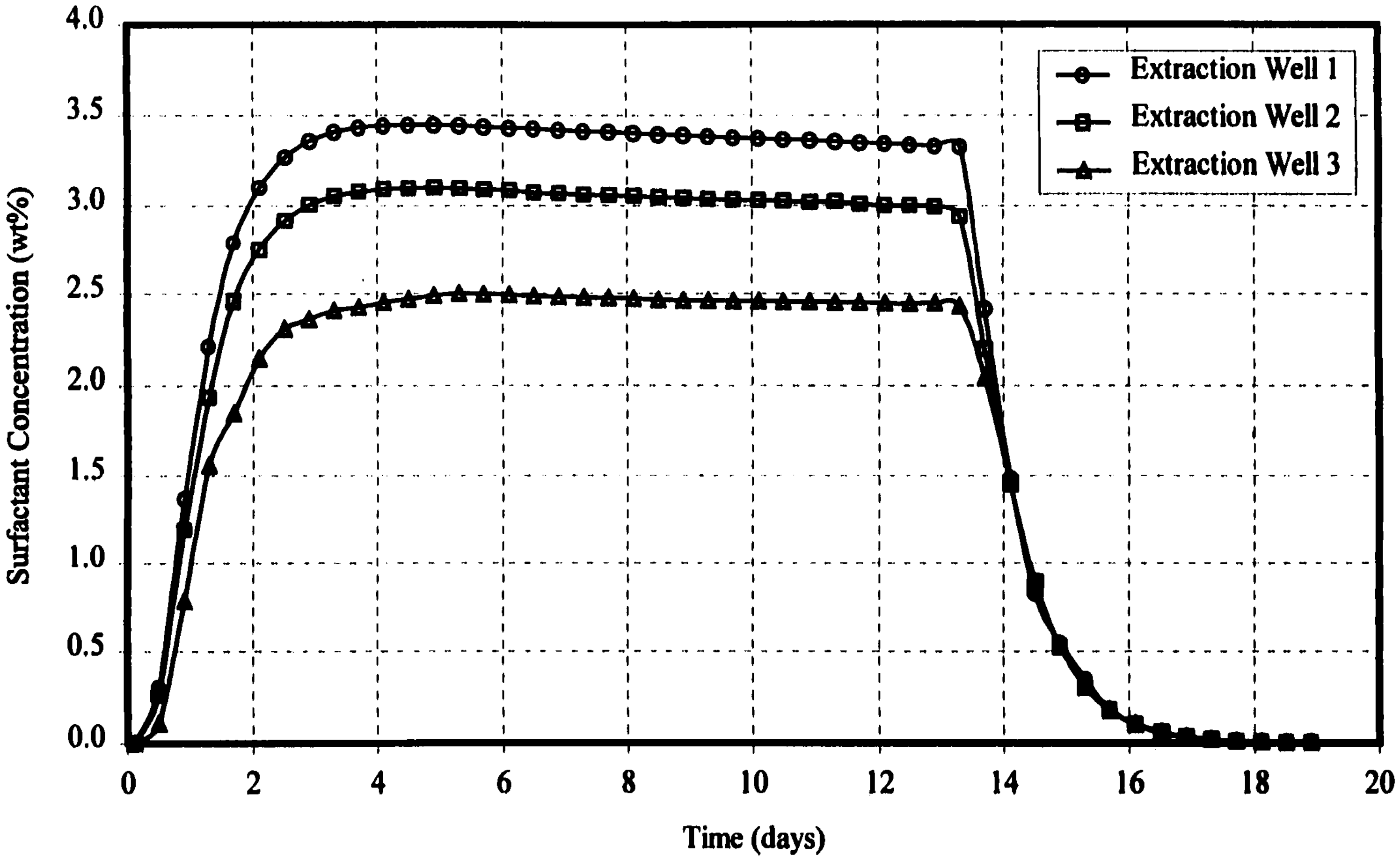

Figure 7.6 Comparison of Initial Simulation Results for Surfactant for Extraction Wells

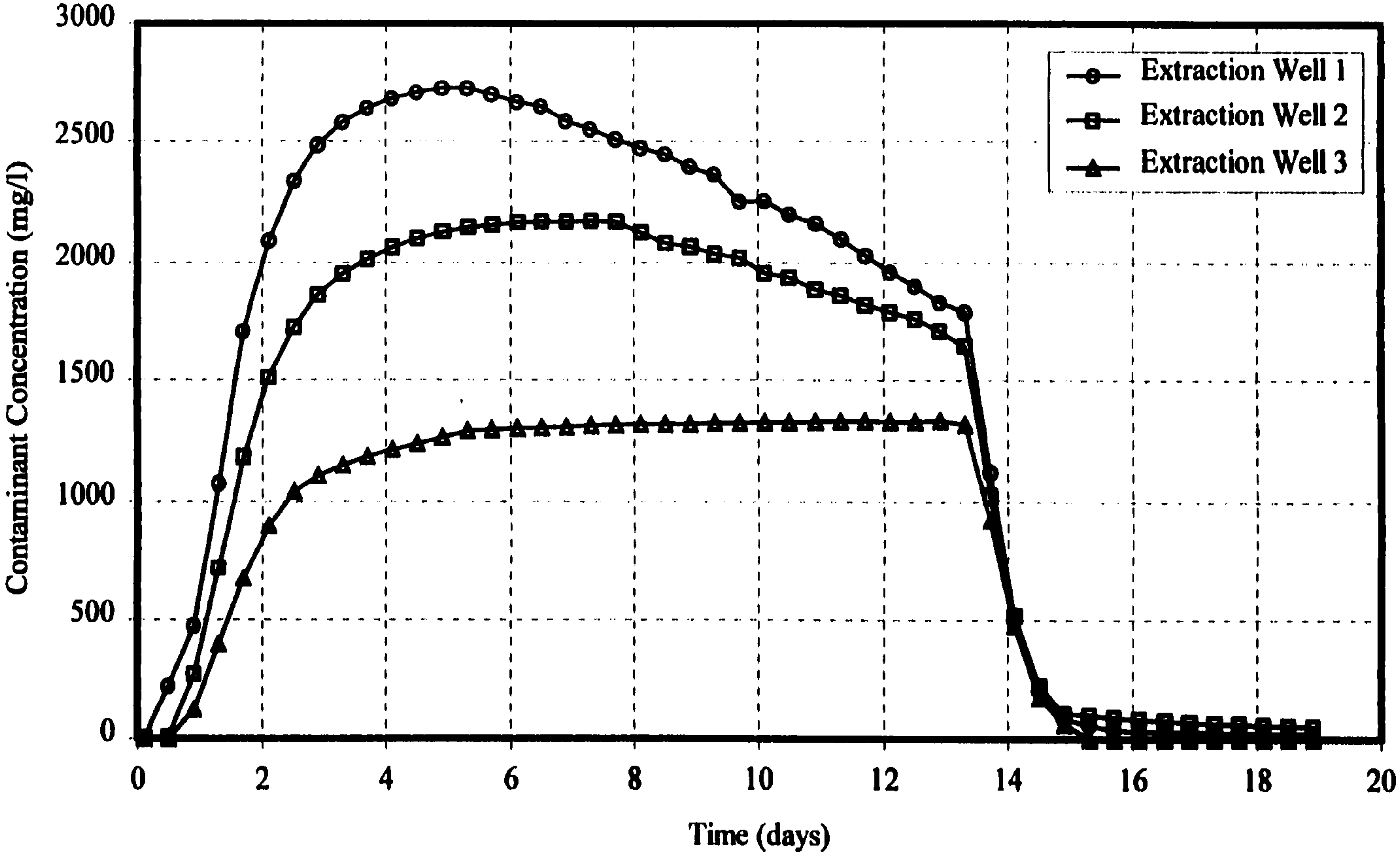

Figure 7.7 Comparison of Initial Simulation Results for Undecane for Extraction Wells

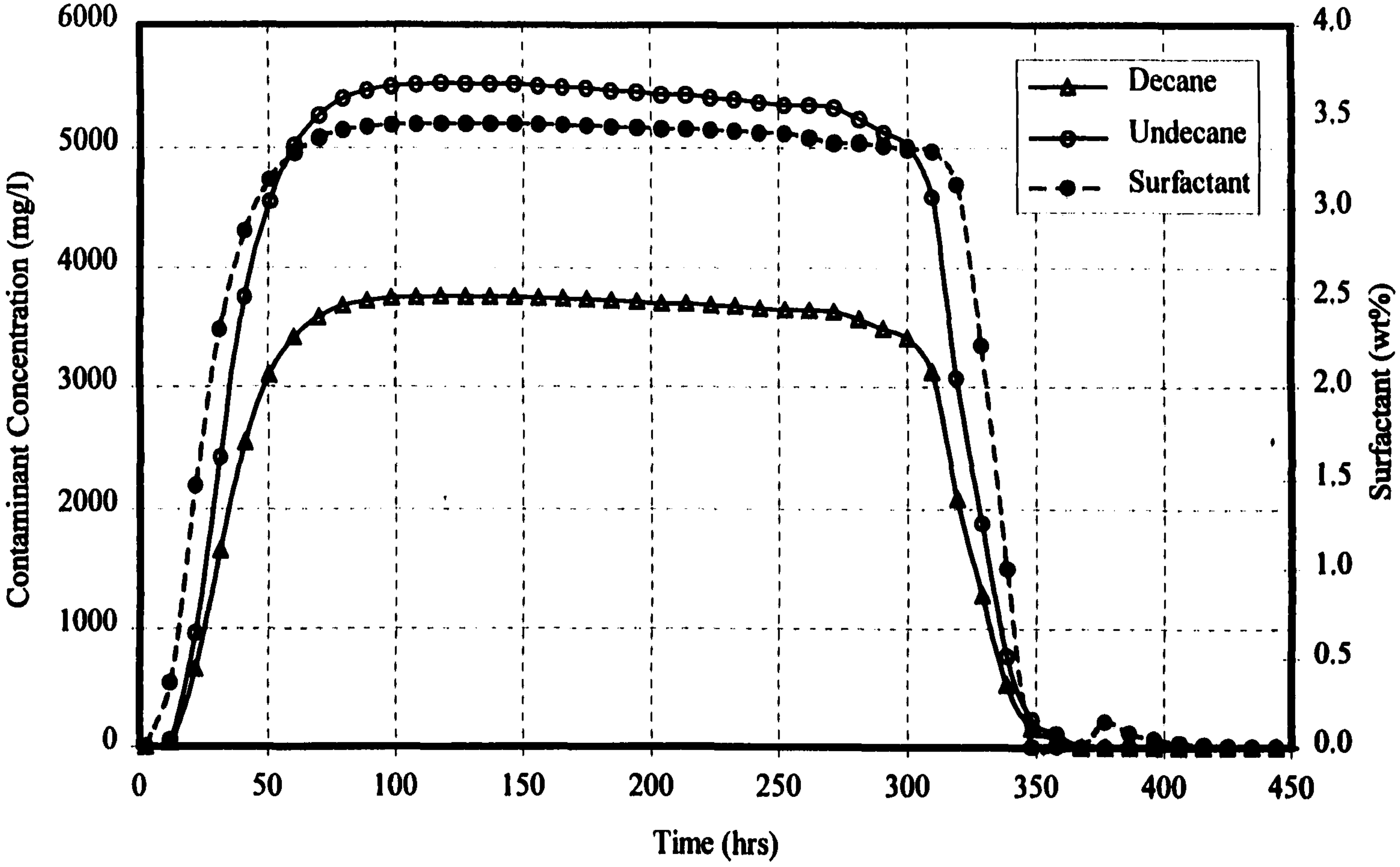

Figure 7.8 Initial Simulation Results for Extraction Well 1 for Contaminants with High Concentrations

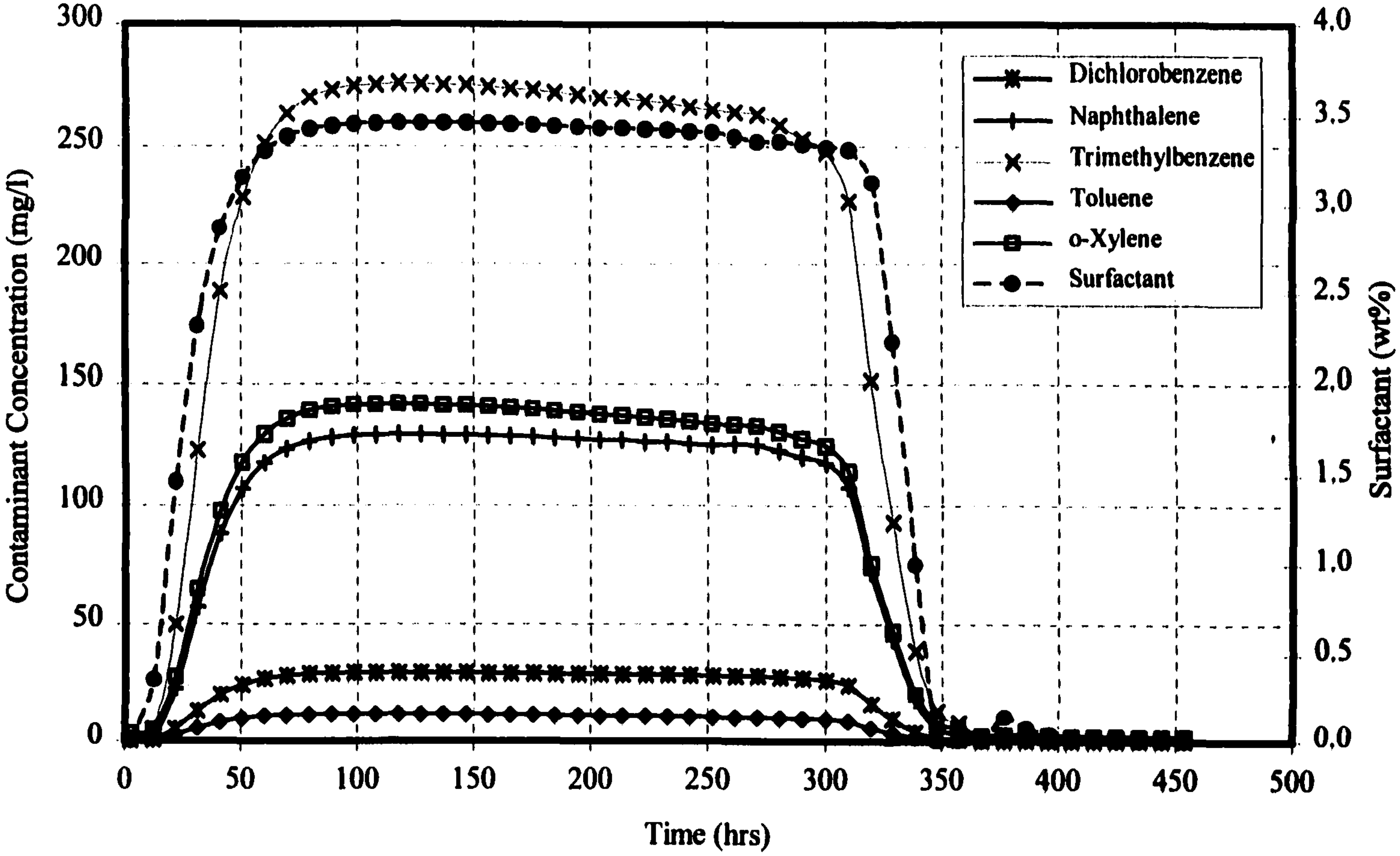

Figure 7.9 Initial Simulation Results for Extraction Well 1 for Contaminants with Low Concentrations

Since comparison of field and simulation data from each extraction well would generate the same discussion, only the complete concentration histories for extraction well 1 are shown in Figures 7.8 and 7.9. When these figures are compared with Figure 5.15, a number of differences are clearly evident, with the most obvious difference concerning the general shapes of the breakthrough curves. While the plots from the field data showed a lot of variability, the simulation results are similar to each other and their relative peak values remain as long as the surfactant is present. However, that was not the case for the field data. These differences can be attributed to the homogeneity assumed for the simulation, which did not account for the heterogeneities that undoubtedly exist for the field conditions.

Another major difference between the field and simulation results is the magnitude of the concentration values. The field concentration histories ranged from less than 1.0 mg/l to almost 50 mg/l, while the simulations indicate a range from 10 mg/l to over 5,000 mg/l. The simulation results are based on the assumption that the residual saturation is comprised only of the seven components reflected in the figures. However, these seven components are only target analytes. If the target analytes are assumed to represent only 1 percent of the total residual saturation, dividing the simulation values by 100 will provide concentration values more similar to the field results. Comparing the values in this manner does not account for interactions from the other components comprising the residual NAPL and should only be done to form generalizations about the data.

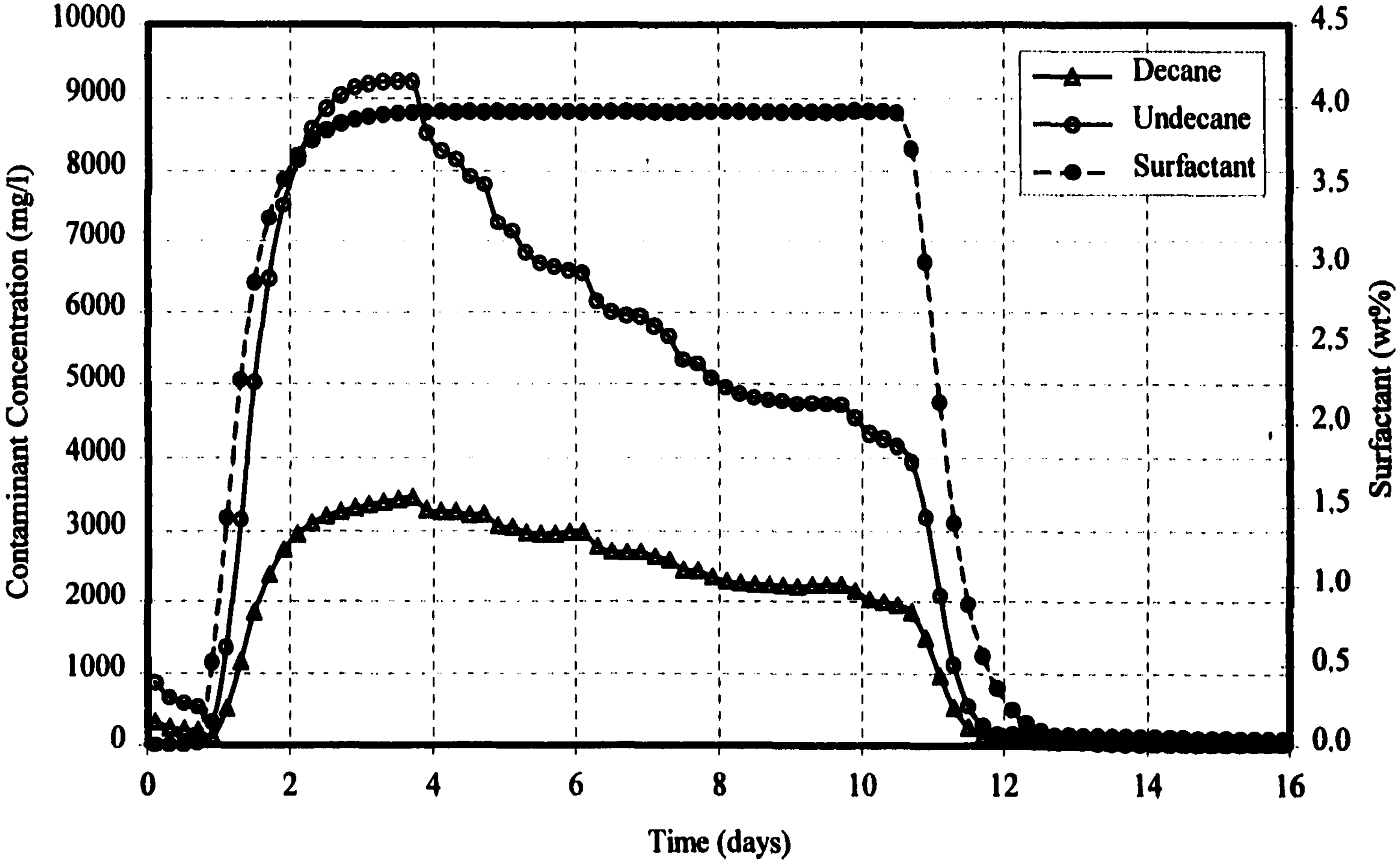

Figure 7.10 Simulation Results for Extraction Well 1 for Indicated Contaminants of Higher Concentration

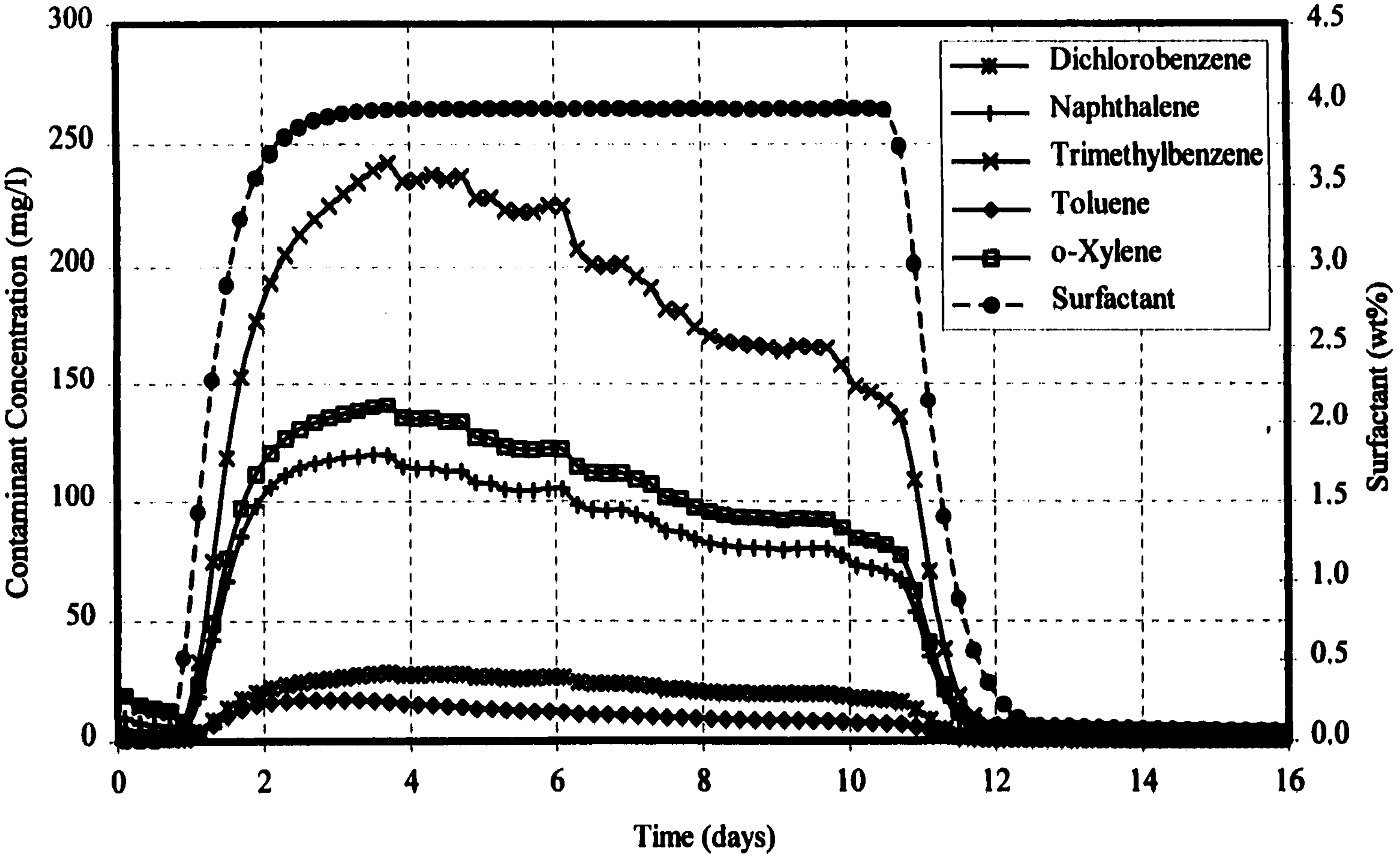

Figure 7.11 Simulation Results for Extraction Well 1 for Indicated Contaminants of Lower Concentration

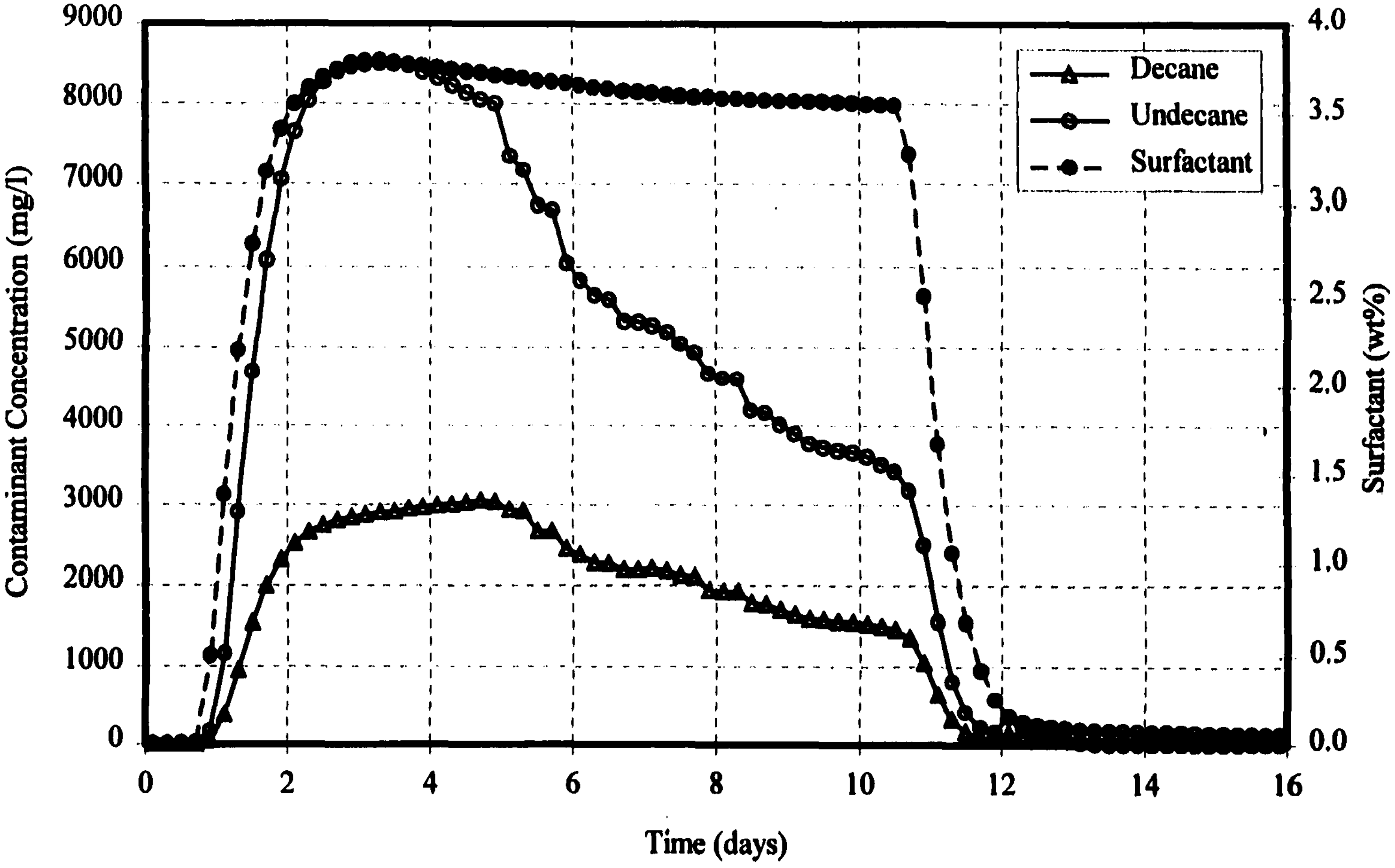

Figure 7.12 Simulation Results for Extraction Well 2 for Indicated Contaminants of Higher Concentration

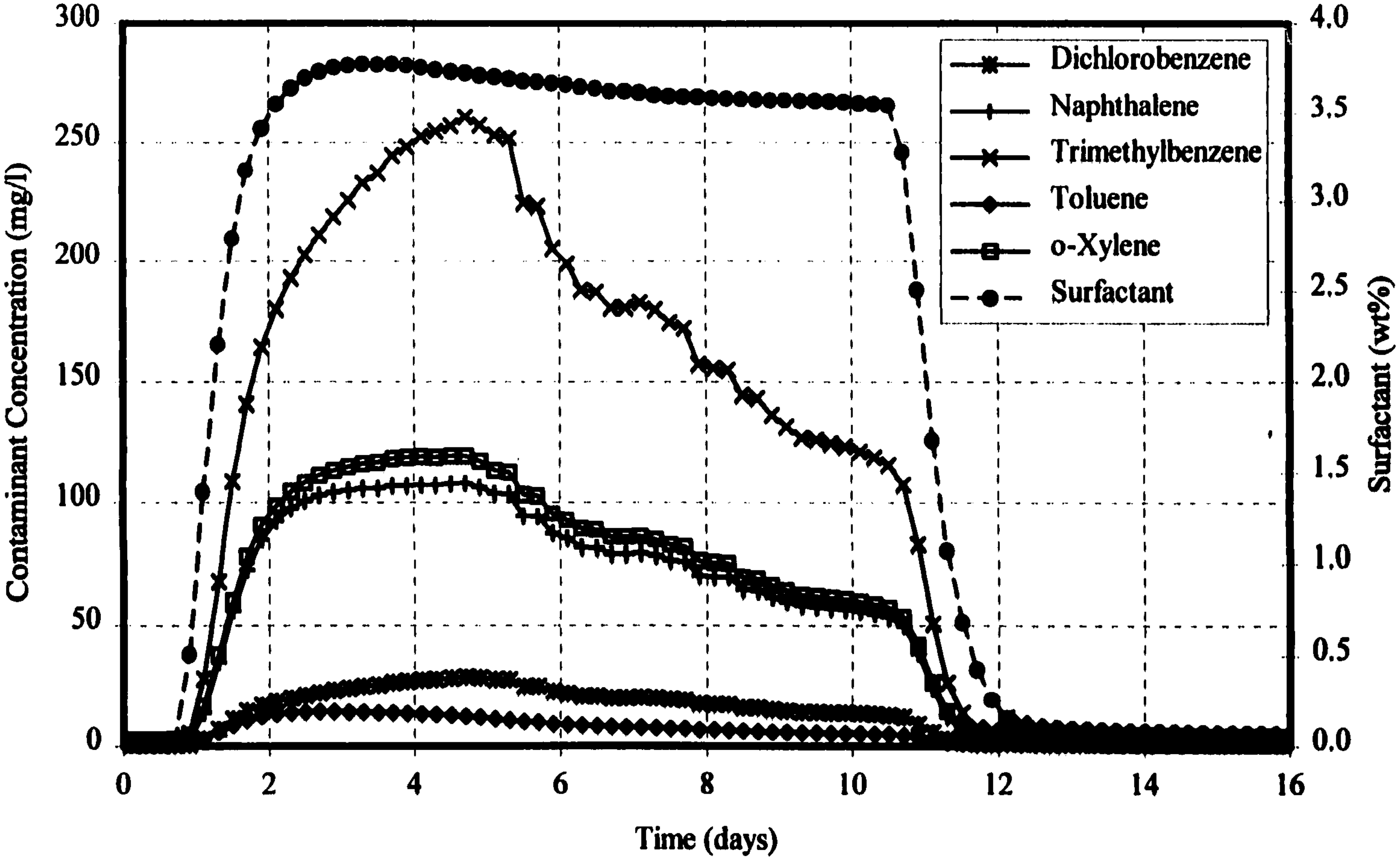

Figure 7.13 Simulation Results for Extraction Well 2 for Indicated Contaminants of Lower Concentration

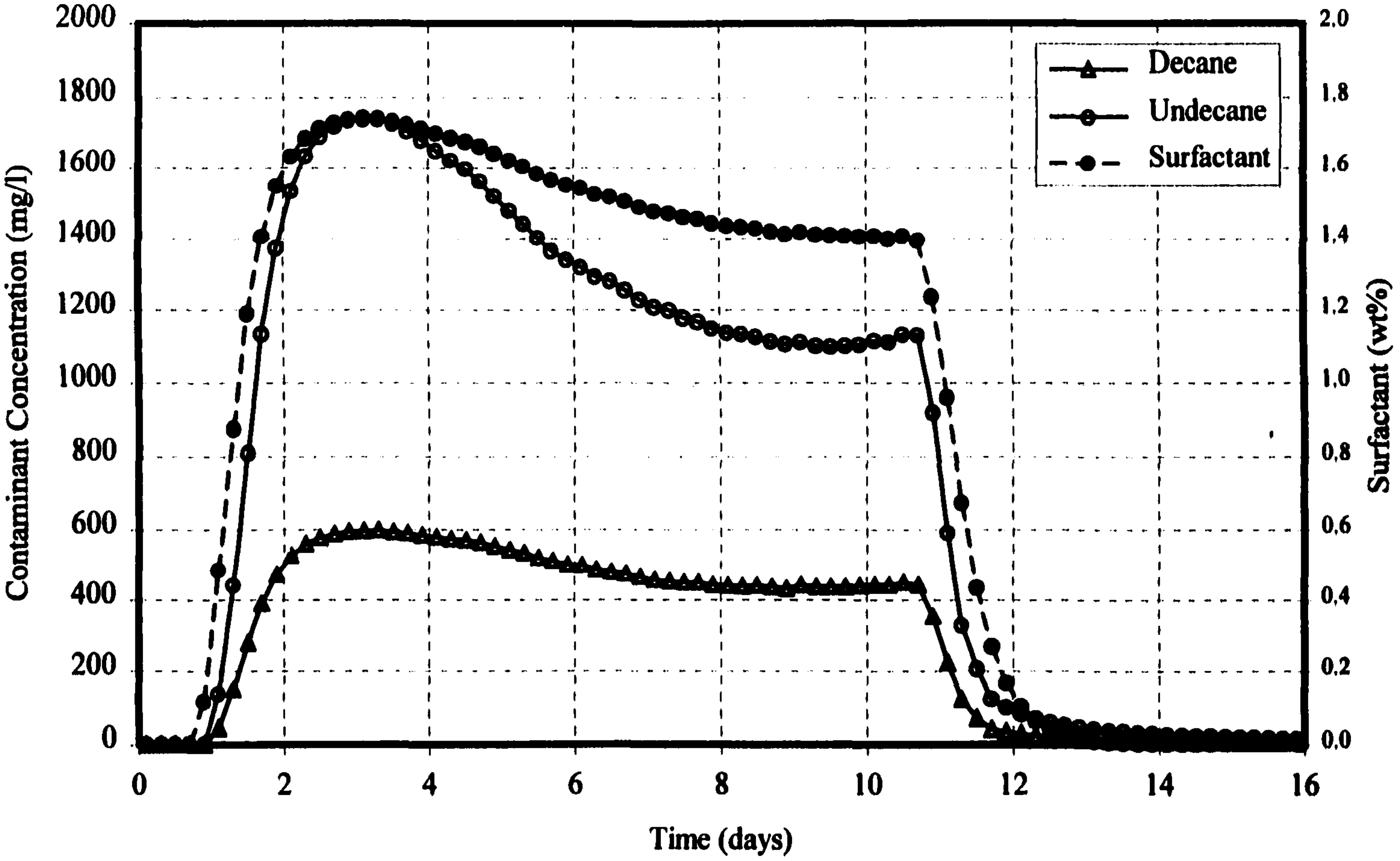

Figure 7.14 Simulation Results for Extraction Well 3 for Indicated Contaminants of Higher Concentration

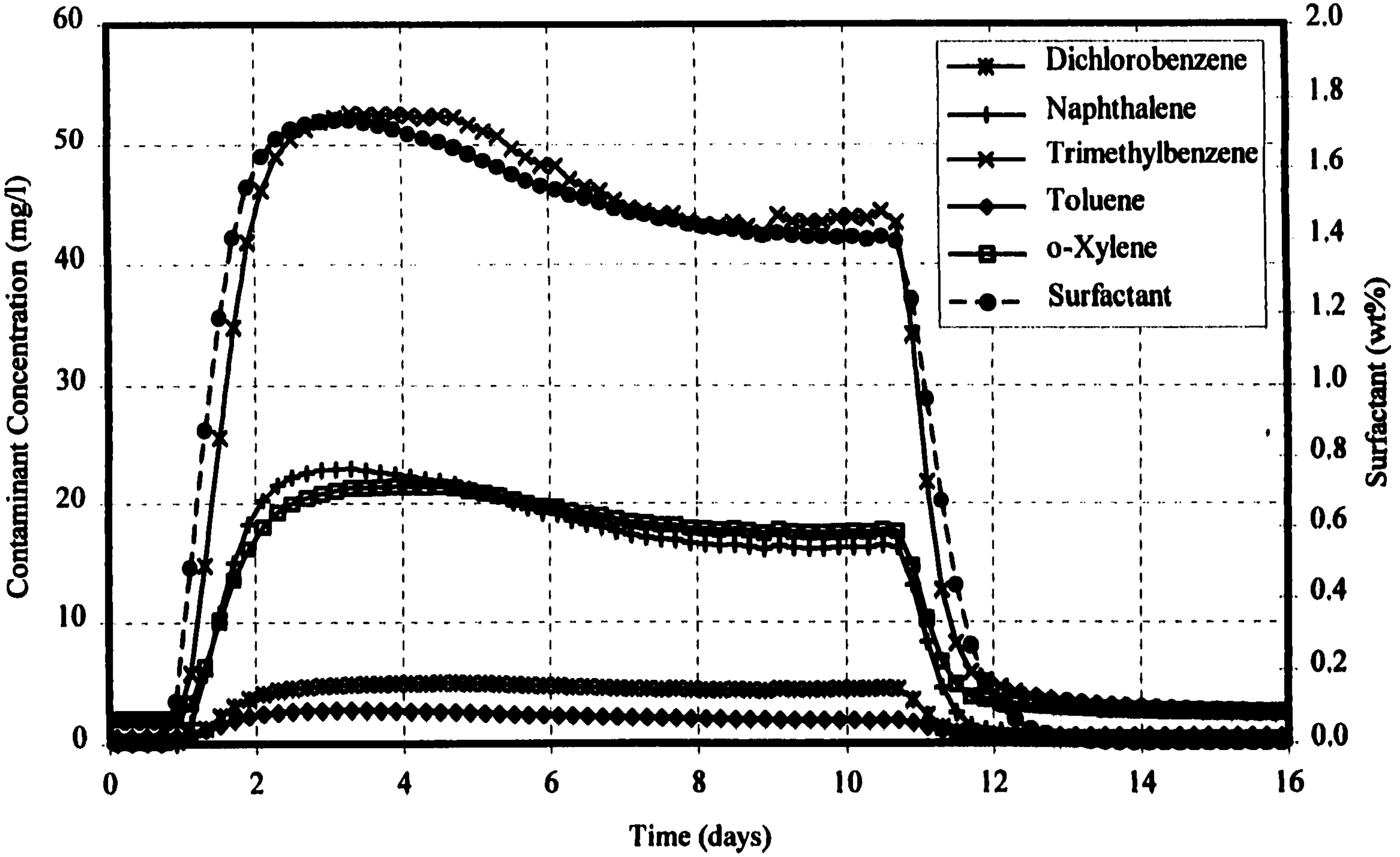

Figure 7.15 Simulation Results for Extraction Well 3 for Indicated Contaminants of Lower Concentration

When residual saturation values and contaminant volume fractions are input for each individual gridblock, the simulations provide slightly different results as shown in Figures 7.10 through 7.15. The order of contaminants, in terms of their respective concentration values, is the same, and the magnitude of the concentration values is very similar to the completely homogeneous case shown in Figures 7.8 and 7.9. However, the more heterogeneous simulation clearly indicates a peak in contaminant concentration values corresponding to the surfactant breakthrough. These peaks are then followed by generally decreasing values, which is the behavior typically expected with surfactant remediation. The surfactants will flow through more permeable areas of the test cell first and solubilize residual NAPL from those areas relatively quickly. As less permeable areas are contacted, the solubilization process becomes slightly less efficient and results in a decrease in effluent concentration values.

Even with more heterogeneity introduced into the simulations, the concentration histories still differ significantly from the field data. Additional field heterogeneities and the assumption that the seven target analytes comprise the complete residual NAPL were already discussed as possible explanations for the differences. Another possible reason is the kriging procedure used to assign residual saturation values to individual gridblocks. Based on a limited sample size, the interpolated values may not be very representative of field conditions. The absence of statistical data to generate a permeability field also hinders the simulation efforts.

7.4 Conclusions

There was reasonably good agreement between field data and the results from simulated tracer tests. Applying the method of moments to the respective data, the calculated mean travel times and residual saturation values were in good agreement as well. Exact, or even near-exact, agreement is not realistic because of the generally homogeneous and isotropic conditions assumed for the simulations. Even when heterogeneity was introduced by varying permeability and residual saturation values, only slight improvement was observed in the agreement between the field and simulated results. The fact that the mean travel time in the field for one of the extraction wells was more than double the simulated value is an indication that significant heterogeneity exists in the associated portion of the test cell. Improved results may be possible if more site data were available and a stochastic permeability field was introduced.

The purpose of any sensitivity analysis should be to identify which parameters require the most accurate estimation and then use various simulations to determine the appropriate tracers, mass of each tracer, and test duration. For this research, altering permeability and capillary pressure values did not appear to affect the results when completely homogeneous conditions were assumed. Inputting residual NAPL saturation values for each layer, or even for each gridblock did not significantly affect the simulations either. Varying permeability values by either layer or gridblock significantly affected the simulations. However, there are no guarantees that the selected values truly represent site conditions. Without statistical data regarding permeability values, no attempt was made to generate a stochastic permeability field. If porosity estimates reflect a 10 percent error, mean travel times and residual saturation values and residual NAPL saturation values will vary by 11 and 1.5 percent, respectively. Dispersivity errors on the order of 50 percent had very little effect on the simulation results (< 1 percent difference).

The surfactant simulations confirmed the expected behavior of NAPL contaminants during enhanced solubilization. However, the results did not agree well with the field data because not enough data was available concerning the heterogeneities of the test cell. Assuming the target analytes comprised the complete residual NAPL and using kriged values for gridblock contaminant concentrations also potentially contributed to the differences.

CHAPTER 8

CONCLUSIONS AND RECOMMENDATIONS

8.1 Conclusions

The primary objective of this research was to determine the relationship between tracer partition coefficients and EACNs of both the NAPL and the alcohol tracer. The secondary objective was to demonstrate the modeling capability of UTCHEM. The combined efforts of this research illustrate the benefits to be gained from being able to use estimated partition coefficients in modeling efforts to improve the design of tracer tests and surfactant flushing demonstrations. The following conclusions were made in support of these objectives.

1. Although alkanes were the only compounds for which a three-phase region was identifiable throughout the various surfactant solutions, the results validated the EACN concept. The linear relationship which existed between the EACNs of the alkanes and the natural logarithm of the system's optimal salinity resulted in k values which were in excellent agreement with values previously reported in the literature.

2. Three-phase regions were identifiable for the aromatics and chlorocarbons only with the 4 wt% SDS solution containing 0.3 grams of iso-butanol as a cosolvent. However, the resulting optimal salinity values were inconsistent with values expected from the literature and did not agree with the linear relationship established for the alkanes.
3. The surfactant solutions appear to be ill-suited for the aromatics and chlorocarbons used in this research for different reasons. It may be more difficult for the aromatics to exhibit classical phase behavior because of their stronger ring structure and multiple double bonds. For the chlorocarbons, it appears as though the more polar the compound, the more difficult it is for the compound to exhibit classical phase behavior.
4. A bilinear relationship was found to exist in which the partitioning coefficient of an alcohol tracer was related to the EACNs of both the contaminant and the alcohol. This relationship was consistent for hydrocarbons and chlorocarbons, as well as for linear and branched alcohol tracers. The resulting bilinear equation was applicable to neat compounds, binary mixtures, and complex mixtures.
5. When the logarithm of the partition coefficients were plotted versus the contaminant EACNs, the data points for dichlorobenzene and carbon tetrachloride were not consistent with the remainder of the data. This discrepancy did not exist when the partition coefficients were plotted versus the alcohol EACNs.

6. The regression equation greatly overestimated the partition coefficients when 4-methyl-3-heptanol and octanol were used with chlorocarbons.

7. Tailing and asymmetry of tracer breakthrough curves during column studies was attributed to either chemical or physical non-equilibrium transport. Physical non-equilibrium was assumed so that UTCHEM's capacitance model can be used.

8. After residual NAPL was established in the soil column, the dispersivity increased by about 11.5 percent. As tracer flow rates increased, a slight decreasing trend in dispersivity values was found. Excluding 2-methyl-2-hexanol, similar values were calculated for pore volume, residual saturation, and tracer retardation factors, respectively. This is an indication that these properties are independent of tracer flow rate.

9. Identifying preferential solubilization was difficult and often misleading because concentration histories do not adequately reflect the wide range in initial aqueous solubilities of respective components. The development of the Solubility Ratio Index (SRI) appeared to provide the best indicator of preferential solubility.

10. The lower the aqueous solubility of a component within a particular series (and the lower the EACN), the greater the increase in solubility due to the surfactant. There is a strong linear relationship between SRI values and aqueous solubility for hydrocarbon compounds.

11. Residual NAPL composition was relatively constant on a mole fraction basis throughout the surfactant flooding process during the column study. The impact on the NAPL EACN was minimal and the calculated partition coefficients were nearly constant.

12. Good agreement was obtained between the laboratory data and the simulation results using UTCHEM only if dead-end pore space and physical non-equilibrium conditions were assumed.

13. During tracer simulations, increasing flow rates caused (1) water flowing fraction values to decrease, (2) mass transfer coefficients to increase, and (3) retardation factors for hexanol and 2-methyl-2-hexanol to decrease. These observations can be attributed to the creation of preferential flow paths and reduced retention times at high flow rates.

14. Given the heterogeneous and anisotropic conditions of the laboratory surfactant flooding experiment and the homogeneous and isotropic assumptions used in the simulations, there was reasonably good agreement between the respective results. In the laboratory experiment, it is hypothesized that the surfactant solution would flow through the more permeable areas of the soil column first and solubilize residual areas from those areas relatively quickly. As less permeable areas are encountered, the solubilization process becomes increasingly less efficient. The one-dimensional nature of the simulations did not account for this variability.

15. A sensitivity analysis helped identify the parameters that appeared to be the most critical to the effective design of a tracer test (i.e., duration and respective tracer masses). The most influential factors are the water flowing fraction and mass transfer coefficients. Although changes in dispersivity and oil flowing fraction values had minor effects on breakthrough curves, there was virtually no effect on the tailing portion of the curves.

16. A similar sensitivity analysis can be performed to determine the required duration of any tracer test and the required mass of individual tracers such that tracer concentrations in the timeframe of interest are above the detection limit of the analytical equipment being used. The method of moments described in earlier chapters can also be used to further refine the tracer test design by helping ensure adequate separation of breakthrough curves and helping determine appropriate sampling times.

17. There was reasonably good agreement between field data and the results from simulated tracer tests. Excellent agreement is not realistic because of the homogeneous and isotropic conditions assumed for the simulations. Even when heterogeneity was introduced into the tracer simulations, only slight improvement was observed in the agreement between the field and simulated results.

18. The surfactant flooding simulations confirmed the expected behavior of NAPL contaminants during enhanced solubilization. However, the results did not agree well with the field data because not enough data was available concerning the heterogeneities of the test cell. Assuming the target analytes comprised the complete residual NAPL and using kriged values for gridblock contaminant concentrations also potentially contributed to the differences.

8.2 Recommendations

Based on the results of this research, the following recommendations are provided as potential areas for further research.

1. The surfactant solutions appear to be ill-suited for the aromatics and chlorocarbons used in this research for different reasons. It may be more difficult for the aromatics to exhibit classical phase behavior because of their stronger ring structure and multiple double bonds. For the chlorocarbons, it appears as though the more polar the compound, the more difficult it is for the compound to exhibit classical phase behavior. Regardless of the reason, these are two areas that deserve further research.

2. Demonstrate the use of the partition coefficient regression equation during the preliminary planning stages of a tracer test.

3. Verify the EACN values for DCB and CTET and investigate why the partition coefficients with these two compounds are inconsistent with the linear relationship established in this research.

4. More research is needed to determine why the partition coefficient for 4-methyl-3-heptanol and octanol, when used with chlorocarbons, are inconsistent with the linear relationship established in this research.

5. A wider range of flow rates should be investigated to verify that method of moment calculations for pore volume, residual saturation, and tracer retardation factors are independent of flow rate.

6. Inconsistencies involving 2-methyl-2-hexanol during the tracer column studies should be researched in more detail.

7. The SRI concept should be used on other hydrocarbon field sites to further validate its applicability. Research to determine if a similar linear relationship exists for chlorocarbons is also needed.

8. Further research may reveal that the adsorption process for some tracers can be described more accurately with a Freundlich or Langmuir model instead of the linear process used in UTCHEM. There may also be a hysteretic effect associated with the desorption of tracers from organic material in the soil.

9. The effect of dead-end pore space during tracer column studies requires investigation to ensure that laboratory results are being interpreted correctly.
10. Continued use of UTCHEM in follow-on experiments and field tests will provide corporate experience that will benefit research through improved planning efforts and a better understanding of subsurface phenomena in terms of site conceptualization.
11. Simulations of field efforts should incorporate more site characterization efforts, such as the generation of a stochastic permeability field.

REFERENCES

Abdul, Abdul S., Thomas L. Gibson, and Devi N. Rai, "Selection of Surfactants for the Removal of Petroleum Products from Shallow Sandy Aquifers," *Ground Water*, 28(6):920-926 (1990).

Abriola, L.M., and G.F. Pinder, "A Multiphase Approach to the Modeling of Porous Media Contamination by Organic Compounds: 1. Equation Development," *Water Resources Research*, 21(1 January):11-18 (1985a).

Abriola, L.M., and G.F. Pinder, "A Multiphase Approach to the Modeling of Porous Media Contamination by Organic Compounds: 2. Numerical Simulation," *Water Resources Research*, 21(1 January):19-26 (1985b).

Agca, C., G. A. Pope, and K. Sepehrnoori, "Modeling and Analysis of Tracer Flow in Oil Reservoirs," *Journal of Petroleum Science and Engineering*, 4:3-19 (1990).

Anderson, M. R., *The Dissolution and Transport of Dense Nonaqueous Phase Liquids in Saturated Porous Media*, Ph.D. Dissertation, Oregon Graduate Center, Beaverton, Oregon (1988).

Ang, C. C., and A. S. Abdul, "Aqueous Surfactant Flushing of Residual Oil Contamination from Sandy Soil," *Ground Water Monitoring Review*, 121-127 (1991).

Atwater, J. W., "A Case Study of a Chemical Spill: Polychlorinated Biphenyls Revisited," *Water Resources Research*, 20(2):317-319 (1984).

Aziz, K., and A. Settari, *Petroleum Reservoir Simulation*, Applied Science Publishers Ltd., London (1979).

Bai, M., Z. Shu, J. Cao, M. Zaman, and J.-C. Roegiers, "A Semi-Analytical Solution for a Two-Dimensional Capacitance Model in Solute Transport," *Journal of Petroleum Science and Engineering*, 22(4):275-295 (1999).

Baran, J.R., Jr., G.A. Pope, W.H. Wade, V. Weerasooriya, and A. Yapa, "Microemulsion Formation with Chlorinated Hydrocarbons of Differing Polarity," *Environmental Science and Technology*, 28(7):1361-1366 (1994).

Bear, J., *Dynamics of Fluids in Porous Media*, Elsevier, New York (1972).

Bedient, P. B., "NAPLs in the Subsurface - A Challenge for the 90s," *Research Journal of the Water Pollution Control Federation*, 63(3):195 (1991).

Borden, R. C., and C. M. Kao, "Evaluation of Groundwater Extraction fro Remediation of Petroleum Contaminated Aquifers," *Water Environmental Resources*, 64(1):28-36 (1992).

Bourrel, M., and R. S. Schecter, *Microemulsions and Related Systems*, Marcel Dekker, Inc. (1988).

Brown, C. L., "Simulation of Surfactant Enhanced Remediation of Aquifers Contaminated with Dense Nonaqueous Phase Liquids," MS Thesis, University of Texas at Austin (1993).

Brown, C. L., G. A. Pope, L. M. Abriola, and K. Sepehrnoori, "Simulation of Surfactant-Enhanced Aquifer Remediation," *Water Resources Research*, 30(11):2959-2977 (1994).

Brusseau, M. L., "Rate-Limited Mass Transfer and Transport of Organic Solutes in Porous Media That Contain Immobile Immiscible Organic Liquid," *Water Resources Research*, 28(1):33-45 (1992).

Camilleri, D., A. Fil, G. A. Pope, B. A. Rouse, and K. Sepehrnoori, "Description of an Improved Compositional Micellar/Polymer Simulator with Laboratory Core Floods," *SPE Reservoir Engineering* (1987a).

Camilleri, D., A. Fil, G. A. Pope, and K. Sepehrnoori, "Improvements in Physical-Property Models Used in Micellar/Polymer Flooding," *SPE Reservoir Engineering* (1987b).

Camilleri, D., E. Lin, T. Ohno, S. Engelsen, G. A. Pope, B. A. Rouse, and K. Sepehrnoori, "Description of an Improved Compositional Micellar/Polymer Simulator," *SPE Reservoir Engineering* (1987c).

Cash, L., J. L. Cayias, G. Fournier, D. Macallister, T. Schares, R. S. Schecter, and W. H. Wade, "The Application of Low Interfacial Tension Scaling Rules to Binary Hydrocarbon Mixtures," *Journal of Colloid and Interface Science*, 59(1):39-44 (1977).

Cayias, J. L., R. S. Schecter, and W. H. Wade, "Modeling Crude Oils for Low Interfacial Tension," *Society of Petroleum Engineers Journal*, 351-357 (1976).

Cayias, J. L., R. S. Schechter, and W. H. Wade, "The Utilization of Petroleum Sulfonates for Producing Low Interfacial Tensions Between Hydrocarbons and Water," *Journal of Colloid and Interface Science*, 59(1):31-38 (1977).

Chang, M., N. L. Maerefat, L. Tomutsa, and M. M. Honarpour, "Evaluation and Comparison of Residual Oil Saturation Determination Techniques," *SPE Formation Evaluation*, March:251-262 (1988).

Chatzis, I., N. R. Morrow, and H. T. Lim, "Magnitude and Detailed Structure of Residual Oil Saturation," *Society of Petroleum Engineering Journal*, April:311-326 (1983).

Cherry, J. A., S. Feenstra, B. H. Kueper, and D. W. McWhorter, "Status of In-Situ Technologies for Cleanup of Aquifers Contaminated by DNAPLs Below the Water Table," paper presented at the International Specialty Conference on *How Clean is Clean? Cleanup Criteria for Contaminated Soil and Groundwater*, Air and Waste Management Association, Washington, D. C., Nov. 6-9, 1990.

Cherry, J. A., S. Feenstra, and D. M. Mackay, "Developing Rational Goals for In Situ Remedial Technologies," in *Proceedings of the Third International Conference for Ground Water Quality Research* (1992).

Christian, S. D., class notes from CHEM 5673, Colloid and Surface Science, Fall Semester (1995).

Coats, K. H., and B. D. Smith, "Dead-End Pore Volume and Dispersion in Porous Media," *SPE Journal*, March:73-84 (1964).

Cohen, Y., and P. A. Ryan, "Multimedia Modeling of Environmental Transport: Trichloroethylene Test Case," *Environmental Science and Technology*, 19(3):33-58 (1985).

Cohen, R. M., R. R. Rasold, C. R. Faust, J. O. Rumbaugh III, and Y. R. Bridge, "Investigation and Hydraulic Containment of Chemical Migration: Four Landfills in Niagra Falls," *Civil Engineering Practice*, spring:33-58 (1987).

Conrad, S.H., J.L. Wilson, W.R. Mason, and W.J. Peplinski, "Visualization of Residual Organic Liquid Trapped in Aquifers," *Water Resources Research*, 28:467-478 (1992).

Cooke, C. E., Jr., "Method of Determining Fluid Saturations in Reservoirs," U. S. Patent No. 3590923 (1971).

Corey, A. T., *Mechanics of Immiscible Fluids in Porous Media*, Water Resources Publications, Littleton, Colorado (1986).

Crichlow, H. B., *Modern Reservoir Engineering - A Simulation Approach*, Prentice-Hall, Englewood Cliffs, New Jersey (1977).

Datta Gupta, A., G. A. Pope, K. Sepehrnoori, and R. L. Thrasher, "A Symmetric, Positive Definite Formulation of a Three-Dimensional Micellar/Polymer Simulator," *SPE Reservoir Engineering*, 1(6):622-632 (1986).

Dawson, H. E., and P. V. Roberts, "Influence of Viscous, Gravitational, and Capillary Forces on DNAPL Saturation," *Ground Water*, 35(2):261-269 (1997).

Delshad, M., "UTCHEM User's Guide and Technical Documentation (undated).

Delshad, M., G.A. Pope, and K. Sepehrnoori, "A Compositional Simulator for Modeling Surfactant Enhanced Aquifer Remediation," *Journal of Contaminant Hydrology*, in press (1996).

Dwarakanath, V., and G. A. Pope, "New Approach for Estimating Alcohol Partition Coefficients between Nonaqueous Phase Liquids and Water, *Environmental Science and Technology*, 32:1662-1666 (1998).

Faust, J. C., J. H. Guswa, and J. W. Mercer, "Simulation of Three-Dimensional Flow of Immiscible Fluids Within and Below the Saturated Zone," *Water Resources Research*, 25(12):2449 (1989).

Feenstra, S., "Evaluation of Multicomponent DNAPL Sources by Monitoring of Dissolved Phase Concentrations," paper presented at the *Conference on Subsurface Contamination by Immiscible Fluids*, International Association of Hydrologists, Calgary, Alberta, April 16-20, 1990.

Feenstra, S., and J.A. Cherry, "Subsurface Contamination by Dense Nonaqueous Phase Liquid (DNAPL) Chemicals," paper presented at International Groundwater Symposium, International Association of Hydrogeologists, Halifax, N. S., May 1-4, 1988.

Feenstra, S., and J. Coburn, "Subsurface Contamination from Spills of Denser Than Water Chlorinated Solvents;" California WPCA Bulletin, 23(4):26-34, 1986.

Foster W. R., "Low-Tension Waterflooding Process," *Journal of Petroleum Technology*, 205-210 (1973).

Fountain, J. C., "Field Tests of Surfactant Flooding," in *Transport and Remediation of Subsurface Contaminants*, ACS Symposium Series 491, edited by D. A. Sabatini and R. C. Knox (1992).

Fountain, J. C., C. Waddell-Sheets, A. Lagowski, C. Taylor, D. Frazier, and M. Byrne, "Enhanced Removal of Dense Nonaqueous Phase Liquids Using Surfactants," in *Surfactant-Enhanced Subsurface Remediation*, ACS Symposium Series 594, edited by D. A. Sabatini, R. C. Knox, and J. H. Harwell (1995).

Fusillo, T. V., J. J. Hochreiter, and D. G. Lord, "Distribution of Volatile Organic Compounds in a New Jersey Coastal Plain Aquifer System," *Ground Water*, 23(3):354-360 (1985).

Geller, J. T., and J. R. Hunt, "Mass Transfer from Nonaqueous Phase Organic Liquids in Water-Saturated Porous Media," *Water Resources Research*, 29(4):833-845 (1993).

Giavedoni, M. D., and J. A. Deiber, "A Model of Mass Transfer Through a Fluid-Fluid Interface," *Chemical Engineering Science*, 41(7):1921-1925 (1986).

Haley, J. L., B. Hanson, C. Enfield, J. Glass, *Ground Water Monitoring Review*, 12:119-124 (1991).

Hansch, C., and T. Fujita, *Classical and Three-Dimensional QSAR in Agrochemistry*, editors, ACS Symposium Series 606, American Chemical Society, Washington, D. C. (1995).

Harten, A., "High Resolution Schemes for Hyperbolic Conservation Laws," *SIAM Review*, 25(1):35-67 (1983).

Harwell, J. H., "Factors Affecting Surfactant Performance in Groundwater Remediation Applications," in *Transport and Remediation of Subsurface Contaminants*, ACS Symposium Series 491, edited by D. A. Sabatini and R. C. Knox (1992).

Healy, R. N., and R. L. Reed, "Physicochemical Aspects of Microemulsion Flooding," *Society of Petroleum Engineers Journal*, 257:491-501 (1974).

Healy, R. N., R. L. Reed, and C. W. Carpenter, Jr., "A Laboratory Study of Microemulsion Flooding," *Society of Petroleum Engineers Journal*, 259:87-100 (1975).

Hinchee, R. E., and J. H. Reisinger, "A Practical Application of Multiphase Transport Theory to Groundwater Contamination Problems," *Ground Water Monitoring Review*, Winter:84-92 (1987).

Hirasaki, G. J., "Application of the Theory of Multicomponent, Multiphase Displacement to Three-Component, Two-Phase Surfactant Flooding," *Society of Petroleum Engineers Journal*, 191-204 (1981).

Huh, C., "Interfacial Tensions and Solubilizing Ability of a Microemulsion Phase that Coexists with Oil and Brine," *Journal of Colloid Interface Science*, 71:408-426 (1979).

Hunt, J. R., N. Sita, and K. S. Udell, "Nonaqueous Phase Liquid Transport and Cleanup, 1, Analysis of Mechanisms," *Water Resources Research*, 24(8):1247-1258 (1988).

James, "Optimal Estimation of Residual Nonaqueous Phase Liquid Saturation Using Partitioning Tracer Concentration Data," *Water Resources Research*, 33(12):2621-2636 (1997).

Jin, M., M. Delshad, V. Dwarakanath, D. C. McKinney, G. A. Pope, K. Sepehrnoori, and C. E. Tilburg, "Partitioning Tracer Test for Detection, Estimation, and Remediation Performance Assessment of Subsurface Nonaqueous Phase Liquids," *Water Resources Research*, 31(5):1201-1211 (1995).

Jin, M., "A Study of Nonaqueous Phase Liquid Characterization and Surfactant Remediation," PhD Dissertation, University of Texas at Austin (1995).

Jin, M., G. W. Butler, R. E. Jackson, P. E. Mariner, J. F. Pickens, G. A. Pope, C. L. Brown, and D. C. McKinney, "Sensitivity Models and Design Protocol for Partitioning Tracer Tests in Alluvial Aquifers," *Ground Water*, 35:964-972 (1997).

Kaluarachchi, J. J., and J. C. Parker, "Modeling Multicomponent Organic Chemical Transport in Three-Fluid Phase Porous Media," *Journal of Contaminant Hydrology*, 5:349-374 (1990).

Kamlet, M. J., R. M. Doherty, M. H. Abraham, Y. Marcus, and R. W. Taft, "Linear Solvation Energy Relationships: 46. An Improved Equation for Correlation and Prediction of Octanol/Water Partition Coefficients of Organic Nonelectrolytes (Including Strong Hydrogen Bond Donor Solutes," *Journal of Physical Chemistry*, 92:5244-5255 (1988).

Kan, A. T., and M. B. Tomson, "UNIFAC Prediction of Aqueous and Nonaqueous Solubilities of Chemicals with Environmental Interest," *Environmental Science and Technology*, 30(4):1369-1376 (1996).

Keely, J. F., *Performance Evaluations of Pump-and-Treat Remediations*, EPA/540/4-89/005, Office of Research and Development, U. S. Environmental Protection Agency, Washington, D. C. (1989).

Knaeppen, W. A., R. Tijssen, and E. A. van den Bergen, "Experimental Aspects of Partitioning Tracer Tests for Residual Oil Saturation Determination with FIA-Based Laboratory Equipment, " *SPE Reservoir Engineering*, May:239-244 (1990).

Knox, R. C., L. W. Canter, D. F. Kincannon, E. L. Stover, and C. H. Ward, "State-of-the-Art of Aquifer Restoration," EPA/600/S2-84/182, U. S. Environmental Protection Agency, Ada, Oklahoma (1986).

Knox, R. C., and D. A. Sabatini, "Introduction," in *Transport and Remediation of Subsurface Contaminants*, ACS Symposium Series 491, edited by D. A. Sabatini and R. C. Knox (1992).

Knox, R. C., D. A. Sabatini, and L. W. Canter, *Subsurface Transport and Fate Processes*, Lewis Publishers, Boca Raton, FL (1993).

Knox, R. C., D. A. Sabatini, and C. Griffin, "Surfactant Remediation Field Demonstration Using a Vertical Circulation Well," *Ground Water*, 35(6):948-953 (1997).

Korfiatis, G. P., and A. Makarigakis, "In Situ Plume Interception and Treatment Technologies: An Overview," in *Nonaqueous Phase Liquids (NAPLs) in Subsurface Environment: Assessment and Remediation*, edited by L. N. Reddi,1996.

Krebs-Yuill, B., J. H. Harwell, D. A. Sabatini, and R. C. Knox, "Economic Considerations in Surfactant-Enhanced Pump-and-Treat Remediation," *Surfactant-Enhanced Subsurface Remediation*, ACS Symposium Series 594, American Chemical Society, Washington, D. C. (1995).

Kueper, B. H., and E. O. Frind, "An Overview of Immiscible Fingering in Porous Media," *Journal of Contaminant Hydrology*, 2(2):95-110 (1988).

Kueper, B. H., W. Abbott, and G. Farquhar, "Experimental Observations of Multiphase Flow in Heterogeneous Porous Media," *Journal of Contaminant Hydrology*, 5(1):83-95 (1989).

Kueper, B. H., and E. O. Frind, "Two-Phase Flow in Heterogeneous Porous Media: 1. Model Development," *Water Resources Research*, 27(6):1049-1057 (1991).

Kueper, B. H., D. Redman, R. C. Starr, S. Reitsma, and M. Mah, "A Field Experiment to Study the Behavior of Tetrachloroethylene Below the Water Table: Spatial Distribution of Residual and Pooled DNAPL," *Ground Water*, 31(5):756-766 (1993).

Kuppusamy, T., J. Sheng, J. C. Parker, and R. J. Lenhard, "Finite Element Analysis of Multiphase Immiscible Flow Through Soils," *Water Resources Research*, 23(4):625-631 (1987).

Lake, L. W., *Enhanced Oil Recovery*, Prentice Hall, Englewood Cliffs, New Jersey (1989).

Lamarche, P., "Dissolution of Immiscible Organics in Porous Media," Ph.D. Dissertation, University of Waterloo, Waterloo, Ontario (1991)

Lesage, S., and S. Brown, "Observation of the Dissolution of NAPL Mixtures," *Journal of Contaminant Hydrology*, 15:57-71 (1994).

Li, L., D. A. Barry, P. J. Culligan-Hensley, and K. Bajracharya, "Mass Transfer in Soils with Local Stratification of Hydraulic Conductivity," *Water Resources Research*, 30(11):2891-2900 (1994).

Lichtenberger, G. J., "Field Applications of Interwell Tracers for Reservoir Characterization of Enhanced Oil Recovery Pilot Areas," SPE 21652, Oklahoma City, Oklahoma, April 7-9 (1991).

Lipe, K. M., D. A. Sabatini, M. A. Hasegawa, and J. H. Harwell, "Micellar-Enhanced Ultrafiltration and Air Stripping for Surfactant-Contaminant Separation and Surfactant Reuse," *Ground Water Monitoring Review*, Winter:85-02 (1996).

Liu, J., "High-Resolution Methods for Enhanced Oil Recovery Simulation," PhD Dissertation, The University of Texas at Austin (1993).

MacDonald, J. A., and M. C. Kavanaugh, *Environmental Science and Technology*, 28:362A-368A (1994).

Mace, R. E., and J. L. Wilson, "Clay and Immiscible Organic Liquids: Greater Capillary Trapping of the Organic Phase," in *Transport and Remediation of Subsurface Contaminants*, ACS Symposium Series 491, edited by D. A. Sabatini and R. C. Knox (1992).

Mackay, D.M., and J.A. Cherry, "Groundwater Contamination: Pump-and-Treat Remediation," *Environmental Science and Technology*, 23(6):630-636 (1989).

Mackay, D.M., P.V. Roberts, and J.A. Cherry, "Transport of Organic Contaminants in Groundwater," *Environmental Science and Technology*, 19(5):384-392 (1985).

Marcus, Y., "Linear Solvation Energy Relationships: Correlation and Prediction of the Distribution of Organic Solutes Between Water and Immiscible Organic Solvents," *Journal of Physical Chemistry*, 95:8886-8891 (1991).

Mayer, A. S. and C. T. Miller, "The Influence of Porous Medium Characteristics and Measurement Scale on Pore-Scale Distributions of Residual Nonaqueous Phase Liquids," *Journal of Contaminant Hydrology*, 11:189-213 (1992).

McKee, J. E., F. B. Laverty, and R. M. Hertel, "Gasoline in Groundwater," *Journal of the Water Pollution Control Federation*, 44(2):292-302 (1972).

Mercer, J.W., and R.M. Cohen, "A Review of Immiscible Fluids in the Subsurface: Properties, Models, Characterization, and Remediation," *Journal of Contaminant Hydrology*, 6:107-163 (1990).

Miller, C. T., M. M. Poirier-McNeill, and A. S. Mayer, "Dissolution of Trapped Nonaqueous Phase Liquids: Mass Transfer Characteristics," *Water Resources Research*, 26(11):2783-2796 (1990).

Mohanty, K. K., H. T. Davis, and L. Scriven, "Physics of Oil Entrapment in Water-Wet Rock," *SPE Reservoir Engineering*, 2:113-128 (1987).

Montgomery Watson, "Draft Phase I Work Plan for Eight Treatability Studies at Operable Unit 1," Project No. 2208.1211, report submitted to Hill Air Force Base, Utah (1995).

Morrow, N. R., and B. Songkran, "Effect of Viscous and Buoyancy Forces on Nonwetting Phase Trapping in Porous Media," in *Surface Phenomena in Enhanced Oil Recovery*, edited by D. O. Shah, Plenum Press, New York (1981).

Morrow, N. R., I. Chatzis, and J. J. Taber, "Entrapment and Mobilization of Residual Oil in Bead Packs," *SPE Reservoir Engineering*, 3(3):927-934 (1988).

Nash, J. H., "Field Studies of In-Situ Washing," U. S. Environmental Protection Agency, EPA/600/2-87/110, Cincinnati, Ohio (1987).

National Resource Council (NCR), *Alternatives for Ground Water Cleanup*, Committee on Ground Water Cleanup Alternatives, Commission on Geosciences, Environment and Resources, National Academy Press, Washington, D. C. (1994).

Nelson, N. T., and M. L. Brusseau, "Field Study of the Partitioning Tracer Method for Detection of Dense Nonaqueous Phase Liquid in a Trichloroethene-Contaminated Aquifer, *Environmental Science and Technology*, 30(9):2859-2863 (1996).

Ng, K. M., H. T. Davis, and L. E. Scriven, "Visualization of Blob Mechanics in Flow Through Porous Media," *Chemical Engineering Science*, 33:1009-1017 (1978).

Nirmalakhandan, N. N., and R. E. Speece, "Prediction of Aqueous Solubility of Organic Chemicals Based on Molecular Structure: 2. Application to PNAs, PCBs, PCDDs, etc," *Environmental Science and Technology*, 23(6):708-713 (1989).

Oolman, T., S. T. Godard, G. A. Pope, M. Jin, and K. Kirchner, "DNAPL Flow Behavior in a Contaminated Aquifer: Evaluation of Field Data," *Ground Water Monitoring Review*, 25-137 (1995).

Osborne, M., and J. Sykes, "Numerical Modeling of Immiscible Organic Transport at the Hyde Park Landfill," *Water Resources Research*, 22(1):25-33 (1986).

Pennell, K. D., G. A. Pope, and L. M. Abriola, "Influence of Viscous and Buoyancy Forces on the Mobilization of Residual Tetrachloroethylene during Surfactant Flushing," *Environmental Science and Technology*, 30(4):1328-1335 (1996).

Pennell, K.D., M. Jin, L.M. Abriola, and G.A. Pope, "Surfactant Enhanced Remediation of Soil Columns Contaminated by Residual Tetrachloroethylene," *Journal of Contaminant Hydrology*, 16:35-53 (1994).

Pennel, K. D., L. M. Abriola, and W. J. Weber, Jr., "Surfactant-Enhanced Solubilization of Residual Dodecane in Soil Columns: 1. Experimental Investigation," *Environmental Science and Technology*, 27(12):2332-2340 (1993).

Perry, P. H., and C. H. Chilton, *Chemical Engineer's Handbook*, McGraw-Hill (1973).

Pfannkuch, H. O., "Determination of the Contaminant Source Strength from Mass Exchange Processes at the Petroleum-Groundwater Interface in Shallow Aquifer Systems," in *Petroleum Hydrocarbons and Organic Chemicals in Ground Water*, National Water Well Association, Dublin, Ohio (1984).

Phillips, G. W., "Underground Tank Technology Update," University of Wisconsin-Madison, 9(6):2 (1995).

Pope, G. A., and R. C. Nelson, "A Chemical Flooding Compositional Simulator," *Society of Petroleum Engineers Journal*, 18(5):339 (1978).

Pope, G. A., and W. H. Wade, "Lessons from Enhanced Oil Recovery Research for Surfactant-Enhanced Aquifer Remediation," in *Surfactant-Enhanced Subsurface Remediation*, ACS Symposium Series 594, edited by D. A. Sabatini, R. C. Knox, and J. H. Harwell (1995).

Poulsen, M. M., and B. H. Kueper, "A Field Experiment to Study the Behavior of Tetrachloroethylene in Unsaturated Porous Media," *Environmental Science and Technology*, 26(5):889-895 (1992).

Powers, S. E., C. O. Loureiro, L. M. Abriola, and W. J. Weber, Jr., "Theoretical Study of the Significance of Nonequilibrium Dissolution of Nonaqueous Phase Liquids in Subsurface Systems," *Water Resources Research*, 27(4):463-477 (1991).

Powers, S. E., L. M. Abriola, and W. J. Weber, Jr., "An Experimental Investigation of Nonaqueous Phase Liquid Dissolution in Saturated Subsurface Systems: Steady State Mass Transfer Rates," *Water Resources Research*, 28(10):2691-2705 (1992).

Powers, S. E., L. M. Abriola, and W. J. Weber, Jr., "An Experimental Investigation of Nonaqueous Phase Liquid Dissolution in Saturated Subsurface Systems: Transient Mass Transfer Rates," *Water Resources Research*, 30(2):321-332 (1994).

Ratnam, S., P. J. Culligan-Hensley, and J. T. Germaine, "Modeling the Behavior of LNAPLs Under Hydraulic Flushing," in *Nonaqueous Phase Liquids (NAPLs) in Subsurface Environment: Assessment and Remediation*, edited by L. N. Reddi,1996.

Razakarisoa, O., J. D. Rasolofoniaina, P. Muntzer, and L. Zillox, "Selective Dissolution and Transport of Hydrocarbons in an Alluvial Aquifer - Role and Impact of Residual Air on Ground Water Contamination, in *Contaminant Transport in Groundwater*, edited by H. E. Kobus and W. Kinzelbach, Balkema, Rotterdam (1989).

Reynolds, D. A., "Three-Dimensional NAPL Dissolution Modeling Using One-Dimensional Dissolution Coefficients," M.S. Thesis, Queen's University, Kingston, Ontario (1995).

Reynolds, D. A., P. Lamarche, and M. Tetreault, "Dissolution of Toluene Residuals: 3-D Laboratory Experiments," in *Nonaqueous Phase Liquids (NAPLs) in Subsurface Environment: Assessment and Remediation*, edited by L. N. Reddi,1996.

Rose, W., and W. A. Bruce, "Evaluation of Capillary Character in Petroleum Reservoir Rock," *Trans. Am. Inst, Min. Metall. Pet. Eng.*, 186:127-142 (1949).

Rosen, M. J., *Surfactants and Interfacial Phenomena*, Wiley, New York (1989).

Rouse, J. D., D. A. Sabatini, and J. H. Harwell, "Minimizing Surfactant Losses Using Twin-Head Anionic Surfactants in Subsurface Remediation," *Environmental Science and Technology*, 27(10):2072-2078 (1993).

Rutan, S. C., P. W. Carr, and R. W. Taft, "Solvatochromic Linear Solvation Energy Relationships for GAS-Liquid Partition Coefficient," *Journal of Physical Chemistry*, 93:4292-4297 (1989).

Sabatini, D. A., R. C. Knox, and J. H. Harwell, "Emerging Technologies in Surfactant-Enhanced Subsurface Remediation," in *Surfactant-Enhanced Subsurface Remediation*, ACS Symposium Series 594, edited by D. A. Sabatini, R. C. Knox, and J. H. Harwell (1995).

Sabatini, D. A., R. C. Knox, and C. C. West, "Design of a Surfactant Remediation Field Demonstration Based on Laboratory and Modeling Studies," *Environmental Science and Technology*, 35(6):954-963 (1997).

Salager, J. L., M. Bourrel, R. S. Schecter, and W. H. Wade, "Mixing Rules for Optimum Phase-Behavior Formulations of Surfactant/Oil/Water Systems," *Society of Petroleum Engineers Journal*, 271-278 (1979).

Schwille, F., "Groundwater Pollution by Mineral Oil Products," in *Proceedings of the Moscow Groundwater Pollution Symposium*, IAHS-AISH, Publication No. 103 (1975).

Schwille, F., *Dense Chlorinated Solvents in Porous and Fractured Media*, translated from German and edited by J. F. Pankow, Lewis Publishers, Chelsea, Michigan (1988).

Schwille, F., "Petroleum Contamination of the Subsoil - A Hydrological Problem," in *The Joint Problems of the Oil and Water Industries, Proceedings of a Symposium*, edited by P. Hepple, Institute of Petroleum, London (1967).

Schwille, F., "Groundwater Pollution in Porous Media by Fluids Immiscible with Water," *Science Total Environment*, 21:173-185 (1981).

Sheely, C. Q., Jr., and D. E. Baldwin, Jr., "Single-Well Tracer Tests for Evaluating Chemical Enhanced Oil Recovery Processes," *Journal of Petroleum Technology*, 1887-1896 (1982).

Shiau, B. J., "Subsurface Remediation of Chlorinated Solvents Using Direct Food Additive Surfactants," PhD Dissertation, University of Oklahoma (1995).

Shiau, B. J., J. D. Rouse, D.A. Sabatini, and J.H. Harwell, "Surfactant Selection for Optimizing Surfactant-Enhanced Subsurface Remediation," in *Surfactant-Enhanced Subsurface Remediation*, ACS Symposium Series 594, edited by D. A. Sabatini, R. C. Knox, and J. H. Harwell (1995).

Sleep, B. E., and J. F. Sykes, "Compositional Simulation of Groundwater Contamination by Organic Compounds: 1. Model Development and Verification," *Water Resources Research*, 29(6):1697-1708 (1993).

Stegemeier, G.L., "Mechanisms of Entrapment and Mobilization of Oil in Porous Media," in *Improved Oil Recovery by Surfactant and Polymer Flooding*, D.O. Shah and R.S. Schechter (eds.), Academic Press, New York, 205-274 (1976).

Tang, J. S., "Interwell Tracer Tests to Determine Residual Oil Saturation to Waterflood at Judy Creek BHL "A" Pool," *Journal of Canadian Petroleum Technology*, 31(8):61-71 (1992).

Tang, J. S., "Partitioning Tracers and In-Situ Fluid-Saturation Measurements," *SPE Formation Evaluation*, March:33-39 (1995).

Tang, J. S., and B. Harker, "Interwell Tracer Test to Determine Residual Oil Saturation in a Gas-Saturated Reservoir. Part II: Field Applications," *Journal of Canadian Petroleum Technology*, 30(4):34-42 (1991).

Texas Research Institute (TRI), Inc., "Test Results of Surfactant Enhanced Gasoline Recovery in a Large Scale Model Aquifer," American Petroleum Institute, Washington, D. C., Publication No. 4390 (1985).

U. S. Environmental Protection Agency, "Santa Clara Valley: Integrated Environmental Management Project (Draft Stage 1 Report)," U. S. Environmental Protection Agency, Region IX, San Francisco, California (1985).

Verschueren, K., *Handbook of Environmental Data on Organic Chemicals*, van Nostrand Reinhold, New York (1983).

Wang, Peng, V. Dwarakanath, B. A. Rouse, G. A. Pope, and K. Sepehrnoori, "Partition Coefficients for Alcohol Tracers Between Nonaqueous-Phase Liquids and Water from UNIFAC-Solubility Method," *Advances in Water Resources*, 21(2):171-181 (1998).

West, C. W., "Surfactant-Enhanced Solubilization of Tetrachloroethylene and Degradation Products in Pump and Treat Remediation," in *Transport and Remediation of Subsurface Contaminants*, ACS Symposium Series 491, edited by D. A. Sabatini and R. C. Knox (1992).

West, C. C., and J. H. Harwell, "Surfactants and Subsurface Remediation," *Environmental Science and Technology*, 26(12):2324-2330 (1992).

Wilson, J. L., and S. H. Conrad, "Is Physical Displacement of Residual Hydrocarbons a Realistic Possibility in Aquifer Restoration?" in *Proceedings of the NWWA Conference on Petroleum Hydrocarbons and Organic Chemicals in Ground Water*, National Water Well Association, Dublin, Ohio (1984).

Wilson, J. L., S. H. Conrad, W. R. Mason, W, Peplinski, and E. Hagan, *Laboratory Investigation of Residual Liquid Organics from Spills, Leaks, and Disposal of Hazardous Wastes in Groundwater*, Final Report, EPA/600/6/90/004, Environmental Protection Agency, Washington, D. C. (1990).

Wilson, R. D., and D. M. Mackay, "Direct Detection of Residual Nonaqueous Phase Liquid in the Saturated Zone Using SF_6 as a Partition Tracer," *Environmental Science and Technology*, 29(5):1255-1258 (1995).

Ziegenfuss, P. S., "The Potential Use of Surfactant and Cosolvent Soil Washing as Adjuvant for In-Situ Aquifer Restoration," M.S. Thesis, Rice University, Houston, Texas (1987).

APPENDIX A

EXAMPLE PITT CALCULATIONS

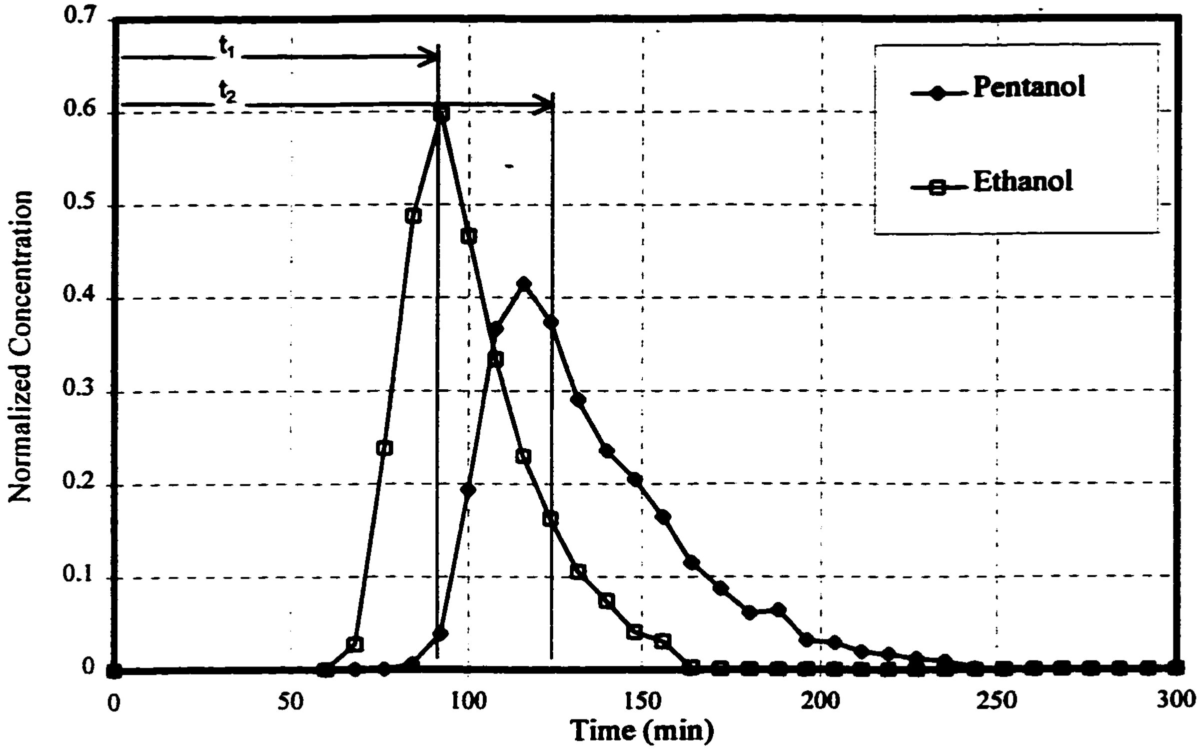

Tracer Breakthrough Curves

t_1 and t_2 are obtained by taking the ratio of the sums of the first and zero moments as shown in the following equation,

$$t = \frac{\int_0^{t_f} tC(t)dt}{\int_0^{t_f} C(t)dt} - \frac{t_s}{2}$$

where t_f is the total duration of the tracer test and t_s is the duration of the tracer slug. For this example, t_1 and t_2 equals 90 and 124 minutes, respectively. With these values and the partitioning coefficients of the tracers, the PITT calculations can be easily accomplished.

APPENDIX B

CALIBRATION-DATA AND CURVES

Table B.1: Calibration Results for Alcohol Tracers

Alcohol	Linear Equation	R^2
1-propanol	$y = 3245.5x$	0.9962
1-pentanol	$y = 3020.1x$	0.9990
1-hexanol	$y = 3900.4x$	0.9939
1-heptanol	$y = 3918.2x$	0.9977
2-octanol	$y = 4243.7x$	0.9979
4-Methyl-3-Heptanol	$y = 3943.8x$	0.9987
6-Methyl-2-Heptanol	$y = 4125.3x$	0.9985
2-Methyl-2-Hexanol	$y = 4014.7x$	0.9990
2-Methyl-3-Hexanol	$y = 4092.9x$	0.9996
2,2-Dimethyl-3-Pentanol	$y = 3765.7x$	0.9961
2,4-Dimethyl-3-Pentanol	$y = 3029.7x$	0.9938
3,3-Dimethyl-1-Butanol	$y = 1119.3x$	0.9993
3,3-Dimethyl-2-Butanol	$y = 3803.2x$	0.9996

Table B.2: Calibration Results for Contaminants

Contaminant	Linear Equation	R^2
Toluene	$y = 212{,}370x$	0.9943
o-Xylene	$y = 196{,}150x$	0.9939
Hexane	$y = 298{,}660x$	0.9957
Heptane/TCE	$y = 75{,}771x$	0.9967
Decane	$y = 219{,}800x$	0.9994
PCE	$y = 197{,}890x$	0.9995

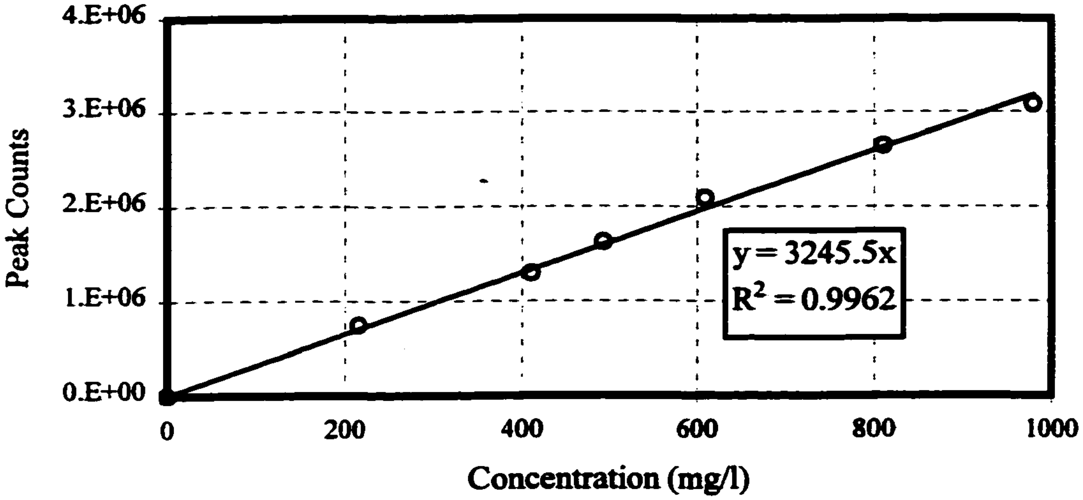

Figure B.1 Calibration Curve for Propanol

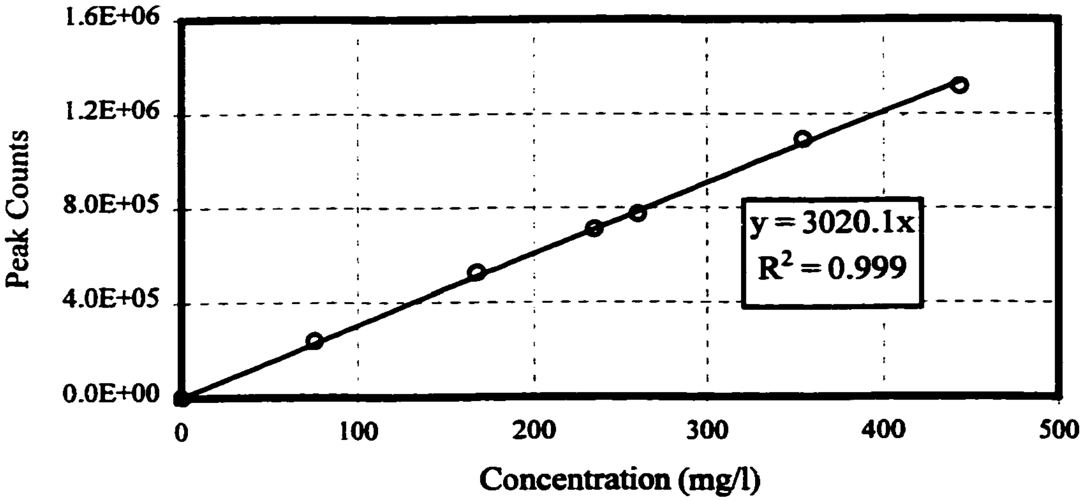

Figure B.2 Calibration Curve for Pentanol

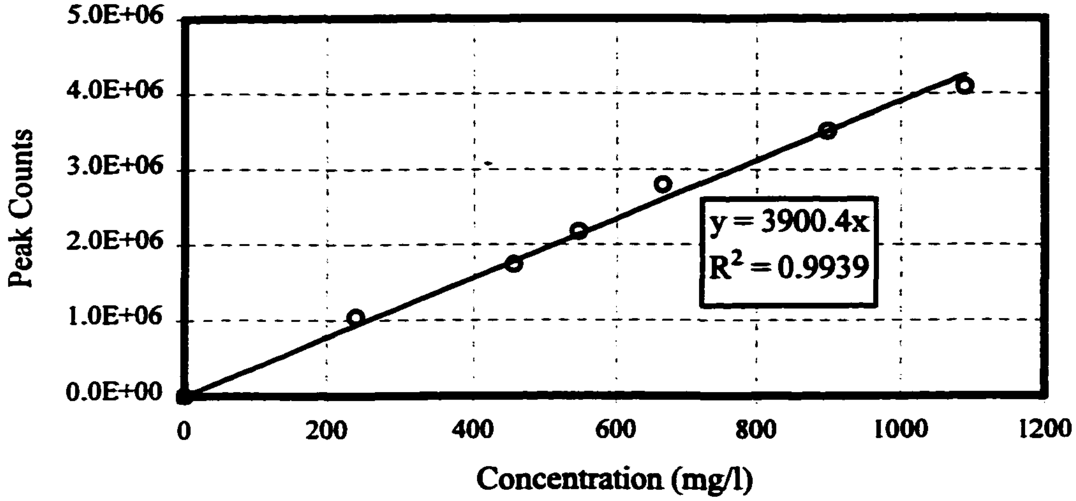

Figure B.3 Calibration Curve for Hexanol

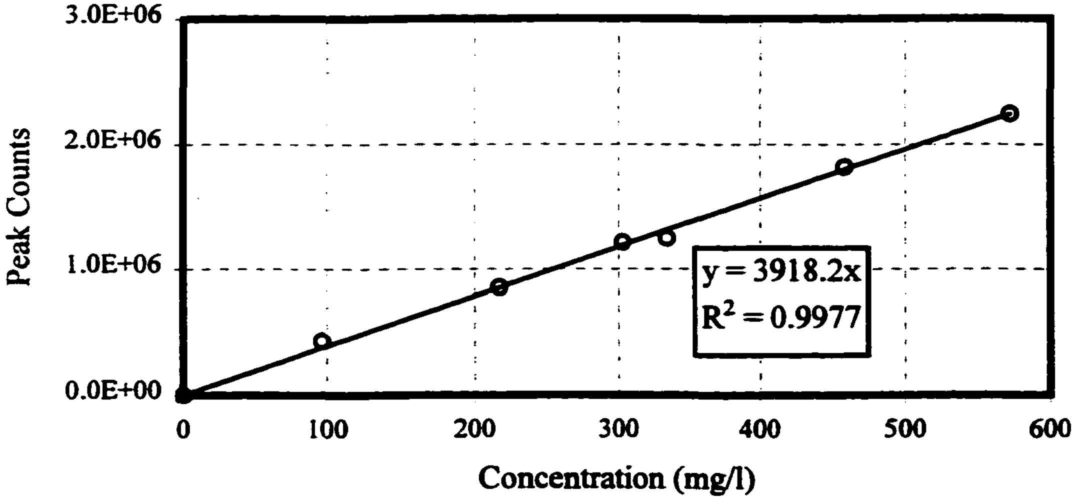

Figure B.4 Calibration Curve for Heptanol

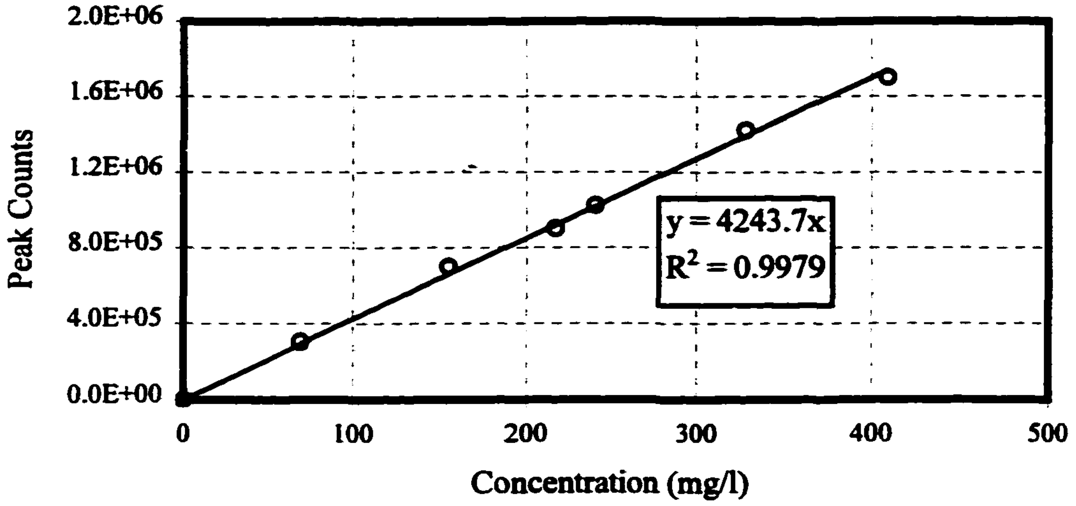

Figure B.5 Calibration Curve for Octanol

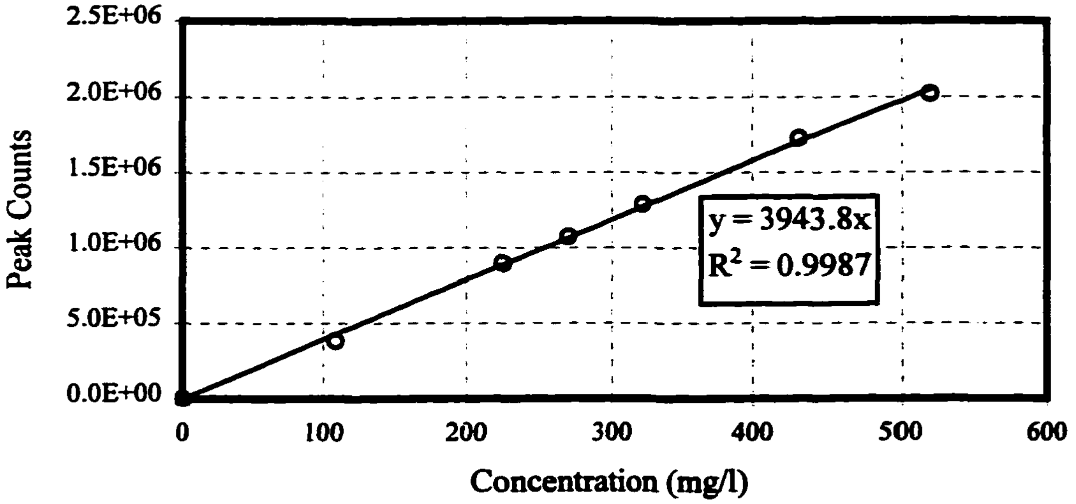

Figure B.6 Calibration Curve for 4-Methyl-3-Heptanol

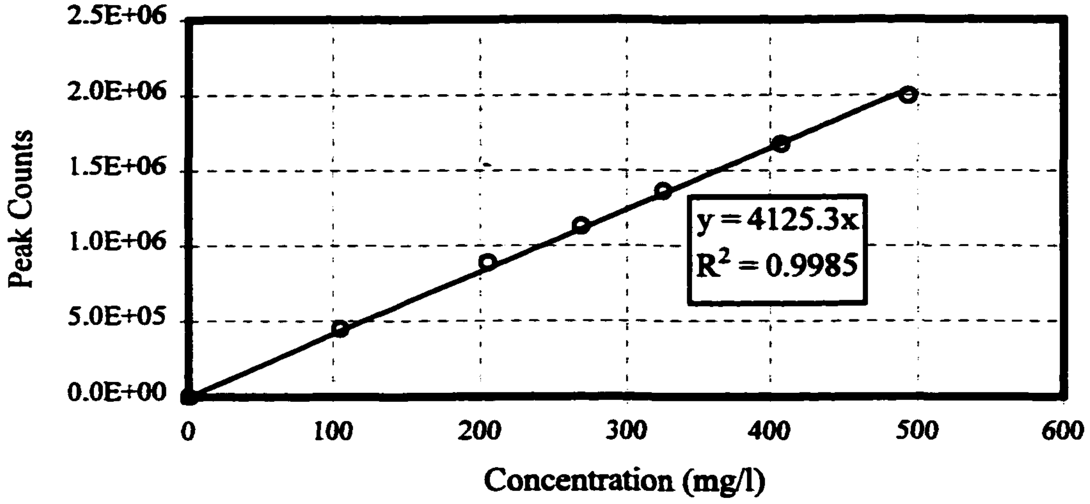

Figure B.7 Calibration Curve for 6-Methyl-2-Heptanol

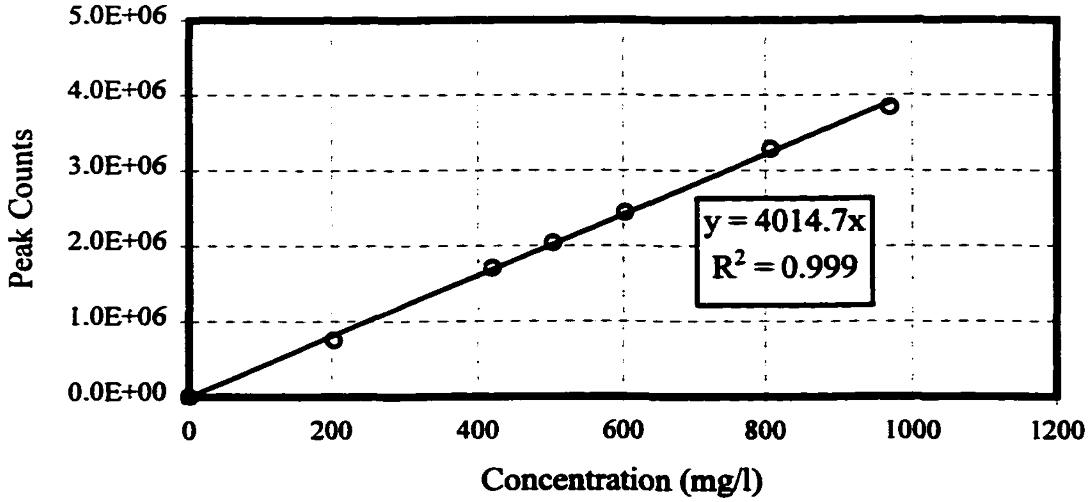

Figure B.8 Calibration Curve for 2-Methyl-2-Hexanol

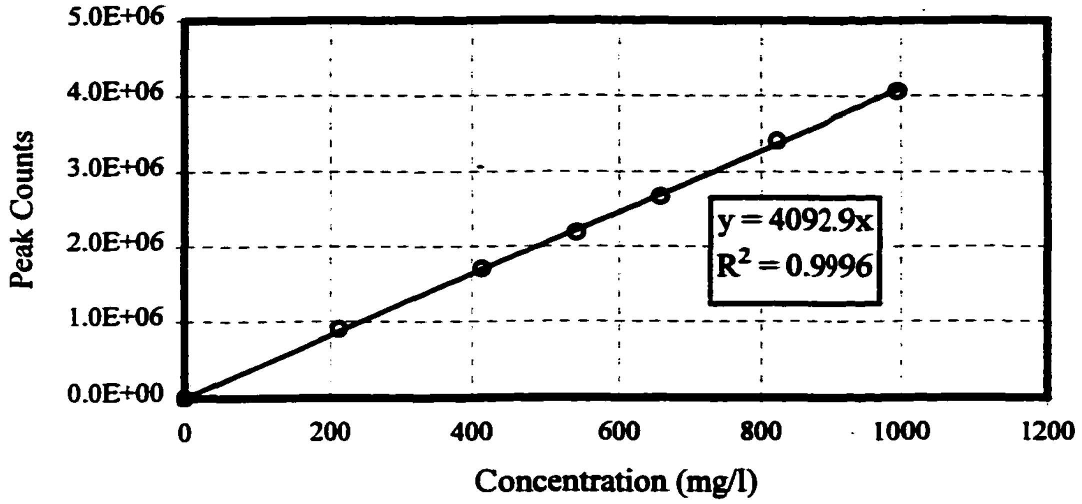

Figure B.9 Calibration Curve for 2-Methyl-3-Hexanol

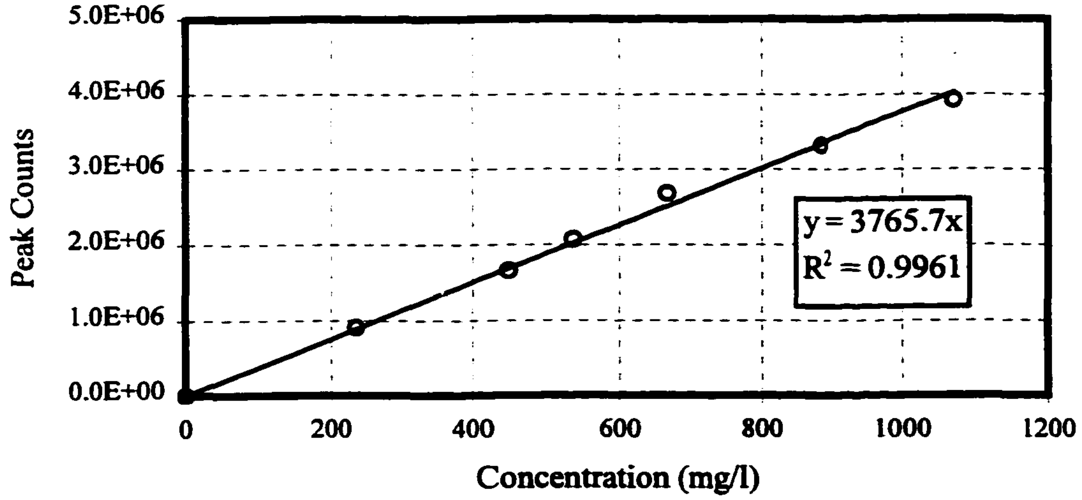

Figure B.10 Calibration Curve for 2,2-Dimethyl-3-Pentanol

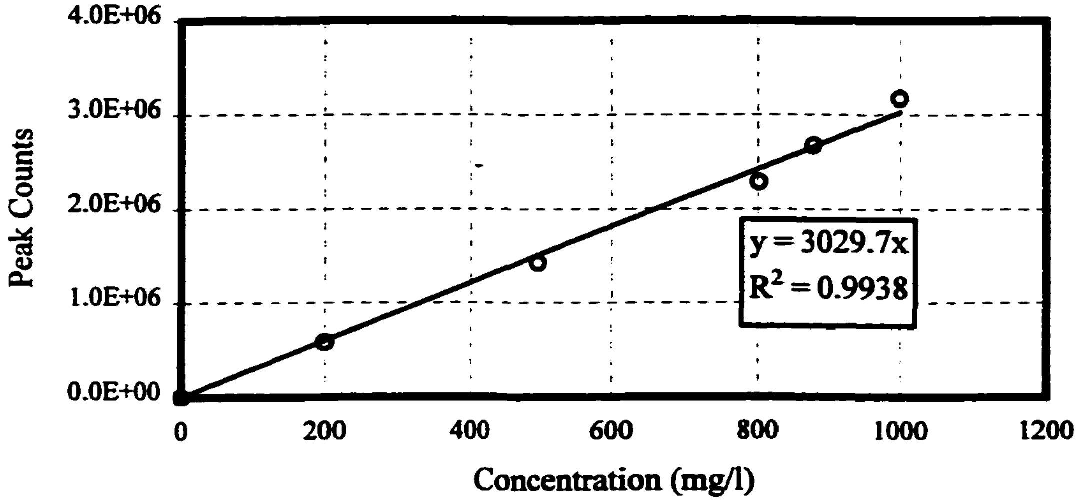

Figure B.11 Calibration Curve for 2,4-Dimethyl-3-Pentanol

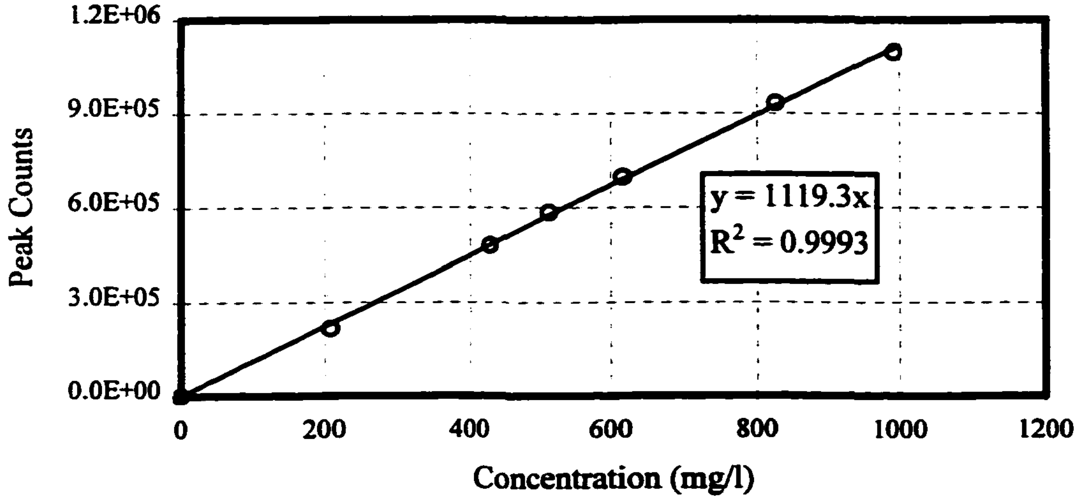

Figure B.12 Calibration Curve for 3,3-Dimethyl-1-Butanol

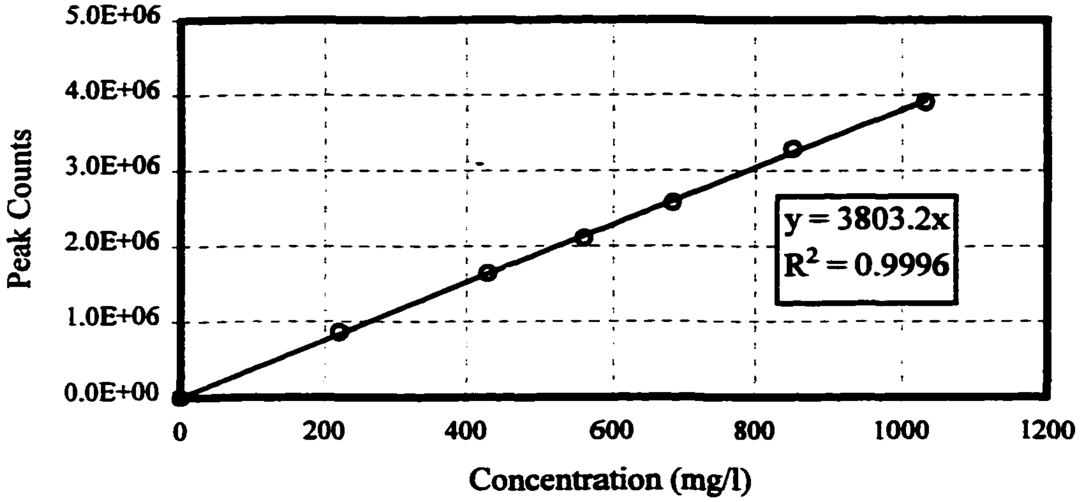

Figure B.13 Calibration Curve for 3,3-Dimethyl-2-Butanol

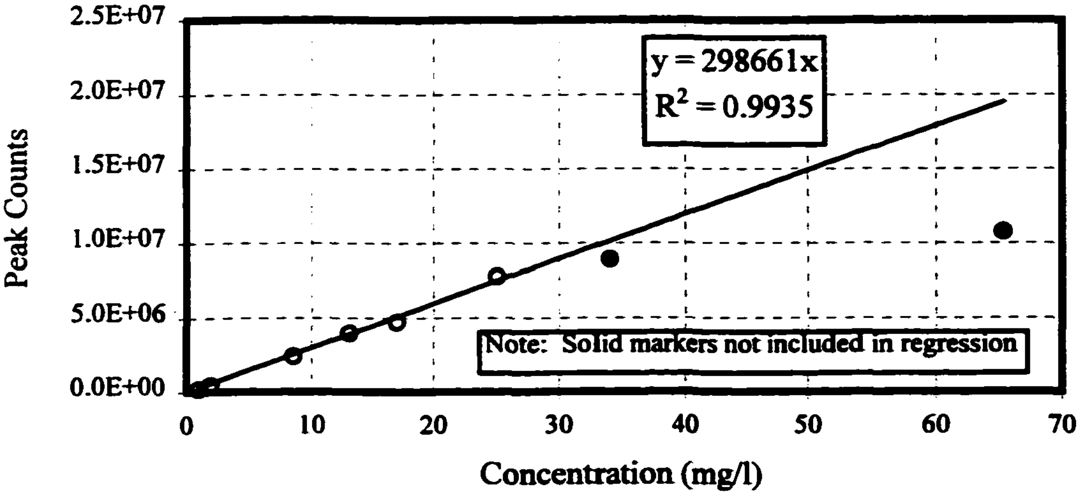

Figure B.14 Calibration Curve for Toluene

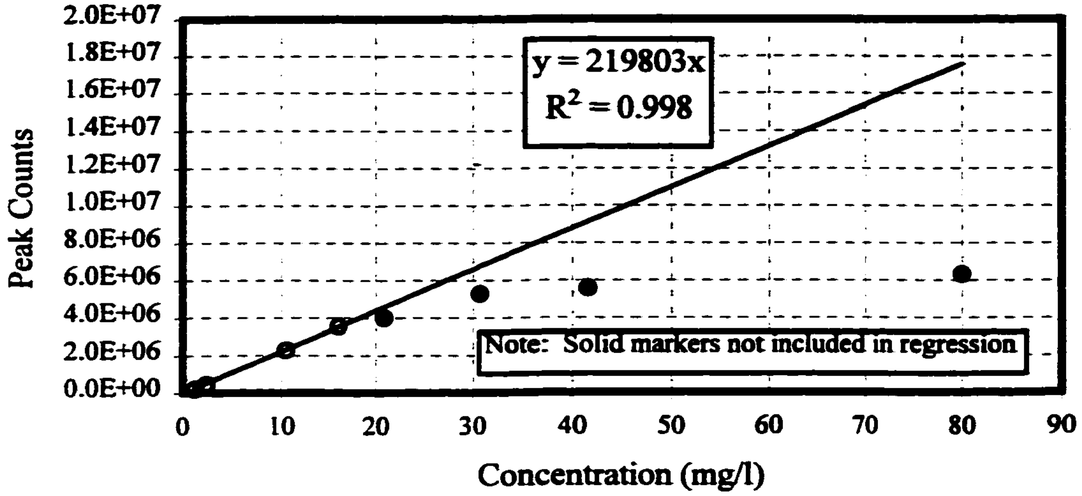

Figure B.15 Calibration Curve for *o* -Xylene

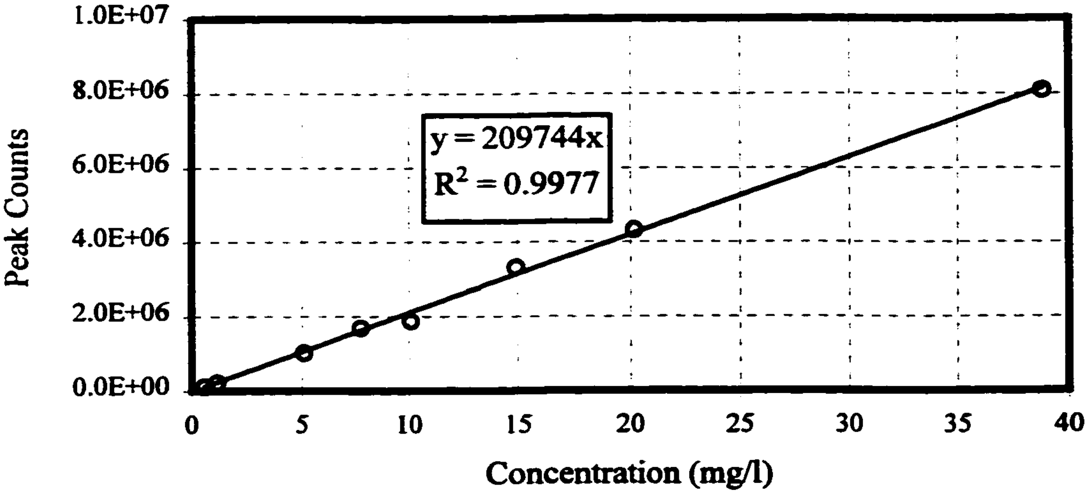

Figure B.16 Calibration Curve for Hexane

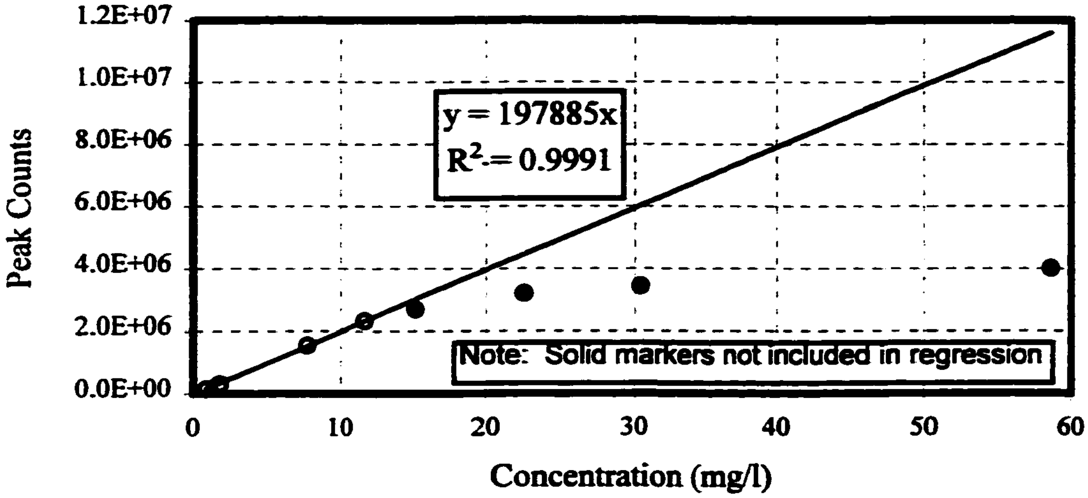

Figure B.17 Calibration Curve for Decane

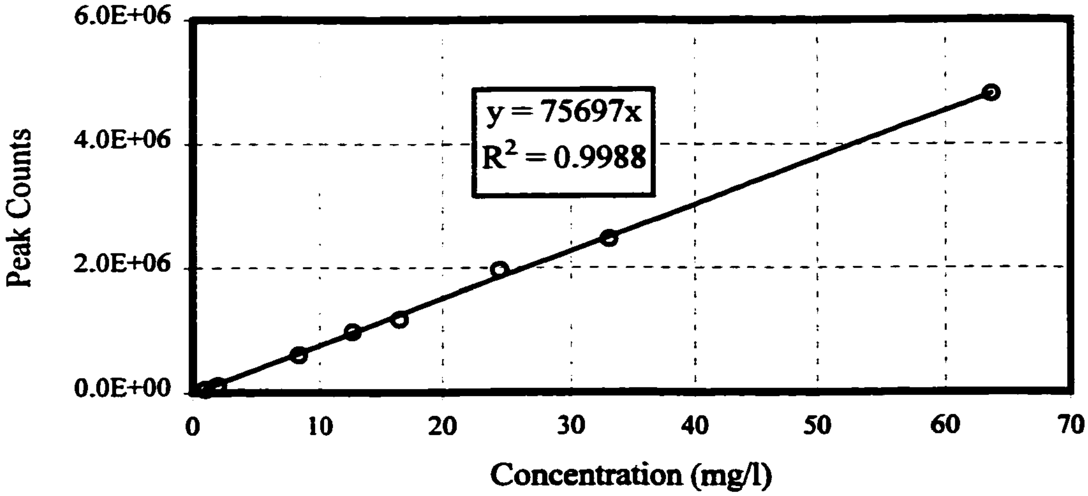

Figure B.18 Calibration Curve for PCE

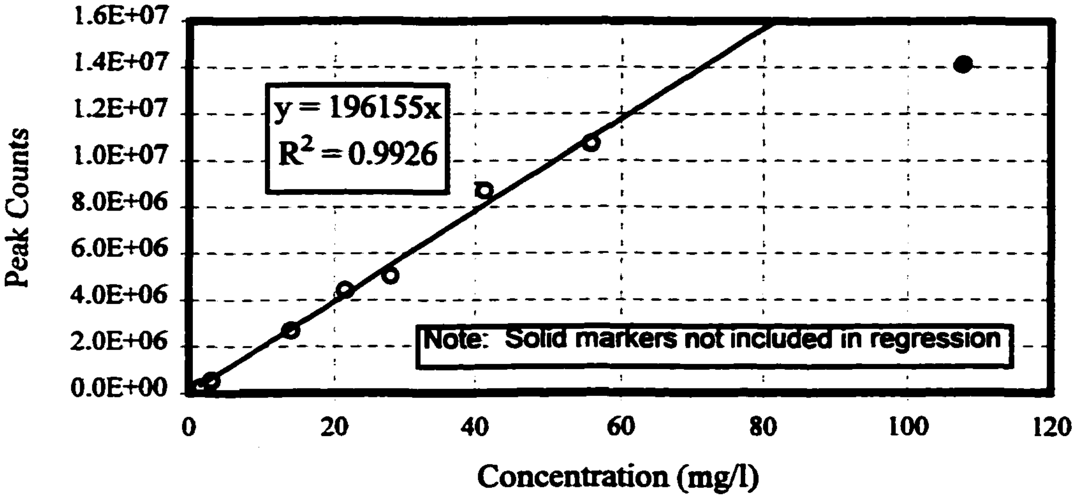

Figure B.19 Calibration Curve for TCE/Heptane

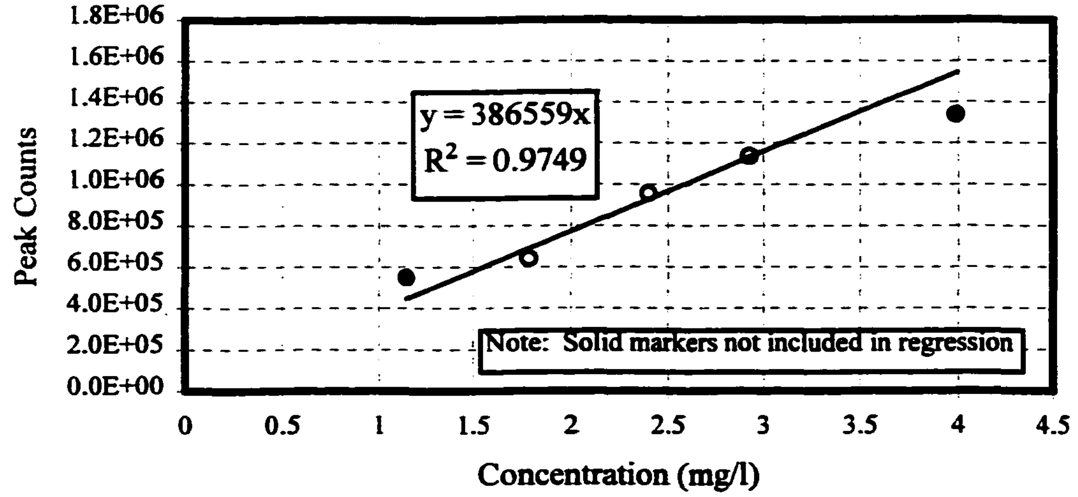

Figure B.20 Calibration Curve for Surfactant

APPENDIX C

MIXTURE COMPOSITIONS

Mix		Xyl	Tol	Hex	Hep	Dec	DCB	CTET	TCE	PCE
1		3.328	5.129						5.718	5.958
	moles	0.031	0.056						0.044	0.036
	M.F.	0.188	0.334						0.261	0.216
	EACN	1.138								
2		1.876	2.718	1.550		2.613				
	moles	0.018	0.029	0.018		0.018				
	M.F.	0.212	0.353	0.215		0.220				
	EACN	4.267								
3								3.066	3.026	3.035
	moles							0.020	0.023	0.018
	M.F.							0.325	0.376	0.299
	EACN	1.377								
4		1.454	1.397						3.313	3.964
	moles	0.014	0.015						0.025	0.024
	M.F.	0.176	0.194						0.323	0.307
	EACN	1.214								
5		1.520	1.444	1.465	1.411	1.438	1.012	1.052	1.011	1.057
	moles	0.014	0.016	0.017	0.014	0.010	0.007	0.007	0.008	0.006
	M.F.	0.145	0.158	0.172	0.142	0.102	0.070	0.069	0.078	0.064
	EACN	3.833								
6		0.760	2.312	0.483	0.316	0.495	0.576	0.854	3.111	1.046
	moles	0.007	0.025	0.006	0.003	0.003	0.004	0.006	0.024	0.006
	M.F.	0.085	0.299	0.067	0.038	0.041	0.047	0.066	0.282	0.075
	EACN	1.641								
7		2.518	2.545						2.556	2.546
	moles	0.024	0.028	0.000	0.000	0.000	0.000	0.000	0.019	0.015
	M.F.	0.275	0.321	0.000	0.000	0.000	0.000	0.000	0.226	0.178
	EACN	1.211								

APPENDIX D

UTCHEM INPUT FILE

y

```
CC*******************************************************************
CC
CC    BRIEF DESCRIPTION OF DATA SET:  UTCHEM (VERSION 6.0)
CC
CC*******************************************************************
CC
CC               SIMULATION OF COLUMN STUDY
CC     (TRACER TEST IN MEDIUM AT 80% RESIDUAL SATURATION)
CC
CC*******************************************************************
CC
CC
CC  COLUMN DIAMETER (CM): 2.5      PROCESS: TRACER TEST
CC  COLUMN LENGTH (CM): 14.8      COORDINATES: CARTESIAN
CC  POROSITY: 0.35              1-D SIMULATION
CC  GRID BLOCKS: 1 X 50
CC
CC  COLUMN AREA ASSUMED TO BE SQUARE WITH DIMENSIONS OF 2.2156 CM
CC
CC*******************************************************************
CC
CC
CC
CC
*----RUN NUMBER
  Column-CONTAMINATED
CC
CC
*----TITLE
CC  1-D SIMULATION OF TRACER TESTS IN COLUMN
CC  80% RESIDUAL SATURATION
CC  4 TRACERS
CC
CC SIMULATION FLAGS
*----IMODE IMES IDISPC ICWM ICAP IREACT IBIO ICOORD ITREAC ITC IGAS IENG
    1  2  3  0  1  0  0  1   0  1  0  0
CC
CC NUMBER OF GRIDBLOCKS, FLAG FOR CONSTANT/VARIABLE GRIDS,
UNIT(1:METRIC)
*----NX  NY  NZ  IDXYZ  IUNIT
   1   1  50   0     1
CC
CC GRIDBLOCK SIZE IN X, Y, AND Z DIRECTION
*----DX1      DY1      DZ1
 0.022156  0.022156  0.00296
CC
CC NUMBER OF COMPONENTS, TRACERS, ETC.
*----N  NO  NBC  NTW  NTA  NGC  NG
  12  0   0    4    0    0    0
CC
CC TRACER NAMES
*----TRNAME(I), FOR I=1,NTW
 ETHANOL
```

```
 1PENTANOL
 1HEXANOL
 2METHYL2HEXANOL
CC
CC FLAG INDICATING IF COMPONENT IS INCLUDED IN CALCULATIONS OR NOT
*----ICF(KC) FOR KC=1,N
   1 1 0 0 0 0 0 0 0 1 1 1 1
CC
CC*******************************************************************
CC
CC   OUTPUT OPTIONS
CC
CC*******************************************************************
CC
CC
CC FLAG FOR PV OR DAYS (1:PV, 0:DAYS)
*----ICUMTM   ISTOP
    0      0
CC
CC FLAG INDICATING IF PROFILE OF KCTH COMPONENT SHOULD BE WRITTEN
*----IPRFLG(KC),KC=1,N
   1 1 0 0 0 0 0 0 0 1 1 1 1
CC
CC FLAG FOR PRESSURE, SATURATION, CONCENTRATION, AND OTHER PROFILES
*----IPPRES IPSAT IPCTOT IPTRAC IPCAP IPGEL IPALK IPTEMP IPOBS IBPR
    0   0   1   0   0   0   0   0   0  0
CC
CC FLAG FOR WRITING SEVERAL PROPERTIES TO UNIT 4 (PROFILES)
*----IPHP IADS ICKL IVEL IVIS IPER ICNM IRKF IPHSE ICSE
   0  0  0  0  0  0  0  0  0  0
CC
CC*******************************************************************
CC
CC   RESERVOIR PROPERTIES
CC
CC*******************************************************************
CC
CC
CC MAXIMUM SIMULATION TIME (DAYS)
*----TMAX
   0.4
CC
CC ROCK COMPRESSIBILITY (1/PSI), STANDARD PRESSURE(KPA)
*----COMPR       PSTAND
   0.0        101.325
CC
CC FLAGS INDICATING CONSTANT/VARIABLE POROSITY AND X, Y, AND Z
PERMEABILITY
*----IPOR1 IPERMX IPERMY IPERMZ IMOD
    0   0   0   0   0
CC
CC CONSTANT POROSITY
*----PORC1
```

```
   0.35
CC
CC PERMEABILITY IN X DIRECTION (MILLIDARCIES)
*----PERMXC
   5000.0
CC
CC PERMEABILITY IN Y DIRECTION (MILLIDARCIES)
*----PERMYC
   5000.0
CC
CC PERMEABILITY IN Z DIRECTION (MILLIDARCIES)
*----PERMZC
   5000.0
CC
CC FLAG FOR CONSTANT OR VARIABLE DEPTH, PRESSURE, WATER SATURATION
*----IDEPTH  IPRESS  ISWI
    0     1     0
CC
CC CONSTANT DEPTH (METERS)
*----D111
   0.0
CC
CC INITIAL PRESSURE (KPA)
*----PINIT    HINIT
  101.325    0.0
CC
CC INITIAL WATER SATURATION
*----SWI
   0.7871
CC
CC CONSTANT CHLORIDE AND CALCIUM CONCENTRATIONS (MEQ/ML)
*----C50      C60
   0.0      0.0
CC
CC*****************************************************************
CC
CC   PHYSICAL PROPERTY DATA
CC
CC*****************************************************************
CC
CC
CC OIL CONC AT PLAIT POINT FOR TYPE II(+) AND TYPE II(-), CMC
*----C2PLC  C2PRC  EPSME  IHAND
   0.0    1.0  0.0001    0
CC
CC FLAG INDICATING TYPE OF PHASE BEHAVIOR PARAMETERS
*----IFGHBN
    1
CC
CC FLAG INDICATING IF PHASE BEHAVIOR DEPENDS ON COMPOSITION
*----IOD
    1
CC
```

```
CC EFFECTIVE SALINITY BTWN LOWER AND OPTIMAL LIMITS FOR TYPE III
*----CS0  SCS0  CS1  SCS1  CS2  SCS2  DCS20
  0.0  0.0   0.0  0.0   0.0  0.0   0.0
CC
CC EFFECTIVE SALINITY SLOPE PARAMETER FOR CALCIUM
*----BETA6
   1.0
CC
CC FLAG INDICATING TYPE OF INTERFACIAL TENSION CORRELATION
*----IFT
   1
CC
CC CONSTANTS IN HUH'S INTERFACIAL TENSION CORRELATION
*----CHUH   AHUH
  0.35   10.0
CC
CC LOG10 OF OIL/WATER INTERFACIAL TENSION
*----XIFTW
  1.6500
CC
CC FLAG FOR OIL SOLUBILITY IN WATER
*----IMASS
   1
CC
CC EQUIL CONC OF OIL IN WATER, NONEQUIL MASS TRANSFER COEFF
*----WSOL    CNEM2    ISOL
 0.0000    0.0       0
CC
CC CAPILLARY DESATURATION PARAMETERS FOR PHASE 1, 2, AND 3
*----ITRAP   T11   T22   T33
   1    0.0  0.0  0.0
CC
CC FLAG FOR DRAINAGE OR IMBIBITION RELATIVE PERMEABILITY CURVES
*----IPERM   IHYST   IPARK
   2     0     0
CC
CC FLAG INDICATING TYPE OF RESIDUAL SAT AND REL PERM PARAMETERS
*----ISRW   IPRW   IEW
   0     0    .0
CC
CC CONSTANT RESIDUAL SATURATION OF PHASES AT LOW CAPILLARY NUMBER
*----S1RWC   S2RWC   S3RWC
  0.240   0.213   0.240
CC
CC CONSTANT RESIDUAL SATURATION OF PHASES AT HIGH CAPILLARY NUMBER
*----S1RC    S2RC    S3RC
  0.12    0.30    0.12
CC
CC WATER AND OIL VISCOSITY, RESERVOIR TEMPERATURE
*----VIS1   VIS2   TSTAND
  1.0    0.89    0.0
CC
CC VISCOSITY PARAMETERS
```

```
*----ALPHA1  ALPHA2  ALPHA3  ALPHA4  ALPHA5
   3.4    1.0    3.0    1.0    1.0
CC
CC PARAMETERS TO CALCULATE POLYMER VISCOSITY AT ZERO SHEAR RATE
*----AP1   AP2   AP3
  52.0  2430.0  40000.0
CC
CC PARAMETER TO COMPUTE CSEP/MIN CSEP AND LOG VIS VS. LOG CSEP SLOPE
*----BETAP  CSE1  SSLOPE (FOR POLYMER PROCESSES)
   2.0  0.01  0.175
CC
CC PARAMETER FOR SHEAR RATE DEPENDENCE OF POLYMER VISCOSITY
*----GAMMAC  GAMHF  POWN
   4.0   20.0   1.1
CC
CC FLAG FOR POLYMER PARTITIONING, PERMEABILITY REDUCTION PARAMETERS
*----IPOLYM  EPHI3   EPHI4   BRK    CRK
    1     1.0     1.0    1000.0  0.0186
CC
CC SPECIFIC WEIGHT FOR COMPONENTS, AND GRAVITY FLAG
*----DEN1  DEN2  DEN3  DEN7  DEN8  IDEN  IODEN
  1.0   0.86  1.0   0.0   0.0    2     1
CC
CC FLAG INDICATING INJECTION/PRODUCTION RATES (0:FT3, 1:BBLS)
*----ISTB
   0
CC
CC COMPRESSIBILITY FOR VOLUME OCCUPYING COMPONENTS
*----COMPC(1)  COMPC(2)  COMPC(3)  COMPC(7)  COMPC(8)
    0.0      0.0      0.0      0.0      0.0
CC
CC FLAG INDICATING CONSTANT/VARIABLE CAP PRESSURE CURVES, OIL/WATER WET
*----ICPC  IEPC  IOW
   0    0    0
CC
CC CAPILLARY PRESSURE ENDPOINT
*----CPC0
  2.9
CC
CC CAPILLARY PRESSURE EXPONENT
*----EPC0
  2.0
CC
CC MOLECULAR DIFFUSIVITY OF KCTH COMPONENT IN PHASE 1 (D(KC),KC=1,N)
*----D(1) D(2) D(3) D(4) D(5) D(6) D(7) D(8) D(9) D(10) D(11) D(12)
  0.  0.  0.  0.  0.  0.  0.  0.  0.  0.  0.  0.
CC
CC MOLECULAR DIFFUSIVITY OF KCTH COMPONENT IN PHASE 2 (D(KC),KC=1,N)
*----D(1) D(2) D(3) D(4) D(5) D(6) D(7) D(8) D(9) D(10) D(11) D(12)
  0.  0.  0.  0.  0.  0.  0.  0.  0.  0.  0.  0.
CC
CC MOLECULAR DIFFUSIVITY OF KCTH COMPONENT IN PHASE 3 (D(KC),KC=1,N)
*----D(1) D(2) D(3) D(4) D(5) D(6) D(7) D(8) D(9) D(10) D(11) D(12)
```

```
  0.  0.  0.  0.  0.  0.  0.  0.  0.  0.  0.  0.
CC
CC LONGITUDINAL AND TRANSVERSE DISPERSIVITY OF PHASE 1 (METERS)
*----ALPHAL(1)    ALPHAT(1)
   0.0005      0.00
CC
CC LONGITUDINAL AND TRANSVERSE DISPERSIVITY OF PHASE 2 (METERS)
*----ALPHAL(2)    ALPHAT(2)
   0.0005      0.00
CC
CC LONGITUDINAL AND TRANSVERSE DISPERSIVITY OF PHASE 3 (METERS)
*----ALPHAL(3)    ALPHAT(3)
   0.0005      0.00
CC
CC FLAG INDICATING IF ORGANIC ADSORPTION IS CONSIDERED
*----IADSO
    0
CC
CC SURFACTANT AND POLYMER ADSORPTION PARAMETERS
*----AD31  AD32   B3D    AD41   AD42   B4D   IADK   IADS1   FADS
  1.0   0.5   1000.   0.7    0.    100.   0      0      0
CC
CC PARAMETERS FOR CATION EXCHANGE OF CLAY AND SURFACTANT
*----QV   XKC   XKS   EQW
  0.0   0.0   0.0   1.0
CC
CC TRACER PARTITION COEFFICIENTS
*----TK(I), FOR I=1,NTW
  0.00   1.34   5.68   11.20
CC
CC SALINITY EFFECT ON TRACER PARTITION COEFFICIENTS
*----TKS(I) FOR I=1,NTW
  0.0   0.0   0.0   0.0
CC
CC TRACER RADIOACTIVE DECAY COEFFICIENT
*----RDC(I) FOR I=1,NTW
  0.0   0.0   0.0   0.0
CC
CC TRACER RETARDATION FACTOR
*----RET(I) FOR I=1,NTW
   0.09   0.25   0.60   0.45
CC
CC WATER PHASE FLOWING FRACTION
*----FFL(1)   FFH(1)   CM(I,1)
  0.72     0.72     0.0004  0.0003  0.00008  0.0001
CC
CC OIL PHASE FLOWING FRACTION
*----FFL(1)   FFH(1)   CM(I,1)
  0.40     0.40     0.0004  0.0003  0.00008  0.0001
CC
CC MICROEMULSION PHASE FLOWING FRACTION
*----FFL(1)   FFH(1)   CM(I,1)
  0.00     0.00     0.0006  0.0003  0.0001  0.0001
```

```
CC
CC*******************************************************************
CC
CC VII   WELL DATA
CC
CC*******************************************************************
CC
CC
CC  FLAG FOR BOUNDARIES
*----IBOUND
    0
CC
CC TOTAL NO. OF WELLS, WELL RADIUS MODEL FLAG
*----NWELL  IRO  ITIME  NWREL
   2  2   1   2
CC
CC WELL LOCATIONS, FLAG FOR WELL TYPE, WELL RADIUS, SKIN, ETC.
*----IDW  IW  JW  IFLAG  RW  SWELL  IDIR  KFIRST  KLAST  IPRF
   1  1  1   1  0.0125 0.0   3     1     1    0
CC
CC NAME OF THE WELL
*----WELNAM
   INJECTION
CC
CC MAX. AND MIN. ALLOWABLE BOTTOMHOLE PRESSURE AND RATE
*----ICHECK    PWFMIN    PWFMAX    QTMIN    QTMAX
    0       0.0      5000.0     0.0    10000.0
CC
CC WELL LOCATION, FLAG FOR WELL TYPE, WELL RADIUS, SKIN, ETC.
*----IDW  IW  JW  IFLAG  RW  SWELL  IDIR  KFIRST  KLAST  IPRF
   2  1  1   2  0.0125 0.0   3     50    50    0
CC
CC NAME OF THE WELL
*----WELNAM
   EXTRACTION
CC
CC MAXIMUM AND MINIMUM ALLOWABLE BOTTOMHOLE PRESSURE AND RATE
*----ICHECK    PWFMIN    PWFMAX    QTMIN    QTMAX
    0       0.0      5000.0     0.0    10000.0
CC
CC INJ. RATE AND INJ. COMP. FOR RATE CONS. WELLS FOR EACH PHASE (L=1,3)
*----QI(M,L)  C(M,KC,L)
 1  0.000432  1.0  0.0  0.0  0.0  0.0  0.0  0.0  0.0  1.0  1.0  1.0 1.0
 1   0.0      0.0  0.0  0.0  0.0  0.0  0.0  0.0  0.0  0.0  0.0  0.0 0.0
 1   0.0      0.0  0.0  0.0  0.0  0.0  0.0  0.0  0.0  0.0  0.0  0.0 0.0
CC
CC MAXIMUM PRESSURE OF PRODUCTION WELL
*----ID    PWF(M)
   2    101.325
CC
CC CUM. IN.PRO:MAPS. PRO:WELL  .HIS1    .CONC   RESTART
*----TINJ   CUMPR1   CUMHI1   WRHPV    WRPRF   RSTC
  0.01389 0.00347 0.00347  0.00347  0.00347 0.01389
```

```
CC
CC INITIAL TIME STEP, CONC. TOLERANCE, MIN/MAX COURANT NUMBERS
*----DT    DCLIM    CNMAX  CNMIN
 0.00001  0.0001  0.025  0.0001
CC
CC DESCRIPTION OF CHANGES
*----IRO  ITIME  IFLAG(M) FOR M=1,NWELL
   2    1      1  2
CC
CC NUMBER OF WELLS WITH LOCATION CHANGES
*----NWEL1
   0
CC
CC NUMBER OF WELLS WITH RATE/CONCENTRATION CHANGES
*----NWEL2  ID
   1    1
CC
CC INJECTION RATE/CONCENTRATION CHANGES
*----ID    QI(ID,L)    C(ID,KC,L)
   1  0.000432  1.0  11*0.0
   1   0.0      12*0.0
   1   0.0      12*0.0
CC
CC CUMULATIVE INJECTION TIME AND INTERVALS
*----TINJ  CUMPR1  CUMHI1  WRHPV  WRPRF  RSTC
   0.35  0.00347  0.00347  0.00347 0.00347  0.25
CC
CC INITIAL TIME STEP, CONC. TOLERANCES, MAX/MIN COURANT NUMBER
*----DT     DCLIM    CNMAX   CNMIN
 0.00001   0.0001   0.025   0.0001
```